GEOMAR
Helmholtz-Zentrum für Ozeanforschung Kiel

Methane hydrates in Black Sea deep-sea fans: Characteristics, implications, and related geohazards

DISSERTATION
zur Erlangung des Doktorgrades
der Mathematisch-Naturwissenschaftlichen Fakultät
der Christian-Albrechts-Universität zu Kiel

vorgelegt von
Timo Zander

Kiel, 2017

Referent:	Prof. Dr. Christian Berndt
Korreferent:	Prof. Dr. Sebastian Krastel-Gudegast
Tag der mündlichen Prüfung:	01. November 2017
Zum Druck genehmigt:	01. November 2017

.....

Die Dekanin

Erklärung

Hiermit erkläre ich, dass ich die vorliegende Doktorarbeit selbstständig und ohne Zuhilfenahme unerlaubter Hilfsmittel angefertigt habe. Sie stellt, abgesehen von der Beratung durch meine Betreuer, nach Inhalt und Form meine eigene Arbeit dar. Weder diese noch eine ähnliche Arbeit wurde an einer anderen Abteilung oder Hochschule im Rahmen eines Prüfungsverfahrens vorgelegt, veröffentlicht oder zur Veröffentlichung vorlegt. Ferner versichere ich, dass die Arbeit unter Einhaltung der Regeln guter wissenschaftlicher Praxis der Deutschen Forschungsgemeinschaft entstanden ist.

Kiel, den 20. Juli 2017

.....

Timo Zander

In memoriam David

26.05.1985 – 10.03.2017

Abstract

The Black Sea is the world's largest anoxic marine basin and offers ideal conditions for the decomposition of organic matter and for gas generation. Methane escape into the water column is observed at abundant sites in the coastal areas and along the shelfbreak, but also in areas within the gas hydrate stability zone (GHSZ), i.e. deeper than 720 m water depth, and at mud volcanoes in the deep basins. The hydrologic structure of the Black Sea is controlled by the inflow of salty waters from the Mediterranean Sea through the Bosphorous, and by the inflow of freshwater from the surrounding rivers, leading to a stratification of the water column with anoxic conditions below 150 m water depth. The rivers formed large deep-sea fan complexes where sedimentation is mainly controlled by glacial cycles and the accompanying sea level rises and falls. Two of these deep-sea fan complexes, the Danube deep-sea fan in the west and the Don Kuban deep-sea fan in the northeast, were investigated in this work in order to study various aspects of gas hydrate complexes in these settings. The area in the Danube deep-sea fan is of particular interest because of the high potential for hosting exploitable gas hydrate reservoirs in high-permeable sediments.

In the first case study, 2D multichannel seismic data were used for identification and mapping of anomalous multiple bottom simulating reflectors (BSR), which were observed in the levee deposits of a buried channel-levee system in the Danube deep-sea fan. BSR formation due to overpressure compartments could be excluded because the necessary gas column height would exceed the vertical distance between two overlying BSRs. Instead, the BSRs are likely paleo-BSRs caused by a change in pressure and temperature conditions during different limnic phases of the Black Sea. The BSRs remain visible in seismic data up to 300,000 yr after they have left the GHSZ, because free gas is still present beneath them. As the free gas can only be transported by diffusion, it largely remains trapped within the fine-grained levee deposits, and therefore only small amounts of gas are released after gas hydrate dissociation.

The second case study is also located in the Danube deep-sea fan and focusses on a potential shallow gas hydrate reservoir that is of interest in terms of exploitation of gas hydrates as an energy resource. The study area is located in a paleo channel-levee system. To determine whether a hypothetical gas production out of the hydrate reservoir induces slope failures along the seabed slopes near the production area, a slope stability analysis was carried out. A screening of the area identified critical slopes at the inner levees along the channel's course. Numerical simulation of hydrate production out of a shallow hydrate reservoir showed that seafloor subsidence due to reservoir compaction likely does not reduce the stability of the nearby slope. Consequently, naturally occurring slope failures are more likely to occur than landslides triggered by gas hydrate production. The mobilization of sediments along the calculated slip zone could generate a landslide that would impact the production site with velocities of up to 10 m s^{-1}.

The third case study focuses on the Kerch seep site located in the Don Kuban deep-sea fan in the northeastern Black Sea. The seep site, composed of three closely-spaced seep domes, is located within the GHSZ in about 900 m water depth. The study consisted of 3D seismic imaging of the seeps' plumbing systems using the P-Cable seismic system, sidescan sonar imaging to analyze seep surface backscatter characteristics, and pore water analyses to investigate the transport mechanism of methane through the sediments towards the seafloor. Each of the three seeps hosts its own gas pocket underneath the seep domes. The transport of biogenic methane predominantly occurs in the form of gas bubbles along narrow pipes through the GHSZ. Based on seismic expressions and surface

backscatter of the seeps, the Kerch seep site is interpreted as a rather young seep system lacking the extensive carbonate crust observed at other seep sites in the Black Sea.

The studies show that the exploitation of gas hydrate out of reservoirs in the sediments of the Danube deep-sea fan likely does not pose a hazard for the triggering of landslides, but more detailed investigations including drilling are required. Similarly, the multiple BSRs underneath the gas hydrate reservoir are not a hazard as they are not related to gas overpressure. The Kerch seep site is an ideal study site for the investigation of short-term and long-term changes of gas migration pathways and seep activity over time. Extending the seismic and hydroacoustic datasets over time should therefore be the objective of future studies.

Zusammenfassung

Das Schwarze Meer ist das größte anoxische Meeresbecken der Welt und bietet ideale Bedingungen für die Zersetzung organischen Materials und die daraus folgende Generierung von Gasen. In flachen Wassertiefen kann an zahlreichen Stellen am Meeresboden entweichendes Methangas beobachtet werden. Vereinzelt treten Gasaustritte auch in Wassertiefen unterhalb der Gashydratstabilitätszone (GHSZ) auf, die bei etwa 720 m Wassertiefe liegt, sowie an Schlammvulkanen in den tieferen Becken. Die Hydrologie des Schwarzen Meeres wird im Wesentlichen durch Salzwassereintrag aus dem Mittelmeer als auch durch Frischwassereintrag aus zahlreichen umliegenden Flüssen beeinflusst, wodurch eine Stratifikation der Wassersäule mit anoxischen Bedingungen unterhalb von 150 m Tiefe entstand. Durch Sedimentablagerungen an den Flussmündungen bildeten sich große Tiefseefächer, deren Sedimentationsrate durch die Glazialzyklen und die daraus resultierenden Meeresspiegelschwankungen gesteuert werden. Gegenstand dieser Arbeit ist die Untersuchung von zwei Tiefseefächern hinsichtlich verschiedener Aspekte von Gashydratvorkommen: der Donau-Tiefseefächer im westlichen Bereich des Schwarzen Meeres, sowie der Don-Kuban-Tiefseefächer im nordöstlichen Bereich. Das Gebiet des Donau-Tiefseefächers ist dabei von besonderem Interesse für die Gashydratforschung, da hier ideale Bedingungen für Gashydratlagerstätten in hochpermeablen Sedimentschichten herrschen.

In der ersten Fallstudie wurden hochauflösende reflexionsseismische Profildaten untersucht, um ungewöhnliche, mehrfach-bodensimulierende Reflektoren (BSR) zu identifizieren und zu kartieren. Diese Mehrfach-BSRs wurden in den Leveeablagerungen eines verschütteten Channel-Leveesystems des Donau-Tiefseefächers entdeckt. Gasüberdruckzonen als Ursache für die BSRs konnte ausgeschlossen werden, da die Höhen der für den Überdruck notwendigen Gassäulen den vertikalen Abstand zwischen zwei BSRs übersteigen würden. Stattdessen konnte gezeigt werden, dass die BSRs vermutlich Paleo-BSRs sind, die durch Druck- und Temperaturschwankungen während limnischer und mariner Phasen bedingt sind. BSRs können somit selbst in Bereichen seismisch erfasst werden, die sich seit über 300.000 Jahren nicht mehr in der GHSZ befinden. Dies liegt daran, dass sich unterhalb der BSRs noch immer durch Gashydratauflösung freigesetztes Gas befindet, welches nur durch Diffusion aufsteigen kann und somit innerhalb der feinkörnigen Leveeablagerungen verbleibt.

Die zweite Fallstudie betrachtet ein potenzielles Gashydratreservoir in flacher Sedimenttiefe, welches sich ebenfalls im Donau-Tiefseefächer befindet. Dieses Gashydratreservoir stellt eine mögliche Lagerstätte für die Gewinnung von Methangas durch Hydratzersetzung dar. Um herauszufinden, ob durch Gasproduktion Hangrutschungen im Bereich der potenziellen Produktionsstätte verursacht werden könnten, wurde eine Hangstabilitätsanalyse durchgeführt. Bei einem Screening des Meeresbodens im Bereich des Donau-Tiefseefächers wurden dabei kritische Hangneigungen an den inneren Levees entlang der Kanäle des Tiefseefächers identifiziert. Anhand einer Simulation der Hydratproduktion wurde untersucht, ob durch eine während der Gashydratproduktion auftretende Kompaktion des Reservoirs eine Absenkung des Meeresbodens hervorgerufen würde, welche die Stabilität des Leveehanges verändern könnte. Die Simulation ergab, dass die Stabilität des Leveehanges nahe der Produktionsstätte wahrscheinlich nicht durch die Produktion beeinträchtigt würde. Demnach ist im Produktionsgebiet die Wahrscheinlichkeit höher, dass eine natürliche Hangrutschung auftritt, als dass Hangrutschungen durch Gashydratproduktion verursacht werden. Eine mögliche mobilisierte Rutschungsmasse könnte mit einer Geschwindigkeit von bis zu 10 m s^{-1} den Bereich der Produktionsstätte treffen.

Die dritte Fallstudie konzentriert sich auf die drei Kerch-Seeps im Don-Kuban-Tiefseefächer des nordöstlichen Schwarzen Meeres. Die Seeps befinden sich in einer Wassertiefe von 900 m und damit innerhalb der GHSZ. Die verwendeten Methoden umfassen P-Cable-3D-Seismik zur Untersuchung der Gasmigrationswege unterhalb der Seeps, Seitensichtsonar zur Analyse der Meeresbodenrückstreuung und Morphologie, sowie die Analyse von Porenwasserdaten, die einen Einblick in die Art des Methantransportes durch die Sedimentschichten geben. Jeder der drei Seeps besteht aus einer Aufwölbungsstruktur, unter der sich biogenes Gas angesammelt hat. Dieses Gas migriert in der Form von Gasblasen entlang schmaler Aufstiegskanäle durch die GHSZ in Richtung Meeresboden. Die seismischen Eigenschaften und die Art der Meeresbodenrückstreuung an den Seeps lässt darauf schließen, dass die Kerch-Seeps ein vergleichsweise junges Seepsystem darstellt, das bislang keine ausgeprägten Karbonatkrusten am Meeresboden ausgebildet hat, welche an anderen Seepsystemen des Schwarzen Meeres zu beobachten sind.

Die Resultate der Studien zeigen, dass eine mögliche Gashydratproduktion in der Region des Donau-Tiefseefächers zwar vermutlich keine Hangrutschungen verursacht, jedoch sind aufgrund fehlender Bodenproben und mangelnden Daten zur Hydratsättigung und der tatsächlichen Ausbreitung und Dimension des Gashydratreservoirs noch weitere Folgestudien notwendig. Die unterhalb des Gashydratreservoirs liegenden Mehrfach-BSRs stellen kein Risiko für die Gashydratproduktion dar, da Gasüberdruckbereiche unterhalb der BSRs ausgeschlossen werden können. Die Kerch-Seeps stellen ein ideales Zielgebiet für die Untersuchung von kurz- und langfristigen Änderungen von Seepaktivitäten und Gas-Migrationswegen dar. Die bereits vorhandene Seismik- und Hydroakustikdatenbank zu erweitern, sollte daher das Ziel zukünftiger Studien in diesem Gebiet sein.

Contents

List of abbreviations

AOM	anaerobic oxidation of methane
BCL	buried channel-levee system
BGHSZ	base of the gas hydrate stability zone
BSR	bottom-simulating reflector
CDP	common depth point
CSEM	controlled source electromagnetic
DSDP	Deep Sea Drilling Program
FoS	factor of safety
GC	gravity cores
GHSZ	gas hydrate stability zone
GMT	Generic Mapping Tools
HMCS	2D high-resolution multichannel seismic survey
IODP	Integrated Ocean Drilling Program
MIC	multiple cores
OBS	ocean bottom seismometer
OFOS	Ocean Floor Observation System
PSF	paleo seafloor
RMCS	2D regional multichannel seismic survey
ROV	remotely operated vehicle
SMOW	standard mean ocean water
SMTZ	sulfate-methane transition zone
TWT	two-way travel time
USBL	ultra-short base line
VPDB	Vienna Pee Dee Belemnite

Motivation and outline

Motivation

Methane hydrates play an important role in the global carbon cycle (Judd and Hovland, 2007). Vast amounts of methane gas are stored in the form of hydrates within the sediments along continental margins. The change of pressure and temperature conditions due to sea level changes and global warming establishes new stability conditions for gas hydrates, which may induce geohazards such as seafloor slope instability and gas venting. Hydrocarbon gas expelled at the seafloor may eventually reach the atmosphere, where it may contribute to global warming. As methane, which is a much stronger greenhouse gas than CO_2 (e.g. Wuebbles and Hayhoe, 2002), is the most common gas in marine sediments (Judd and Hovland, 2007), the potential impact of expelled methane on global warming is of high interest for research studies. Additionally, gas hydrate reservoirs have raised interest as a possible alternative energy resource (e.g. Burwicz et al., 2011; Wallmann et al., 2012; Piñero et al., 2013). The exploitation of gas hydrate reservoirs has been tested at several sites around the world, e.g. in the Gulf of Mexico (Collett et al., 2005), in the Nankai Trough off Japan (Tsuji et al., 2009), and most recently in the South China Sea (Jia, 2017). The identification of the presence of gas hydrates through bottom simulating reflectors (BSR) in seismic data is widely accepted, as the reflector corresponds to the base of the gas hydrate stability zone (BGHSZ).

One of the most interesting research areas in the world regarding gas hydrates and fluid flow systems is the Black Sea. Only a single connection through the Sea of Marmara and the Mediterranean Sea links the global oceans with the Black Sea, making it the world's largest body of anoxic water (Ryan et al., 1997). Conditions in the Black Sea changed completely from marine to lacustrine during glacial times, when the sea level fell and the Black Sea was isolated from saline water inflow through the Bosphorus (Ryan et al., 1997). Under these conditions, high amounts of hydrocarbons formed in the sediments of the Black Sea. As gas hydrates are stable below ~720 m water depth (Naudts et al., 2006), the Black Sea provides a great potential to study complex gas hydrate systems and associated fluid flow.

In the Danube deep-sea fan in the western Black Sea (study area 1; Fig. I), abundant BSRs in seismic data indicate the presence of gas hydrates in high-permeable sediments, which makes this a promising area for a potential gas hydrate exploitation in the future (Haeckel et al., 2015). However, the removal of massive amounts of solid gas hydrates by depressurizing a permeable reservoir may cause a significant subsidence at the seafloor, which may cause seafloor instability and induce slope failures. Furthermore, the presence of multiple BSRs underneath the potential gas hydrate reservoirs in this area is not well understood. If these anomalous BSRs are caused by overpressured gas compartments, they pose an additional hazard for gas hydrate production, as uncontrolled gas release and blowouts are possible.

In the Black Sea, gas is expelled at numerous vent sites such as shallow-water pockmarks, cold seeps, and mud volcanoes in the deeper basins. The factors controlling fluid migration underneath the seep sites, as well as seep surface expressions, have been studied in detail over the past decades in numerous locations around the world, including areas within the gas hydrate stability zone (GHSZ; e.g. Cartwright, 1994; Suess et al., 1999; Judd and Hovland, 2007; Greinert et al., 2010; Dumke et al., 2014). These studies also provide insights into origins and transport processes of the expelled gas (e.g. Haeckel et al., 2004; Hensen et al., 2004). Therefore, the investigation of cold seep sites through multidisciplinary studies provides the possibility to gain insight into the local tectonic and fluid

migration processes involved, and to increase our knowledge on cold seep sites in general. One example is the Kerch seep site in the northwestern Black Sea offshore Crimea (study area 2; Fig. I), which is located within the GHSZ in about 900 m water depth. It is still unclear how gas migrates through the GHSZ at this seep site, and how this is influenced by its location in a channel-levee system.

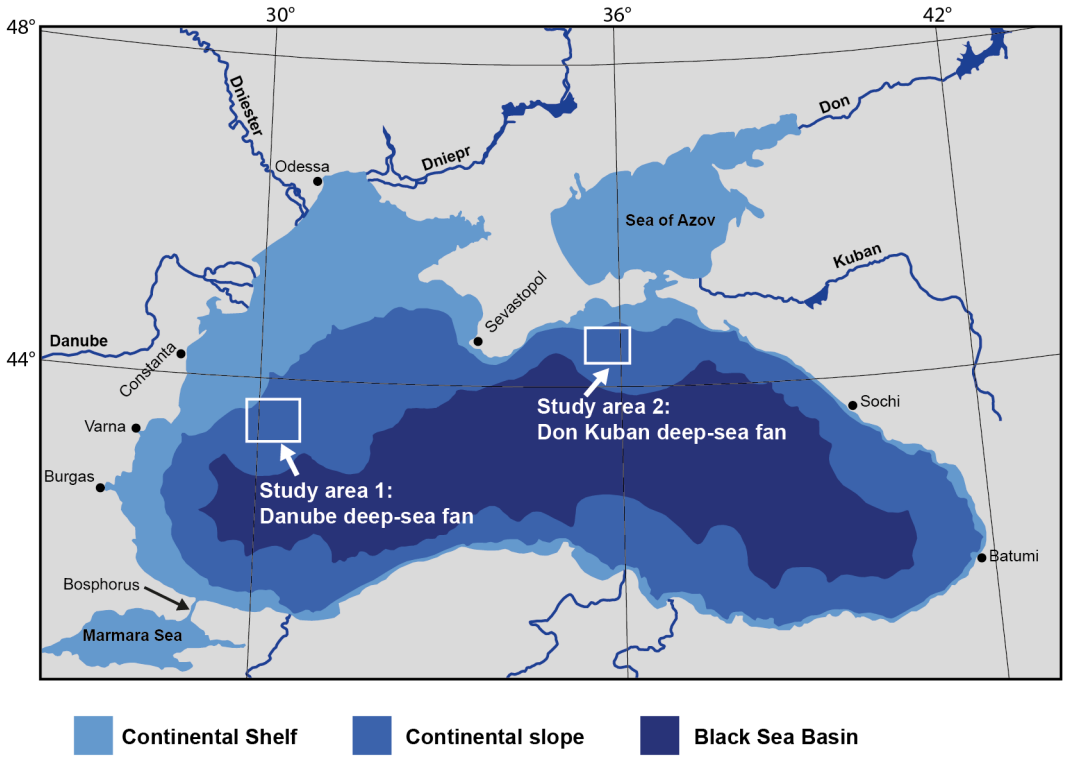

Fig. I: Overview map of the Black Sea. The two study areas are marked by white rectangles.

Purpose of this study

The two study areas in the Black Sea, the Danube deep-sea fan and the Don Kuban deep-sea fan (Fig. I), were investigated using a variety of tools such as 2D and 3D high resolution reflection seismics, multibeam echosounder, subbottom profiler, sidescan sonar, and pore water analyses. The specific objectives of this thesis are:

- to study the character and distribution of anomalous multiple BSRs in the study area of the Danube deep-sea fan. These BSRs are one of the most spectacular examples of multiple BSRs in the world.
- to develop and test new hypotheses that explain these anomalous multiple BSRs
- to find out if production of gas out of a shallow hydrate reservoir in the study area can be performed safely with respect to slope stability
- to find out how gas migrates through the GHSZ at the Kerch seep site in the northwestern Black Sea

SUGAR and MIDAS projects

Data from the Danube deep-sea fan (study area 1) were acquired during two research expeditions: MSM34 (legs 1 and 2, 2013-2014) onboard *RV Maria S. Merian*, and GHASS cruise (2015) onboard *RV Pourquoi Pas?*. The research was funded by the Federal Ministry of Education and Research (BMBF) and the Federal Ministry of Economy and Energy (BMWi) through the SUGAR project (Submarine Gas Hydrate Reservoirs), and by the European Union Seventh Framework Programme under the MIDAS project (Managing Impacts of Deep-Sea Research Exploitation). SUGAR aims at the preparation of a large-scale European gas hydrate initiative and a field test in European waters where gas is produced from hydrates using novel production technologies. The Black Sea was selected as a target area during phase II of the project, which ended in July 2014. MIDAS aimed at investigating the environmental impacts of extracting mineral and energy resources from the deep-sea environment. The project ended in November 2016. As part of work package 1, the work of this thesis was performed alongside the scientific progress of the SUGAR project, with the specific objective to study the potential hazards for slope failure during a simulated hydrate production at the SUGAR test site. Study results for the Danube deep-sea fan are presented in Chapters 2 and 3.

Fig. II: Logos of the scientific projects SUGAR (left) and MIDAS (right)

DOKU-GAS project

Data from the Don Kuban deep-sea fab (study area 2) were obtained during the RV Poseidon expedition P427 (2012) and complemented using data from the RV Meteor expedition M84/2 (2011). The research was funded by the German Research Foundation (DFG) through the DOKU-GAS project, which ended in 2014. The aim of the project was to image different fluid expulsion systems and to deduce the functioning of these focused fluid flow systems. Therefore, an anomalous active seep site within the GHSZ was selected as a study area complementing to this thesis. Study results for the Don Kuban deep-sea fan are presented in Chapter 4.

Thesis outline

This PhD thesis was written at the GEOMAR Helmholtz-Centre for Ocean Reseach Kiel, Germany. The basic work has been carried out from October 2013 until June 2017.

The thesis is structured into five chapters. **The first chapter** introduces the central topics of the thesis. The introduction starts with an overview of gas and gas hydrates in marine sediments, beginning with the origin of methane and flow mechanisms, followed by a brief introduction into gas hydrate formation and cold seep systems. The introduction further discusses the state of gas hydrates as a potential future energy resource and possible production methods especially in the marine environment. This is followed by a discussion of marine geohazards that are related to gas hydrate production. Then, gas and gas hydrate identification methods based on geophysical data are presented. The introduction closes with an overview over the study area, the Black Sea, and briefly introduces to the areas which are in focus in the following chapters. Three manuscripts comprise the central part of the thesis. They represent stand-alone manuscripts with their own abstract, introduction, methods, results, discussion, and conclusions sections. Short outlines of **chapters 2-4** including the contributions of the involved co-authors are given below. The thesis closes with **chapter 5**, which sums up the main findings of the work presented in chapters 2-4 and presents future perspectives.

Chapter 2 presents new findings on a stack of anomalous multiple BSRs that were identified in the levee deposits of a buried channel-levee system of the paleo Danube deep-sea fan. Based on new reflection seismic data, we were able to study the distribution of the BSRs throughout the area in more detail compared to previous studies, and to relate them to different sealevel lowstands during lacustrine stages of the Black Sea. We further present new explanations for the cause of these BSRs which are related to the permeability of the sediments in which the BSRs are observed.

This chapter is published in *Earth and Planetary Science Letters* as Zander, T., Haeckel, M., Berndt, C., Chi, W.C., Klaucke, I., Bialas, J., Klaeschen, D., Koch, S., and Atgın, O. (2017), On the origin of multiple BSRs in the Danube deep-sea fan, Black Sea. Earth and Planetary Science Letters 462, pp. 15-25. Supporting Information can be found in the Appendices A.1 – A.3.

Contributions to Chapter 2: J. Bialas led the survey. J. Bialas, I. Klaucke, M. Haeckel, S. Koch, O. Atgın, and T. Zander contributed to the acquisition of the seismic, multibeam, and geochemical data. T. Zander, D. Klaeschen, and S. Koch processed the seismic data. T. Zander, M. Haeckel, and W.C. Chi performed the thermal and geochemical models. T. Zander analyzed the data and wrote the manuscript, with contributions by C. Berndt and M. Haeckel. All co-authors helped improving and revising the manuscript.

Chapter 3 describes a multidisciplinary study combining geophysical data and geomechanical modeling in order to investigate potential hazards of slope failure due to gas hydrate exploitation. The study was conducted in the same area of the paleo Danube deep-sea fan as the work presented in Chapter 2. Here, we assume a hypothetical gas hydrate reservoir in shallow sub-seafloor depth and simulate hydrate production using the depressurization method. Our geomechanical model identifies the zone with the lowest factor of safety against slope failure along the levee wall located close to the production area, and analyses if a submarine landslide might be triggered by the production operation.

This chapter has been submitted to *Marine and Petroleum Geology* as Zander, T., Choi, J.C., Vanneste, M., Berndt, C., Dannowski, A., Carlton, B., and Bialas, J., Potential impacts of gas hydrate exploitation on slope stability in the Danube deep-sea fan, Black Sea.

Contributions to Chapter 3: J. Bialas led the survey. J. Bialas, A. Dannowski, and T. Zander contributed to the acquisition and processing of the seismic and multibeam data. J.C. Choi, M. Vanneste, B. Cartlon, and T. Zander performed the geomechanical screening, models, and simulations. T. Zander wrote the manuscript with contribution by J.C. Choi, M. Vanneste, and C. Berndt. All co-authors helped improving and revising the manuscript.

Chapter 4 presents new findings of the Kerch seep plumbing system in the northwestern Black Sea based on 3D seismic and sidescan sonar data that were acquired in 2012. The seeps site is located well within the GHSZ and features anomalous gas escape into the water column. We show that the seep sites are directly connected to several gas pockets in shallow depth, which push the sediments upward, leading to domes at the seafloor.

This chapter will be submitted to *Marine Geology* as Zander, T., Haeckel, M., Klaucke, I., Berndt, C., Bialas, J., Klaeschen, D., and Papenberg, C., New insights into the Kerch seep plumbing system in the Black Sea.

Contributions to Chapter 4: J. Bialas led the survey. J. Bialas, D. Klaeschen, C. Papenberg, and T. Zander contributed to the acquisition of the seismic, sidescan, and subbottom profiler data. D. Klaeschen and C. Papenberg processed the seismic data, and T. Zander and I. Klaucke processed the sidescan and subbottom profiler data. T. Zander and M. Haeckel performed the pore water analysis and modeling. T. Zander wrote the manuscript, with contributions by I. Klaucke, M. Haeckel, and C. Berndt. All co-authors helped improving and revising the manuscript.

1. Introduction

1.1 Gas and gas hydrates in marine sediments

1.1.1 Natural gas in the marine environment

Gas in marine sediments is dominated by methane, which mainly originates from biogenic methane generation, i.e., microbial and thermogenic processes. In addition, methane can also be formed from inorganic processes, which is referred to as abiogenic methane generation (e.g. Schoell, 1988; Welhan, 1988; Whiticar, 1999).

Microbial methane originates from methanogenic processes in shallow sediments. CO_2, originating from organic matter and from sulfate reduction in shallow sediments (about 1 m depth), is reduced to methane, which is the most dominant methane-forming process in marine sediments (Whiticar et al., 1986). In freshwater sediments, methane is generally formed through fermentation. Ideal conditions for methane generation are found in continental margins, which are characterized by high biogenic productivity and high sedimentation rates, leading to the presence of large amounts of organic matter in the sediments. Optimal conditions for microbial methanogenesis in anoxic conditions are provided by temperatures around 35-45 °C (Rice, 1992). The temperature for methane production ranges from 4 °C to up to 97 °C, and therefore microbial methanogenesis typically occurs within the upper 2 m of sediment (Rice, 1992; Wiese and Kvenvolden, 1993). The lower limit is defined by the temperature and hence the sedimentation rate, and can therefore be expected to occur in depths of >1 km (Judd and Hovland, 2007).

At greater depth, organic matter eventually becomes kerogen, which can release methane and higher hydrocarbons by catagenesis (Judd, 2003). The type of petroleum produced depends on the type of kerogen (defined by the ratios of hydrogen to carbon (H/C) and oxygen to carbon (O/C)) and the origin of organic matter (Tissot and Welte, 1994; Judd and Hovland, 2007). Methane is characterized by the lowest hydrocarbon complexity of one carbon atom (C_1) and requires kerogen of low H/C and high O/C ratios with organic matter of terrestrial origin (Tissot and Welte, 1994). Methane can also form when petroleum (C_{2+}) that remains in the source rock and does not migrate upwards into a cooler environment is broken down into lower hydrocarbon complexity (Judd and Hovland, 2007). The temperature window for thermogenic hydrocarbon production is around 60-260 °C, corresponding to depths of >10 km (Judd and Hovland, 2007).

Abiogenic methane is formed through inorganic processes. It is suggested to occur at hydrothermal systems at mid ocean ridges (Welhan, 1988; Minshull et al., 1998) or onshore (Fiebig et al., 2009).

The origin of methane can be derived from the molecular ratio of higher hydrocarbons. The C_1/C_{2+} ratios of microbially generated hydrocarbons are generally high (>1000) compared to thermogenic hydrocarbons characterized by lower ratios (Fig. 1.1A; Bernard et al., 1976; Whiticar, 1999). Additionally, the stable isotope analysis of light and heavy isotopes ($^{12}C/^{13}C$ and $D/^{1}H$) can give insight into the origin of methane (Fig. 1.1B). Microbially generated methane is depleted in ^{13}C (-110‰ to -50‰), whereas thermogenic methane is more enriched in ^{13}C (-50‰ to -20‰) (Whiticar, 1999). The $D/^{1}H$ ratio, or δD relative to the SMOW (standard mean ocean water) standard can be used to infer

the process of methane generation. δD values lower than -250‰ characterize methane originating from microbial acetate fermentation, whereas δD values in the range of -250‰ to -150‰ indicate methane originating from microbial CO_2 reduction (Whiticar et al., 1986).

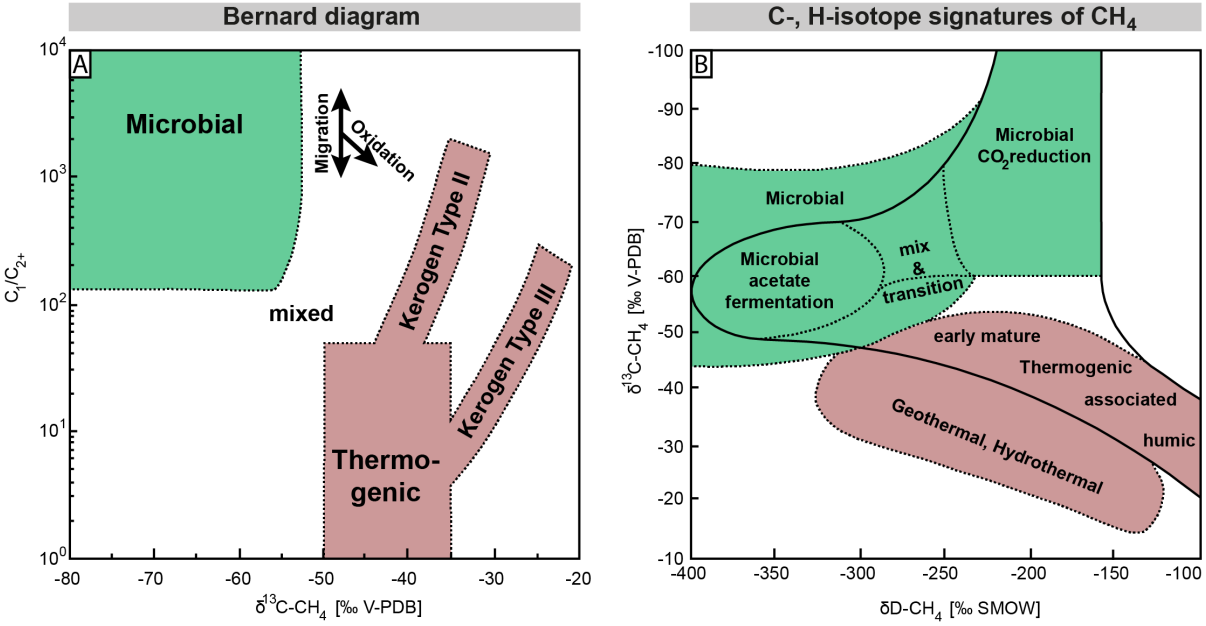

Fig. 1.1 A: Bernard diagram (modified after Whiticar, 1999) showing biogenic, thermogenic, and mixed origin of methane, which depend on the molecular and isotopic composition of carbon. B: Cross plot of carbon and hydrogen isotope signatures for the illustration of the classification of microbial and thermogenic methane (modified after Whiticar, 1999). V-PDB = Vienna Pee Dee Belemnite, SMOW = standard mean ocean water.

The driving factors for the transport of methane from depth towards shallower sediments depend on whether methane is in solution in the pore water or exists as free gas bubbles, and whether the dominant transport system is diffusive or focused (Ginsburg and Soloviev, 1997; Clennell et al., 2000). The flow of fluids is controlled by the pressure field in the sediments, as described by Darcy's Law (Eq. 1.1):

$$\frac{Q}{A} = -\frac{k}{\mu} grad(P) \qquad \textit{Eq. 1.1}$$

where Q is the volumetric flow per time, A is the sectional area, k is the intrinsic permeability, μ is the fluid's viscosity, and grad(P) is the gradient in excess fluid pressure. Advective and diffusive flows of dissolved methane are generally inefficient transport mechanisms over time and distance (Clennell et al., 2000). Advective flow is limited by the low concentration of methane in solution. In diffusive flow, the methane flux is controlled by the gradient of methane concentration in solution of the pore water. This gradient is generally small (Clennell et al., 2000). If the gas concentration is above solubility, buoyancy is the dominant force driving the gas bubbles towards the surface (Clennell et al., 2000). For example, methane density in 3-4 km water depth is in the order of 200-300 kg m^{-3} compared to a density of 1025 kg m^{-3} for seawater. The diffusive fluid flow is further controlled by the sediment permeability (Eq. 1.1), and sediment layers can act as permeability barriers or seals (Cartwright et al., 2007) for the rising fluids.

Focused flow of fluids and gas is more efficient in transporting methane towards shallower sediments. For upward fluid migration to occur, overpressure is required, which can be achieved through stress changes (disequilibrium compaction, tectonic stress) or changes in the pore fluid volume

due to temperature increase, the addition of fluids through fluid migration or generation of new fluids (such as water generation through mineral transformation of hydrocarbon generation) (Tacket and Puckette, 2012).

Overpressured gas and fluids can overcome the permeability barrier's resistance against capillary or fracture failure (Clayton and Hay, 1994). Favorable pathways for rising fluids are existing faults and fractures, and dipping permeable stratigraphic horizons (Stakes et al., 1999). Closed fractures may be reopened by the rising fluids, and periodic closing and reopening of fractures in response to pore pressure changes (e.g. driven by tidal changes or seismic activity) was also observed (Cartwright, 1994, Leifer et al., 2004). Polygonal fault systems may also act as migration pathways (Gay et al., 2007). Diapirism can create migration pathways by faulting, steepening and pushing up of sediments (Clennell et al., 2000).

1.1.2 Gas hydrates

Gas hydrates are ice-like, crystalline solid structures (clathrates) in which gas molecules (e.g. methane) are trapped within a host lattice consisting of water molecules (hence the term "hydrate"; Fig. 1.2). Therefore, gas hydrates do not have a fixed chemical composition and are stable without a direct chemical bonding. A minimum of 70% of the cages have to be filled in order for gas hydrates to be stable, and in naturally occurring hydrates around 95% of the cages are filled (Holder and Hand, 1982; Circone et al., 2005).

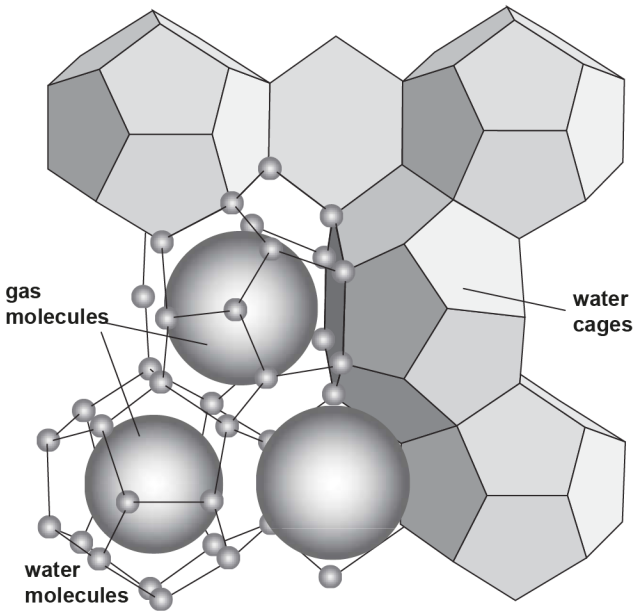

Fig. 1.2: Schematic of structure I gas hydrate (after Maslin et al., 2010). Guest molecules (e.g. methane) are trapped in cage structures formed by water molecules.

Three different structures of gas hydrates are commonly known, which differ in cage size and thereby both in the amount of water molecules and in the size of the hosted guest molecules (Sloan and Koh, 2007):

- Structure I: guest molecule diameters between 4.2 – 6 Å (e.g. methane, carbon dioxide, nitrogen)
- Structure II: guest molecule diameters between 6-7 Å (e.g. ethane, propane)
- Structure H: guest molecule diameters between 7-9 Å (e.g. metycyclohexane)

Since most natural gas hydrates consist of more than 99% of methane, structure I hydrates are the type of hydrates that is most commonly observed in marine sediments (Kvenvolden, 1995) and hence the term "methane hydrates" is commonly used to describe gas hydrates in the literature. Structure II hydrates are much less common, and structure H hydrates are extremely rare.

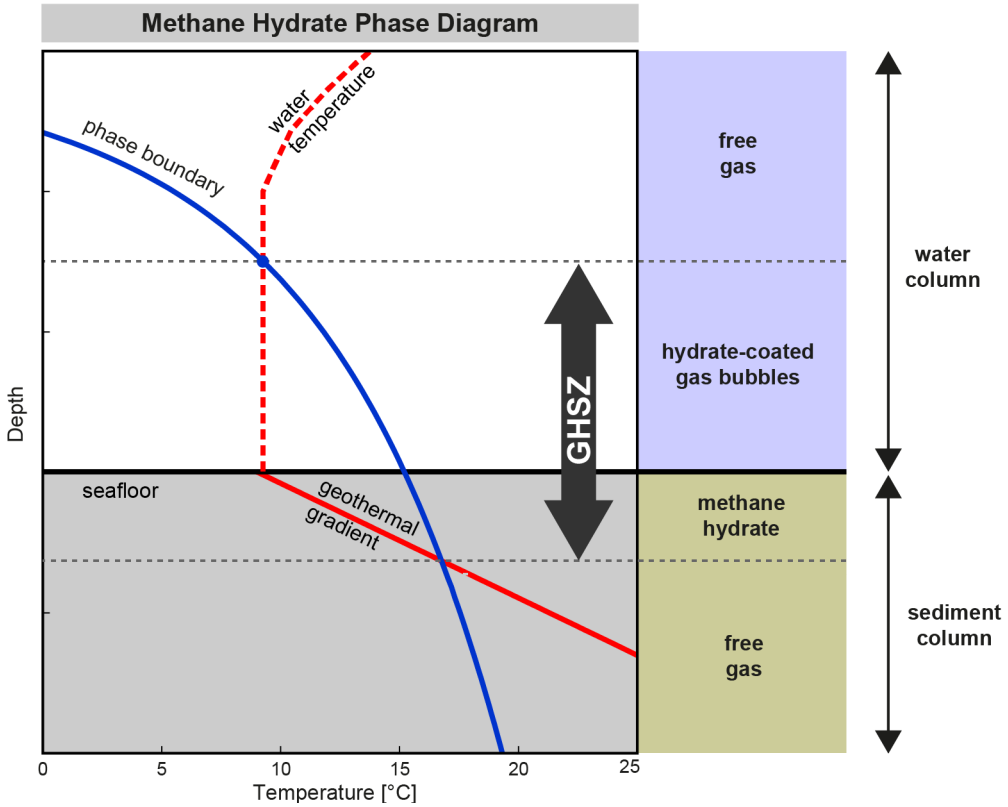

Fig. 1.3: Methane hydrate phase diagram illustrating the hydrate stability defined by temperature and pressure. The area of the gas hydrate stability zone is defined by the intersections of the temperature profiles with the phase boundary. Within the gas hydrate stability zone (GHSZ), hydrate forms around gas bubbles in the water column, or is generated within the pore space of sediments if sufficient supplies of gas and water are available.

The stability of gas hydrates is mainly controlled by pressure and temperature, assuming that sufficient supplies of gas and water are given (Fig. 1.3). In general, gas hydrates form in a high pressure and low temperature environment (Kvenvolden, 1995; Sloan and Koh, 2007). The stability of gas hydrates is further controlled by the presence of higher hydrocarbons and by the pore water salinity with higher hydrocarbons and lower salinity shifting the stability towards higher temperatures at a given pressure.

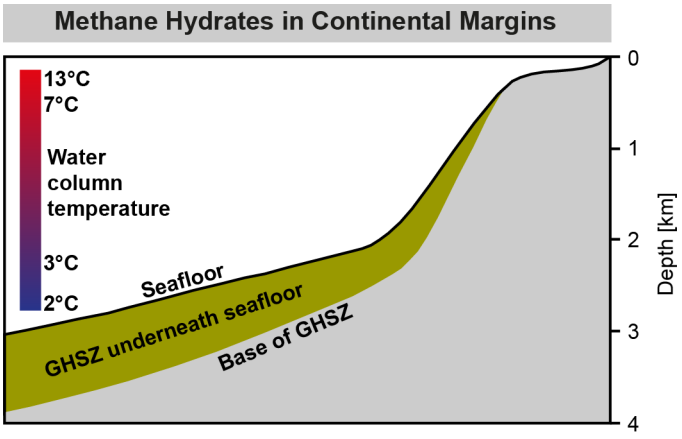

Fig. 1.4: Schematic of a continental margin and the inferred thickness of the GHSZ underneath the seafloor (after Bohrmann and Torres, 2006).

Due to their stability field, the occurrence and distribution of gas hydrates around the world is restricted to permafrost regions in Arctic areas and deep marine environments such as continental margins, as well as deep cold-water lakes such as Lake Baikal (Kvenvolden, 1988). In permafrost regions, e.g. Siberia (Makogon et al.,1972) and the Mackenzie Delta (Kvenvolden and Grantz, 1989), the top of the gas hydrate stability zone (GHSZ) typically occurs about 150–300 m below the surface, and the GHSZ can extend more than 500 m below the base of the permafrost (Kvenvolden, 1988). Offshore, gas hydrates can occur at water depths exceeding 300 m, with bottom water temperatures typically lower than 10 °C (Fig. 1.4 and Fig. 1.5; e.g. Kvenvolden, 1988; Bohrmann and Torres, 2006; Judd and Hovland, 2007; Ruppel, 2007; Sarkar et al., 2012).

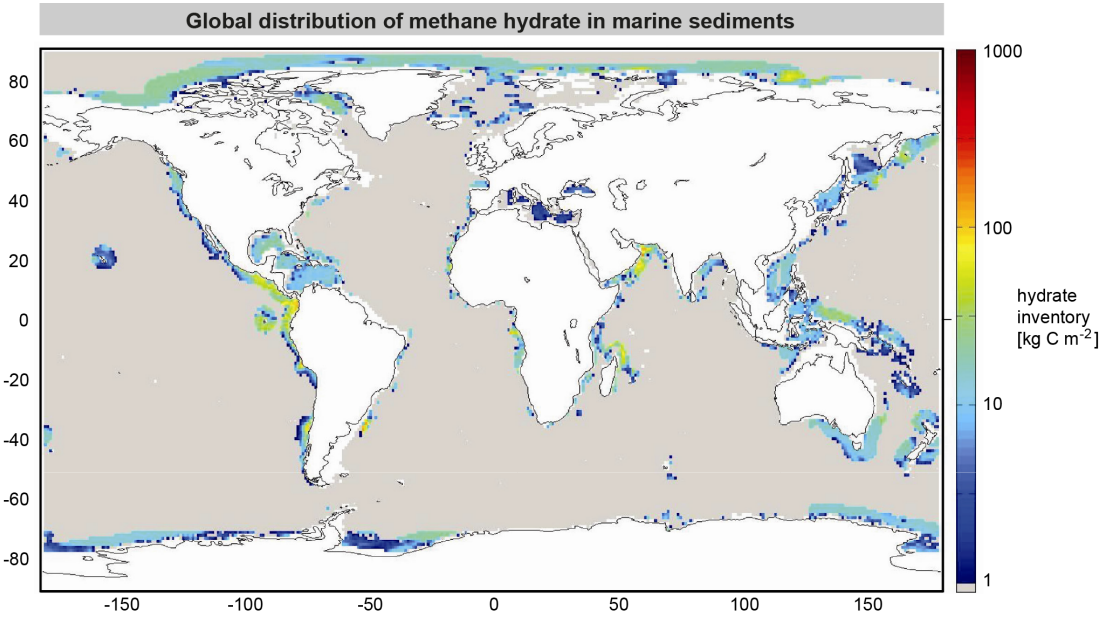

Fig. 1.5: Global distribution of methane hydrate in marine sediments (modified after Wallmann et al. (2012)). The global inventory of gas hydrates derived from these estimates is 455 Gt of C (Wallmann et al., 2012).

In offshore regions, the lower boundary of the GHSZ is limited by the temperature and thereby the temperature gradient in the sedimentary column. Since the pore pressure controlling the hydrate stability is hydrostatic (Hart et al., 1995), the BGHSZ typically follows the isotherms in an equilibrated environment (Kvenvolden and Lorenson, 2001). Locally increased heatflow (e.g. through fluid migration) leads to a shoaling of the BGHSZ, whereas a cooling of the sediments (e.g. through topographic effects) leads to a downshift of the BGHSZ (e.g. Chen et al., 2014; Chi et al., 2014).

1.1.3 Cold seep systems

Cold seeps define seafloor sites where fluids such as hydrocarbon gases, oil, or gas-rich pore waters rise from deeper strata to the shallow subsurface and eventually escape into the water column. Most seep sites are dominated by methane (Judd, 2003; Bohrmann and Torres, 2006). Cold seeps consist of four main structural elements: one or more fluid sources, upward migration pathways, a plumbing system, and seafloor venting structures (Klaucke et al., 2006; Talukder, 2012; Koch et al., 2015; Luo et al., 2016). Studies showed that some mud volcanoes are sourced by fluids trapped in oceanic crusts older than 140 Ma (Hensen et al., 2015). In some places, seeps can indicate active deep petroleum systems, but the relationship between seafloor seepage and deep reservoirs, and in particular the migration of free gas through the GHSZ, can be complex (Talukder, 2012).

Multiple studies described cold seeps in many different geological settings at active (e.g. Stakes et al., 1999; Klaucke et al., 2008; Greinert et al., 2010) and passive continental margins (e.g. Sahling et al., 2008) around the world. Cold seeps appear to be preferentially located on topographic highs such as accretionary ridges or erosional ridges (e.g. Crutchley et al., 2010; Klaucke et al., 2010) or atop subsurface highs such as diapirs or local highs of the bottom simulating reflector (BSR; e.g. Crutchley et al., 2014). This distribution suggests that cold seep locations are controlled by local subsurface traps just like conventional hydrocarbon reservoirs. Fluid migration to the surface is either structurally or stratigraphically controlled, but can also be controlled by a combination of both mechanisms (Krabbenhoeft et al., 2013).

At numerous seep sites gas escape into the water column has been observed, even within the GHSZ (e.g. Suess et al., 1999; Klaucke et al., 2006, 2012; Greinert et al., 2010; Römer et al., 2012). Hydroacoustic flares indicating escaping gas bubbles have been observed to rise up to 1300 m from the seabed (Greinert et al., 2006). The surface expressions of seeps are typically associated with a rough topography due to the precipitation of authigenic carbonates (e.g. Klaucke et al., 2012; Dumke et al., 2014), doming structures due to gas hydrate formation (pingoes; Hovland and Svensen, 2006; Paull et al., 2008) or gas overpressure (Koch et al., 2015), mud volcanism (Bohrmann et al., 2003) or seafloor depressions (pockmarks; Judd and Hovland, 2007; Riboulot et al., 2016). These structures can reach diameters of up to several 100 m and heights of several tens of meters (Hovland and Judd, 1988).

Anaerobic oxidation of methane (AOM) and the coupled sulfate depletion in the sulfate-methane transition zone (SMTZ) is observed at all cold seep sites (Boetius et al., 2000). AOM is performed by microbial communities and is an efficient sink for seeping methane (Hinrichs and Boetius, 2002), thereby affecting the amount of methane which is released into the water column. The analysis of these pore water profiles at active seep sites and comparison with background profiles provides insight into the processes involved at local seep sites, such as origin, quantification, and transport mechanisms of methane (e.g. Haeckel et al., 2004, 2007; Bhatnagar et al., 2008; Regnier et al., 2011; Koch et al., 2016).

AOM occurs in conjunction with sulfate reduction:

$$CH_4 + SO_4^{2-} \rightarrow HS^- + HCO_3^- + H_2O \qquad \text{Eq. 1.2}$$

Over time, AOM leads to the precipitation of carbonates. Authigenic carbonates at active seep sites can grow up to several tens of meters into the water column (Teichert et al., 2003; Dumke et al., 2014).

1.2 Gas hydrates as an energy resource

Gas hydrates occur in various types in the marine environment, and not all of these types of occurrence represent a resource potential for the production of free gas:

1. **Massive units of solid gas hydrates**, which occur primarily at or near the seafloor. These gas hydrates are often observed near vent sites and are described as hydrate mounds. Although rather easily to detect through hydroacoustic surveys, these gas hydrate mounds are considered irrelevant as an energy resource as they are generally very small in size and are unsuitable for gas production with existing technologies (Boswell et al., 2012).
2. **Grain-displacing gas hydrates** in the form of solid nodules disseminated within fine-grained sediments, filling fractures or veins (Park et al., 2008), where the gas hydrate saturation can reach up to 40 % (Lee and Collett, 2009). In this case, gas production is not favorable because of the geomechanical instabilities in such systems (Moridis et al., 2013).
3. **Pore-occupying gas hydrates** in coarse-grained and fine-grained sediments. Hydrate saturation increases with grain size (Boswell et al., 2012). Field expeditions have shown that in fine-grained sediments, pore-filling gas hydrate saturations are generally in the order of 10 % or less, but can reach up to 90 % in coarse-grained silts and sands (Park et al., 2008; Tsuji et al., 2009; Moridis et al., 2011; Boswell et al., 2012).

Therefore, sandy gas hydrate reservoirs with potentially very high saturations are in the focus of research in terms of potential gas production from hydrates. The high permeability of the sediments initially allows the fluids and gas to migrate and to form gas hydrate accumulations within the pore space with high resource concentration (Moridis et al., 2011). In terms of production, high permeability allows the spreading of pressure and temperature from a fixed wellbore into the gas hydrate bearing reservoir, as well as the creation of migration pathways for the released gas towards the well (Boswell et al., 2009; Moridis et al., 2011).

Gas-hydrate-bearing sands with promising reservoir conditions have been studied in detail over the past two decades. These reservoirs are located, e.g., in the Nankai Trough, Japan (Tsuji et al., 2009; Fujii et al., 2015;), in the Gulf of Mexico (Collett et al., 2005; Boswell et al., 2012), offshore India (Collett et al., 2008), offshore Korea (Park et al., 2008), and in permafrost regions in Alaska (Collett, 1993) and Canada (Dallimore et al., 1999).

1.2.1 Production methods

To produce gas out of hydrates, new technologies had to be developed as conventional oil and gas recovery technologies are not applicable to gas hydrates, due to their solid phase structure (Lee and Holder, 2001). At present, four production methods exist (three of them illustrated in Fig. 1.6), all of which are based on the dissociation of gas hydrates through disturbance of their thermodynamic conditions (Makogon, 1997; Lee and Holder, 2001):

1. **Thermal stimulation**: Temperature T is raised above the hydration temperature at the prevailing pressure p
2. **Depressurization**: Lowering the pressure p to a level lower than the hydration pressure at the prevailing temperature T
3. **Chemical stimulation**: Use of inhibitors (i.e. salts, alcohols) to shift the p/T equilibrium
4. **CH_4/CO_2 exchange**: Methane exchange with another hydrate-forming gas such as CO_2, H_2S, N_2 or O_2, with the greenhouse gas CO_2 being preferred in most applications (Sloan and Koh, 2007; Lee et al., 2013).

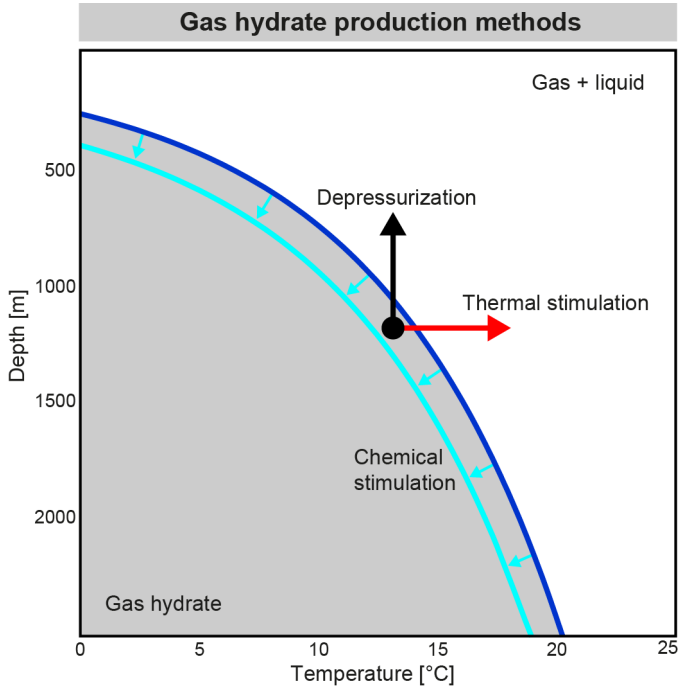

Fig. 1.6: Illustration of three different methods which aim at the dissociation of gas hydrates through disturbance of their thermodynamic conditions: thermal stimulation (heating), depressurization, and chemical stimulation.

Thermal stimulation

The concept of the thermal stimulation method is based on the in situ heating of gas hydrates until they start to dissociate. Heating is realized by the injection of hot water or brine through a wellbore into the gas hydrate reservoir.

The method was tested successfully in the Mackenzie Delta (Canada) in 2002, using hot-water circulation. However, during five days of production, only 468 m^3 of methane were produced (Hancock

et al., 2005). While this test demonstrated that it is possible to produce gas out of gas hydrate reservoirs, the results also showed that thermal stimulation is not economical and therefore unattractive for gas hydrate production. A major economic problem is the waste of heat, as it is mostly water which is heated in the process, due to the nature of hydrate (1 volume of gas hydrate contains around 0.87 volumes of water) (Moridis et al., 2011).

Depressurization

The method involves drilling a vertical production well into the gas hydrate reservoir, and pressure reduction by pumping along the entire reservoir interval. (Fig. 1.7). Pressure reduction forces hydrate dissociation, which gradually spreads out from the well into the surrounding hydrate reservoir (Moridis et al., 2011). The high permeability of the sandy reservoir results in a steady stream of free gas and free water towards the well (Moridis et al., 2011). Therefore, the production of gas out of gas hydrates needs to take the steady co-production of water into account.

Typically, the pore pressure around the well is reduced to a specific target pressure, e.g. 2.7 MPa at Walker Ridge (Myshakin et al., 2012) and 3 MPa at Nankai (Yamamoto et al., 2014). In 1500 m water depth, this pressure reduction is comparable to a sea level fall of 1200 m. The sediment volume affected by pressure reduction is expected to remain relatively limited to the vicinity of the well location, i.e., 100 m around the well (Kvalstad et al., 2011; Konno et al., 2017).

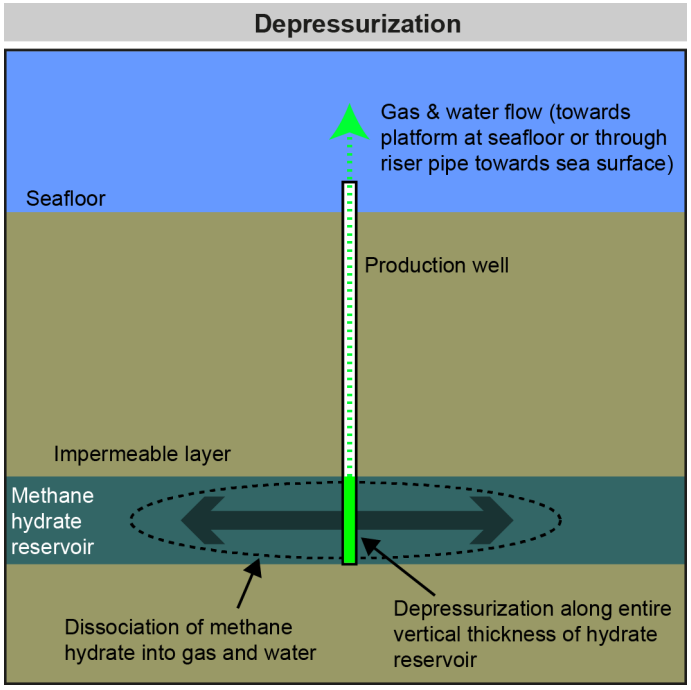

Fig. 1.7: Schematic of the depressurization method applied in a marine environment. A methane hydrate reservoir located in high-permeable sediments (dark green) is depressurized along a vertical drillhole (bright green area), and the gas hydrate dissociates from the well into the reservoir (dashed line). The gas flows through the well towards the production infrastructure (dashed green arrow).

Currently, depressurization is considered the most effective and most economical production method for gas hydrates (Zhao et al., 2013). The depressurization method was first tested successfully in the Mackenzie Delta (Canada) in 2007-2008, and unlike the thermal stimulation production test conducted five years earlier in the same area, the test revealed that depressurization is a promising gas

hydrate production method (Dallimore et al., 2012). During six days of production, about 13,000 m^3 of methane were produced (Yamamoto and Dallimore, 2013). In 2013, the world's first offshore production test using the depressurization method was conducted in the Nankai Trough off Japan (Yamamoto et al., 2014). 119,500 m^3 of gas volume were produced continuously over six days until abrupt sand production stopped the test. These tests demonstrated the applicability of the depressurization method as a methane hydrate production technology without thermal energy input.

Chemical stimulation

The chemical stimulation is based on chemical inhibitors which are injected into the reservoir. These inhibitors change the hydrate equilibrium conditions, thereby destabilizing hydrate in natural conditions (Chong et al., 2016). Thermodynamic inhibitors are, e.g., methanol and ethylene glycol (Dong et al., 2009). Kinetical inhibitors slow down the formation of hydrate. Recent research identified that NaCl is both a thermodynamic inhibitor and a kinetic inhibitor (Mekala et al., 2014).

On an economical scale, chemical stimulation is not feasible on a reservoir scale, because the ratio of inhibitor to hydrate is significantly high (Moridis et al., 2011; Chong et al., 2016). Currently, it is discussed if chemical stimulation can increase the effectiveness of both the depressurization and thermal stimulation by lowering the heat of dissociation (Chong et al., 2016).

CH_4/CO_2 exchange

The CH_4/CO_2 exchange method is based on the hydrate kinetics, because CO_2 hydrate is more stable at low temperatures (<10 °C) compared to CH_4 hydrate (Chong et al., 2016). CO_2 has a molecular diameter of 5.12 Å (slightly larger compared to the molecular diameter of 4.36 Å of CH_4), and forms as well hydrates of structure 1 (Sloan and Koh, 2007). The exothermic formation of CO_2 hydrate thereby releases more heat (57.98 kJ mol^{-1}) than is required for the endothermic dissociation of CH_4 (Goel, 2006).

In an ideal scenario, the CH_4/CO_2 exchange method becomes carbon neutral. Further advantages are that sediment strengths in the reservoir are maintained due to the solid CO_2 hydrate generation, which also consumes the released water of the CH_4 dissociation. The storage of CO_2 in solid form further reduces the mobility of the greenhouse gas, which is a further advantage compared to current sequestering methods where CO_2 is stored in liquid or gaseous forms (Chong et al., 2016).

The CH_4/CO_2 exchange method has so far not been tested in a field test, and many challenges have to be solved. These challenges are a more deeper understanding of the kinetics regarding the transport of heat and mass (especially of the released water), the interplay between CH4 hydrate dissociation and CO2 hydrate formation, the role of permeability and sediment properties, and the calculation of models for optimal well placements and production strategies (Chong et al., 2016).

1.3 Marine geohazards related to gas hydrate production

One of the most important offshore geohazards is submarine slope failure (Vanneste et al., 2014). Sediment failure occurs when shear stress (e.g. the gravitational downslope force) exceeds shear strength (resisting forces) (Fig. 1.8A). In geomechanics, the stability of a slope is defined by the factor of safety (FoS), which is defined as resisting forces against driving forces. Therefore, theoretically a slope with a FoS of less than 1.0 is prone to fail. Failure can occur along a planar surface (more typical in sandy soils) or along a curved surface along with rotation of the failure mass around a virtual point above the slope (typical in clayey soils) (Fig. 1.8B; Abramson et al., 2002). After failure occurred, the slope often features a steep scarp, which can retreat further upslope if retrogressive failures affect the area upslope of the scarp (Kvalstad, 2007).

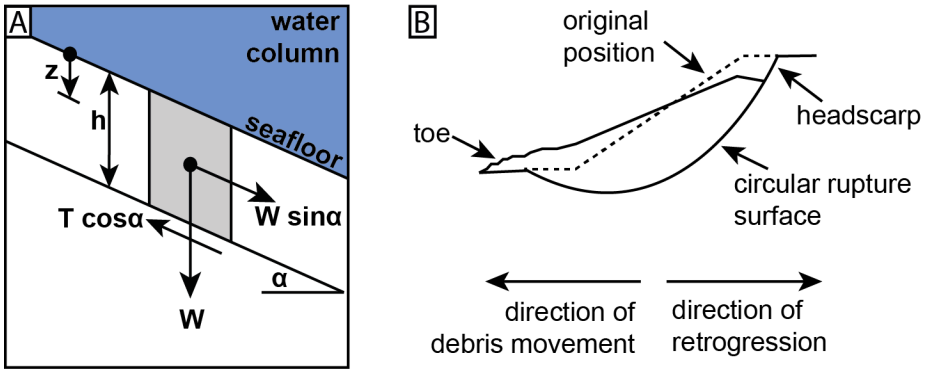

Fig. 1.8 A: Schematic of the forces acting on a slice (grey) in a submarine infinite slope. T cos α = shear resistance of sediment, W sin α = gravitational shear stress acting in the direction of potential movement, W = vertical component of body force of the slice, z = sub seafloor depth, h = height of the slice, α = slope angle. Modified after Hampton et al. (1996). B: Illustration of a circular mass failure on a clayey slope, modified after Abramson et al. (2002)

To determine of the stability of a given slope, the slip zone with the least FoS under static conditions is calculated. Because of uncertainties due to simplified modeling and parameter uncertainties, a FoS of 1.5 is generally used to define a stable slope, but this depends on the infrastructure at risk as well as local standards and guidelines (e.g. CEN, 2004). Pseudo-static models are additionally applied to simulate seismic effects. Under pseudo-static condition, a minimum FoS of 1.1 is generally required. Note that typically a full dynamic site response analysis requiring a reliable time history is preferred over pseudo-static models. Geomechanical models and slope stability analyses require knowledge of the slope geometry, subsurface geology, soil strength parameters, and unit weights.

Areas with steep slopes, e.g. in submarine channels and canyons, are more susceptible to slope failure than the surrounding areas (Kvalstad, 2007). Instable slopes may cause sliding or slumping of the seafloor sediments, and even on gently dipping slopes mobilized mass can travel over large distances during a landslide. The area between the instable slope and the run-out line is defined as “hazard lands” and represent the area characterized by a FoS of less than 1.5 against being affected by slope failure (Abramson et al., 2002).

Seabed failures can be triggered by both natural causes and human interferences such as oversteepening of the slope, uneven deposition or erosion, increase of shear stress (loading, lateral pressure), reduction of shear strength, and seismic events (lateral and vertical ground shaking due to earthquakes). Slope stability assessments are generally based on a conservative scenario, i.e., the

worst-case scenario which is often associated with an earthquake (Abramson et al., 2002). The transported mass of a submarine landslide can affect seabed installations in many ways including loss of foundation area, destruction of facilities by debris impact, partial or total burial of seabed facilities, and even generation of tsunamis affecting not only seabed installations but entire coastal communities over potentially large areas (Kvalstad, 2007).

So far, it remains unclear whether natural gas hydrate dynamics have triggered slope failures. If gas hydrates that are hosted in a sediment matrix dissociate into free gas and excess pore water, the geomechanical stability of the host sediment may be significantly reduced (Collett et al., 2015). However, a review of landslide inventories carried out by Urlaub et al. (2013) did not find evidence for a large-scale triggering of landslides due to gas hydrate dissociation caused by the glacial-interglacial pressure and temperature changes. Nevertheless, gas hydrate dissociation may be considered as a preconditioning mechanism instead of an actual trigger for certain submarine landslides (Crutchley et al., 2016). There is also evidence that some submarine landslides have developed differently in areas with hydrate than in hydrate-free areas (Micallef et al., 2009).

Gas hydrate production campaigns, as already pointed out in chapter 1.2, are focused on potential reservoirs in high-permeable sediments such as those encountered in paleo deep-sea fans along continental margins. Therefore, certain mitigation measures against potential slope failures have to be taken into account in the planning of gas hydrate production in areas that may be at risk of slope failure. However, there is a lack of experience regarding geohazards associated with gas hydrate exploitation, and therefore more research has to be taken out at the individual production sites in order to understand the complexity of these geohazards (Collett et al., 2015).

1.3.1 Reservoir compaction and seabed subsidence

The stress regime in marine sediments is defined as

$$\sigma_n = \sigma_{eff} + \mu \qquad \textit{Eq. 1.3}$$

where σ_n is the normal stress, σ_{eff} is the effective stress of the sediment matrix and μ is the pore pressure. Gas hydrate production through depressurization in the reservoir causes a pore pressure depletion, which immediately leads to an increase in effective stress. The geomechanical response to the stress changes in the reservoir is reservoir compaction (Fig. 1.9; Moridis et al., 2011). Simulations showed that the radial displacement are smaller than the vertical displacements, with the latter being largest in the direct vicinity of the wellbore and close to zero underneath the well (Zhou et al., 2014). Due to the high porosity and poor consolidation, marine sands such as those encountered in potential gas hydrate reservoirs may be prone to formation failure due to pore collapse and rearrangement of inelastic grains (Moridis et al., 2011).

A compacting reservoir may lead to subsidence at the seafloor (Fig. 1.9; Fjaer et al., 2008; Kim et al., 2014). The factors controlling the subsidence are the pressure depletion in the reservoir, the thickness of reservoir and overburden, and the stiffness of the overburden. In permafrost regions, e.g., the subsidence is rather low due to the stiff soils (Rutquist et al., 2009).

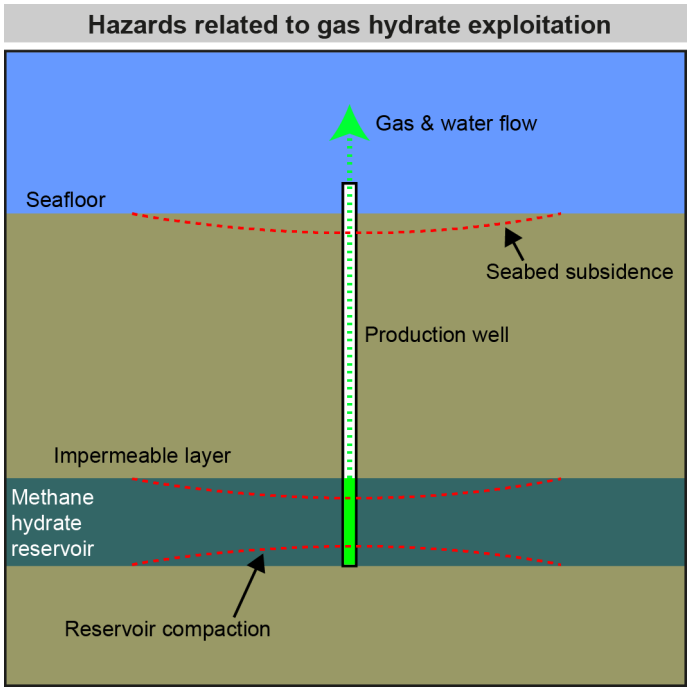

Fig. 1.9: Illustration of the hazard of reservoir compaction and seafloor subsidence related to the depressurization method of gas hydrate exploitation.

Seafloor subsidence, although likely occurring uniformly over a large distance from the well (Rutquist et al., 2009), has to be taken into account as a potential hazard for the overlying production infrastructure at the seabed. Furthermore, when the production area is located in a sloping seabed environment, subsidence may change the stress/strength equilibrium of the slope, potentially lowering the FoS against slope failure (Fig. 1.10).

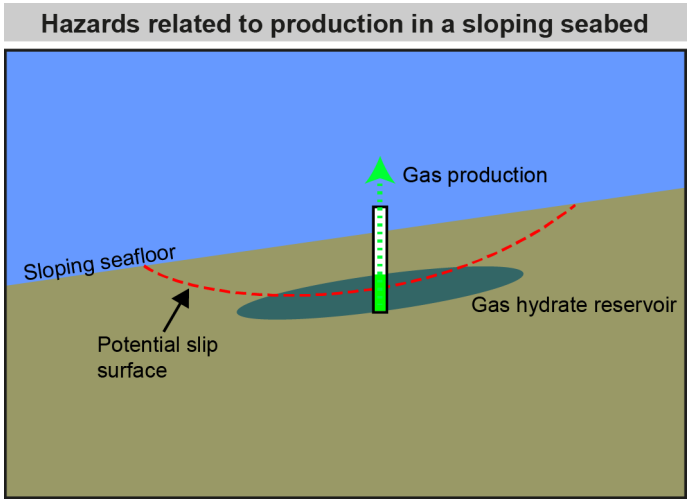

Fig. 1.10: Schematic of a production site in a sloping seabed environment, illustrating the hazard of an interaction between a gas hydrate reservoir, which may compact due to pore pressure depletion, thereby changing the stress/strength equilibrium along the potential slip surface with the lowest FoS (Factor of Safety).

1.3.2 Sand production

If shear failure in the reservoir sands occurs, solid particles can flow towards the wellbore and are co-produced as well, besides gas and water. As a result, cavities may be generated around the wellbore (Moridis et al., 2011). Sand production abruptly occurred during the 2007 onshore production test in the Mackenzie Delta (Canada) and led to an abortion of the test. The installation of a sand screen into the wellbore in 2008, however, allowed continuous gas production over a period of six days (Yamamoto and Dallimore, 2008). During the 2013 production test in the Nankai Trough (Japan), sand production occurred as well after six days, ending the production test (Konno et al., 2017).

1.4 Gas and gas hydrate manifestations in geophysical data

1.4.1 Gas signatures

Shallow free gas accumulations are often easy to identify in high-resolution seismic data. The presence of gas causes a strong decrease in seismic velocity, which results in a negative impedance contrast. Gas concentrations as low as 0.5 % of the sediment pore space already decrease the acoustic impedance of sediment significantly (Judd and Hovland, 2007), especially in unconsolidated sand/shale sequences (Cooper and Hart, 2003). Studies showed that the largest velocity drop already occurs at gas concentrations of less than 4% (Fig. 1.11; Andreassen et al., 2007). Therefore, seismic methods alone are not sensitive enough to detect variations in gas concentrations.

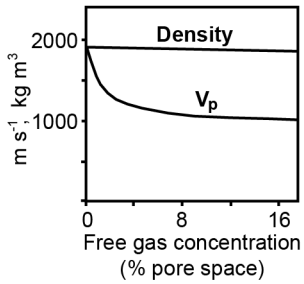

Fig. 1.11: P-wave velocity and bulk density calculated as a function of gas saturation for sediments with porosity of 0.4 and V_p = 1900 m s^{-1} (after Andreassen et al., 2007).

Gas bubbles in the sediments produce a variety of seismic anomalies, which largely depend on the acoustic frequency and the size of the bubbles. Typical anomalies are bright spots, which are high-amplitude reflections at the interface between a gas-free zone and an underlying gas-bearing zone. They are caused by the strong negative impedance contrast and are typically characterized by a phase reversal (Judd and Hovland, 1992; Løseth et al., 2009). The low-velocity regions frequently result in pull-down effects of the entire underlying strata (Løseth et al., 2009). Often, low-frequency events are observed underneath a bright spot, because high-frequency components of the seismic energy are absorbed by the gas bubbles (Geletti and Busetti, 2011). In sediment echosounder data, the acoustic energy is scattered at the gas bubbles, and these effects of acoustic turbidity often lead to a complete washout or blanking of the stratigraphic events underneath (Judd and Hovland, 1992; Klaucke et al., 2006).

Vertical migration pathways of focused flow of gas or gas-bearing fluids are generally described as chimneys or pipes in seismic data (Cartwright et al., 2007; Løseth et al., 2009). These vertical pathways can exceed diameters of a few kilometers (Løseth et al., 2009) and are often characterized by scattered low amplitudes caused by the attenuation of the acoustic signal (Hovland and Judd, 1988). At the margins of gas chimneys and pipes, a reflection pull-up is often observed (Hustoft et al., 2007; Westbrook et al., 2008; Plaza-Faverola et al., 2011). This effect is caused by higher seismic velocities associated with the formation of gas hydrates or carbonates at the chimney walls.

1.4.2 Bottom-simulating reflector

A common indicator for the presence of gas hydrates along continental slopes is the bottom-simulating reflector (BSR) in reflection seismic data. Its name derives from its typical behavior of mimicking the seafloor topography, running along isotherms and thereby cutting across stratigraphic reflections, typically with opposite polarity compared to the seafloor reflection (Fig. 1.12A, B; Hyndman and Davies, 1992). BSRs were first identified in the 1970s at Blake Ridge (Shipley et al., 1979). The BSR is caused by the negative impedance contrast between high-velocity gas-hydrate-bearing sediments above and low-velocity gas-bearing sediments below (Hyndman and Davies, 1992). Therefore, the cause of a BSR is not necessarily the presence of gas hydrates, but the presence of free gas underneath, which causes a strong decrease in seismic velocity (Paull et al., 1996). Moreover, the absence of a BSR does not preclude the presence of gas hydrates, as hydrates have also been observed in areas where a BSR is absent (Mathews and von Huene, 1985; Haacke et al., 2007). On many occasions, the BSR is patchy and discontinuous (Fig. 1.12C). Hillman et al. (2017) argued that all BSRs are discontinuous in nature, and the appearance in seismic data depends largely on the resolution of the imaging tools. Gas is also more likely trapped in highly permeable sediment layers (e.g. sands and silts) bounded by impermeable layers (Judd and Hovland, 2007), which explains the patchy appearance of a BSR in many areas. Studies showed that free-gas concentrations of only a few percent of the pore volume below the hydrate-bearing zone are sufficient to create a distinct BSR (Andreassen et al., 2007; Haacke et al., 2007; Judd and Hovland, 2007).

The BSR alone is not a sufficient indicator for the presence of gas hydrates, as it only indicates the presence of free gas accumulations underneath the BGHSZ. If large amounts of gas hydrate are present in the pore space, they cause a positive impedance contrast in seismic data due to their high seismic velocity. The positive impedance contrast results in high amplitude anomalies and a relatively high interval velocity.

The BSR is often used to derive information about the thermal state at its location, including the local and regional heat flow as well as thermal anomalies. Thermal anomalies indicate that a BSR is out of equilibrium, e.g. due to higher or lower temperatures and fluid flow (Davies et al., 1990; Hyndman et al., 1992; Grevemeyer and Villinger, 2001; Wood et al., 2002).

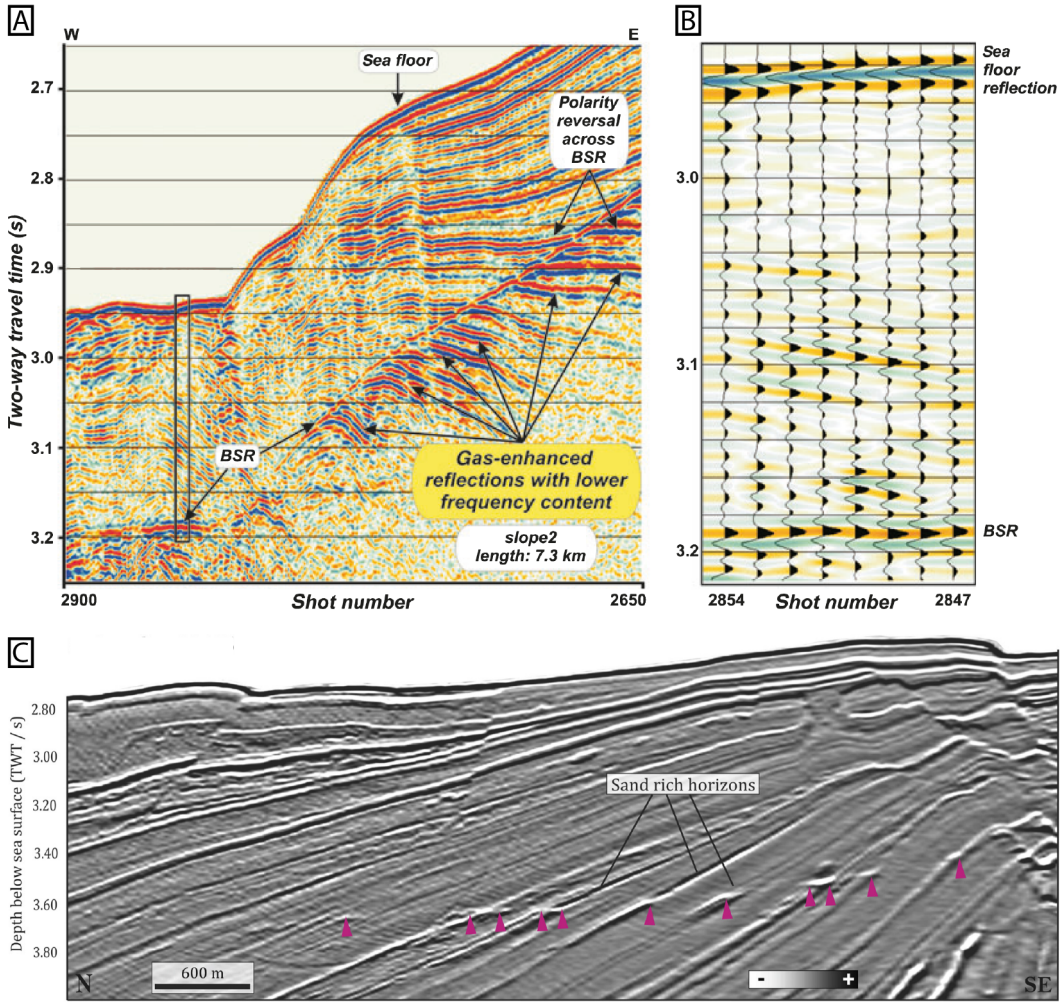

Fig. 1.12 A: Seismic reflection profile illustrating the BSR running sub-parallel to the seafloor offshore Svalbard. B: Wiggle trace display from the area marked with the black box in A. Note the high reflectivity and reversed polarity of the BSR compared to the seafloor. A and B modified after Vanneste et al. (2005). C: Example for a patchy and discontinuous BSR (pink triangles) in conventional 3D seismic data. The BSR signal is strong along permeable sand-rich horizons. Adapted from Hillman et al. (2017).

1.4.3 Gas hydrate identification workflow

The hydrocarbon industry with focus on gas hydrates distinguishes between the terms *hydrate stability zone* (where gas hydrates are theoretically stable), *hydrate bearing zone* (zones of high permeability above the BGHSZ, which theoretically yield a good reservoir potential), and *hydrate concentrated zone* (Fig. 1.13). The hydrate concentrated zone can be identified in seismic data with the following indicators as proposed by Saeki et al. (2008):

- Presence of a BSR
- Zone of turbidity above the BGHSZ (such as those encountered in paleo-channel systems)
- Positive high-amplitude reflections within the turbidity zones
- Relatively higher interval velocities compared to the surrounding

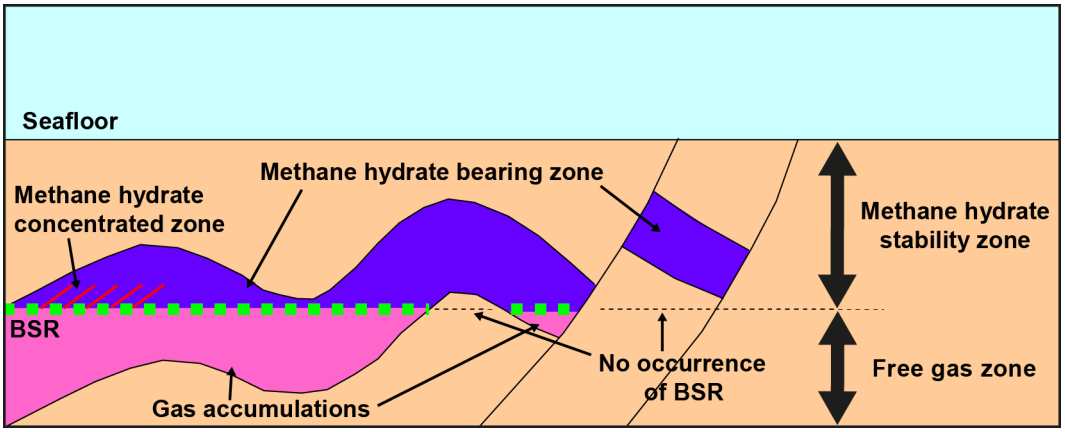

Fig. 1.13: Illustration of the relationship between "gas hydrate stability zone", "gas hydrate bearing zone", and "gas hydrate concentrated zone" as defined by the hydrocarbon industry, modified after Saeki et al. (2008). Where free gas is present at the BGHSZ, a BSR can occur. Gas hydrate bearing zones within the stability zone can exist where a BSR is absent. Methane hydrate concentrated zones occur most likely close to the BSR in sediments with high permeability.

Additional information on the distribution of gas hydrates can be gained through the analysis of S-wave velocities. S-waves have lower frequencies than P-waves and also travel much slower, resulting in a higher resolution of the subsurface. As S-waves can only propagate through solid media, free gas accumulations as well as the BSR cannot be imaged. However, it is possible to estimate the thickness of a zone hosting gas hydrates via the P-to-S ratio (Dannowski et al., 2017). The gas hydrate concentration cannot be estimated using this method (Dannowski et al., 2017). S-wave studies require multicomponent seismometers installed at the seafloor, which can be deployed as part of seismic surveys. Because the seismic signal is produced by an airgun towed behind a vessel and S-waves cannot travel through the water column, the seismometers record transformed S-waves, i.e. P-waves converted to S-waves at sediment interfaces.

1.4.4 Multiple BSRs

The formation of two or more overlying BSRs, which are typically spaced apart by a few tens of meters is not well understood. In most studies, the shallowest BSR is considered as the seismic manifestation of the BGHSZ. The additional BSRs are usually weaker in amplitude and can occur with normal or reversed polarity. The presence of two or more BSRs at a specific location allows drawing multiple conclusions related to their origin. A general explanation does not exist and multiple BSRs are therefore considered as local features that require individual explanations regarding their origin:

- **Gas composition**: Additional BSRs may reflect active lower boundaries of the GHSZ for structure II hydrates containing higher hydrocarbons that result in a lowering of the BGHSZ. Tinivella and Giustiniani (2013) considered that if the thickness of the layer between two BSRs is "very high" (i.e., more than 200 m in shallow waters), it is more likely that the BSRs are caused by different gas compositions. Double BSRs caused by different gas compositions were suggested for, e.g., off the coast of the Antarctica (Geletti and Busetti, 2011) and offshore western Norway (Andreassen et al., 2000).

- **Thickness of the free gas zone underneath the BSR**: Tinivella and Guistiniani (2013) suggested that the second BSR, which was observed by Foucher et al. (2002) at the Nankai slope and has a positive polarity, might reflect the bottom of the free gas zone.
- **Thickness of the gas hydrate-bearing zone**: A second shallower BSR with positive reflectivity was observed by Posewang and Mienert (1999) offshore Norway and interpreted as a reflection of the top of the hydrate-bearing layer. The thickness of the gas hydrate-bearing zone could therefore be derived from the distance between the two overlying BSRs, assuming that the lower BSR reflects the BGHSZ.
- **Pressure distribution in the subsurface**: Tinivella and Giustiniani (2013) suggested that overpressure conditions below the theoretical BSR depth have to be taken into account in order to understand double BSRs. The authors differentiated between hydrostatic BSRs and overpressure BSRs and discussed that anomalous pore pressures might also explain the often observed mismatch between the theoretical BGHSZ and the seismic BSR depth. In addition, free gas columns existing below hydrate provinces in basin settings can also cause critical pore pressures (Hornbach et al., 2004).
- **Paleo stability conditions**: Some double BSRs are not related to current equilibrium features, but may indicate a downward or upward shift of the BGHSZ. Downward shifting of the BGHSZ due to sediment erosion and preservation of the former BSR was reported from the Nankai Trough, Japan (Bangs et al., 2010). Upward shifting of the BGHSZ due to rapid sedimentation, resulting in a remaining paleo-BSR was reported from the Yaquina forearc basin, Peru (Netzeband et al., 2005), offshore Mauritania (Davies et al., 2012), and offshore mid-Norway (Plaza-Faverola et al., 2012). Tectonic uplift as the driver for a rapid shoaling of the GHSZ can also cause the preservation of a paleo-BSR, which has been suggested for the Nankai slope, Japan (Foucher et al., 2002). Remnant BSRs related to sealevel variations (e.g. the rise after the last glacial maximum) were reported for Hydrate Ridge, Oregon (Bangs et al., 2005).
- **BSRs that are unrelated to gas or gas hydrates** can be caused by the diagenesis of siliceous sediments from Opal A to Opal CT, by the smectite-illite conversion, or by authigenic carbonates within the sediments, as suggested by Berndt et al. (2005) for the mid-Norwegian margin.

1.4.5 Seep detection

The detection of seep sites can occur through direct or indirect investigation methods. Active cold seep sites that show gas bubble streams rising from the seafloor can be observed directly through video operations, e.g. cameras installed on a remotely operated vehicle (ROV; Römer et al., 2012, 2014), or deep-towed cameras behind the vessel (OFOS, Greinert et al., 2010). In hydroacoustic data, gas bubbles are indicated by strong acoustic returns (so-called flares) in the water column, which are caused by the high acoustic impedance contrast between the water and free gas (Judd and Hovland, 1992; Greinert et al., 2006; Naudts et al., 2008). These flares can be detected by multibeam or sediment echosounder systems (Fig. 1.14B, C; Naudts et al., 2006; Greinert et al., 2010; Römer et al., 2012, 2014), as well as by sidescan sonar systems (Fig. 1.14A; Klaucke et al., 2006, Dupré et al., 2010).

The detection of seep sites that are characterized by distinct morphological features such as pockmarks, mud volcanoes, and carbonate build-ups, is often possible through bathymetric surveys (Fig. 1.14D; Bohrmann et al., 2003; Dupré et al., 2010, 2015; Riboulot et al, 2016). Seep sites with authigenic carbonate precipitates at the seafloor often lead to an increased backscatter intensity in sidescan sonar data (Fig. 1.14A), which allows the detection of these sites (Klaucke et al., 2006, 2016; Dumke et al., 2014).

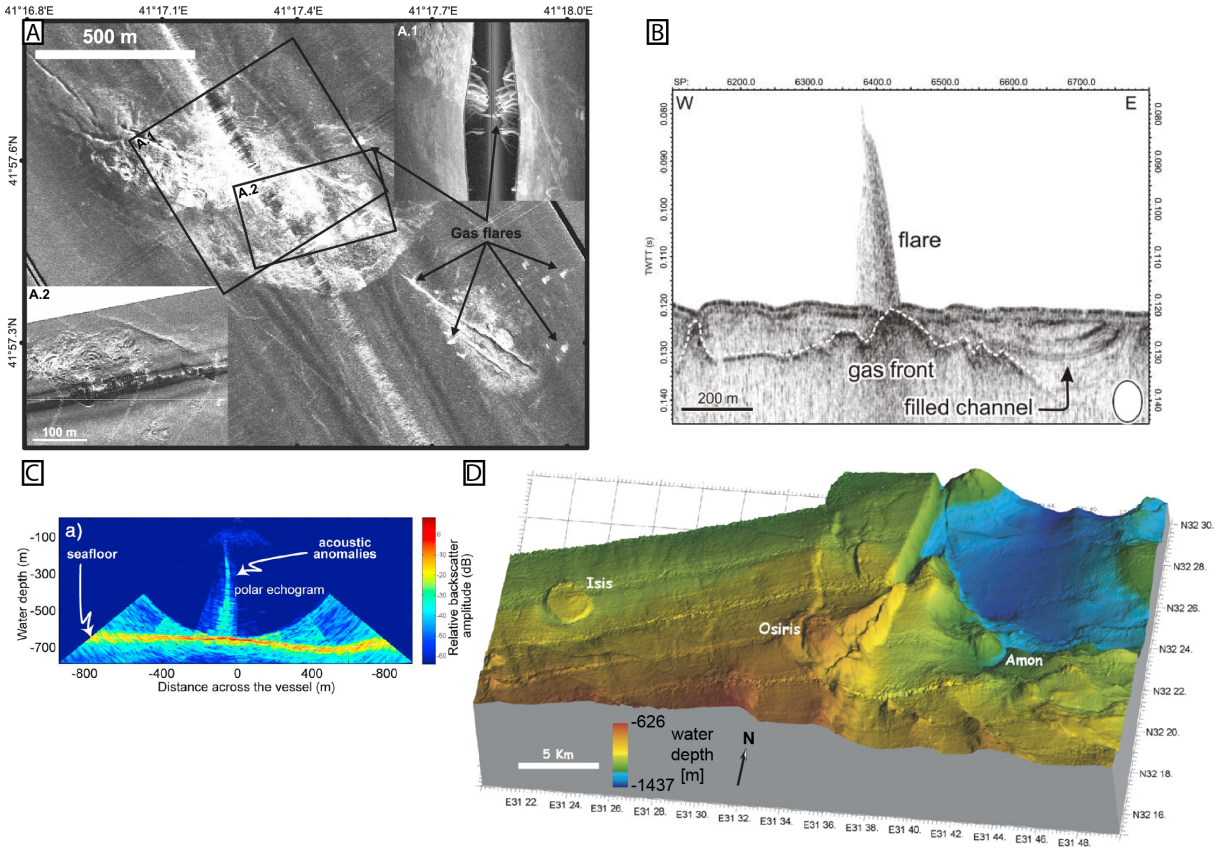

Fig. 1.14: Examples of different surface expressions of seep sites and mud volcanoes, as well as acoustic anomalies in the water column caused by escaping gas bubbles. A: High backscatter anomalies in 75-kHz sidescan data indicating cold seep carbonates in the eastern Black Sea. Inset A.1: Hydroacoustic flares in the water column of the raw sidescan data indicate gas bubble venting. A.2: 410 kHz sidescan data of the same seep site (location shown in A). Modified after Klaucke et al. (2005). B: 5 kHz sediment echosounder data showing acoustic turbidity underneath the seafloor, which is interpreted as the top of a shallow gas front, and water column anomalies interpreted as a gas flare. Adapted from Naudts et al. (2009). C: Raw echogram from EM302 multibeam echosounder showing acoustic anomalies in the water column related to gas flares. Adapted from Dupré et al. (2015). D: Bathymetry in 3D showing the surface expressions of three mud volcanoes (Isis, Osiris and Amon) from the Central Nile Deep-Sea Fan. Modified after Dupré et al. (2007).

1.5 Study area: The Black Sea

1.5.1 Tectonic setting

The Black Sea is a marginal ocean located between Ukraine, Russia, Georgia, Turkey, Bulgaria, and Romania. Two prominent ridges, the Andrusov Ridge and the Archangelsky Ridge, subdivide the Black Sea into two separated basins, the Eastern and the Western Basins (Fig. 1.15; Tugolesov et al., 1985; Nikishin et al., 2003), with maximum water depths of about 2.2 km. The ridges consist of continental crust and are overlain by 5-6 km of sediment. The Western Basin is underlain by oceanic to suboceanic crust with a sedimentary cover of up to 19 km thickness, while the Eastern Basin is underlain by thinned continental crust of about 10 km thickness covered with about 12 km thick sediment (Nikishin et al., 2003). Recent studies suggest that the Eastern Basin might also have been oceanic in the past (Shilington et al., 2008).

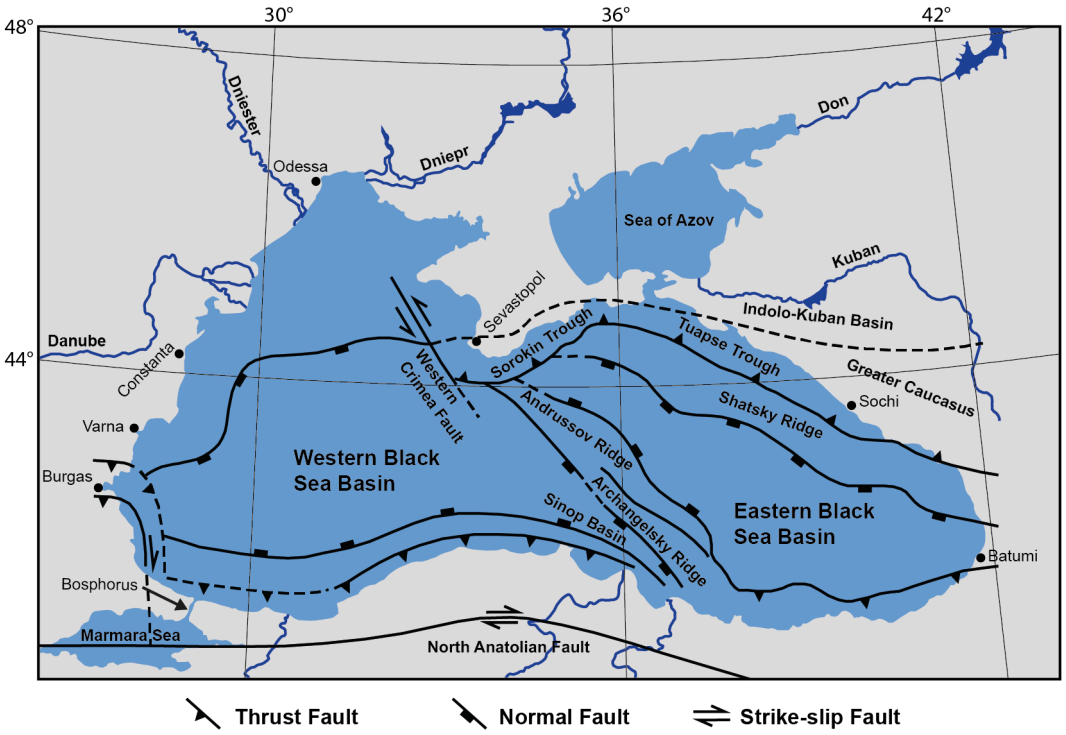

Fig. 1.15: Tectonic map of the Black Sea (modified after Robinson et al., 1996; Cifçi et al., 2003).

The Black Sea is presumably of extensional origin, as it evolved as a back-arc basin in late Cretaceous times during the northward subduction of the Thethyan Ocean under the volcanic arc of the Balkanides and Pontides (Nikishin et al., 2003). Since then, the area changed to a compressional environment that resulted from the collision between the Arabian, Anatolian, and Eurasian Plates, which was interpreted from modern stress field observations (Reilinger et al., 1997; Nikishin et al., 2003). Overall, the tectonic evolution of the basins involved multiple phases of extension and compression as well as subsidence, which resulted in the separation of the basins (Nikishin et al., 2003).

At the end of the last glaciation, sea water flowed into the freshwater sea during sea level lowstand (Reeburgh et al., 1991). The Black Sea thus changed from a lacustrine to a marine environment, which could have been completed over the course of a few years during a flooding event that occurred at 7150 +/- 100 yr BP at the end of the last Quaternary glaciation (Ryan et al., 1997). Seawater from the Mediterranean Sea entered through the Bosphorus into the Black Sea, where the sealevel was about 120-150 m lower compared to today (Ryan et al., 1997; Lericolais et al., 2009). As a consequence, the flooding event led to a submergence of 100,000 km^2 of eroded land which now makes up the Black Sea's continental shelf (Ryan et al., 1997). These changes between limnic and marine conditions occurred recurrently during the past glacial cycles and can be traced down to at least 300 ka BP, based on sediment sulfur concentrations in the Deep-Sea Drilling Project (DSDP) cores 379 and 379A collected during the campaign 42B (Fig. 1.16; Calvert and Batchelor, 1978; Manheim and Schug, 1978; Muratov et al., 1978).

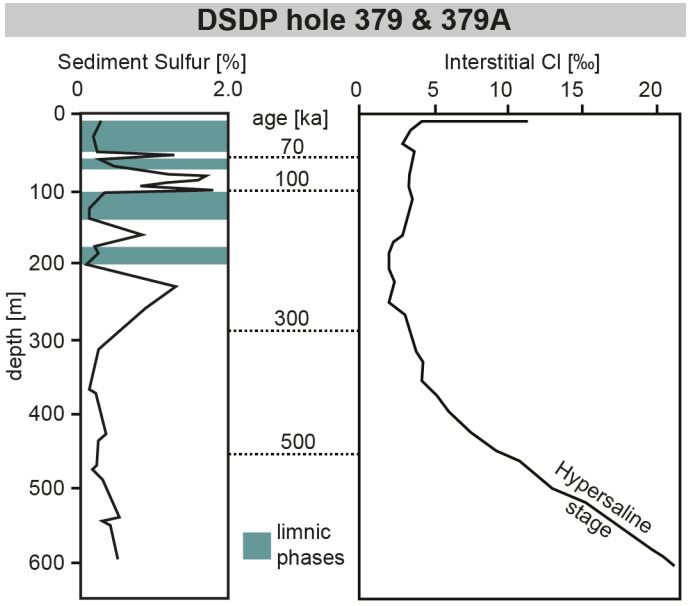

Fig. 1.16: Distribution of sediment sulfur concentration (left) and interstitial chlorinity (right) in the DSDP holes 379 and 379A (modified after Manheim and Schug, 1978). The intervals of limnic phases after Calvert and Batchelor (1978) are highlighted (green). The age of the depth interval is based on the interpretation of Muratov et al. (1978).

The continuous inflow of dense Mediterranean waters through the Bosphorus causes a strong stratification of the water column in the Black Sea. The upper layer is characterized by cold fresh water supplied by large rivers (Fig. 1.17; e.g. Danube, Dnepr, Dniestr, Don) at oxic conditions (Özsoy and Ünlüata, 1997). At about 150 m water depth, a change to anoxic conditions is observed, with warmer, more saline water supplied mainly by water inflow from the Mediterranean (Özsoy and Ünlüata, 1997).

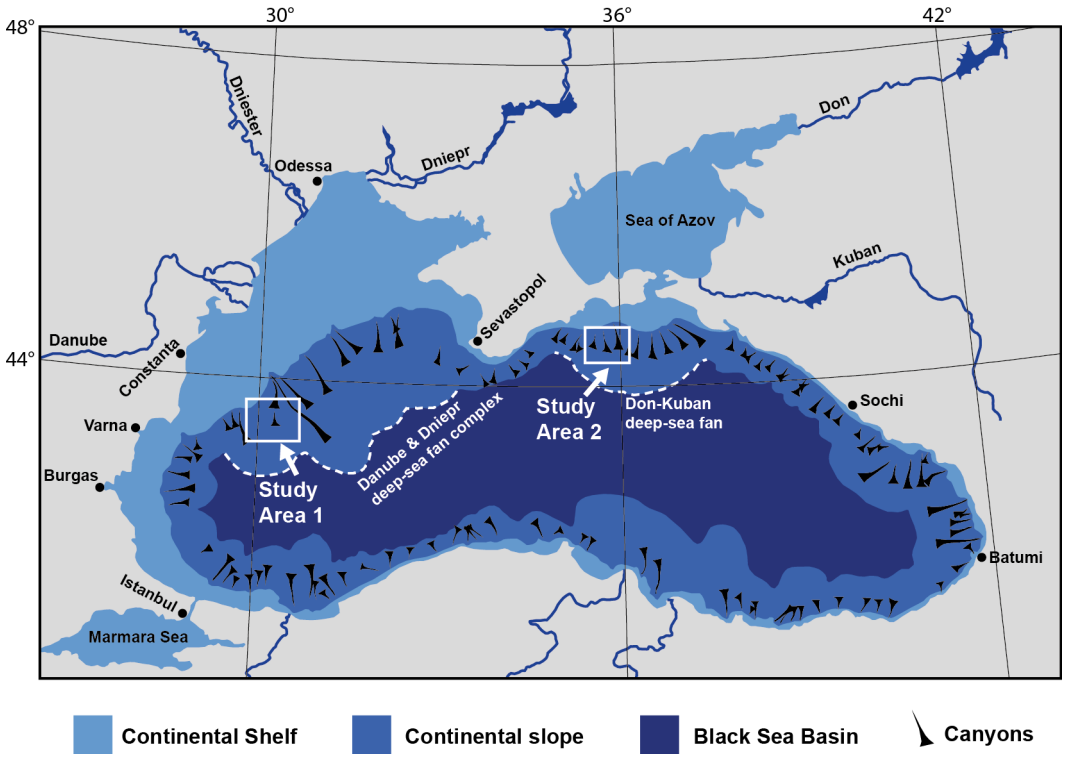

Fig. 1.17: Illustration of the main morphologic units of the Black Sea. During glacial sea level lowstands, the large rivers discharged at the shelf break. The paleo-fans are characterized by numerous channels and canyons, which transported large amounts of sediments into the basins. Modified after Popescu et al. (2015).

1.5.2 Gas and gas hydrates in the Black Sea

In the Black Sea, warm bottom water temperatures of 9 °C and salinities of 22.3 control the GHSZ, which occurs in water depths greater than ~720 m (Haeckel et al., 2015). The bottom-water temperature is remarkably uniform on regional and temporal scales (Degens and Ross, 1974; Vassilev and Dimitrov, 2002). However, due to the rapid salinity decrease in shallow sediment depth (Fig. 1.16; Manheim and Schug, 1978; Soulet et al., 2010), the upper boundary of the GHSZ may extent upwards to a water depth of ~665 m, which leads to a gas/gas hydrate intermediate zone between 665 m and 720 m (Fig. 1.18).

Gas hydrates in the sediments of the Black Sea are suggested to control the upward migration of gas towards the seafloor as they act as a permeability barrier. This is supported by several studies which reported a depth limit of around 720 m water depth for gas emission sites (Fig. 1.19; Naudts et al., 2006; Römer et al., 2012, Bialas et al., 2014).

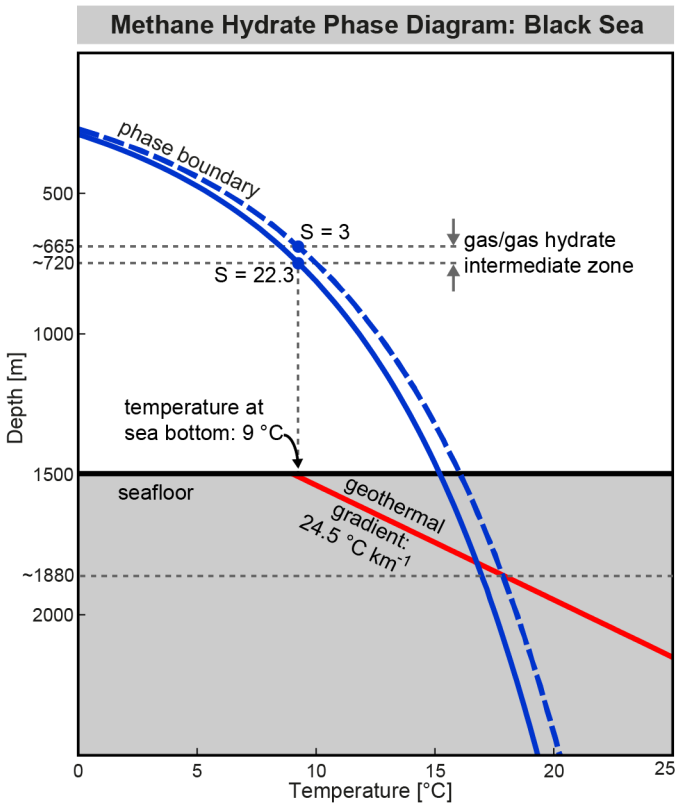

Fig. 1.18: Methane hydrate phase diagram for temperature conditions typically observed in the Black Sea. The salinity decrease of 22.3 in seawater (solid blue line) to ~3 in shallow sediment (dashed blue line) leads to a shift of the BGHSZ towards greater sediment depth.

BSRs as an indicator for the presence of gas hydrates are documented for several areas in the Black Sea, e.g. in the southwestern margin (Dondurur et al., 2013; Küçük et al., 2015) and the eastern margin (Wagner-Friedrichs, 2007; Bocharova et al., 2009; Minshull and Keddie, 2010). Several studies carried out in the Danube and Dniepr paleo deep-sea fan complex in the northwestern Black Sea revealed large BSR patches (Lüdmann et al., 2004; Baristeas, 2006; Popescu et al., 2006; 2007; Haeckel et al., 2015; Ker and Riboulot, 2015).

The first discovery of natural gas hydrates in the Black Sea dates back to 1970-1972 (Vassilev and Dimitrov, 2002; Starostenko et al., 2010, and references therein). Since then, multiple studies have reported successful sampling of gas hydrates in multiple locations around the Black Sea (e.g. Bohrmann et al., 2003; Heeschen et al., 2011; Römer et al., 2012; Ker and Riboulot, 2015). Gas hydrates were also sampled in areas where BSRs are absent (Krastel et al., 2003).

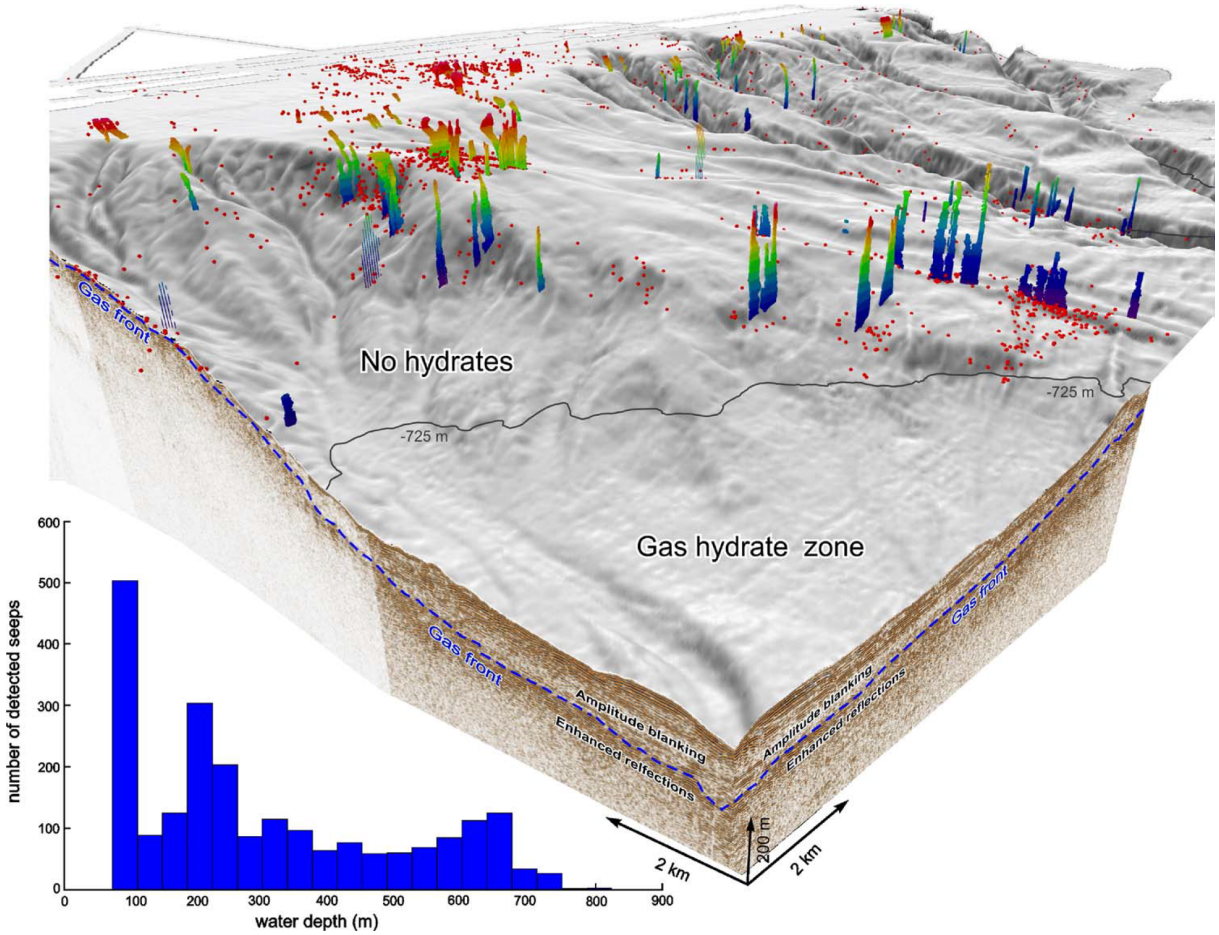

Fig. 1.19: Seep distribution at the Dniepr paleo-delta, plotted as red dots and 3D gas flares. Seeps are abundant above the upper limit of gas hydrate stability (plotted here at the 725 m isoline), with one cluster at 650 m water depth. From Naudts et al. (2006).

1.5.3 Multiple BSRs in the Black Sea

The Black Sea is well known for the presence of double and multiple BSRs. Multiple BSRs with up to four BSRs in the Danube deep-sea fan were first discovered by Popescu et al. (2006). These BSRs were observed in 2D seismic profiles that cross a buried channel-levee system in water depths of 1000-1500 m. All observed BSRs are sub-parallel to the seafloor. Popescu et al. (2006) excluded that the multiple BSRs are caused by gas hydrate layers with different gas compositions. Instead, they suggested that the lower BSRs represent paleo-BSRs corresponding to stable cold climatic episodes of the Black Sea. Based on the current seafloor level and paleo bottom water temperatures, Popescu et al. (2006) calculated the depth of the BGHSZ for lower sea stands during different glacial periods. The same approach was later applied to a site at the Tuapse Trough in the northeastern Black Sea, which is characterized by a stack of three BSRs that run parallel to the seafloor and are also thought to be related to lower sealevels (Bocharovka et al., 2009). Additional studies on multiple BSRs were carried out offshore Amasra, Bartın, and Zonguldak-Kozlu in the central Black Sea (Küçük et al., 2015). These authors concluded that the multiple BSRs are related to different gas compositions due to the presence of thermogenic gas.

1.5.4 Cold seeps and natural gas emissions in the Black Sea

In general, three types of seeps are observed in the Black Sea: shallow seeps, deep-sea seeps, and seeps within the GHSZ. Shallow water gas emissions are located above the GHSZ in water depths of 60-720 m (Dimitrov, 2002; Cifçi et al., 2003; Naudts et al., 2006; Schmale et al., 2010; Römer et al., 2012). These shallow gas emissions are commonly observed at morphological features such as pockmarks, canyon flanks, ridges, and slump scars. They are generally not associated with distinct backscatter anomalies (Klaucke et al., 2006). The emitted gas is predominantly of microbial origin with molecular compositions of >99% methane (Poort et al., 2005; Naudts et al., 2006).

In water depths of 1000-2000 m, deep-sea seep sites can be observed in the deep Black Sea basins. They result from the expulsion of warm fluids and mud, originating from the late Oligocene-Miocene Maikopian formation (Klaucke et al., 2006). Examples of this type are the well-studied mud volcanoes in the Sorokin Trough (Blinova et al., 2003; Bohrmann et al., 2003; Krastel et al., 2003; Sahling et al., 2009; Papenberg et al., 2013).

The third type of cold seeps in the Black Sea is located within the GHSZ, i.e., below 720 m water depth. This type includes the Kerch seep site at the Don Kuban deep-sea fan (Bialas, 2012; Römer et al., 2012), which is characterized by active methane emission of microbial origin (Römer et al., 2012). Another well-studied example is the Batumi seep site offshore Georgia. It is located in water depths of 850-900 m on the Kobuleti ridge (Klaucke et al., 2006). Multiple studies were carried out to investigate these seeps based on deep-towed sidescan sonar data (Klaucke et al., 2006), multichannel seismic data (Wagner-Friedrichs, 2007), pore water analysis (Pape et al., 2010; Reitz et al., 2011), pressure coring (Heeschen et al., 2011) and satellite imagery (Körber et al., 2014). The emitted hydrocarbons are of microbial as well as thermogenic origin (Reitz et al., 2011), and oil seepage was also observed (Körber et al., 2014).

1.5.5 Fate of released methane

As methane is one of the most abundant greenhouse gases, its role in global climate change is of high interest (Wuebbles and Hayhoe, 2002). The fate of methane that is released into the water column has been studied intensively, especially in the Black Sea as the world's largest anoxic basin. In general, rising heights are controlled by the seafloor depth at which the gas is expelled, gas bubble size, rising velocity, methane concentration in the seawater, and the presence of upwelling flows (Leifer and Judd, 2002). During gas bubble ascent, methane dissolves in the methane-undersaturated seawater.

Recent studies showed that only gas bubbles larger than 6 mm in diameter and release shallower than 200 m water depth have the potential to reach the sea surface and escape into the atmosphere (McGinnis et al., 2006; Schmale et al., 2010; IRIS, 2015). Gas bubbles released below the upper boundary of the GHSZ (> 720 m water depth) form a protective hydrate coat which slows down methane dissolution (Rehder et al., 2002), they are nonetheless completely dissolved within 150-200 m above the GHSZ (IRIS, 2015).

Water column imaging surveys confirmed that gas bubbles expelled at deep-sea vent sites are eventually dissolved in the water column. For example, gas bubbles released at mud volcanoes in 2080 m water depth were traced up to 1300 m above the seafloor, indicating that the bubbles are completely dissolved while still within the GHSZ (Greinert et al., 2006). Bubbles released at the Kerch seep site in around 900 m water depth were traced up to 350 – 460 m above the seafloor (Römer et al., 2012).

1.5.6 Gas hydrate production in the Black Sea

Reservoir-quality gas hydrate accumulations are expected to occur in highly permeable sand of the paleo-river depositional areas around the Black Sea (Fig. 1.17; Haeckel et al., 2015; Merey and Sinayuk, 2016a). The most promising research program focusing on gas hydrates as an energy resource (SUGAR – Submarine Gas Hydrate Reservoirs) is currently carried out in the Danube deep-sea fan (Haeckel et al., 2015). In terms of production methods suitable in the Danube deep-sea fan, the exchange of CH_4 with CO_2 is not feasible due to the high bottom water temperatures around 9 °C (Merey and Sinayuk, 2016b). Based on the models and experiences gained in other potential production areas (discussed in chapter 1.2.1), the depressurization method was considered feasible for the Black Sea (Haeckel et al., 2015). The high bottom water temperatures in the Black Sea would thereby increase the efficiency of the depressurization method (Merey and Sinayuk, 2016b).

Accidental gas release during production operations from shallow gas hydrate reservoirs is considered a minor hazard, since gas hydrate reservoirs are, unlike conventional oil and gas reservoirs, not over-pressured (IRIS, 2015). Methane release would therefore be comparable to already well-known seep sites in the deeper part of the Black Sea where the released gas is completely dissolved in the water column.

1.6 References

Abramson, L.W., Lee, T.S., Sharma, S., and Boyce, G.M., 2002. Slope stability and stabilization methods (Second Edition). John Wiley & Sons Inc., New York, USA.

Andreassen, K., Mienert, J., Bryn, P., and Singh, S.C., 2000. A double gas-hydrate related bottom simulating reflector at the Norwegian continental margin. Annals of the New York Academy of Sciences 912, pp. 126-135, doi:10.1111/j.1749-6632.2000.tb06766.x.

Andreassen, K., Nilssen, E.G., and Ødegaard, C.M., 2007. Analysis of shallow gas and fluid migration within the Plio-Pleistocene sedimentary succession of the SW Barents Sea continental margin using 3D seismic data. Geo-Marine Letters 27, pp. 155-171, doi:10.1007/s00367-007-0071-5.

Bangs, N.L.B., Musgrave, R.J., and Tréhu, A.M., 2005. Upward shifts in the southern Hydrate Ridge gas hydrate stability zone following postglacial warming, offshore Oregon. Journal of Geophysical Research: Solid Earth 110, B03102, doi:10.1029/2004JB003293.

Bangs, N.L., Hornbach, M.J., Moore, G.F., and Park, J.O., 2010. Massive methane release triggered by seafloor erosion offshore southwestern Japan. Geology 38, pp. 1019-1022, doi:10.1130/G31491.1.

Baristeas, N., 2006. Seismische Fazies, Tektonik und Gashydratvorkommen im nordwestlichen Schwarzen Meer. Diploma Thesis, University of Hamburg, 110 pp.

Bernard, B.B., Brooks, J.M., and Sackett, W.M., 1976. Natural gas seepage in the Gulf of Mexico. Earth and Planetary Science Letters 31, pp. 48-54, doi:10.1016/0012-821X(76)90095-9.

Berndt, C., 2005. Focused fluid flow in passive continental margins. Philosophical Transactions of the Royal Society A 363, pp. 2855-2871, doi:10.1098/rsta.2005.1666.

Bhatnagar, G., Chapman, W.G., Dickens, G.R., Dugan, B., and Hirasaki, G.J., 2008. Sulfate-methane transition as a proxy for average methane hydrate saturation in marine sediments. Geophysical Research Letters 35, L03611, doi:10.1029/2007GL032500.

Bialas, J. (Ed.), 2012. FS POSEIDON Fahrtbericht / Cruise Report POS427 – Fluid emissions from mud volcanoes, cold seeps and fluid circulation at the Don-Kuban deep-sea fan (Kerch peninsula, Crimea, Black Sea), 23.02.-19.03.2012, Burgas, Bulagria – Heraklion, Greece. GEOMAR Report, N. Ser. 003. GEOMAR Helmholtz-Zentrum für Ozeanforschung Kiel, Germany, 28 pp, doi:10.3289/GEOMAR_ REP_NS_3_2012.

Bialas, J., Klaucke, I., and Haeckel, M. (Eds.), 2014. FS MARIA S. MERIAN Fahrtbericht / Cruise Report MSM-34/1 & 2 - SUGAR Site, 06.12.13-16.01.14, Varna – Varna. GEOMAR Report, N. Ser. 015. GEOMAR Helmholtz-Zentrum für Ozeanforschung Kiel, Germany, 111 pp., doi:10.3289/GEOMAR_REP_ NS_15_2014.

Blinova, V.N., Ivanov, M.K., and Bohrmann, G., 2003. Hydrocarbon gases in deposits from mud volcanoes in the Sorokin Trough, north-eastern Black Sea. Geo-Marine Letters 23, pp. 250-257, doi:10.1007/s00367-003-0148-8.

Bocharova, A., Volkonskaya, A., Ivanov, M. K., Bouriak, S. V., and Almendinger, O., 2009. Origin of multiple bottom simulating reflectors in the Black Sea. 71st EAGE Conference & Exhibition, Amsterdam, Netherlands, 8-11 June 2009, 6 pp.

Boetius, A., Ravenschlag, K., Schubert, C.J., Rickert, D., Widdel, F., Gieseke, A., Amann, R., Jørgensen, B.B., Witte, U., and Pfannkuche, O., 2000. A marine microbial consortium apparently mediating anaerobic oxidation of methane. Nature 407, pp. 623-626, doi:10.1038/35036572.

Bohrmann, G., Ivanov, M., Foucher, J.P., Spiess, V., Bialas, J., Greinert, J., Weinrebe, W., Abegg, F., Aloisi, G., Artemov, Y., Blinova, V., Drews, M., Heidersdorf, F., Krabbenhoeft, A., Klaucke, I., Krastel, S., Leder, T., Polikarpov, I., Saburova, M., Schmale, O., Seifert, R., Volkonskaya, A., and Zillmer, M., 2003. Mud volcanoes and gas hydrates in the Black Sea: new data from Dvurechenskii and Odessa mud volcanoes. Geo-Marine Letters 23, pp. 239-249, doi:10.1007/s00367-003-0157-7.

Bohrmann, G., and Torres, M., 2006. Gas hydrates in marine sediments. In: Schulz, H.D., and Zabel, M. (Eds.), Marine Geochemistry. Springer, pp. 481-512.

Boswell, R., Shelander, D., Lee, M., Latham, T., Collett, T., Guerin, G., Moridis, G., Reagan, M., Goldberg, D., 2009. Occurrence of gas hydrate in Oligocene Frio sand: Alaminos Canyon Block 818: Northern Gulf of Mexico. Marine and Petroleum Geology 26, pp. 1499-1512, doi: 10.1016/j.marpetgeo.2009.03.005.

Boswell, R., Collett, T.S., Frye, M., Shedd, W., McConnell, D.R., and Shelander, D., 2012. Subsurface gas hydrates in the northern Gulf of Mexico. Marine and Petroleum Geology 34, pp 4-30, doi:10.1016/j.marpetgeo.2011.10.003.

Burwicz, E.B., Rüpke, L.H., and Wallmann, K., 2011. Estimation of the global amount of submarine gas hydrates formed via microbial methane formation based on numerical reaction-transport modelling and a novel parameterization of Holocene sedimentation. Geochimica et Cosmochimica Acta 75, pp. 4562-4576, doi: 10.1016/j.gca.2011.05.029.

CEN, 2004. EN-1998-1: Eurocode 8: Design of Structures for Earthquake Resistance. European Committee for Standardization, Brussels, 229 pp.

Calvert, S.E., and Batchelor, C.H., 1978. Major and minor element geochemistry of sediments from Hole 379A, Leg 42B, Deep-Sea Drilling Project. Initial Reports of the Deep Sea Drilling Project 42, Part 2, pp. 527-541.

Cartwright, J., 1994. Episodic basin-wide fluid expulsion from geopressured shale sequences in the North Sea basin. Geology 22, pp. 447-450, doi:10.1130/0091-7613(1994)022<0447:EBWFEF>2.3.CO;2.

Cartwright, J., Huuse, M., and Aplin, A., 2007. Seal bypass systems. AAPG Bulletin 91, pp. 1141-1166, doi:10.1306/04090705181.

Chen, L., Chi, W.C., Wu, S.K., Liu, C.S., Shyu, C.T., Wand, Y., and Lu, C.Y., 2014. Two dimensional fluid flow models at two gas hydrate sites offshore southwestern Taiwan. Journal of Asian Earth Sciences 92, pp. 245-253, doi:10.1016/j.jseases.2014.01.004.

Chi, W.C., Lin, Y.S., Berndt, C., Wu, S.K., Crutchley, G., Chen, L., Liu, C.S., Shyu, C.T., Chian, H.T., Lin, S., Han, W.C., Hsu, H.H., Peng, Y.S., and Wang, Y., 2014. Processes affecting the depth of the gas hydrate stability zone in the accretionary prism offshore southwestern Taiwan. OCEANS'14 MTS/IEEE Conference, Taipei, Taiwan, 7-10 April 2014, 4 pp, doi:10.1109/OCEANS-TAIPEI.2014.6964594.

Chong, Z.R., Yang, S.H.B., Babu, P., Linga, P., and Li, X.S., 2016. Review of natural gas hydrates as an energy resource: Prospects and challenges. Applied Energy 162, pp. 1633-1652, doi:10.1016/j.apenergy.2014.12.061.

Cifçi, G., Dondurur, D., and Ergün, M., 2003. Deep and shallow structures of large pockmarks in the Turkish shelf, Eastern Black Sea. Geo-Marine Letters 23, pp. 311-322, doi:10.1007/s00367-003-0138-x.

Circone, S., Kirby, S.H., and Stern, L.A., 2005. Direct measurement of methane hydrate composition along the hydrate equilibrium boundary. The Journal of Physical Chemistry B 109, pp. 9468-9475, doi:10.1021/jp050487.

Clayton, C.J., and Hay, S.J., 1994. Gas migration mechanism from accumulation to surface. Bulletin of the Geological Society of Denmark 41, pp. 12-23.

Clennell, M.B., Judd, A., and Hovland, M., 2000. Movement and accumulation of methane in marine sediments: relation to gas hydrate systems. In: Max, M.D. (Ed.), Natural Gas Hydrate in Oceanic and Permafrost Environments. Kluwer Academic Publishing, Netherlands, pp. 105-122.

Collett, T.S., 1993. Natural gas hydrates of the Prudhoe Bay and Kuparuk River area, North Slope, Alaska. AAPG Bulletin 77, pp. 793-812.

Collett, T.S., Lewis, R.E., and Dallimore, S.R., 2005. Mallik 5L-38 gas hydrate production research well downhole well-log and core montages for the JAPEX/JNOC/GSC et al. Mallik 5L-38 Gas Hydrate Production Research Well. In: Dallimore, S.R., and Collett, T.S. (Eds.), Scientific Results from the Mallik 2002 Gas Hydrate Production Well Program, Mackenzie Delta, Northwest Territories, Canada. Geological Survey of Canada, Bulletin 585, Ottawa, Canada, XX pp.

Collett, T.S., Riedel, M., Cochran, J., Boswell, R., Presley, J., Kumar, P., Sathe, A., Sethi, A., Lall, M. and Sibal, V., 2008. Indian National Gas Hydrate Program Expedition 01 Initial Reports: Expedition 01 of the Indian National Gas Hydrate Program from Mumbai, India to Chennai, India; Sites NGHP-01-01 through NGPH-01-21, April 2006 – August 2006. Initial Report, Directorate General of Hydrocarbons, Ministry of Petroleum and Natural Gas, Noida, India, XX pp.

Collett, T., Bahk, J.J., Baker, R., Boswell, R., Divins, D., Frye, M., Goldberg, D., Husebø, J., Koh, C., Malone, M., Morell, M., Myers, G., Shipp, C., and Torres, M., 2015. Methane hydrates in nature – current knowledge and challenges. Journal of Chemical & Engineering Data 60, pp. 319-329, doi:10.1021/je500604h.

Cooper, A.K., and Hart, P.E., 2003. High-resolution seismic reflection investigation of the northern Gulf of Mexico gas-hydrate stability zone. Marine and Petroleum Geology 19, pp. 1275-1293, doi: 10.1016/S0264-8172(02)00107-1.

Crutchley, G.J., Geiger, S., Pecher, I.A., Gorman, A.R., Zhu, H., and Henrys, S.A., 2010. The potential influence of shallow gas and gas hydrates on sea floor erosion of Rock Garden, an uplifted ridge offshore of New Zealand. Geo-Marine Letters 30, pp. 283-303, doi: 10.1007/s00367-010-0186-y.

Crutchley, G.J., Klaeschen, D., Planert, L., Bialas, J., Berndt, C., Papenberg, C., Hensen, C., Hornbach, M.J., Krastel, S., and Brueckmann, W., 2014. The impact of fluid advection on gas hydrate stability: Investigations at sites of methane seepage offshore Costa Rica. Earth and Planetary Science Letters 401, pp. 95-109, doi:10.1016/j.epsl.2014.05.045.

Crutchley, G.J., Mountjoy, J.J., Pecher, I.A., Gorman, A.R., and Henrys, S.A., 2016. Submarine slope instabilities coincident with shallow gas hydrate systems: Insights from New Zealand examples. In: Lamarche, G., Mountjoy, J., Bull, S., Hubble, T., Krastel, S., Lane, E., Micallef, A., Moscardelli, L., Mueller, C., Pecher, I., and Woelz, S. (Eds.), Submarine Mass Movements and their Consequences. Advances in Natural and Technological Hazards Research 41, Springer, pp. 401-409.

Dallimore, S.R., Collett, T.S., and Uchida, T., 1999. Scientific results from JAPEX/JNOG/GSC Mallik 2L-38 gas hydrate research well, Mackenzie Delta, Northwest Territories, Canada. In: Dallimore, S.R., Uchida, T., and Collett, T.S. (Eds.). Geological Survey of Canada, Bulletin 544, Ottawa, Canada.

Dallimore, S.R., Wright, J.F., Yamamoto, K., and Bellefleur, G., 2012. Proof of concept for gas hydrate production using the depressurization technique, as established by the JOGMEC/NRCan/Aurora Mallik 2007-2008 Gas Hydrate Production Research Well Program. In: Dallimore, S.R., Yamamoto, K., Wright, J.F., and Bellefleur, G. (Eds.), Scientific results from the JOGMEC/ NRCan/Aurora Mallik 2007-2008 gas hydrate production research well program, Mackenzie Delta, Northwest Territories, Canada. Geological Survey of Canada, Bulletin 601, pp. 1-15.

Dannowski, A., Bialas, J., Schwalenberg, K., Gehrmann, R., Zander, T., and Klaeschen, D., 2017. Shear wave modelling of high resolution OBS data with a comparison to CSEM data in a gas hydrate environment in the Danube deep-sea fan, Black Sea. 9th International Conference on Gas Hydrates, ICGH9, 25-30 June 2017, Denver, Colorado, USA.

Davies, E.E., Hyndman, R.D., and Villinger, H., 1990. Rates of fluid expulsion across the Northern Cascadia accretionary prism: Constraints from new heat flow and multichannel reflection data. Journal of Geophysical Research: Solid Earth 95, pp. 8869-8889, doi:10.1029/JB095iB06p08869.

Davies, R.J., Thatcher, K.E., Armstrong, H., Yang, J., and Hunter, S., 2012. Tracking the relict bases of marine methane hydrates using their intersections with stratigraphic reflections. Geology 40, pp. 1011-1014, doi:10.1130/G33297.1.

Degens, E.T., and Ross, D.A. (Eds.), 1974. The Black Sea – Geology, Chemistry, and Biology. AAPG Memoir 20, American Association of Petroleum Geologists.

Dimitrov, L.I., 2002. Mud volcanoes – the most important pathway for degassing deeply buried sediments. Earth-Science Reviews 59, pp.49-76, doi:10.1016/S0012-8252(02)00069-7.

Dondurur, D., Küçük, H.M., and Cifçi, G., 2013. Quaternary mass wasting on the western Black Sea margin, offshore of Amasra. Global and Planetary Change 103, pp. 248-260, doi:10.1016/ j.gloplacha.2012.05.009.

Dong, F., Zang, X., Li, D., Fan, S., and Liang, D., 2009. Experimental investigation on propane hydrate dissociation by high concentration methanol and ethylene glycol solution injection. Energy Fuels 23, pp. 1563-1567, doi:10.1021/ef800660m.

Dumke, I., Klaucke, I., Berndt, C., and Bialas, J., 2014. Sidescan backscatter variations of cold seeps on the Hikurangi Margin (New Zealand): indications for different stages in seep development. Geo-Marine Letters 34, pp. 169-184, doi:10.1007/s00367-014-0361-7.

Dupré, S., Woodside, J., Foucher, J.P., de Lange, G., Mascle, J., Boetius, A., Mastalerz, V., Stadnitskaia, A., Ondréas, H., Huguen, C., Harmégnies, F., Gontharet, S., Loncke, L., Deville, E., Niemann, H., Omoregie, E., Olu-Le Roy, K., Fiala-Medioni, A., Dählmann, A., Caprais, J.C., Prinzhofer, A., Sibuet, M., Pierre, C., Damsté, J.S., and the NAUTINIL Scientific Party, 2007. Seafloor geological studies above active gas chimneys off Egypt (Central Nile Deep Sea Fan). Deep-Sea Research I 54, pp. 1146-1172, doi:10.1016/j.dsr.2007.03.007.

Dupré, S., Woodside, J., Klaucke, I., Mascle, J., and Foucher, J.P., 2010. Widespread active seepage activity on the Nile Deep Sea Fan (offshore Egypt) revealed by high-definition geophysical imagery. Marine Geology 275, pp. 1-19, doi:10.1016/j.margeo.2010.04.003.

Dupré, S., Scalabrin, C., Grall, C., Augustin, J.M., Henry, P., Şengör, A.M.C., Görür, N., Çağatay, M.N., and Géli, L., 2015. Tectonic and sedimentary controls on widespread gas emissions in the Sea of Marmara: Results from systematic, shipborne multibeam echo sounder water column imaging. Journal of Geophysical Research: Solid Earth 120, pp. 2891-2912, doi:10.1002/2014JBO11617.

Fiebig, J., Woodland, A.B., D'Alessandro, W., and Püttmann, W., 2009. Excess methane in continental hydrothermal emissions is abiogenic. Geology 37, pp. 495-498, doi:10.1130/G25598A.1.

Fjaer, E., Holt, R.M., Horsrud, P., Raaen, A.M., and Risnes, R., 2008. Petroleum Related Rock Mechanics (Second Edition). Developments in Petroleum Science 53, Elsevier.

Foucher, J.P., Nouzé, H., and Henry, P., 2002. Observation and tentative interpretation of a double BSR on the Nankai slope. Marine Geology 187, pp. 161-175, doi:10.1016/S0025-3227(02)00264-5.

Fujii, T., Suzuki, K., Takayama, T., Tamaki, M., Komatsu, Y., Konno, Y., Yoneda, J., Yamamoto, K., and Nagao, J., 2015. Geological setting and characterization of a methane hydrate reservoir distributed at the first offshore production test site on the Daini-Atsumi Knoll in the eastern Nankai Trough, Japan. Marine and Petroleum Geology 66, pp. 310-322, doi:10.1016/j.marpetgeo.2015.02.037.

Gay, A., Lopez, M., Berndt, C., and Séranne, M., 2007. Geological controls on focused fluid flow associated with seafloor seeps in the Lower Congo Basin. Marine Geology 244, pp. 68-92, doi:10.1016/ j.margeo.2007.06.003.

Geletti, R., and Busetti, M., 2011. A double bottom simulating reflector in the western Ross Sea, Antarctica. Journal of Geophysical Research: Solid Earth 116, B04101, doi:10.1029/2010JB007864.

Ginsburg, G.D., and Soloviev, V.A., 1997. Methane migration within the submarine gas hydrate stability zone under deep-water conditions. Marine Geology 137, pp. 49-57 doi:10.1016/S0025-3227(96)00078-3.

Goel, N., 2006. In situ methane hydrate dissociation with carbon dioxide sequestration: current knowledge and issues. Journal of Petroleum Science and Engineering 51, pp. 169-184, doi:10.1016/j.petrol.2006.01.005.

Greinert, J., Artemov, Y., Egorov, V., De Batist, M., and McGinnis, D., 2006. 1300-m-high rising bubbles from mud volcanoes at 2080 m in the Black Sea: Hydroacoustic characteristics and temporal variability. Earth and Planetary Science Letters 244, pp. 1-15, doi:10.1016/j.epsl.2006.02.011.

Greinert, J., Lewis, K.B., Bialas, J., Pecher, I.A., Rowden, A., Bowden, D.A., De Batist, M., and Linke, P., 2010. Methane seepage along the Hikurangi Margin, New Zealand: Overview of studies in 2006 and 2007 and new evidence from visual, bathymetric and hydroacoustic investigations. Marine Geology 272, pp. 6-25, doi:10.1016/j.margeo.2010.01.017.

Grevemeyer, I., and Villinger, H., 2001. Gas hydrate stability and the assessment of heat flow through continental margins. Geophysical Journal International 145, pp. 647-660, doi:10.1046/j.0956-540x.2001.01404.x.

Haacke, R.R., Westbrook, G.K., and Hyndman, R.D., 2007. Gas hydrate, fluid flow and free gas: formation of the bottom-simulating reflector. Earth and Planetary Science Letters 261, pp. 407-420, doi:10.1016/ j.epsl.2007.07.008

Haeckel, M., Suess, E., Wallmann, K., and Rickert, D., 2004. Rising methane gas bubbles form massive hydrate layers at the seafloor. Geochimica et Cosmochimica Acta 68, pp. 4335-4345, doi:10.1016/ j.gca.2004.01.018.

Haeckel, M., Boudreau, B.P., and Wallmann, K., 2007. Bubble-induced porewater mixing: A 3-D model for deep porewater irrigation. Geochimica et Cosmochimica Acta 71, pp. 5135-5154, doi:10.1016/ j.gca.2007.08.011

Haeckel, M., Bialas, J., Klaucke, I., Wallmann, K., Borhmann, G., Schwalenberg, K., and SUGAR participants, 2015. Gas hydrate occurrences in the Black Sea – New observations from the German SUGAR project. Fire in the Ice: Methane Hydrate Newsletter 15 (2), pp. 6-9.

Hampton, M.A., Lee, H.J., and Locat, J., 1996. Submarine landslides. Reviews of Geophysics 34, pp. 33-59, doi:10.1029/95RG03287.

Hancock, S.H., Collett, T.S., Dallimore, S.R., Satoh, T., Inoue, T., Huenges, E., Henninges, J., and Weatherill, B., 2005. Overview of thermal stimulation production-test results for the JAPEX/JNOC/GSC et al. Mallik 5L-38 gas hydrate production research well. In: Dallimore, S.R., and Collett, T.S. (Eds.), Scientific Results from the Mallik 2002 Gas Hydrate Production Research Well Program, Mackenzie Delta, Northwest Territories, Canada. Geological Survey of Canada, Bulletin 585, Ottawa, Canada, 15 pp.

Hart, B.S., Flemings, P.B., and Deshpande, A., 1995. Porosity and pressure: Role of compaction disequilibrium in the development of geopressures in a Gulf Coast Pleistocene basin. Geology 23, pp. 45-48, doi:10.1130/0091-7613(1995)023<0045:PAPROC>2.3.CO;2.

Heeschen, K.U., Haeckel, M., Klaucke, I., Ivanov, M.K., and Bohrmann, G., 2011. Quantifying in-situ gas hydrates at active seep sites in the eastern Black Sea using pressure coring technique. Biogeosciences 8, pp. 3555-3565, doi:10.5194/bg-8-3555-2011.

Hensen, C., Wallmann, K., Schmidt, M., Ranero, C.R., and Suess, E., 2004, Fluid expulsion related to mud extrusion off Costa Rica—A window to the subducting slab. Geology 32, pp. 201-204, doi:10.1130/G20119.1.

Hensen, C., Scholz, F., Nuzzo, M., Valadaresm V., Gràcia, E., Terrinha, P., Liebetrau, V., Kaul, N., Silva, S., Martínez-Loriente, S., Bartolome, R., Piñero, E., Magalhães, V.H., Schmidt, M., Weise, S.M.,

Cunha, M., Hilario, A., Perea, H., Rovelli, L., and Lackschewitz, K., 2015. Strike-slip faults mediate the rise of crustal-derived fluids and mud volcanism in the deep sea. Geology 43, pp. 339-342, doi: 10.1130/G36359.

Hillman, J.I.T., Cook, A.E., Sawyer, D.E., Küçük, H.M., and Goldberg, D.S., 2017. The character and amplitude of 'discontinuous' bottom-simulating reflectors in marine seismic data. Earth and Planetary Science Letters 459, pp. 157-169, doi:10.1016/j.epsl.2016.10.058.

Hinrichs, K.U., and Boetius, A., 2002. The anaerobic oxidation of methane: New insights in microbial ecology and biogeochemistry. In: Wever, G., Billett, D., Hebbeln, D., Jørgensen, B.B., Schlüter, M., and van Weering, T.C.E. (Eds.), Ocean Margin Systems. Springer Verlag, Heidelberg, pp. 457-577.

Holder, G.D., and Hand, J.H., 1982. Multiple-phase equilibria in hydrates from methane, ethane, propane, and water mixtures. AlChE Journal 28, pp. 440-447, doi:10.1002/aic.690280312.

Hornbach, M. J., Saffer, D. M., and Holbrook, W. S. (2004). Critically pressured free-gas reservoirs below gas-hydrate provinces. Nature 427, pp. 142-144, doi: 10.1038/nature02172.

Hovland, M., and Judd, A.G., 1988. Seabed pockmarks and seepages: Impact on geology, biology and the marine environment. Graham and Trotman, London.

Hovland, M., and Svensen, H., 2006. Submarine pingoes: Indicators of shallow gas hydrates in a pockmark at Nyegga, Norwegian Sea. Marine Geology 228, pp. 15-23, doi:10.1016/j.margeo.2005.12.005.

Hustoft, S., Mienert, J., Bünz, S., and Nouzé, H., 2007. High-resolution3D-seismic data indicate focused fluid migration pathways above polygonal fault systems of the mid-Norwegian margin. Marine Geology 245, pp. 89-106, doi: 10.1016/j.margeo.2007.07.004

Hyndman, R. D., and Davis, E. E., 1992. A mechanism for the formation of methane hydrate and seafloor bottom-simulating reflectors by vertical fluid expulsion. Journal of Geophysical Research: Solid Earth 97, pp. 7025-7041, doi:10.1029/91JB03061.

Hyndman, R. D., Foucher, J.-P., Yamano, M., and Fisher, A., 1992. Deep sea bottom-simulating-reflectors: calibration of the base of the hydrate stability field as used for heat flow estimates. Earth and Planetary Science Letters 109, pp. 289-301 doi:10.1016/0012-821X(92)90093-B.

IRIS (International Research Institute of Stavanger), 2015. Report of the assessment of the severity of methane release from gas hydrate extraction activities and potential impacts on deep-sea ecosystems. MIDAS Deliverable Report 5.1, MIDAS project, European Commission Seventh Framework Programme, 13 pp.

Jia, H., 2017. China opens up new energy front as it succeeds in tapping gas hydrates. Chemistry World, https://www.chemistryworld.com/news/china-opens-up-new-energy-front-as-it-taps-gas-hydrates/3007662.article, retrieved 2017-07-12.

Judd, A.G., and Hovland, M., 1992. The evidence of shallow gas in marine sediments. Continental Shelf Research 12, pp. 1081-1095, doi:10.1016/0278-4343(92)90070-Z.

Judd, A.G., 2003. The global importance and context of methane escape from the seabed. Geo-Marine Letters 23, pp. 147-154 doi:10.1007/s00367-003-0136-z.

Judd, A., and Hovland, M., 2007. Seabed Fluid Flow: The Impact on Geology, Biology and the Marine Environment. Cambridge University Press, Cambridge.

Ker, S., and Riboulot, V., 2015. GHASS Cruise Report. Ifremer, France, 53 pp.

Kim, A.R., Cho, G.C., Song, K.I., and Kim, S.J., 2014. Settlement prediction in the Ulleung Basin due to gas hydrate production. Offshore Technology Conference, OTC25308-MS, Houston, Texas, USA, 5-8 May 2014, 10 pp.

Klaucke, I., Sahling, H., Bürk, D., Weinrebe, W., and Bohrmann, G., 2005. Mapping deep-water gas emissions with sidescan sonar. Eos Transactions 86, pp. 341-352.

Klaucke, I., Sahling, H., Weinrebe, W., Blinova, V., Bürk, D., Lursmanashvili, N., and Bohrmann, G., 2006. Acoustic investigation of cold seeps offshore Georgia, eastern Black Sea. Marine Geology 231, pp. 51-67, doi:10.1016/j.margeo.2006.05.011.

Klaucke, I., Masson, D.G., Petersen, C.J., Weinrebe, W., and Ranero, C.R., 2008. Multifrequency geoacoustic imaging of fluid escape structures offshore Costa Rica: Implications for the quantification of seep processes. Geochemistry Geophysics Geosystems 9, Q04010, doi:10.1029/2007GC001708.

Klaucke, I., Weinrebe, W., Petersen, C.J., and Bowden, D., 2010. Temporal variability of gas seeps offshore New Zealand: Multi-frequency geoacoustic imaging of the Wairarapa area, Hikurangi margin. Marine Geology 272, pp. 49-58, doi:10.1016/j.margeo.2009.02.009.

Klaucke, I., Weinrebe, W., Linke, P., Klaeschen, D., and Bialas, J., 2012. Sidescan sonar imagery of widespread fossil and active cold seeps along the central Chilean continental margin. Geo-Marine Letters 32, pp. 489-499, doi:10.1007/s00367-012-0283-1.

Klaucke, I., Berndt, C., Crutchley, G.J., Chi, W.C., Lin, S., and Muff, S., 2016. Fluid venting and seepage at accretionary ridges: the Four Way Closure Ridge offshore SW Taiwan. Geo-Marine Letters 36, pp. 165-174, doi:10.1007/s00367-015-0431-5.

Koch, S., Berndt, C., Bialas, J., Haeckel, M., Crutchley, G. J., and Papenberg, C., 2015. Gas-controlled seafloor doming. Geology 43, pp. 571-57, doi:10.1130/G36596.1.

Koch, S., Schroeder, H., Haeckel, M., Berndt, C., Bialas, J., Papenberg, C., Klaeschen, D., and Plaza-Faverola, A., 2016. Gas migration through Opouawe Bank at the Hikurangi margin offshore New Zealand. Geo-Marine Letters 36, pp. 187-196, doi:10.1007/s00367-016-0441-y.

Konno, Y., Fujii, T., Sato, A., Akamine, K., Naiki, M., Masuda, Y., Yamamoto, K., and Nagao, J., 2017. Key findings of the world's first offshore methane hydrate production test off the coast of Japan: Toward future commercial production. Energy & Fuels 31, pp. 2607-2616, doi:10.1021/acs.energyfuels.6b03143.

Körber, J.H., Sahling, H., Pape, T., dos Santos Ferreira, C., MacDonald, I., and Bohrmann, G., 2014. Natural Oil seepage at Kobuleti Ridge, eastern Black Sea. Marine and Petroleum Geology 50, pp. 68-82, doi:10.1016/j.marpetgeo.2013.11.007.

Krabbenhoeft, A., Bialas, J., Klaucke, I., Crutchley, G., Papenberg, C., and Netzeband, G.L., 2013. Patterns of subsurface fluid-flow at cold seeps: The Hikurangi Margin, offshore New Zealand. Marine and Petroleum Geology 39, pp. 59-73, doi:10.1016/j.marpetgeo.2012.09.008.

Krastel, S., Spiess, V., Ivanov, M., Weinrebe, W., Bohrmann, G., Shashkin, P., and Heidersdorf, F., 2003. Acoustic investigations of mud volcanoes in the Sorokin Trough, Black Sea. Geo-Marine Letters 23, pp.230-238, doi:10.1007/s00367-003-0143-0.

Küçük, H.M., Dondurur, D., Özel, Ö., Sınayuç, Ç., Merey, S., Parlaktuna, M., Çifçi, G., 2015. Acoustic investigations of gas and gas hydrate formations, offshore southwestern Black Sea. AGU Fall Meeting, San Francisco, USA, 14-18 December 2015.

Kvalstad, T.J., 2007. What is the current "best practice" in offshore geohazard investigations? A state-of-the-art review. Offshore Technology Conference, OTC18545, Houston, Texas, USA, 30 April - 3 May 2007, 14 pp.

Kvalstad, T.J., Yamamoto, K., Noguchi, S., Uchida, S., and Soda, K., 2011. Effect of gas hydrate production on seabed stability in the eastern Nankai Trough area. Proceedings of the 7th International Conference on Gas Hydrates (ICGH), Edinburgh, Scotland, 17-21 July 2011, 10 pp.

Kvenvolden, K.A., 1988. Methane hydrate – a major reservoir of carbon in the shallow geosphere? Chemical Geology 71, pp. 41-51, doi:10.1016/0009-2541(88)90104-0.

Kvenvolden, K., 1995. A review of the geochemistry of methane in natural gas hydrate. Organic Geochemistry 23, pp. 997-1008, doi:10.1016/0146-6380(96)00002-2.

Kvenvolden, K.A., and Grantz, A., 1989. Gas hydrates of the Arctic region. In: Grantz, A., Johnson, L., and Sweeney, J.F. (Eds.), The Arctic Ocean Region: The Geology of North America. Geological Society of America, Washington DC, USA, pp. 539-549.

Kvenvolden, K.A., and Lorenson, T.D., 2001. The global occurrence of natural gas hydrate. Geophysical Monograph 124, pp. 3-16, doi:10.1029/GM124p0003.

Lee, M.W., and Collett, T.S., 2009. Gas hydrate saturations estimated from fractured reservoir at Site NGHP-01-10, Krishna-Godavari Basin, India. Journal of Geophysical Research: Solid Earth 114, B07102, doi:10.1029/2008JB006237.

Lee, S.-Y., and Holder, G. D., 2001. Methane hydrates potential as a future energy source. Fuel Processing Technology 71, pp. 181-186, doi:10.1016/S0378-3820(01)00145-X.

Lee, S., Lee, Y., Lee, J., Lee, H., and Seo, Y., 2013. Experimental verification of methane–carbon dioxide replacement in natural gas hydrates using a differential scanning calorimeter. Environmental Science & Technology 47, pp. 13184-13190, doi:10.1021/es403542z.

Leifer, I., and Judd, A.G., 2002. Oceanic methane layers: the hydrocarbon seep bubble deposition hypothesis. Terra Nova 14, pp. 417-424, doi:10.1046/j.1365-3121.2002.00442.x.

Leifer, I., Boles, J.R., Luyendyk, B.P., and Clark, J.F., 2004. Transient discharges from marine hydrocarbon seeps: spatial and temporal variability. Environmental Geology 46, pp. 1038-1052, doi:10.1007/s00254-004-1091-3.

Lericolais, G., Bulois, C., Gillet, H., and Guichard, F., 2009. High frequency sea level fluctuations recorded in the Black Sea since the LGM. Global and Planetary Change 66, pp. 65-75, doi:10.1016/ j.gloplacha.2008.03.010.

Løseth, H., Gading, M., and Wensaas, L., 2009. Hydrocarbon leakage interpreted on seismic data. Marine and Petroleum Geology 26, pp. 1304-1319, doi:10.1016/j.marpetgeo.2008.09.008.

Lüdmann, T., Wong, H.K., Konerding, P., Zillmer, M., Petersen, J., and Flüh, E., 2004. Heat flow and quantity of methane deduced from a gas hydrate field in the vicinity of the Dnieper Canyon, northwestern Black Sea. Geo-Marine Letters 24, pp. 182-193, doi:10.1007/s00367-004-0169-y.

Luo, M., Dale, A.W., Haffert, L., Haeckel, M., Koch, S., Crutchley, G., De Stigter, H., Chen, D., and Greinert, J., 2016. A quantitative assessment of methane cycling in Hikurangi Margin sediment (New Zealand) using geophysical imaging and biogeochemical modeling. Geochemistry, Geophysics, Geosystems 17, 10 pp., doi: 10.1002/2016GC006643

Makogon, Y.F., Trebin, F.A., Trofimuk, A.A., Tsarev, V.P., and Cherskiy, N.V., 1972. Detection of a pool of natural gas in a solid (hydrated gas) state. Transactions (Doklady) of the USSR Academy of Sciences, Earth Science Sections 196, pp. 197-200.

Makogon, Y.F., 1997. Hydrates of Hydrocarbons. PennWell Publishing Company, Tulsa, USA.

Manheim, F.T., and Schug, D.M., 1978. Interstitial waters of Black Sea cores. Initial Reports of the Deep Sea Drilling Project 42, Part 2, pp. 637-651.

Maslin, M., Owen, M., Betts, R., Day, S., Dunkley Jones, T., and Ridgwell, A., 2010. Gas hydrates: past and future geohazards? Philosophical Transactions of the Royal Society A 368, pp. 2369-2392, doi:10.1098/ rsta.2010.0065.

Mathews, M.A., and von Huene, R., 1985. Site 570 methane hydrate zone. In: Orlofsky, S. (Ed.), Initial Reports of the Deep Sea Drilling Project 84, U.S. Government Printing Office, Washington, pp. 773-790.

McGinnis, D.F., Greinert, J., Artemov, Y., Beaubien, S.E., and Wüest, A., 2006. Fate of rising methane bubbles in stratified waters: How much methane reaches the atmosphere? Journal of Geophysical Research: Oceans 111, C09007, doi: 10.1029/2005JC003183.

Mekala, P., Babu, P., Sangwai, J.S., and Linga, P., 2014. Formation and dissociation kinetics of methane hydrates in seawater and silica sand. Energy & Fuels 28, pp. 2708-2716, doi:10.1021/ef402445k.

Merey, S., and Sinayuc, C., 2016a. Investigation of gas hydrate potential of the Black Sea and modelling of gas production from a hypothetical Class 1 methane hydrate reservoir in the Black Sea conditions. Journal of Natural Gas Science and Engineering 29, pp. 66-79, doi: 10.1016/j.jngse.2015.12.048.

Merey, S., and Sinayuc, C., 2016b. Experimental set-up design for gas production from the Black Sea gas hydrate reservoirs. Journal of Natural Gas Science and Engineering 33, pp. 162-185, doi:10.1016/ j.jngse.2016.04.030

Micallef, A., Masson, D.G., Berndt, C., and Stow, D.A.V., 2009. Development and mass movement processes of the north-eastern Storegga Slide. Quaternary Science Reviews 28, pp. 433-448, doi:10.1016/ j.quascirev.2008.09.026.

Minshull, T.A., Muller, M.R., Robinson, C.J., White, R.S., and Bickle, M.J., 1998. Is the oceanic Moho a serpentinization front? Geological Society, London, Special Publications 148, pp. 71-80, doi:10.1144/GSL.SP.1998.148.01.05.

Minshull, T.A., and Keddie, A., 2010. Measuring the geotherm with gas hydrate bottom-simulating reflectors: a novel approach using three-dimensional seismic data from the eastern Black Sea. Terra Nova 22, pp. 131-136, doi:10.1111/j.1365-3121.2010.00926.x.

Moridis, G.J., Collett, T.S., Pooladi-Darvish, M., Hancock, S., Santamarina, C., Boswell, R., Kneafsey, T., Rutqvist, J., Kowalsky, M.B., Reagan, M.T., Sloan, E.D., Kum, A.K., Koh, C.A., 2011. Challenges, uncertainties, and issues facing gas production from gas-hydrate deposits. SPE Reservoir Evaluation and Engineering 14, pp. 76-112.

Moridis, G.J., Collett, T.S., Boswell, R., Hancock, S., Rutqvist, J., Santamarina, C., Kneafsey, T., Reagan, M.T., Darvish, M.P., Kowalsky, M., Sloan, E.D., and Coh, C., 2013. Gas hydrates as a potential energy source: State of knowledge and challenges. In: Lee, W.J. (Ed.), Advanced Biofuels and Bioproducts. Springer, New York, pp. 977-1033, doi:10.1007/978-1-4614-3348-4_37.

Muratov, M.V., Neprochnox, Y.P., Ross, D.A., and Trimonis, E.S., 1978. Basic features of the Black Sea Late Cenozoic history based on results of deep-sea drilling. Initial Reports of the Deep Sea Drilling Project 42, Part 2, pp. 1141-1148.

Myshakin, E.M., Gaddipati, M., Rose, K., and Anderson, B.J., 2012. Numerical simulations of depressurization-induced gas production from gas hydrate reservoirs at the Walker Ridge 313

site, northern Gulf of Mexico. Marine and Petroleum Geology 34, pp. 169-185, doi:10.1016/j.marpetgeo.2011.09.001.

Naudts, L., Greinert, J., Artemov, Y. G., Staelens, P., Poort, J., Van Rensbergen, P., and De Batist, M., 2006. Geological and morphological setting of 2778 methane seeps in the Dnepr paleo-delta, northwestern Black Sea. Marine Geology 227, pp. 177–199, doi:10.1016/j.margeo.2005.10.005.

Naudts, L., Greinert, J., Artemov, Y., Beaubien, S.E., Borowski, C., and de Batist, M., 2008. Anomalous sea-floor backscatter patterns in methane venting areas, Dnepr paleo-delta, NW Black Sea. Marine Geology 251, pp. 253-267, doi:10.1016/j.margeo.2008.03.002.

Naudts, L., De Batist, M., Greinert, J., and Artemov, Y., 2009. Geo- and hydro-acoustic manifestations of shallow gas and gas seeps in the Dnepr paleodelta, northwestern Black Sea. The Leading Edge 28, pp. 1030-1040, doi:10.1190/1.3236372.

Netzeband, G.L., Hübscher, C.P., Gajewski, D., Grobys, J.W.G., and Bialas, J., 2005. Seismic velocities from the Yaquina forearc basin off Peru: evidence for free gas within the gas hydrate stability zone. International Journal of Earth Sciences 94, pp. 420-432, doi:10.1007/s00531-005-0483-2.

Nikishin, A.M., Korotaev, M.V., Ershov, A.V., and Brunet, M.F., 2003. The Black Sea basin: tectonic history and Neogene-Quaternary rapid subsidence modeling. Sedimentary Geology 156, pp. 149-168, doi:10.1016/S0037-0738(02)00286-5.

Özsoy, E., and Ünlüata, Ü., 1997. Oceanography of the Black Sea: a review of some recent results. Earth-Science Reviews 42, pp. 231-272, doi:10.1016/S0012-8252(97)81859-4.

Pape, T., Bahr, A., Rethemeyer, J., Kessler, J.D., Sahling, H., Hinrichs, K.U., Klapp, S.A., Reeburgh, W.S., and Bohrmann, G., 2010. Molecular and isotopic partitioning of low-molecular-weight hydrocarbons during migration and gas hydrate precipitation in deposits of a high-flux seepage site. Chemical Geology 269, pp. 350-363, doi:10.1016/j.chemgeo.2009.10.009.

Papenberg, C., Krabbenhoeft, A., Klaeschen, D., and Bialas, J., 2013. Distribution of free gas and 3D mirror image structures beneath Sevastopol mud volcano, Black Sea, from 3D high resolution wide-angle seismic data. AGU Fall Meeting, San Francisco, USA, 9-13 December 2013.

Park, K.P., Bahk, J.J., Kwon, Y., Kim, G.Y., Riedel, M., Holland, M., Schultheiss, P., Rose, K., and the UBGH-1 Scientific Party, 2008. Korean National Program expedition confirms rich gas hydrate deposits in the Ulleung basin, East Sea. Fire in the Ice (US DOE-NETL newsletter), pp. 6-9.

Paull, C.K., Matsumoto, R., and Wallace, P.J., 1996. Proceedings of the ODP, Initial Reports 164. College Station, Texas, USA, 623 pp., doi:10.2973/odp.proc.ir.164.1996.

Paull, C.K., Normark, W.R., Ussler III, W., Caress, D.W., and Keaten, R., 2008. Association among active seafloor deformation, mound formation, and gas hydrate growth and accumulation within the seafloor of the Santa Monica Basin, offshore California. Marine Geology 250, pp. 258-275, doi:10.1016/ j.margeo.2008.01.011.

Piñero E, Marquardt M, Hensen C, Haeckel M, and Wallmann K, 2013. Estimation of the global inventory of methane hydrates in marine sediments using transfer functions. Biogeosciences 10, pp. 959–975, doi:10.5194/bg-10- 959-2013

Plaza-Faverola, A., Bünz, S., and Mienert, J., 2011. Repeated fluid expulsion through sub-seabed chimneys offshore Norway in response to glacial cycles. Earth and Planetary Science Letters 305, pp. 297-308, doi:10.1016/j.epsl.2011.03.001.

Plaza-Faverola, A., Bünz, S., and Mienert, J., 2012. The free gas zone beneath gas hydrate bearing sediments and ist link to fluid flow: 3-D seismic imaging offshore mid-Norway. Marine Geology 291-294, pp. 211-226, doi:10.1016/j.margeo.2011.07.002.

Poort, J., Vassilev, A., and Dimitrov, L., 2005. Did postglacial catastrophic flooding trigger massive changes in the Black Sea gas hydrate reservoir? Terra Nova 17, pp. 135–140, doi:10.1111/j.1365-3121.2005.00599.x.

Popescu, I., De Batist, M., Lericolais, G., Nouzé, H., Poort, J., Panin, N., Versteeg, W., and Gillet, H., 2006. Multiple bottom-simulating reflections in the Black Sea: Potential proxies of past climate conditions. Marine Geology 227, pp. 163-176, doi:10.1016/j.margeo.2005.12.006.

Popescu, I., Lericolais, G., Panin, N., De Batist, M., and Gillet, H., 2007. Seismic expression of gas and gas hydrates across the western Black Sea. Geo-Marine Letters 27, pp. 173-183, doi:10.1007/s00367-007-0068-0.

Popescu, I., Panin, N., Jipa, D., Lericolais, G., and Ion, G., 2015. Submarine canyons of the Black Sea basin with a focus on the Danube Canyon. In: Briand, F. (Ed.), CIESM Monograph 47, Submarine canyon dynamics in the Mediterranean and tributary seas – An integrated geological, oceanographic and biological perspective. CIESM Publisher, Monaco, pp. 103-121.

Posewang, J., and Mienert, J., 1999. The enigma of double BSRs: indicators for changes in the hydrate stability field? Geo-Marine Letters 19, pp. 157-163, doi:10.1007/s003670050103.

Reeburgh, W.S., Ward, B.B., Whalen, S.C., Sandbeck, K.A., Kilpatrick, K.A., and Kerkhof, L.J., 1991. Black Sea methane geochemistry. Deep-Sea Research 38, pp. S1189-S1210, doi:10.1016/S0198-0149(10)80030-5.

Regnier, P., Dale, A.W., Arndt, S., LaRowe, D.E., Mogollon, J., and Van Capellen, P., 2011. Quantitative analysis of anaerobic oxidation of methane (AOM) in marine sediments: A modeling perspective. Earth-Science Reviews 106, pp. 105-130, doi:10.1016/j.earscirev.2011.01.002.

Reilinger, R.E., McClusky, S.C., Oral, M.B., King, R.W., Toksoz, M.N., Barka, A.A., Kinik, I., and Sanli, I., 1997. Global Positioning System measurements of present-day crustal movements in the Arabia-Africa-Eurasia plate collision zone. Journal of Geophysical Research: Solid Earth 102, pp. 9983-9999, doi:10.1029/96JB03736.

Rehder, G., Brewer, P.W., Peltzer, E.T., and Friedrich, G., 2002. Enhanced lifetime of methane bubble streams within the deep ocean. Geophysical Research Letters 29, pp. 1731-1734, doi:10.1029/2001GL013966.

Reitz, A., Pape, T., Haeckel, M., Schmidt, M., Berner, U., Scholz, F., Liebetrau, V., Aloisi, G., Weise, S.M., and Wallmann, K., 2011. Sources of fluids and gases expelled at cold seeps offshore Georgia, eastern Black Sea. Geochimica et Cosmochimica Acta 75, pp. 3250-3268, doi:10.1016/j.gca.2011.03.018.

Riboulot, V., Sultan, N., Imbert, P., and Ker, S., 2016. Initiation of gas-hydrate pockmark in deep-water Nigeria: Geo-mechanical analysis and modelling. Earth and Planetary Science Letters 434, pp. 252-263, doi:10.1016/j.epsl.2015.11.047.

Rice, D.D., 1992. Controls, habitat, and resource potential of ancient bacterial gas. In: Vially, R. (Ed.), Bacterial Gas. Editions Technip, Paris, pp. 91-118.

Robinson, A.G., Rudat, J.H., Banks, C.J., and Wiles, R.L.F., 1996. Petroleum geology of the Black Sea. Marine and Petroleum Geology 13, pp. 195-223, doi:10.1016/0264-8172(95)00042-9.

Römer, M., Sahling, H., Pape, T., Bahr, A., Feseker, T., Wintersteller, P., and Bohrmann, G., 2012. Geological control and magnitude of methane ebullition from a high-flux seep area in the Black Sea – the Kerch seep area. Marine Geology 319-322, pp. 57-74, doi: 10.1016/j.margeo.2012.07.005.

Römer, M., Torres, M., Kasten, S., Kuhn, G., Graham, A.G.C., Mau, S., Little, C.T.S., Linse, K., Pape, T., Geprägs, P., Fischer, D., Wintersteller, P., Marcon, Y., Rethemeyer, J., Bohrmann, G., and shipboard scientific party ANT-XXIX/4, 2014. First evidence of widespread active methane seepage in the Southern Ocean, off the sub-Antarctic island of South Georgia. Earth and Planetary Science Letters 403, pp. 166-177, doi:10.1016/j.epsl.2014.06.036.

Ruppel, C., 2007. Tapping methane hydrates for unconventional natural gas. Elements 3, pp. 193-199, doi:10.2113/gselements.3.3.193.

Rutqvist, J., Moridis, G.J., Grover, T., and Collett, T., 2009. Geomechanical response of permafrost-associated hydrate deposits to depressurization-induced gas production. Journal of Petroleum Science and Engineering 67, pp. 1-12, doi:10.1016/j.petrol.2009.02.013.

Ryan, W.B.F., Pitman III, W.C., Major, C.O., Shimkus, K., Moskalenko, V., Jones, G.A., Dimitrov, P., Gorür, N., Sakinc, M., and Yüce, H., 1997. An abrupt drowning of the Black Sea Shelf. Marine Geology 138, pp. 119-126, doi:10.1016/S0025-3227(97)00007-8.

Saeki, T., Fujii, T., Inamori, T., Kobayashi, T., Hayashi, Nagakubo, S., and Takano, O., 2008. Extraction of methane hydrate concentrated zone for resource assessment in the Eastern Nankai Trough, Japan. Offshore Technology Conference, OTC19311, Houston, Texas, USA, 5-9 May 2008, 8p.

Sahling, H., Bohrmann, G., Spiess, V., Bialas, J., Breitzke, M., Ivanov, M., Kasten, S., Krastel, S., and Schneider, R., 2008. Pockmarks in the Northern Congo Fan area, SW Africa: Complex seafloor features shaped by fluid flow. Marine Geology 249, pp. 206-225, doi:10.1016/j.margeo.2007.11.010.

Sahling, H., Bohrmann, G., Artemov, Y.G., Bahr, A., Brüning, M., Klapp, S.A., Klaucke, I., Kozlova, E., Nikolovska, A., Pape, T., Reitz, A., and Wallmann, K., 2009. Vodyanitskii mud volcano, Sorokin trough, Black Sea: Geological characterization and quantification of gas bubble streams. Marine and Petroleum Geology 26, pp. 1799-1811, doi:10.1016/j.marpetgeo.2009.01.010.

Sarkar, S., Berndt, C., Minshull, T.A., Westbrook, G.K., Klaeschen, D., Masson, D.G., Chabert, A., and Thatcher, K.E., 2012. Seismic evidence for shallow gas-escape features associated with a retreating gas hydrate zone offshore west Svalbard. Journal of Geophysical Research: Solid Earth 117, B09102, doi: 10.1029/2011JB009126.

Schmale, O., Beaubien, S.E., Rehder, G., Greinert, J., and Lombardi, S., 2010. Gas seepage in the Dnepr paleo-delta area (NW-Black Sea) and its regional impact on the water column methane cycle. Journal of Marine Systems 80, pp. 90-100, doi:10.1016/j.marsys.2009.10.003.

Schoell, M., 1988. Multiple origins of methane in the earth. Chemical Geology 71, pp. 1-10, doi:10.1016/0009-2541(88)90101-5.

Shillington, D.J., White, N., Minshull, T.A., Edwards, G.R.H., Jones, S.M., Edwards, R.A., and Scott, C.L., 2008. Cenozoic evolution of the eastern Black Sea: A test of depth-dependent stretching models. Earth and Planetary Science Letters 265, pp. 360-378, doi:10.1016/j.epsl.2007.10.033.

Shipley, T. H., Houston, M. H., and Buffler, R. T., 1979. Seismic evidence for widespread occurrence of possible gas-hydrate horizons on continental slopes and rises. AAPG Bulletin 63, pp. 2204-2213.

Sloan, E.D., and Koh, C.A., 2007. Clathrate Hydrates of Natural Gases (Third Edition). CRC Press.

Soulet, G., Delaygue, G., and Vallet-Coulomb, C., 2010. Glacial hydrologic conditions in the Black Sea reconstructed using geochemical pore water profiles. Earth and Planetary Science Letters 296, pp. 57-66, doi:10.1016/j.epsl.2010.04.045.

Stakes, D.S., Orange, D., Paduan, J.B., Salamy, K.A., and Maher, N, 1999. Cold-seeps and authigenic carbonate formation in Monterey Bay, California. Marine Geology 159, pp. 93-109, doi:10.1016/S0025-3227(98)00200-X.

Starostenko, V.I., Rusakov, O.M., Shnyukov, E.F., Kobolev, V.P., and Kutas, R.I., 2010. Methane in the northern Black Sea: characterization of its geomorphological and geological environments. Geological Society, London, Special Publications 340, pp. 57-75, doi:10.1144/SP340.5.

Suess, E., Torres, M.E., Bohrmann, G., Collier, R.W., Greinert, J., Linke, P., Rehder, G., Trehu, A., Wallmann, K., Winckler, G., and Zuleger, E., 1999. Gas hydrate destabilization: enhanced dewatering, benthic material turnover and large methane plumes at the Cascadia convergent margin. Earth and Planetary Science Letters 170, pp. 1-15, doi:10.1016/S0012-821X(99)00092-8.

Tacket, J., and Puckette, J., 2012. Lithologic controls of pressure distribution in sedimentary basins. AAPG Search and Discovery Article #40898, 58 pp.

Talukder, A.R., 2012. Review of submarine cold seep plumbing systems: leakage to seepage and venting. Terra Nova 24, pp. 255-272, doi: 10.1111/j.1365-3121.2012.01066.x.

Teichert, B.M.A., Eisenhauer, A., Bohrmann, G., Haase-Schramm, G., Bock, A., and Linke, P., 2003. U/Th systematics and ages auf authigenic carbonates from Hydrate Ridge, Cascadia Margin: recorders of fluid flow variations. Geochimica et Cosmochimica Acta 67, pp. 3845-3857, doi:10.1016/S0016-7073(03)00128-5.

Tinivella, U., and Giustiniani, M., 2013. Variations in BSR depth due to gas hydrate stability versus pore pressure. Global and Planetary Change 100, pp. 119-128, doi:10.1016/j.gloplacha.2012.10.012.

Tissot, B.P., and Welte, D.H., 1994. Petroleum Formation and Cccurrence (Second Edition). Springer, New York.

Tsuji, Y., Namikawa, T., Fujii, T., Hayashi, M., Kitamura, R., Nakamizu, M., Ohbi, K., Saeki, T., Yamamoto, K., Inamori, T., Oikawa, N., Shimizu, S., Kawasaki, M., Nagakubo, S., Matsushima, J., Ochiai, K., and Okui, T., 2009. Methane-hydrate occurrence and distribution in the eastern Nankai Trough, Japan: findings of the Tokai-oki to Kumano-nada methane-hydrate drilling program. In: Collett, T., Johnson, A., Knapp, C., Boswell, R. (Eds.), Natural Gas Hydrates-Energy Resource Potential and Associated Geologic Hazards. AAPG Memoir 89, pp. 228-246, doi:10.1306/13201103M893129.

Tugolesov, D.A., Gorshkov, A.S., Meisner, L.B., Soloviev, V., and Khakhalev, E.M., 1985. Tectonics of the Mesozoic-Cenozoik deposits of the Black Sea (in Russian). Nedra, Moscow.

Urlaub, M., Talling, P.J., and Masson, D.G., 2013. Timing and frequency of large submarine landslides: implications for understanding triggers and future geohazard. Quaternary Science Reviews 72, pp. 63-82, doi:10.1016/j.quascirev.2013.04.020.

Vanneste, M., Guidard, S., and Mienert, J., 2005. Bottom-simulating reflections and geothermal gradients across the western Svalbard margin. Terra Nova 17, pp. 510-516, doi:10.1111/j.1365-3121.2005.00643.x.

Vanneste, M., Sultan, N., Garziglia, S., Forsberg, C.F., and L'Heureux, J.S., 2014. Seafloor instabilities and sediment deformation processes: The need for integrated, multi-disciplinary investigations. Marine Geology 352, pp. 183-214, doi:10.1016/j.margeo.2014.01.005.

Vassilev, A., and Dimitrov, L., 2002. Spatial and quantity evaluation of the Black Sea gas hydrates. Geologiya I Geofizika 43, pp. 672–684.

Wagner-Friedrichs, M., 2007. Seafloor seepage in the Black Sea: Mud volcanoes, seeps and diapiric structures imaged by acoustic methods. PhD Thesis, University of Bremen, Bremen, 154 pp.

Wallmann, K., Pinéro, E., Burwicz, E.B., Haeckel, M., Hensen, C., Dale, A., and Ruepke, L., 2012. The global inventory of methane hydrate in marine sediments: a theoretical approach. Energies 5, pp. 2449-2498, doi:10.3390/en5072449.

Welhan, J., 1988. Origins of methane in hydrothermal systems. Chemical Geology 71, pp. 183-198, doi:10.1016/0009-2541(88)90114-3.

Westbrook, G.K., Exley, R., Minshull, T., Nouzé, H., Gailler, A., Jose, T., Ker, S., and Plaza-Faverola, A., 2008. High-resolution 3D seismic investigations of hydrate-bearing fluid-escape chimneys in the Nyegga region of the Vøring Plateau, Norway. Proceedings of the 6th International Conference on Gas Hydrates (ICGH 2008), Vancouver, British Columbia, Canada, 6-20 July 2008, 12 pp.

Whiticar, M.J., Faber, E., and Schoell, M., 1986. Biogenic methane formation in marine and freshwater environments: CO_2 reduction vs. acetate fermentation – isotope evidence. Geochimica et Cosmochimica Acta 50, pp. 693-709, doi:10.1016/0016-7037(86)90346-7.

Whiticar, M.J., 1999. Carbon and hydrogen isotope systematics of bacterial formation and oxidation of methane. Chemical Geology 161, pp. 291-314, doi:10.1016/S0009-2541(99)00092-3.

Wiese, K., and Kvenvolden, K.A., 1993. Introduction to microbial and thermal methane. U.S. Geological Survey Professional Paper 1570, pp. 13-20.

Wood, W.T., Gettrust, J.F., Chapman, N.R., Spence, G.D., and Hyndman, R.D., 2002. Decreased stability of methane hydrates in marine sediments owing to phase-boundary roughness. Nature 420, pp. 656-660, doi:10.1038/nature01261.

Wuebbles, D.J., and Hayhoe, K., 2002. Atmospheric methane and global change. Earth-Science Reviews 57, pp. 177-210, doi: 10.1016/S0012-8252(01)00062-9.

Yamamoto, K., and Dallimore, S., 2008. AURORA-JOGMEX-NRCAN Mallik 2006-2008 Gas Hydrate Research Project Progress. Fire in the Ice, Methane Hydrate Newsletter 2008, pp.1-5.

Yamamoto, K., Terao, Y., Fujii, T., Ikawa, T., Seki, M., Matsuzawa, M., and Kanno, T., 2014. Operational overview of the first offshore production test of methane hydrates in the Eastern Nankai Trough. Offshore Technology Conferency, OTC25243-MS, Houston, Texas, USA, 5-8 May 2014, 11 pp.

Zhao, J. F., Yu, T., Song, Y., Liu, D., Liu, W. G., Liu, Y., Yang, M. J., Ruan, X. K., and Li, Y. H., 2013. Numerical simulation of gas production from hydrate deposits using a single vertical well by depressurization in the Qilian Mountain permafrost, Qinghai-Tibet Plateau, China. Energy 52, pp. 308–319, doi:10.1016/ j.energy.2013.01.066.

Zhou, M., Soga, K., Xu, E., Uchida, S., and Yamamoto, K., 2014. Numerical study on Eastern Nankai Trough gas hydrate production test. Offshore Technology Conference, OTC25169, Houston, Texas, USA, 5-8 May 2014, 19 pp.

2. On the origin of multiple BSRs in the Danube deep-sea fan, Black Sea

Timo Zander[a], Matthias Haeckel[a], Christian Berndt[a], Wu-Cheng Chi[b], Ingo Klaucke[a], Jörg Bialas[a], Dirk Klaeschen[a], Stephanie Koch[c], Orhan Atgın[d]

[a]*GEOMAR Helmholtz Centre for Ocean Research Kiel, Germany*

[b]*Institute of Earth Sciences, Academia Sinica, Taipei, Taiwan*

[c]*ifb group, Köln, Germany*

[d]*Institute of Marine Sciences and Technology, Dokuz Eylül University, Izmir, Turkey*

Published in Earth and Planetary Science Letters 462 (2017), 15-25.

2.1 Abstract

High-resolution 2D seismic data reveal the character and distribution of up to four stacked bottom simulating reflectors (BSR) within the channel-levee systems of the Danube deep-sea fan. The theoretical base of the gas hydrate stability zone (GHSZ) calculated from regional geothermal gradients and salinity data is in agreement with the shallowest BSR. For the deeper BSRs, BSR formation due to overpressure compartments can be excluded because the necessary gas column would exceed the vertical distance between two overlying BSRs. We show instead that the deeper BSRs are likely paleo-BSRs caused by a change in pressure and temperature conditions during different limnic phases of the Black Sea. This is supported by the observation that the BSRs correspond to paleo seafloor horizons located in a layer between a buried channel-levee system and the levee deposits of the Danube channel. The good match of the observed BSRs and the BSRs predicted from deposition of these sediment layers indicates that the multiple BSRs reflect stages of stable sealevel lowstands possibly during glacial times. The observation of sharp BSRs several 10,000 of years but possibly up to 300,000 years after they have left the GHSZ demonstrates that either hydrate dissociation does not take place within this time frame or that only small amounts of gas are released that can be transported by diffusion. The gas underneath the previous GHSZ does not start to migrate for several thousands of years.

2.2 Introduction

A bottom simulating reflector (BSR) in seismic reflection data is a common indicator for gas hydrates in marine sediments. It is a distinct reflector that is caused by the negative impedance contrast between high-velocity gas-hydrate-bearing sediments above and low-velocity gas-bearing sediments below (Hyndman and Davis, 1992). It follows the base of the gas hydrate stability field and is consequently sub-parallel to the seafloor, frequently crosscutting reflectors and stratigraphic sequences. On many occasions, the BSR is patchy and discontinuous, depending on the geology, as gas is more likely trapped in highly permeable layers bounded by impermeable layers (Judd and Hovland, 2007). The gas hydrate stability field is controlled by pressure, temperature (bottom-water temperature and geothermal gradient in the sedimentary column), salinity, and gas composition (Shipley et al., 1979). In the marine environment, gas hydrates primarily consist of methane and dominantly form in crystallographic structure I (e.g. Sloan, 1998).

Studies showed that free-gas concentrations of only a few percent of the pore volume below the hydrate-bearing zone are sufficient to create a distinct BSR (e.g. Andreassen et al., 2007; Haacke et al., 2007, and references therein). Higher amounts of gas below a BSR may build up overpressure and lead to low-frequency events in seismic data, since high-frequency components of the seismic energy are absorbed by gas (Geletti and Busetti, 2011). The BSR can be used to derive information about the thermal state at its location, including the local and regional heat flow as well as thermal anomalies that are indicated by a BSR out of equilibrium due to higher or lower temperatures and fluid flow (Hyndman et al., 1992; Grevemeyer and Villinger, 2001; Wood et al., 2002).

The formation of two or more BSRs located a few tens of meters above each other has been reported from multiple sites (Foucher et al., 2002; Popescu et al., 2006; Geletti and Busetti, 2011), but their causes are not well understood. In most of these studies, the shallowest BSR is considered as the seismic manifestation of the current base of the gas hydrate stability zone (BGHSZ). The additional BSRs are usually weaker in amplitude and can occur with normal or reversed polarity compared to the seafloor reflection. Suggested explanations for the occurrence of multiple BSRs include different gas compositions (Geletti and Busetti, 2011), top and base of the free gas zone (Tinivella and Giustiniani, 2013), top and base of the hydrate-bearing zone (Posewang and Mienert, 1999), overpressure conditions below the depth of the theoretical BSR (Tinivella and Giustiniani, 2013), BSRs unrelated to gas and gas hydrates (Berndt et al., 2004), and BSRs representing former stable conditions for the BGHSZ (Foucher et al., 2002; Netzeband et al., 2005; Popescu et al., 2006). The latter are often related to distinct changes in the glacial-interglacial cycles (Bangs et al., 2005; Davies et al., 2012).

One of the most spectacular examples of multiple BSRs has been reported by Popescu et al. (2006) for the Danube deep-sea fan in the Black Sea, where up to four different BSRs with reversed amplitude are observed. These BSRs were observed in small segments of 2D seismic profiles that crossed a buried channel-levee system in water depths between 1000 m and 1500 m. All BSRs observed in that study are sub-parallel to the seafloor. Popescu et al. (2006) excluded that these BSRs reflect gas hydrate layers for different gas compositions as they are in sharp contradiction with the general background of the gas composition in the study area. The authors concluded that the deeper BSRs are paleo-BSRs corresponding to stable cold climatic episodes of the Black Sea. In their model, the authors calculated the depth of the BGHSZ based on the current seafloor for sealevel lowstands and bottom-water temperatures for different glacial periods, but they assumed a constant sedimentary overburden during the glacial cycles.

Here, we show that the deeper BSRs are unrelated to the current seafloor topography and that the sediment overburden was not constant during the last glacial cycles. We use new 2D seismic data to investigate the character and distribution of multiple bottom-simulating reflections in the vicinity of a channel-levee system in the Danube deep-sea fan. The multiple BSRs consequently require a new explanation taking into account the asymmetric deposition of the Danube levee sediments. Therefore, we tested two hypotheses that may explain the formation of the lower BSRs. The first hypothesis is that overpressured gas pockets exist below the BSR leading to different depths at which hydrates are stable. The second hypothesis is that the multiple BSRs are indeed paleo-BSRs caused by the complex interplay between bottom water temperature and sealevel variations and the depositional history of the Danube deep-sea fan during glacial periods.

2.3 Geological Setting

The deep-sea fans of the Danube and Dniepr rivers are located in the northwestern part of the Black Sea (Fig. 2.1) and began to develop at about 900 ka BP (Winguth et al., 2000). They are the result of sediment discharge by the rivers Danube, Dniepr, Dniestr and Bug during the last glaciation (Winguth et al., 2000; Popescu et al., 2001). The continental shelf is up to 120 km wide and the Danube deep-sea fan developed downslope of the shelf break at about 100 m water depth down to the abyssal plain in 2200 m water depth (Wong et al., 1997). The canyons and channels of the fan are characterized by erosional processes on the upper slope and by depositional processes on the middle and lower slope (Popescu et al., 2001). Eight seismic sequences were identified in the Danube deep-sea fan, consisting of stacked channel-levee systems, overbank sediments and mass transport deposits (Wong et al., 1997).

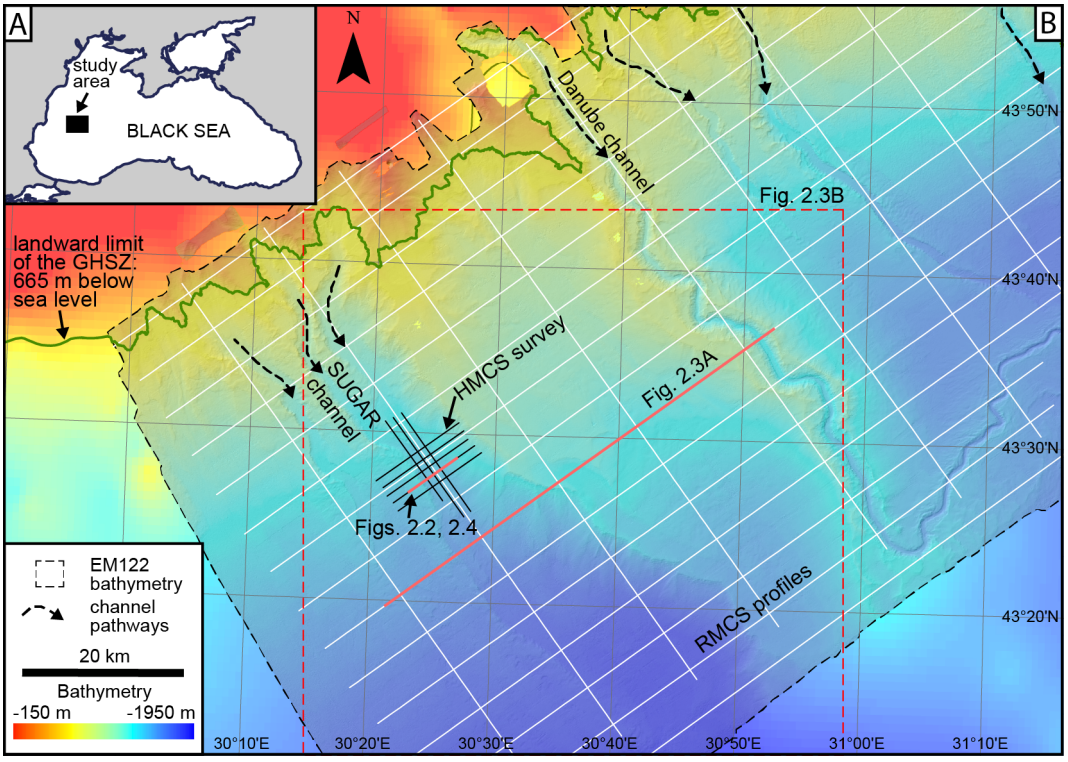

Fig. 2.1A: Location of the study area in the northwestern Black Sea. B: Overview map of the study area in the Danube deep-sea fan. GHSZ = gas hydrate stability zone, HMCS = 2D high-resolution multichannel seismic survey, RMCS = 2D regional multichannel seismic survey. Bathymetry and seismic data were acquired during R/V Maria S. Merian cruise MSM34 in 2013-2014.

The most recent active channel of the Danube fan is the Danube channel (Fig. 2.1), which was connected to the mouth of the Danube river by the Viteaz canyon at the shelf break (Popescu et al., 2001). The erosive Viteaz canyon terminates in a channel-levee system at about 800 m water depth (Lericolais et al., 2013) and developed during the last glacial period about 25 ka BP when the sealevel was up to 150 m lower than today (Winguth et al., 2000). As observed in other river fans of the northern hemisphere, the right-hand (western) levees are more pronounced than the left-hand (eastern) levees because of the Coriolis force (Popescu et al., 2001). Several older channels can be identified from the bathymetry such as a channel westwards of the Danube channel named SUGAR channel in this study (Fig. 2.1).

The upper limit of the gas hydrate stability zone (GHSZ), calculated for the observed bottom water temperature of 9 °C and a limnic pore water salinity of 3, is located in a water depth of 665 m. This is supported by the observation of numerous gas flares in water depths shallower than 665 m and much fewer gas flares at greater water depth in parts of the Danube fan (Bialas et al., 2014), and other areas of the Black Sea such as the Dniepr fan (Naudts et al., 2006) or the Don-Kuban fan (Römer et al., 2012). The expelled gas is primarily composed of methane of biogenic origin with concentrations of 99.1 – 99.9 % (Poort et al., 2005; Römer et al., 2012; Bialas et al., 2014).

2.4 Data and Methods

All data presented in this study were collected during cruise MSM34 onboard the German research vessel MARIA S. MERIAN from December 2013 to January 2014. A total of 26 2D regional multichannel seismic (RMCS) profiles were recorded using a 1050 m long streamer with 168 channels and a group distance of 6.25 m (Bialas et al., 2014). Sixteen profiles were acquired across the Danube fan with a spacing of 5 km and lengths of 45 – 110 km, and 10 profiles were acquired in downslope direction with a length of 40 – 70 km (Fig. 2.1).

Additionally, a 2D high-resolution multichannel seismic survey (HMCS) was acquired using a 62.6 m long streamer with 40 channels and a group distance of 1.56 m. Eight profiles were recorded over an area of two merging channel-levee systems: three profiles along the channel's direction (14 km length each) and five profiles across the channels (11 km length each). A 105/105 in^3 GI gun was used as a source for the RMCS survey, and a 45/45 in^3 GI gun was used for the HMCS survey. The shot interval was 5 s. After navigation processing, Omega (WesternGeco) was used for signal-processing, stacking, semblance picking (only RMCS) and true-amplitude time migration. No gain was applied during processing. The RMCS data has a CDP spacing of 3.12 m and a center frequency of 70 Hz, and the HMCS data has a CDP spacing of 1.56 m and a center frequency of 130 Hz. As the short streamers do not allow for semblance analysis of the HMCS data the velocity information of the RMCS profiles was extrapolated to the HMCS area. Both the RMCS and HMCS profiles were converted from time to depth domain using the RMCS-derived velocity information and cross-checked with P-wave velocities from ocean bottom seismometers that were available in the study area (Bialas et al., 2014).

Multibeam bathymetry data were collected during the entire RMCS survey using the ship-mounted EM122 echosounder (Kongsberg). The resulting map comprises a grid of 25 m x 25 m resolution.

In order to calculate an average temperature gradient, we assumed that the location of the shallowest BSR corresponds to the present BGHSZ. We fitted the methane hydrate phase boundary that was calculated using the SUGAR Toolbox (Kossel et al., 2013) for different temperature gradients in the interval between the seafloor and the shallowest BSR.

2.5 Results

The multiple BSRs were imaged by three different recording systems, which confirm their existence more than 10 years after their discovery as described by Popescu et al. (2006). This observation also rules out that the BSRs are ephemeral features, or the product of incorrect processing or artifacts.

2.5.1 Character and distribution of multiple BSRs

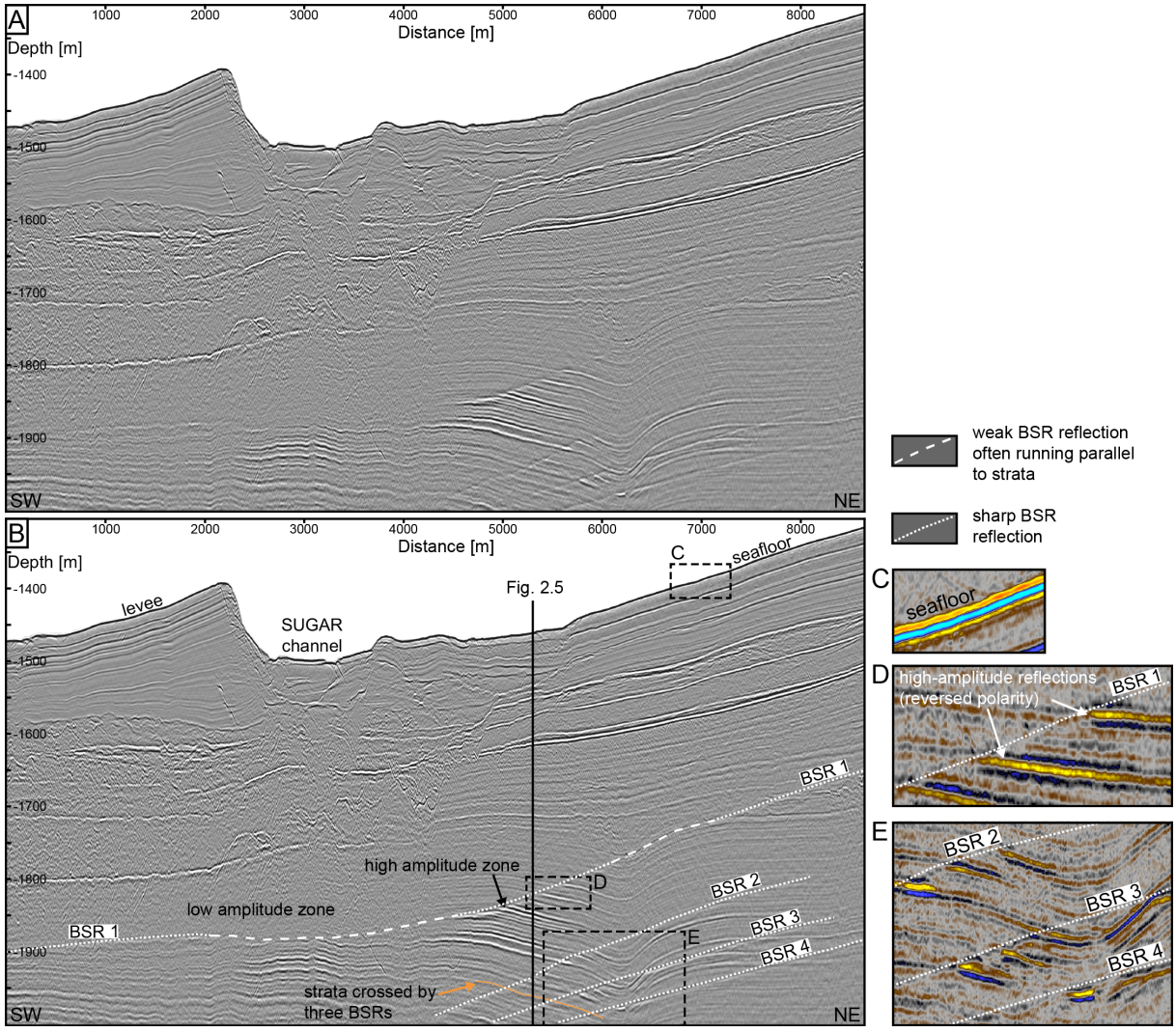

Fig. 2.2 A: 2D HMCS line 1107 across the SUGAR channel-levee system. The location is shown in Fig. 2.1. B: Interpreted section showing the general character of the four stacked multiple BSRs. C-E: Insets with different colour scale highlight the positive polarity of the seafloor (C) and the negative polarities of the reflections underneath the shallowest BSR 1 (D) and BSRs 2-4 (E).

The shallowest BSR occurs in depths of about 320-380 m below the seafloor and generally runs parallel to the seafloor. It can be identified in large patches throughout the Danube deep-sea fan, as already observed in previous studies (Popescu et al., 2006; Bialas et al., 2014).

The reflection amplitudes are generally low in an almost transparent seismic facies above the BSR, while they are high and of reversed polarity below the BSR (Fig. 2.2C, D). The appearance of the BSR is continuous and sharp where it crosscuts strata (Fig. 2.2B). Where it is parallel to the strata, the BSR is characterized by an abrupt amplitude increase with depth. The strongest amplitudes below the BSR are observed underneath the eastern levee, where several high-amplitude reflections pass from below the BSR into the transparent zone while undergoing a phase reversal at the BSR (Fig. 2.2D). The observed increased amplitudes below the BSR are often limited to individual reflectors that underlie a reflector of weaker amplitude (Fig. 2.2D).

Three additional BSRs are observed in the MCS data, named BSR 2-4 from top to bottom, and underlying the shallowest BSR described above (Fig. 2.2B, E). These BSRs are generally weaker in amplitude compared to the shallowest BSR, but they also represent a sharp and continuous boundary towards increased amplitudes below. Each of the additional BSRs shows reversed polarity compared to the seafloor. Some BSRs cross the same strata (Fig. 2.2B) while they exhibit slightly varying individual dips.

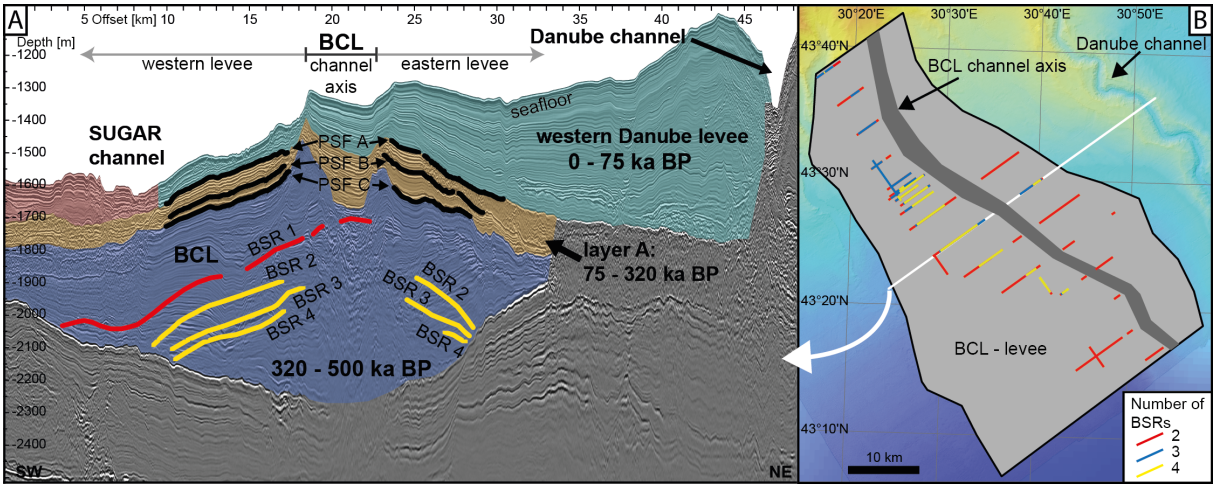

Fig. 2.3 A: 2D RMCS line 09 across the SUGAR channel (red unit) and the western Danube channel levee (green unit) in the northeast. A buried channel-levee system (BCL) is identified in the subsurface (blue unit), underneath layer A (brown unit). The multiple BSRs (yellow lines) are solely observed in the levees of the BCL. Time frames for the deposition of the different facies units are adapted from the interpretation of Winguth et al. (2000) (Figure 4 in their study). Three paleo seafloors were defined for the modelling of the BGHSZ under paleo conditions (black lines PSF A-C). B: Extent of the BCL based on seismic data and highlighting the occurrence of more than one BSR. Locations of A and B are shown in Fig. 2.1. An uninterpreted version of the seismic section is presented in the Supplementary material.

The stack of BSRs 2-4 is only observed in the well-stratified levee deposits of a buried channel-levee system (BCL) identified in the subsurface (Fig. 2.3). The BSRs are generally limited to the western levee of the BCL, but on few RMCS profiles we also observed the BSR stack in the eastern levee (Fig. 2.3B) where the overburden is thicker compared to the western levee (Fig. 3A). The multiple BSRs are not observed in or underneath the channel axis, and the reflections of all BSRs fade out where they intersect with the base of the BCL (Fig. 2.3A).

The BCL is overlain by the outer levee deposits of the Danube channel (Fig. 2.3A). A sediment unit (layer A) exists between the BSL and the Danube levee and is characterized by an average thickness of about 80 m. The structure of layer A is homogeneous and layered sub-horizontally. Earlier studies by Winguth et al. (2000) indicate the depositional ages of the main depositional units in this area. The Danube levee was deposited over the past 75 ka during the last major glacial cycle, and the BCL was deposited during the period of 500 – 320 ka BP. Layer A consequently was deposited during the period of 320 – 75 ka BP.

2.5.2 Thermal Modeling

The thermodynamic stability of gas hydrates depends on local pressure, temperature, gas composition, and pore water salinity (Sloan, 1998). In the Black Sea the bottom-water temperature of 9 °C is well constrained by numerous studies and is remarkably uniform on regional and temporal scales (Degens and Ross, 1974; Vassilev and Dimitrov 2002). The gas composition in our model is assumed to be pure methane because of the $\delta^{13}C$ values of CH_4 between -84‰ and -70‰ observed in the surface sediments at seeps and in the BSR areas of the study area (unpublished data). Due to past limnic phases of the Black Sea, the pore water salinity in the sediments decreases rapidly from ~22.3 at the seafloor (Özsoy and Ünülata, 1997) to ~2-5 in shallow subbottom depth as observed in DSDP cores (Calvert and Batchelor, 1978) and surface sediment cores from our study area (Soulet et al., 2010). A geothermal gradient of 24.5 °C/km ± 0.5 °C/km fits best along the northeastern area of the SUGAR channel at HMCS line 1107 where the slope is gentle and the topographic effects are minimal (Fig. 4A). Below the SUGAR channel and its western levee, we observe an increasing mismatch with the BSR-derived temperature of up to 2 °C lower compared to the regional temperature field (Fig. 2.4A).

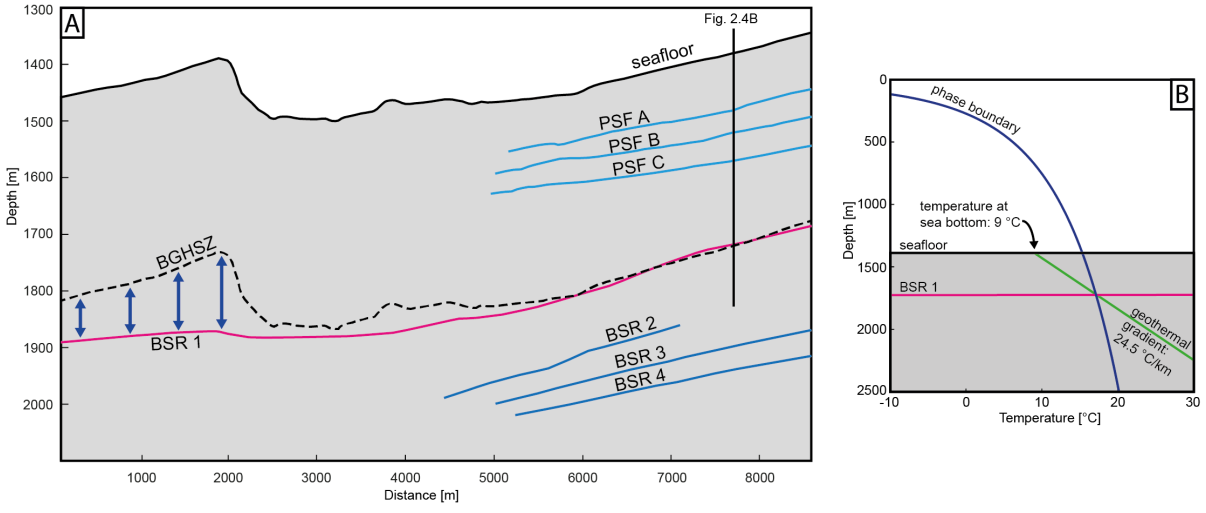

Fig. 2.4A: Interpretated 2D HMCS line 1107 from Fig. 2.2, reduced to the relevant horizons of this study. The BSR is plotted as a pink line. The theoretical BGHSZ fits best to the BSR with a regional geothermal gradient of ~24.5 °C/km below the northeastern levee where the topographic effect is expected to be minor. Towards the channel and western levee, the mismatch between the shallower BGHSZ and the BSR indicate a local thermal gradient that is up to 5 °C/km lower compared to the regional temperature field (blue arrows). B: Phase diagram illustrating the stability conditions of methane hydrates at the location depicted in A. PSF = paleo seafloor.

2.6 Discussion

2.6.1 Thermal state of the channel-levee system

With each BSR showing reversed polarities compared to the seafloor reflection and increased amplitudes underneath, we can confirm that the impedance contrast causing the crosscutting BSRs in the seismic data is most likely caused by free gas. The regional temperature gradient of ~24.5 °C/km that we derived from the BSR temperature at the location of the multiple BSRs is lower compared to temperature gradients of other studies (30 °C/km; Popescu et al., 2006; Vassilev and Dimitrov, 2002). A possible explanation for this difference might be incorrect velocity estimates used by Popescu et al. (2006) for depth conversion of their seismic data. Lacking alternative velocity information, Popescu et al. (2006) converted travel time to depth by assuming velocities between 1600 m/s and 1800 m/s based on velocity profiles from the Storegga site offshore Norway published in Posewang and Mienert (1999), and from the Dniepr deep-sea fan as published in Lüdmann et al. (2000). However, our velocity analysis of the RMCS profiles and data from ocean bottom seismometers (OBS) indicate that the seismic velocity increases from 1485 m/s at the seafloor up to 1950 m/s at BSR level in 380 m depth. Thus, the depth of the BSRs might be underestimated in the studies of Popescu et al. (2006), which consequently leads to a higher geothermal gradient derived from the shallower BSR.

Below the western levee of the SUGAR channel, the BSR-derived temperature indicates a local geothermal gradient even lower than ~24.5 °C/km (Fig. 2.4A). This observation suggests that the gas hydrate system of the Danube deep-sea fan is not in a steady state. The misfit may have been caused by rapid levee deposition. However, in the multiple BSR area, the temperature field is likely equilibrated, as the BSR 1 is in good agreement with the theoretical BGHSZ. This match between predicted and observed BSR 1 is particularly important. In the absence of deep sources for heat flow variations (e.g. volcanic intrusions), it is expected that with increasing depth the thermal field is increasingly in steady state, as the effects of surface processes are averaged out by thermal diffusion.

The levee deposits of the Danube fan extend far into the area of the SUGAR channel. With increasing distance from the Danube channel, the thickness of the levee deposits decreases, which leads to a thicker overburden above the eastern levee of the BCL compared the western levee (Fig. 2.3). Considering the thickness variations of individual sedimentary layers (Fig. 2.2 and Fig. 2.3), it is evident that the sediment load above the multiple BSRs grew during the past glacial cycles and was not constant as stated by Popescu et al. (2006). As we also observe multiple BSRs in the eastern levee of the BCL modeling these BSRs from current seafloor depth would require high variations of pressure and temperature. This introduces large errors when the BSRs are linked to ranges of lower bottom-water temperatures during stable cold climate periods, as noted by Popescu et al. (2006).

2.6.2 Multiple BSRs due to overpressure compartments

Methane hydrates are stable under high pressure and low temperature (Kvenvolden, 1995), with temperature controlled by bottom-water temperature and the regional geothermal gradient. Pressure, on the other hand, is mainly controlled by hydrostatic pressure in the relevant sediment depths (Berndt, 2005) and hence, increases linearly with depth. As a result, the base of gas hydrate stability is defined by a sharp boundary. If, however, the pore pressure is above hydrostatic conditions, the base of gas hydrate stability moves towards greater depths. Fluid overpressure can be caused by fluid volume changes (i.e. due to temperature increase, fluid hydrocarbon generation from kerogen, or

H_2O release in the smectite-illite transformation reaction), fluid movements (due to buoyancy or osmosis), or compaction (e.g. reservoir compaction due to tectonic stress or rapid deposition) (Tacket and Puckette (2012) and references therein). Overpressures can also be caused by free gas, for which the amount of pressure increase depends on the height of the gas column. The presence of free gas is not only indicated by the BSRs but also by bright spots of varying intensity, which are observed beneath each BSR (e.g. the high amplitude zone in Fig. 2.2).

Stepped or tiered overpressure systems have been reported from several sedimentary basins, such as the North Sea Basin (3.4 km depth; Heritier et al., 1979), the Sacramento Basin (1.8 km depth; Tacket and Puckette, 2012), or the Anadarko Basin (3 km depth; Al-Shaieb et al., 1994). These overpressure systems are linked to permeability barriers in the sediment column and are observed in much greater depths compared to the typical thickness of the GHSZ, which ranges between 0 m and 900 m (e.g. Wallmann et al., 2012).

In order to test whether overpressured compartments in the subsurface may form pockets of stable gas hydrates, we calculated a 1D model for a location in 1460 m water depth with four sharp BSRs (location in Fig. 2.2B) and a regional geothermal gradient that is assumed to be stable at 24.5 °C/km. The gas composition for all BSRs was assumed to be pure methane and the pore water salinity was set to 5.

The resulting phase boundary for stable methane hydrates at this location is in a depth of 1827.5 m below sea surface, fitting well with the shallowest BSR in a depth of 1828 m (Fig. 2.5). The required pressures for stable methane hydrates at BSRs 2-4 are the sum of the hydrostatic pressure at the respective depths and the overpressures $P_{DBSR2,3,4}$.

Based on the overpressures required for stable methane hydrates above the deeper BSRs, we calculated the required height of the gas column generating this pore overpressure:

$$H_{BSR2,3,4} = P_{DBSR2,3,4}/g * (\rho_w - \rho_{CH_4}) \quad (2.1)$$

where $H_{BSR2,3,4}$ is the height of the gas column, $P_{DBSR2,3,4}$ are the overpressures for each of the multiple BSRs, g is the gravitational acceleration (9.81 m/s^2), ρ_w is the density of the formation water (1025 kg/m^3), and ρ_{CH_4} is the density of methane, which depends on the temperature and pressure. ρ_{CH_4} was thus calculated separately for P and T at each BSR level, using the SUGAR toolbox (Kossel et al., 2013).

The 1D calculation for the selected site shows that the calculated gas column heights for piercing the phase boundary for stable methane hydrates are 24-36 times higher than the vertical distance between two BSRs. For example, the vertical distance between BSRs 2 and 3 is ~39 m, whereas the required height of the gas column underneath BSR 2 would be ~766 m (Table 2.1). This gas column height exceeds the range of gas column height required for fault reactivation at Blake Ridge (150-290 m; Hornbach et al., 2004), seal failure in the North Sea (263 m; Karstens and Berndt, 2015), or sediment doming offshore New Zealand (37-121 m; Koch et al., 2015).

Table 2.1 Overpressure parameters required for stable methane hydrates at each BSR level.

Reflector	Depth below sea surface [m]	Hydrostatic pressure [MPa]	Total required pressure [MPa]	PD [MPa]	Lithostatic pressure[a] [MPa]	Density of methane [kg/m³]	Gas column height [m]
Seafloor	1460 +/- 5						
BSR 1	1828 +/- 10						
BSR 2	1941 +/- 10	19.5	25.7	6.2	22.6 – 23.6	~196.9	~766
BSR 3	1980 +/- 10	19.9	28.9	9.0	23.9 – 25.0	~211.7	~1134
BSR 4	2011 +/- 10	20.2	31.8	11.6	24.5 – 25.6	~223.1	~1474

[a] *lithostatic pressure derived from density using a density-velocity correlation (details are provided in the Supplementary materials)*

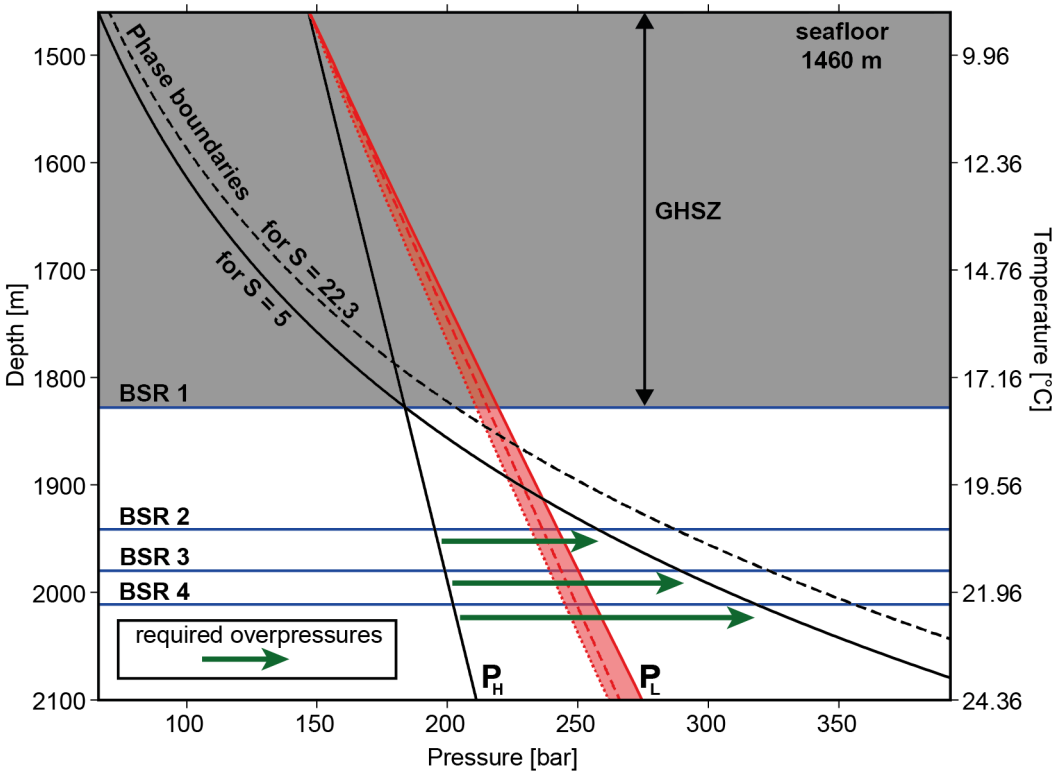

Fig. 2.5 Phase diagram for pure methane hydrates at our model site in 1460 m water depth. The calculated BGHSZ of our 1D model fits well with the location of BSR 1. The required overpressures at each BSR level (green arrows, see Table 1) are likely above lithostatic pressure for the multiple BSRs (P_L, red area, calculated with a density-velocity correlation based on two different approaches as described in the Supplementary material. Red dashed line: lithostatic pressure measured in the Gulf of Mexico). The increased pore water salinity (S) is plotted as a dashed black line, indicating a further increase in overpressure with increasing salinity for stable methane hydrates at the BSR levels. The location for this model is shown in Fig. 2.2B.

Data for lithostatic pressure in the Danube fan were unavailable for this study. Therefore, we calculated likely lithostatic pressure profiles from density using a density-velocity correlation (Table 2.1). More details of the calculation are provided in the Supplementary materials. Furthermore, we compared the lithostatic pressures to measurements from the Mississippi delta in the Gulf of Mexico, which is located in a comparable setting to the Danube deep-sea fan. During IODP expedition 308, measured lithostatic pressures were in the order of 18.6 kPa/m (Behrmann et al., 2006). The lithostatic pressures (Fig. 2.5) show that the required pressures for stable gas hydrates at the multiple BSRs likely exceed lithostatic pressure.

DSDP cores from site 379A show an increase in salinity into the hypersaline stage starting at ~350 m below the seafloor (Calvert and Batchelor, 1978), which is in the depth range of the deeper BSRs at our study site. An increase in pore water salinity results in a shift of the phase boundary towards higher pressures (Fig. 2.5). The top of the hypersaline stage lies probably in greater depth at the Danube fan compared to the DSDP site, due to greater sediment thickness.

Based on our calculations, it is unlikely that pockets with overpressured gas are present in the Danube fan area and cause the observed BSRs. Lithological boundaries, which would support the formation of pressure compartments, are not observed. Instead, the same strata are crossed by two or more BSRs at the same location (Fig. 2.2). Some patches below each BSR may be gas-charged as suggested by their high amplitude contrast and polarity change. However, the height of the gas column beneath each BSR appears to be small, as indicated by the overall small amplitude attenuation below each BSR with almost no loss in frequency content.

2.6.3 Multiple BSRs caused by temporally changing pressure and temperature conditions in different limnic phases

If the multiple BSRs can be linked to events of climate change (i.e., sealevel variations, changes in bottom water temperatures), the sedimentation above the BCL has to be taken into account. The deposition of the western Danube levee above the BCL lead to an asymmetrical growth of the overburden above the BCL, which is thicker towards the Danube channel in the northeast (Fig. 2.3). Deposition of the western levee occurred over a relatively short time of 75 ka BP during the last major sealevel lowstand (e.g. Winguth et al., 2000; Popescu et al., 2001). Therefore, we need to find the corresponding paleo seafloors (PSFs) for these events. These horizons can be found in layer A, which is located between the BCL and the base of the Danube levee (Fig. 2.3). This layer was well mapped by cross-correlating the available seismic data along the study area. The thickness of this layer is in the range of ~70 m to ~120 m. According to Winguth et al. (2000), the age of this layer is in the range of 75 ka to 320 ka and thus spans at least three major limnic phases of the Black Sea (Manheim and Shug, 1978; Muratov et al., 1978).

Due to the large uncertainty of the real age of layer A (drilling data are not available), we defined and picked three reasonably spaced horizons representing the PSFs in layer A. We used these PSFs for modelling the BGHSZ at paleo levels: The upper boundary of layer A was assumed to correspond to the paleo seafloor for BSR 2 (PSF A), the lower boundary was assumed to correspond to BSR 4 (PSF C), and a horizon in the center of layer A (PSF B) was assumed to correspond to BSR 3 (Fig. 2.3).

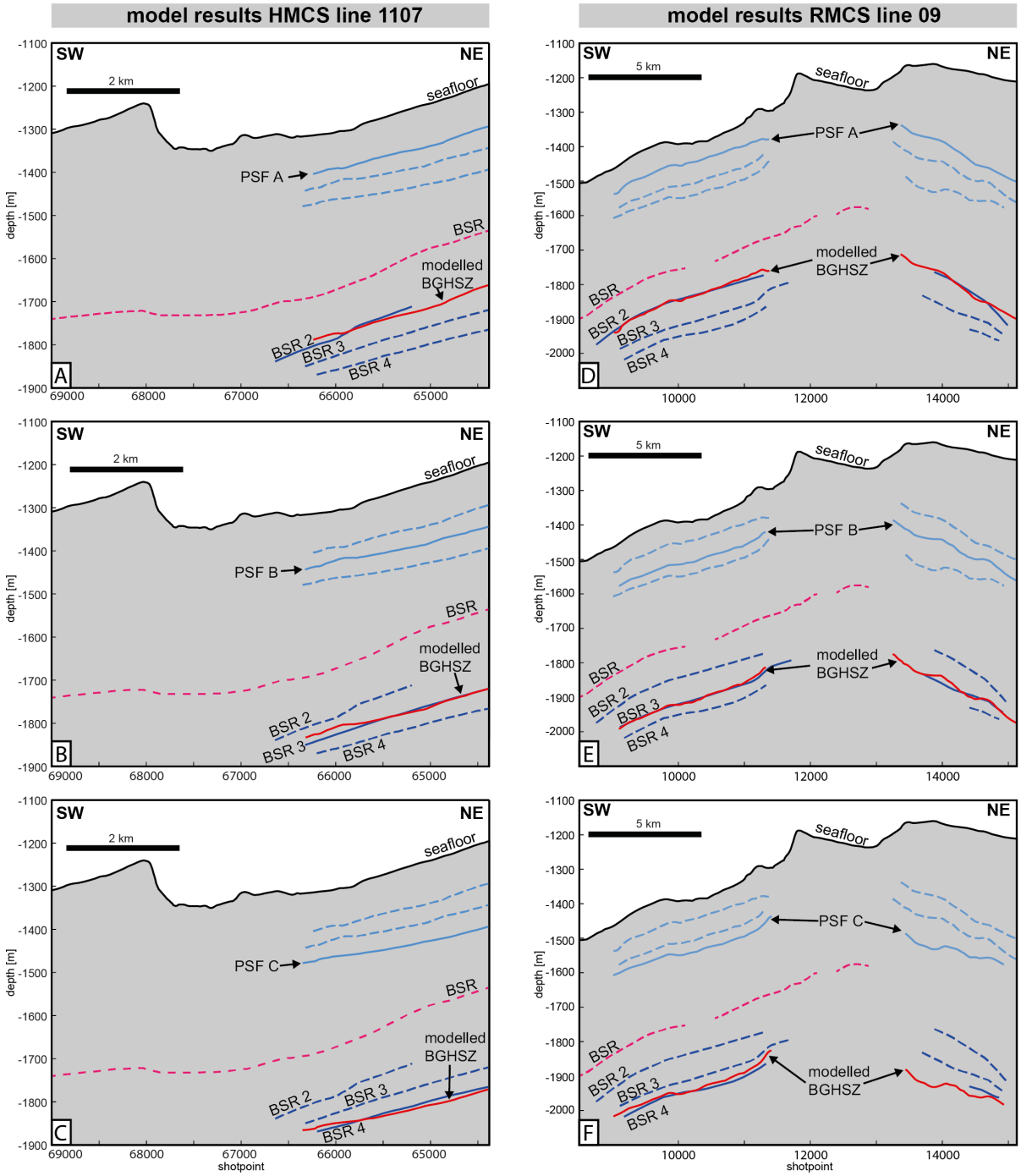

Fig. 2.6 Model results for matching the paleo-BSRs with the paleo seafloors. A-C: Results for HMCS line 1107 near the SUGAR channel. The BGHSZ (red line) is calculated from the paleo seafloor (PSF, light blue) and compared to the paleo-BSRs (dark blue). Model parameters are described in the discussion. D-E: Results for RMCS line 09, where the paleo-BSR stack is also observed further to the northeast.

We observed that in the multiple BSR area, the present-day BSR is stable and follows the temperature field (Fig. 2.4A). Therefore, it is reasonable to test paleo pressure and temperature conditions for the PSFs as boundary parameters for the paleo-BSRs. In our 2D model approach, we calculated the BGHSZ for each of the PSFs under assumed paleo conditions, which included a 120-150 m lower sealevel compared to today (e.g. Ryan et al., 1997; Lericolais et al., 2009) and a lower bottom water temperature than today's 9°C. Poort et al. (2005) inferred a temperature decrease of 2.0-5.5 °C at

about 7.1 ka BP, while Soulet et al. (2010) reconstructed 4 °C for the last glacial maximum based on $\delta^{18}O$ pore water data. Because 4 °C is also the density maximum for fresh water, we used this value as a start for the model, but also ran it with higher temperatures of 5 °C and 6 °C. The pore water salinity was kept at 5.

In this approach, the temperature gradient in the sediments was set as a variable, because we expected a higher temperature gradient in the upper sediment column due to the lower bottom-water temperature. By varying the temperature gradients, we fitted the modelled BGHSZ for the individual PSFs to the paleo-BSRs. The model shows a good fit of the BGHSZ models to the corresponding paleo-BSRs for temperature gradients in the range of 35 – 37.5 °C/km at 4 °C bottom water temperature and for a 150 m lower sealevel. The results are shown for the two profiles HMCS line 1107 (Fig. 2.6 A-C) and RMCS line 09 (Fig. 2.6 D-F). Lowering the sealevel by only 120 m instead of 150 m results in slightly higher (by ~0.5 °C/km) temperature gradients, whereas an increase of the bottom water temperature by 1 °C results in a reduction of the required temperature gradients by 2.0-2.5 °C/km.

Our results show that it is possible to link the paleo-BSRs to paleo seafloor horizons in layer A (Fig. 2.6). The depositional history of layer A indicates that the paleo-BSRs reflect stages of stable sealevel lowstands under glacial conditions. The glacial-interglacial cycles are more distinctive in the Black Sea compared to other areas due to the isolation from the Mediterranean during sealevel lowstands. The preservation of paleo-BSRs may have been favored by the development of the Danube deep-sea fan under lacustrine conditions (Popescu et al., 2001) controlled by rapid sealevel changes in the order of 120–150 m.

However, high uncertainties beyond small-scale misfits of modelled BGHSZ and paleo-BSRs are associated with our model approach. The largest uncertainties originate from the choice of the PSF horizons, which are exchangeable as they are all deposited sub-parallel. Only drilling into this layer can provide more certainty. The errors of the PSFs and the BSRs are mainly related to uncertainties in the velocities, but also to the picking accuracy, static errors, and imaging problems. High uncertainties of the model are also related to the paleo parameters (bottom-water temperature and paleo sealevel). Taking all these uncertainties into account, we estimate that an average geothermal gradient of 35±5 °C/km best reflects stable conditions for the paleo-BSRs.

The question remains whether the derived temperature gradient for the paleo-BSRs is reasonable. Even though we have to estimate larger errors for the range of the geothermal gradients, the geothermal gradients are nevertheless higher (35±5° C/km) compared to the regional geothermal gradient derived from the shallowest BSR (24.5 °C/km). The only temperature data that is available from greater depth is from DSDP core 379A in the central Black Sea and is in the range of 32 – 38 °C/km (Erickson and Von Herzen, 1978). These results indicate that the paleo-BSRs probably reflect the true geotherm of the Black Sea basin. Today's lower geothermal gradient derived from the shallow BSR temperature is still influenced by the increase of the bottom water temperature from about 4 °C to today's 9 °C since the last glacial maximum (Appendix A.1, Fig. A 1). We therefore suggest that the thermal system in the Danube fan still adapts to this change and is not in steady state. The BGHSZ will probably become shallower over the next tens of thousands of years (also pointed out by Poort et al., 2005) as the geotherm increases due to thermal diffusion.

2.6.4 Preservation of paleo-BSRs

The observation of multiple BSRs, which mimic several older seafloors and are partly at steep angles to the present-day seafloor, provides unequivocal evidence that the BSRs must be old structures. The limited age control that exists for the Danube fan suggests that the BSRs must be at least several 10,000 years old and possibly as much as 300,000 years old. After a change of stability conditions by sediment loading due to rapid deposition, the regional geothermal gradient would start to equilibrate by heat conduction from below the GHSZ. This would lead to the dissociation of the lowermost gas hydrates and latent heat absorbed during the dissociation might subsequently cause cooling from this endothermic reaction. Depending on how high the hydrate saturation above the BSR is, cooling would increasingly buffer the temperature field, but, even with high hydrate saturation the dissipation of the cooling presumably should not take longer than a few decades. Consequently, we conclude that despite buffering by latent heat, it is unlikely that gas hydrates still exist above the paleo-BSRs, as they would start to dissociate immediately once they leave the stability field.

Dissociation of hydrates should lead to free gas formation within the former GHSZ, but we do not observe any high amplitude reflections directly above the paleo-BSRs. In fact, the paleo-BSRs in the high-resolution seismic data are remarkably sharp. This strongly suggests that the amount of gas that was formed by gas hydrate dissociation is very small. It also suggests that the free gas that still exists in the zone below the previous GHSZs has not yet begun to migrate upwards causing todays paleo-BSRs. It seems likely that the upward migration of the free gas due to its own buoyancy forces is inhibited by low free gas saturation and a general low permeability of the host sediment. The upward migration of gas is controlled by the irreducible gas saturation S_{GC}, which is typically in the range of 0.01–0.1 (Garg et al., 2008), and has to be exceeded in the pore space to enable gas migration (Wallmann et al., 2012). The largest drop in P-wave velocities occurs at gas concentrations lower than 4% (Andreassen et al., 2007). Therefore the free gas concentrations at each paleo-BSR must be low enough for the free gas not to migrate further upwards, but high enough to cause a clear impedance contrast in seismic data. It is likely that only diffusive transport of dissolved gas plays a role in this setting and that the biogenic gas, which is observed in the organic-rich sediment column, is solely produced within the GHSZ. This is supported by the low vertical permeability of the levee sediments in which the BSRs are located, and by the absence of vertical migration pathways in the seismic data. Gas that is produced underneath the BCL may migrate upslope along coarse-grained sediment deposits such as those encountered in the numerous channels and bases of the channel-levee systems, all of which areas where multiple BSRs are not observed.

2.7 Conclusions

The existence of previously identified multiple BSRs of the Danube deep-sea fan has been confirmed by new 2D multichannel seismic data. A stack of four BSRs was observed in the levee deposits of a buried channel-levee system. The multiple BSRs do not represent gas composition changes or overpressured compartments, but reflect past pressure and temperature conditions. Our modeling results suggest that temperature effects of rapid sediment deposition rather than bottom-water temperature change or sealevel variations dominate the pressure and temperature conditions leading to the multiple BSRs. These changes are more distinctive in the Black Sea and especially in the Danube area because of the isolation of the Black Sea from the Mediterranean during sealevel lowstands. Because hydrate dissociation may not occur for several thousands of years, such paleo-BSRs remain well defined in seismic data. We propose that small amounts of free gas are present beneath each of the paleo-BSRs. The gas saturation is high enough to cause an impedance contrast in seismic data, but low enough to inhibit buoyancy-driven upward migration. The paleo-BSRs possibly reflect the real geotherm in the order of 35±5 °C/km, which is higher than the local geotherm of 24.5±0.5 °C/km derived from the shallowest (current) BSR. This also suggests that the Danube area is not in thermal steady state and still adapting to increasing bottom water temperatures since the last glacial maximum.

2.8 Acknowledgements

The research leading to these results has received funding from the European Union Seventh Framework Programme (FP7/2007-2013) under the MIDAS project, grant agreement no. 603418, from the German Ministry of Education and Research (BMBF) and from the Federal Ministry of Economy and Energy (BMWi) through the SUGAR project (grant nos. 03G0819A, 03SX320A, 03G0856A). The RMCS line 09 was kindly provided by the Institute of Marine Science and Technology (IMST-Seislab) of the Dokuz-Eylül University, Izmir, Turkey. We would like to thank the captains and crew of RV MARIA S. MERIAN cruise MSM34 as well as the GEOMAR lab technicians for their excellent support. We thank reviewers Marc de Batist and Ingo Pecher and editor Peter Shearer for their constructive comments that greatly helped to improve the manuscript.

2.9 References

Al-Shaieb, Z., Puckette, J.O., Abdalla, A.A., and Ely, P.B., 1994. Megacompartment complex in the Anadarko basin: a completely sealed overpressured phenomenon. In: Ortoleva, P.J. (Ed.), Basin compartments and seals. AAPG Memoir 61, pp. 55-68.

Andreassen, K., Nilssen, E.G., and Ødegaard, C.M., 2007. Analysis of shallow gas and fluid migration within the Plio-Pleistocene sedimentary succession of the SW Barents Sea continental margin using 3D seismic data. Geo-Marine Letters 27, pp. 155–171, doi:10.1007/s00367-007-0071-5.

Bangs, N.L.B., Musgrave, R.J., and Tréhu, A.M., 2005. Upward shifts in the southern Hydrate Ridge gas hydrate stability zone following postglacial warming, offshore Oregon. Journal of Geophysical Research 110, B03102, doi:10.1029/2004JB003293.

Behrmann, J., Flemings, P.B., and John, C.M., 2006. Rapid sedimentation, overpressure, and focused fluid flow, Gulf of Mexico Continental Margin. Scientific Drilling 3, pp. 12-17, doi:10.2204/iodp.sd.3.03.2006.

Berndt, C., Bünz, S., Clayton, T., Mienert, J., and Saunders, M., 2004. Seismic character of bottom simulating reflectors: examples from the mid-Norwegian margin. Marine and Petroleum Geology 21, pp. 723-733, doi:10.1016/j.marpetgeo.2004.02.003.

Berndt, C., 2005. Focused fluid flow in passive continental margins. Philosophical Transactions of the Royal Society A 363, pp. 2855-2871, doi:10.1098/rsta.2005.1666.

Bialas, J., Klaucke, I., and Haeckel, M. (Eds.), 2014. FS MARIA S. MERIAN Fahrtbericht / Cruise Report MSM34/1 & 2 SUGAR Site; Varna – Varna, 06.12.13-16.01.14. GEOMAR Report, N. Ser., 015. GEOMAR Helmholtz-Zentrum für Ozeanforschung, Kiel, Germany, 111 pp., doi:10.3289/GEOMAR_REP_NS_15_2014.

Calvert, S.E., and Batchelor, C.H., 1978. Major and minor element geochemistry of sediments from Hole 379A, Leg 42B, Deep-Sea Drilling Project. Initial Reports of the Deep Sea Drilling Project 42 Part 2, pp. 527-541.

Degens, E.T., and Ross, D.A., 1974. The Black Sea – Geology, Chemistry, and Biology. The American Association of Petroleum Geologists, Tulsa, USA.

Davies, R.J., Thatcher, K.E., Armstrong, H., Yang, J., and Hunter, S., 2012. Tracking the relict bases of marine methane hydrates using their intersections with stratigraphic reflections. Geology 40, 1011-1014, doi:10.1130/G33297.1.

Erickson, A.J., and Von Herzen, R.P., 1978. Downhole temperature measurements and heat flow data in the Black Sea; DSDP Leg 42B. Initial Reports of the Deep Sea Drilling Project 42 Part 2, pp. 1085-1103.

Foucher, J.P., Nouzé, H., and Henry, P., 2002. Observation and tentative interpretation of a double BSR on the Nankai slope. Marine Geology 187, pp. 161-175, doi:10.1016/S0025-3227(02)00264-5.

Garg, S. K., Pritchett, J. W., Katoh, A., Baba, K., and Fujii, T., 2008. A mathematical model for the formation and dissociation of methane hydrates in the marine environment. Journal of Geophysical Research: Solid Earth 113, B01201, doi:10.1029/2006JB004768.

Geletti, R., and Busetti, M., 2011. A double bottom simulating reflector in the western Ross Sea, Antarctica. Journal of Geophysical Research: Solid Earth 116, B04101, doi:10.1029/2010JB007864.

Grevemeyer, I., and Villinger, H., 2001. Gas hydrate stability and the assessment of heat flow through continental margins. Geophysical Journal International 145, pp. 647–660, doi:10.1046/j.0956-540x.2001.01404.x.

Haacke, R.R., Westbrook, G.K., and Hyndman, R.D., 2007. Gas hydrate, fluid flow and free gas: Formation of the bottom-simulating reflector. Earth and Planetary Science Letters 261, pp. 407-420, doi:10.1016/ j.epsl.2007.07.008.

Heritier, F.E., Lossel, P., and Wathne, E., 1979. Frigg Field – large submarine-fan trap in lower Eocene rocks of the North Sea Viking Graben. AAPG Bulletin 63, pp. 1999-2020.

Hornbach, M.J., Saffer, D.M., and Holbrook, W.S., 2004. Critically pressured free-gas reservoirs below gas-hydrate provinces. Nature 427, pp. 142-144, doi:10.1038/nature02172.

Hyndman, R.D., and Davis, E.E., 1992. A mechanism for the formation of methane hydrate and seafloor bottom-simulating reflectors by vertical fluid expulsion. Journal of Geophysical Research: Solid Earth 97, pp. 7025-7041, doi:10.1029/91JB03061.

Hyndman, R.D., Foucher, J.-P., Yamano, M., and Fisher, A., 1992. Deep sea bottom-simulating-reflectors: calibration of the base of the hydrate stability field as used for heat flow estimates. Earth and Planetary Science Letters 109, pp. 289–301, doi:10.1016/0012-821X(92)90093-B.

Judd, A., and Hovland, M., 2007. Seabed Fluid Flow: The Impact on Geology, Biology and the Marine Environment. Cambridge University Press, Cambridge.

Karstens, J., and Berndt, C., 2015. Seismic chimneys in the Southern Viking Graben – Implications for palaeo fluid migration and overpressure evolution. Earth and Planetary Science Letters 412, pp. 88-100, doi:10.1016/j.epsl.2014.12.017.

Koch, S., Berndt, C., Bialas, J., Haeckel, M., Crutchley, G.J., and Papenberg, C., 2015. Gas-controlled seafloor doming. Geology 43, pp. 571-57, doi:10.1130/G36596.1.

Kossel, E., Bigalke, N., Piñero, E., and Haeckel, M., 2013. The SUGAR Toolbox – A library of numerical algorithms and data for modelling of gas hydrate systems and marine environments. GEOMAR Report No. 8, 160 pp, doi:10.3289/geomar_rep_ns_8_2013.

Kvenvolden, K. A., 1995. A review of the geochemistry of methane in natural gas hydrate. Organic Geochemistry 23, pp. 997-1008, doi:10.1016/0146-6380(96)00002-2.

Lericolais, G., Bulois, C., Gillet, H., and Guichard, F., 2009. High frequency sea level fluctuations recorded in the Black Sea since the LGM. Global and Planetary Change 66, pp. 65-75, doi:10.1016/ j.gloplacha.2008.03.010.

Lericolais, G., Bourget, J., Popescu, I., Jermannaud, P., Mulder, T., Jorry, S., and Panin, N., 2013. Late Quaternary deep-sea sedimentation in the western Black Sea: New insights from recent coring and seismic data in the deep basin. Global and Planetary Change 103, pp. 232-247, doi:10.1016/j.gloplacha.2012.05.002.

Lüdmann, T., Wong, H., Konerding, P., Zillmer, M., Petersen, C J., and Flüh, E., 2004. Heat flow and quantity of methane deduced from a gas hydrate field in the vicinity of the Dnieper Canyon, northwestern Black Sea. Geo-Marine Letters 24, pp. 182-193, doi:10.1007/s00367-004-0169-y.

Manheim, F.T., and Schug, D.M., 1978. Interstitial waters of Black Sea cores. Initial Reports of the Deep Sea Drilling Project 42 Part 2, 637 – 651.

Muratov, M.V., Neprochnox, Y.P., Ross, D.A., and Trimonis, E.S., 1978. Basic features of the Black Sea late Cenozoic history based on results of deep-sea drilling. Initial Reports of the Deep Sea Drilling Project 42 Part 2, pp. 1141-1148.

Naudts, L., Greinert, J., Artemov, Y.G., Staelens, P., Poort, J., Van Rensbergen, P., and De Batist, M., 2006. Geological and morphological setting of 2778 methane seeps in the Dnepr paleo-delta, northwestern Black Sea. Marine Geology 227, pp. 177-199, doi:10.1016/j.margeo.2005.10.005.

Netzeband, G.L., Hübscher, C.P., Gajewski, D., Grobys, J.W.G., and Bialas, J., 2005. Seismic velocities from the Yaquina forearc basin off Peru: evidence for free gas within the gas hydrate stability zone. International Journal of Earth Sciences 94, pp. 420-432, doi:10.1007/s00531-005-0483-2.

Özsoy, E., and Ünlüata, Ü., 1997. Oceanography of the Black Sea: a review of some recent results. Earth-Science Reviews 42, pp. 231-272, doi:10.1016/S0012-8252(97)81859-4.

Poort, J., Vassilev, A., and Dimitrov, L., 2005. Did postglacial catastrophic flooding trigger massive changes in the Black Sea gas hydrate reservoir? Terra Nova 17, pp. 135-140, doi:10.1111/j.1365-3121.2005.00599.x.

Popescu, I., Lericolais, G., Panin, N., Wong, H.K., and Droz, L., 2001. Late Quaternary channel avulsions on the Danube deep-sea fan, Black Sea. Marine Geology 179, pp. 25-37, doi:10.1016/S0025-3227(01)00197-9.

Popescu, I., De Batist, M., Lericolais, G., Nouzé, H., Poort, J., Panin, N., Versteeg, W., and Gillet, H., 2006. Multiple bottom-simulating reflections in the Black Sea: Potential proxies of past climate conditions. Marine Geology 227, pp. 163-176, doi:10.1016/j.margeo.2005.12.006.

Posewang, J., and Mienert, J., 1999. The enigma of double BSRs: indicators for changes in the hydrate stability field? Geo-Marine Letters 19, pp. 157-163, doi:10.1007/s003670050103.

Römer, M., Sahling, H., Pape, T., Bahr, A., Feseker, T., Wintersteller, P., and Bohrmann, G., 2012. Geological control and magnitude of methane ebullition from a high-flux seep area in the Black Sea – the Kerch seep area. Marine Geology 319-322, pp. 57-74, doi:10.1016/j.margeo.2012.07.005.

Ryan, W.B.F., Pitman III, W.C., Major, C.O., Shimkus, K., Moskalenko, V., Jones, G.A., Dimitrov, P., Gorür, N., Sakinc, M., and Yüce, H., 1997. An abrupt drowning of the Black Sea Shelf. Marine Geology 138, pp. 119-126, doi:10.1016/S0025-3227(97)00007-8.

Sclater, J.G., Jaupart, C., Galson, D., 1980. The heat flow through oceanic and continental crust and the heat loss of the earth. Reviews of Geophysics 18, pp. 269-311, doi:10.1029/RG018i001p00269.

Shipley, T. H., Houston, M. H., and Buffler, R. T., 1979. Seismic evidence for widespread occurrence of possible gas-hydrate horizons on continental slopes and rises. AAPG Bulletin 63, pp. 2204-2213.

Sloan, E.D., 1998. Clathrate hydrates of natural gases. Marcel Dekker, New York.

Soulet, G., Delaygue, G., and Vallet-Coulomb, C., 2010. Glacial hydrologic conditions in the Black Sea reconstructed using geochemical pore water profiles. Earth and Planetary Science Letters 296, pp. 57-66, doi:10.1016/j.epsl.2010.04.045.

Tacket, J., and Puckette, J., 2012. Lithologic controls of pressure distribution in sedimentary basins. AAPG Search and Discovery Article #40898, 58 pp.

Tinivella, U., and Giustiniani, M., 2013. Variations in BSR depth due to gas hydrate stability versus pore pressure. Global and Planetary Change 100, pp. 119-128, doi:10.1016/j.gloplacha.2012.10.012.

Vassilev, A., and Dimitrov, L., 2002. Spatial and quantity evaluation of the Black Sea gas hydrates. Geologiya I Geofizika 43, pp. 672-684.

Wallmann, K., Piñero, E., Burwicz, E.B., Haeckel, M., Hensen, C., Dale, A., and Ruepke, L., 2012. The global inventory of methane hydrate in marine sediments: A theoretical approach. Energies 5, pp. 2449-2498, doi:10.3390/en5072449.

Winguth, C., Wong, H.K., Panin, N., Dinu, C., Georescu, P., Ungureanu, G., Krugliakov, V.V., and Podshuveit, V., 2000. Upper Quaternary water level history and sedimentation in the northwestern Black Sea. Marine Geology 167, pp. 127-146, doi:10.1016/S0025-3227(00)00024-4.

Wong, H.K., Winguth, C., Panin, N., Dinu, C., Wollschläger, M., Georgescu, P., Ungereanu, G., Krugliakov, V.V., and Podshuveit, V., 1997. The Danube and Dniepr fans, morphostructure and evolution. GeoEcoMarina 2, pp. 77-102.

Wood, W.T., Gettrust, J.F., Chapman, N.R., Spence, G.D., and Hyndman, R.D., 2002. Decreased stability of methane hydrates in marine sediments owing to phase-boundary roughness. Nature 420, pp. 656-660, doi:10.1038/nature0126.

3. Potential impacts of gas hydrate exploitation on slope stability in the Danube deep-sea fan, Black Sea

Timo Zander[a], Jung Chan Choi[b], Maarten Vanneste[b], Christian Berndt[a], Anke Dannowski[a], Brian Carlton[b], Jörg Bialas[a]

[a]*GEOMAR Helmholtz Centre for Ocean Research Kiel, Germany*

[b]*Norwegian Geotechnical Institute (NGI), Oslo, Norway*

Submitted to Marine and Petroleum Geology

3.1 Abstract

Methane production from gas hydrate reservoirs is only economically viable for hydrate reservoirs in permeable sediments. The most suitable known prospect in European waters is the paleo Danube deep-sea fan in the Bulgarian exclusive economic zone in the Black Sea where a gas hydrate reservoir is found 60 m below the seafloor in water depths of about 1500 m. To investigate the hazards associated with gas production-induced slope failures we carried out a slope stability analysis for this area. Screening of the area based on multibeam bathymetry data shows that the area is overall stable with some critical slopes at the inner levees of the paleo channels. Hydrate production using the depressurization method will increase the effective stresses in the reservoir beyond pre-consolidation stress, which results in sediment compaction and seafloor subsidence. The modeling results show that subsidence would locally be in the order of up to 0.4 m, but it remains confined to the immediate vicinity above the production site. Our simulations show that the Factor of Safety against slope failure (1.27) is not affected by the production process, and it is more likely that a landslide is triggered by an earthquake than by production itself. If a landslide were to happen, the mobilized sediments on the most likely failure plane could generate a landslide that would impact the production site with velocities of up to 10 m s^{-1}. This case study shows that even in the case of production from very shallow gas hydrate reservoirs the threat of naturally occurring slope failures may be greater than that of hydrate production itself and has to be considered carefully in hazard assessments.

3.2 Introduction

Gas hydrates are ice-like crystals that occur in large quantities along continental margins and permafrost regions. Their stability depends on high pressure and low temperature as well as on salinity and gas composition (Shipley et al., 1979). In the marine environment, gas hydrates primarily consist of methane and dominantly form in crystallographic structure I (e.g. Sloan, 1998).

Gas hydrates are considered a potential energy resource and research programs in several countries including Japan, Korea, and India are dedicated to the exploration and ultimately the exploitation of offshore gas hydrate reservoirs. The German SUGAR project aims at developing technologies for the exploration and exploitation of methane hydrates within European waters. Economically viable hydrate reservoirs occur in sands and coarse silts with permeability that is high enough to sustain gas flow towards the well during production. The paleo Danube deep-sea fan in the Black Sea offers the best conditions for hydrate production in Europe because it contains sandy sediments and a widespread bottom simulating reflector (BSR) in seismic data that indicates the presence of gas hydrates (Popescu et al., 2006, Zander et al., 2017).

Several production technologies have been considered to produce methane from gas hydrates. All are based on the dissociation of hydrates following a gas flow towards a production well. Applicable methods include warming of hydrated sediments by injection of warm water and chemical stimulation of methane hydrate with an agent such as nitrogen, methylene or carbon dioxide. However, the economically most favorable production method is depressurization (Fig. 3.1). The concept of depressurization was applied and validated in a production test in the Nankai Trough offshore Japan in 2013 (Yamamoto et al., 2014). Studies showed that the high bottom water temperature of around 9 °C in the Black Sea is not conducive to hydrate dissociation by CO_2 or N_2 injection, while such high temperatures increase the efficiency of the depressurization method (Merey and Sinayuk, 2016a).

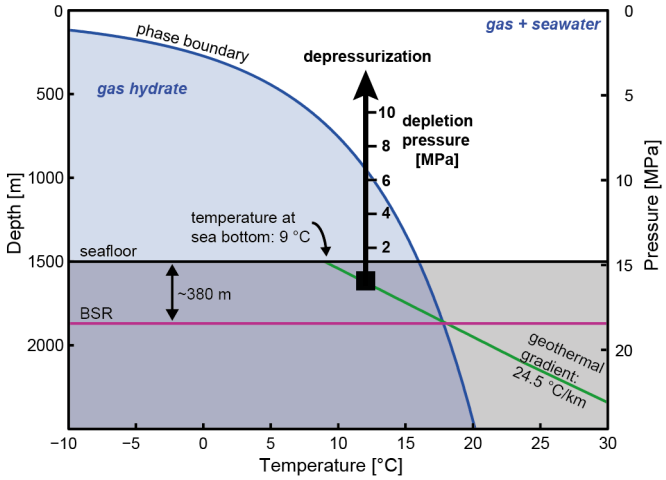

Fig. 3.1: Gas hydrate phase diagram showing the gas hydrate stability zone in the upper ~380 m below the seafloor and the pressure path during gas hydrate dissociation under pressure reduction (black arrow).

The basic concept of the depressurization method involves a borehole which is drilled vertically into the gas hydrate reservoir, and pressure reduction by pumping along the entire reservoir interval. Pressure reduction forces hydrate dissociation, which gradually spreads out from the well into the surrounding hydrate reservoir. Typically, the pore pressure around the well is reduced to a specific target (e.g. 2.7 MPa at Walker Ridge (Myshakin et al., 2012) and 3 MPa at Nankai (Yamamoto et al.,

2014)). Models showed that a pressure target of 3 MPa yields the highest gas production in Black Sea sediments (Merey and Sinayuc, 2016b). In 1500 m water depth, this pressure reduction is comparable to a sea level fall of 1200 m. The area affected by pressure reduction is expected to remain relatively limited to the vicinity of the well location, i.e., 100 m around the well (Kvalstad et al., 2011).

Following depressurization, hydrate dissociation in the sandy sediments will cause an increase in permeability. Hydrates typically are load-bearing and grain-supporting when their saturation exceeds 25 – 40 % (Waite et al., 2009). Thus, the disappearance of the cementing hydrates will typically lead to a softening of the sediments. Consequently, the effective stress in the reservoir will increase, which leads to sediment compaction towards the dissociation area in all directions (Zhou et al., 2014). Simulations showed that the radial displacements are smaller than the vertical displacements, with the latter being largest directly above the production zone and close to zero underneath the production zone (Zhou et al., 2014). As a result, gas production from a shallow compacting reservoir may cause subsidence at the seafloor (Fjaer et al., 2008; Kim et al., 2014).

One of the most important offshore geohazards is submarine slope failure (Vanneste et al., 2014). Areas with steep slopes, caused, e.g. by submarine channels such as those encountered in the Danube deep-sea fan, are more susceptible to slope failure than the surrounding areas (Kvalstad, 2007). Instable slopes may cause sliding or slumping of the seafloor sediments, and even on gently dipping slopes mobilized mass can travel over large distances during a landslide. Sediment failure occurs when the shear stress (e.g. the gravitational downslope force) exceeds the shear strength (resisting forces). The initiation of seabed failures can be triggered by both natural causes and human interference such as over-steepening of the slope, uneven deposition or erosion, increase of shear stress (loading, lateral pressure), reduction of shear strength, and seismic events (lateral and vertical ground shaking due to earthquakes). So far it remains unclear whether natural gas hydrate dynamics have triggered slope failures. A review of landslide inventories carried out by Urlaub et al. (2013) did not find evidence for a large-scale triggering of landslides due to gas hydrate dissociation caused by the glacial-interglacial pressure and temperature changes. Nevertheless, gas hydrate dissociation may be considered as a preconditioning mechanism instead of an actual trigger for certain submarine landslides (Crutchley et al., 2016) and there is evidence that some submarine landslides have developed differently in areas with hydrate than in those without (Micallef et al., 2009). The transported mass of a submarine landslide can affect installations in various forms such as loss of foundation area, debris impact causing destruction of facilities, or even partial or total burial of seabed facilities, and generation of tsunamis affecting coastal communities over potentially large areas (Kvalstad, 2007).

In this study, we focus on a part of the paleo Danube deep-sea fan which has been investigated with various geophysical tools in the German SUGAR project to investigate its suitability as a gas hydrate production test site. Our aim is to find out if production of gas from a shallow hydrate reservoir can be performed safely at this location, particularly with respect to slope stability. The objectives are (i) to identify slopes with the lowest Factor of Safety (FoS) near the target area and to assess whether the slope in this area can be considered stable; (ii) to simulate hydrate production in a 2D slope stability model to constrain the amount and timing of expected slope deformation; and (iii) to determine the run-out distance and potential implications for infrastructure and installations at the production site through simulation of a landslide along the most critical segment of the slope as modeled in the previous step.

3.3 Geological Setting

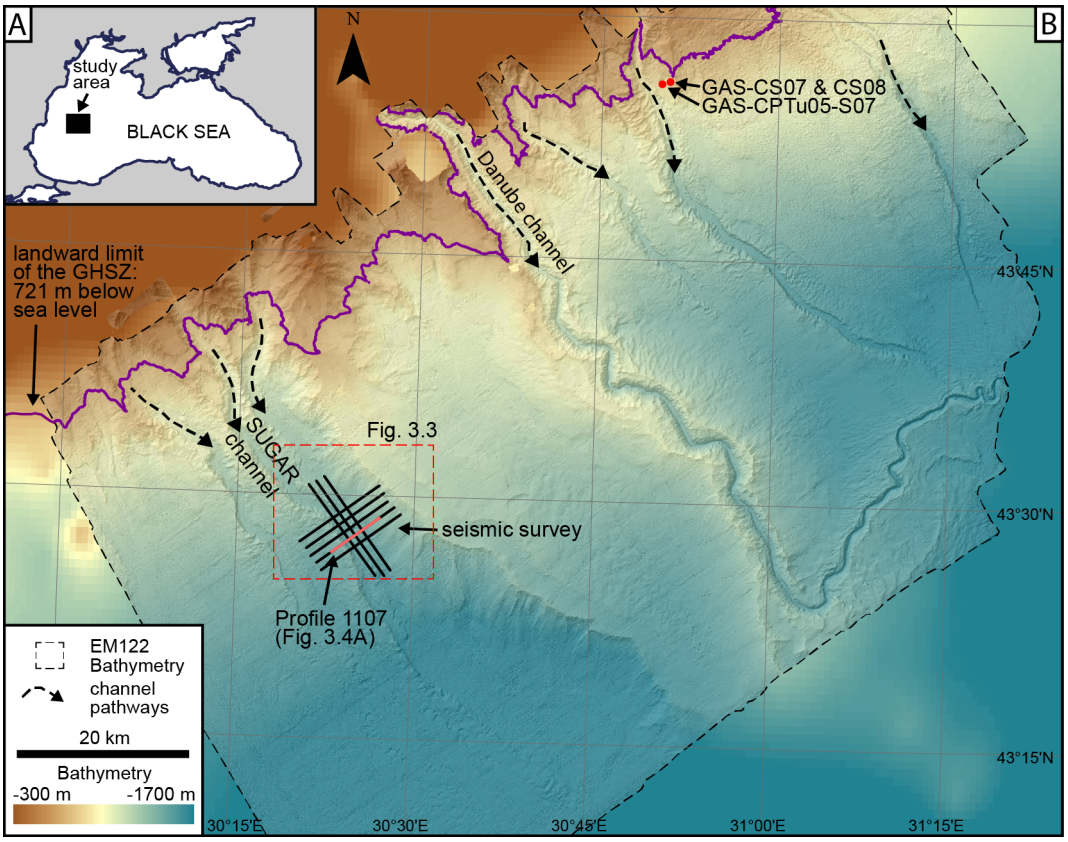

Fig. 3.2: Bathymetric map (25 m x 25 m resolution) of the Danube deep-sea fan in the Black Sea. Note the prominent channel-levee systems, which transport sand into the study area. This sand provides the host rock for the gas hydrate accumulations.

The continental shelf of the northwestern Black Sea basin is up to 120 km wide. During the last glaciation, the rivers Danube, Dniepr, Dniestr and Bug discharged large amounts of sediments off the shelf break at about 100 m water depth down to the abyssal plain at 2200 m water depth (Wong et al., 1997). The depositional areas, which constitute the paleo Danube and Dniepr deep-sea fans, are characterized by numerous canyons and channels (Fig. 3.2), which formed by erosion on the upper slope and by deposition on the middle and lower slope (Popescu et al., 2001). These canyons and channels formed additional slopes along their courses. The highest slope angles typically occur along the inner levee walls of channel-levee systems (Hansen et al., 2015). As observed in other river fans of the northern hemisphere, the right-hand (western) levees are more pronounced than the left-hand (eastern) levees because of the Coriolis force (Popescu et al., 2001). Several older channels can be identified from the bathymetry, such as a channel westwards of the Danube channel which was named SUGAR channel (Fig. 3.2); Zander et al., 2017).

For the observed bottom water temperature of 9 °C (Degens and Ross, 1974) and a salinity of 22.3 (Özsoy and Ünlüata, 1997) the upper limit of the gas hydrate stability zone is located at a water depth of 721 m. The pore water salinity decreases rapidly in shallow depth below the seafloor to a level of 3-5 (Soulet et al., 2010), which shifts the phase boundary for methane hydrates upwards. Indirect indicators for gas hydrates exist in the form of a BSR which is observed in reflection seismic data (Popescu et al., 2006; Zander et al., 2017), and gas hydrate was sampled during a research cruise in 2015

(Ker and Riboulot, 2015). Anomalous multiple BSRs were identified in the levees of a buried channel-levee system underneath the SUGAR channel. These additional BSRs are caused by changes in pressure and temperature conditions during the glacial cycle and indicate that the Danube area is not in a steady state (Zander et al., 2017).

The SUGAR project targets a potential gas hydrate reservoir at the base of the SUGAR channel in about 1500 m water depth. Preliminary results of controlled source electromagnetic (CSEM) data (Schwalenberg et al., 2016) and a shear wave anomaly observed in ocean bottom seismometer (OBS) data (Dannowski et al., 2016) suggest a shallow zone (~60 m depth) of increased gas hydrate saturation with potentially up to 40% hydrate concentration in the pore space.

3.4 Data and Methods

Slope stability assessments are generally based on a conservative scenario. To get an idea of the stability of a given slope, the slip zone with the least FoS in static models is determined. The FoS is defined as resisting forces against driving forces, and theoretically a slope with a FoS of less than 1.0 is prone to fail. However, because of uncertainties due to simplified modeling and parameter variations, a FoS of 1.5 is generally used to define a stable slope, but this depends on the infrastructure at risk as well as local standards and guidelines (CEN, 2004). Pseudo-static models are additionally applied to simulate seismic effects. Under pseudo-static condition, a minimum FoS of 1.1 is generally required. Note that typically a full dynamic site response analysis is preferred over pseudo-static models.

The constraints for geomechanical models and slope stability analyses ideally comprise the geometry of the slope, the geology of the subsurface, strength parameters of the soils and the unit weights. However, for this study, not all of these input parameters were available due to a limited number of boreholes and the complexities of measuring the strength of weak soils. Furthermore, the sampling program was not ideal for geotechnical analyses as only academic methods were available. We therefore used simplified scenarios and approximate some of the parameters. On the other hand, our high-resolution 2D seismic data are excellent, with resolution two to three times better than the resolution of common industry-type 3D seismic data, as the survey focused on the upper 500 m of gas hydrate-hosting sediments. Seismic and bathymetry data were collected during cruise MSM34 onboard the German research vessel MARIA S. MERIAN from December 2013 to January 2014 (Bialas et al., 2014).

3.4.1 Multibeam bathymetry

Multibeam bathymetry data were collected using the ship-mounted EM122 echosounder (Kongsberg). The resulting maps are based on a grid of 25 m x 25 m bin size for the Danube deep-sea fan survey (Fig. 3.2) and 10 m x 10 m bin size for the study area (Fig. 3.3).

3.4.2 2D reflection seismic data

A 2D high-resolution multichannel seismic survey was conducted using a 62.6 m-long streamer with 40 channels and a group distance of 1.56 m. Eight profiles were recorded over an area of two merging channel-levee systems: three profiles along the channel's direction (14 km length each), and five across the channel (11 km length each; Fig. 3.2). A 45/45 in^3 GI gun was used as a source with a shot interval of 5 s. After navigation processing, Omega (WesternGeco) was used for signal processing, stacking, and amplitude-preserving time migration. No gain was applied during processing. Due to the short streamers, velocity data could not be derived and had to be extrapolated from other seismic data discussed in a previous study (Zander et al., 2017). These extrapolated velocities were cross-checked with P-wave velocities derived from OBS stations that were also deployed in the study area (Dannowski et al., 2016). We used these data to convert the seismic data from time to depth domain.

3.4.3 Soil properties

Only very sparse geotechnical and geomechanical data are available from the Black Sea, and to our knowledge, no such data exist for the target area itself. Our 2D slope stability model is therefore based on two different soil parameter sets: one for the gas hydrate reservoir and one for the surrounding sediments (in the following referred to as the overburden). Due to the rather uniform sedimentation in the top 10 m – 30 m of sediments in the Black Sea (e.g. Ross and Degens, 1974; Soulet et al., 2010; Bialas et al, 2014), we decided to estimate the overburden soil parameters from measurements taken during a cruise onboard the RV Pourquoi Pas? in 2015, which was carried out in the northeastern part of the Danube deep-sea fan in Romanian territory (Ker and Riboulot, 2015, Garziglia, 2016). The reservoir's soil parameters were estimated based on published parameters from the successful hydrate production test site in the Nankai Trough offshore Japan (Santamarina et al., 2015; Yoneda et al., 2015). The hydrate reservoir in the Nankai area is located in the sandy channel bed deposits of a buried channel-levee system about 300 m below the seafloor in a water depth of about 1 km (Saeki et al., 2008).

Overburden

In 2015, piezocone and pore pressure data were collected in the Romanian territory of the Danube deep-Sea fan in a water depth of 729 m, at the top of a bathymetric high running N-S along a distance of 3 km with a maximum height of about 50 m above the surrounding area (Fig. 3.2; Ker and Riboulot, 2015). The results obtained from triaxial tests on cores GAS-CS07 and GAS-CS08 were used for correlation with the cone penetration test GAS-CPTu05-S07 (Garziglia, 2016; and pers. communication). We applied these parameters to the overburden soil properties used in this study (Table 3.1).

Table 3.1: Overburden soil parameters (Garziglia, 2016; and pers. communication). γ is the total unit soil weight, G is the shear modulus, s_u is the undrained shear strength, $\sigma'v$ is the effective vertical in situ stress. The locations of the cores are shown in Fig. 3.2.

Parameter	Notation	Value	Reference
Total unit soil weight	γ	17.5 kN m^{-3}	
Rigidity index	G/s_u	140	GAS-CS07, GAS-CS08
Poisson's ratio	ν	0.49	
Undrained shear strength ratio	$s_u/\sigma'v$	0.4	GAS-CPTu05-S07

Gas hydrate reservoir

Shear strength and elastic stiffness of sandy hydrate-bearing sediments are sensitive to hydrate saturation and confining pressure (Yoneda et al., 2015). Extensive laboratory test programs were carried out in the Nankai Trough, where gas production from hydrates was tested successfully (Yamamoto et al., 2014). The results show that the shear strength and elastic stiffness tend to increase with the hydrate saturation. Strengthening is most likely caused by the cohesion induced by hydrate bonding (Santamarina et al., 2015, Yoneda et al., 2015). To obtain realistic parameters for the hydrate reservoir in the Black Sea target area, the material properties of the studied area were thus calibrated as a function of hydrate saturation and the in situ stress condition (Yoneda et al., 2015). The input properties applied in this study are summarized in Table 3.2.

Table 3.2: Parameters for the geotechnical model of the gas hydrate reservoir based on laboratory tests on borehole samples from the Nankai Trough (obtained from Santamarina et al. (2015) and calibrated through relations published in Yoneda et al. (2015)). Mbsf = meter below seafloor

Depth [mbsf]	Confining stress [MPa]	Saturation	E50 [MPa]	Poisson's ratio	Shear modulus [MPa]	Cohesion [MPa]	Friction angle [°]
60	~0.35	Before dissociation					
		0.4	100	0.22	41	1.5	25-30
		After dissociation					
		0	80	0.22	32.8	0 – 0.5	25-30

3.4.4 Slope stability screening tool

In order to select a potentially unstable area and suitable transects to perform a 2D slope stability analysis, a screening of the area based on bathymetric data and geotechnical soil parameters was performed within the top 30 m of soil. The functionality of the screening tool is described in Carlton et al. (2017). The tool estimates the FoS using the infinite slope method (Morgenstern, 1967) and the probability against failure using the First Order Second Moment (FOSM) method. For our simplified soil model parameters, the FoS decreases with depth below the surface, and is largely controlled by the slope angle. Additionally, seismically induced permanent displacements are calculated in the pseudo-static slope stability analysis.

Table 3.3: Input parameters for the screening tool. s_u is the undrained shear strength.

Parameter	Notation	Value	Reference
Maximum depth below seafloor of the analysis	Z_{max}	30 m	-
Pseudo-static coefficient	k	0.05 g	-
Coefficient of variation of k	COV_k	0.2	-
Momentum magnitude	M_w	7.2	Matova, 2000
Peak ground acceleration	PGA	0.1	GSHAP (Giardini, 1999)
Pore pressure ratio	r_u	0	-
Coefficient of variation of s_u	COV_{su}	0.2	-

3.4.5 2D geomechanical analysis

The numerical 2D static geomechanical analysis provides key information on the static and pseudo-static FoS as well as the deformation of the subsurface during hydrate dissociation. The numerical analysis calculates both the most likely failure plane and the volume of sediment that may fail. The simulation was carried out using the commercial finite element software PLAXIS 2D (Brinkgreve et al, 2007). The FoS was calculated by reducing the shear strength parameters until the soil mass failed, which is known as the 'phi-c reduction method' (Griffiths and Lane, 1999). Variations in terrain and stratigraphy were derived from the interpretation of the 2D seismic profiles, and soil strength parameters were incorporated. The software first calculated the slip zone with the least FoS against sliding. The production of methane out of a methane hydrate reservoir was then simulated by reducing the pressure and changing the reservoir's material properties given in Table 3.2 within a certain range. The FoS was then calculated again to determine any change of slope stability due to a potential change in topography resulting from seafloor subsidence as well as changes in shear strength in the subsurface. In addition to the simulation under static conditions, a pseudo-static simulation was carried out which included horizontal forces caused by earthquake loading.

3.4.6 Landslide dynamics simulation

Landslides due to hydrate exploitation were modeled to assess the potential run-out distance and velocities for a downslope travelling landslide from the adjacent steep levee walls. The analysis will help to determine potential mitigation measures (e.g. relocation options, design criteria) that may need to be considered for the production infrastructure at the sea bottom.

For the run-out simulations, we used a propriety NGI code for visco-plastic flows in quasi-2D (i.e. depth-averaged). The code is based on the BING code from St. Anthony Falls Laboratory (Imran et al., 2001) and the various extensions to this code were described by De Blasio et al. (2004). The BING3 model performs an analysis of the run-out of an arbitrarily shaped slide block along a predefined geometry (extended slip plane). The model is specifically developed for submarine conditions. The code is based on a non-linear Herschel-Bulkley rheology coupled with depth-averaged mass and momentum continuity equations that were solved using a Lagrangian scheme. The model includes hydrodynamic pressure and friction drag during run-out as well as strength degradation, and can also be used for debris flows with embedded rafted blocks (e.g., Vanneste et al., 2011). Further options are hydroplaning and erosion or entrainment of seabed material, but we did not use these options as there was too little information on the boundary conditions.

The results of the 2D slope stability model from PLAXIS (for both static and pseudo-static analysis) were used as input for the landslide dynamics modeling to guarantee consistency of the results. As there is significant uncertainty on the soil properties, we have run several simulations using a range of realistic soil parameters (Table 3.4). The most critical parameters are:

$\tau_{y,s}$ Initial yield strength of the soil at the time of failure (kPa)

$\tau_{y,r}$ Fully remolded yield strength of the soil (kPa)

R_c Remolding coefficient, with a high value corresponding to rapid remolding during the flow (-)

ν Kinematic viscosity at the flow node ($m^2\ s^{-1}$)

n Herschel-Bulkley exponent (n = 1 implies Bingham fluid)

C_P Pressure drag coefficient, -

C_{FR} Friction drag coefficient, -

In principle, these properties may vary at each node, but we used constant values. We also kept the density of the slurry constant at 1680 kg m^{-3}. We ran the model with a 5 m cell length for the flow, following stability testing. The same properties were used for the static and pseudo-static cases. The parameter range was constrained from either the limited site-specific data of NGI's soil data base for similar soil types as well as the results from the screening tool and PLAXIS simulations. The parameter range includes relatively weak as well as relatively strong conditions, representing end-members for the simulation.

Results of the run-out simulations are: (1) final deposit (thickness) of the mass along the flow path; (2) toe velocity during the flow; (3) peak height at each point along the flow path and (4) peak velocity at each point along the flow path. Limitations are that lateral spreading cannot be taken into account in this quasi-2D model, as a result, the landslide velocity and peak heights may be overestimating high.

Table 3.4: Input parameters for the landslide dynamics simulation. $\tau_{y,s}$ = initial yield strength of the soil at the time of failure, $\tau_{y,r}$ = fully remolded yield strength of the soil, R_c = remolding coefficient, with a high value corresponding to rapid remolding during the flow, ν = Kinematic viscosity at the flow node, n = Herschel-Bulkley exponent, C_P = Pressure drag coefficient, C_{FR} = Friction drag coefficient

model	$\tau_{y,s}$	$\tau_{y,r}$	R_c	ν	*n*	C_P	C_{FR}
	kPa	kPa	-	m2 s^{-1}	-	-	-
1	0.75	0.75	0	0.237	0.25	1	0.001
2	4.50	4.50	0	0.237	0.15	1	0.001
3	3.00	3.00	0	0.237	0.15	1	0.001
4	3.00	3.00	0	0.237	0.35	1	0.001
5	3.00	3.00	0	0.400	0.35	1	0.001
6	4.50	1.50	0.0001	0.237	0.15	1	0.001
7	4.50	0.75	0.001	0.500	0.15	1	0.001
8	4.50	0.75	0.01	0.500	0.15	1	0.001
9	4.50	0.75	0.001	0.500	0.25	1	0.001
10	4.50	0.75	0.001	0.500	0.35	1	0.001
11	3.00	0.75	0.001	0.300	0.15	1	0.001
12	7.50	1.50	0.001	0.300	0.15	1	0.001
13	4.50	1.88	0.001	0.250	0.15	1	0.001
14	4.50	1.88	0.001	0.250	0.15	1	0.001
15	4.50	2.25	0.001	0.250	0.15	1	0.001
16	7.50	2.25	0.0001	0.250	0.15	1	0.001
17	7.50	2.25	0.005	0.250	0.15	1	0.001
18	4.50	0.60	0.001	0.500	0.15	1	0.001
19	11.20	2.80	0.01	2.400	0.15	0.5	0.005
20	11.20	2.80	0.01	0.600	0.15	0.5	0.005
21	11.20	2.80	0.01	0.300	0.15	0.5	0.005
22	11.20	2.80	0.1	2.400	0.15	0.5	0.005
23	11.20	2.80	0.1	0.300	0.15	0.5	0.005
24	11.20	2.52	0.1	0.300	0.15	0.5	0.005
25	11.20	2.10	0.1	0.300	0.15	0.5	0.005
26	11.20	1.40	0.01	2.400	0.15	0.5	0.005
27	11.20	1.40	0.1	2.400	0.15	0.5	0.005

3.5 Results

3.5.1 Initial screening

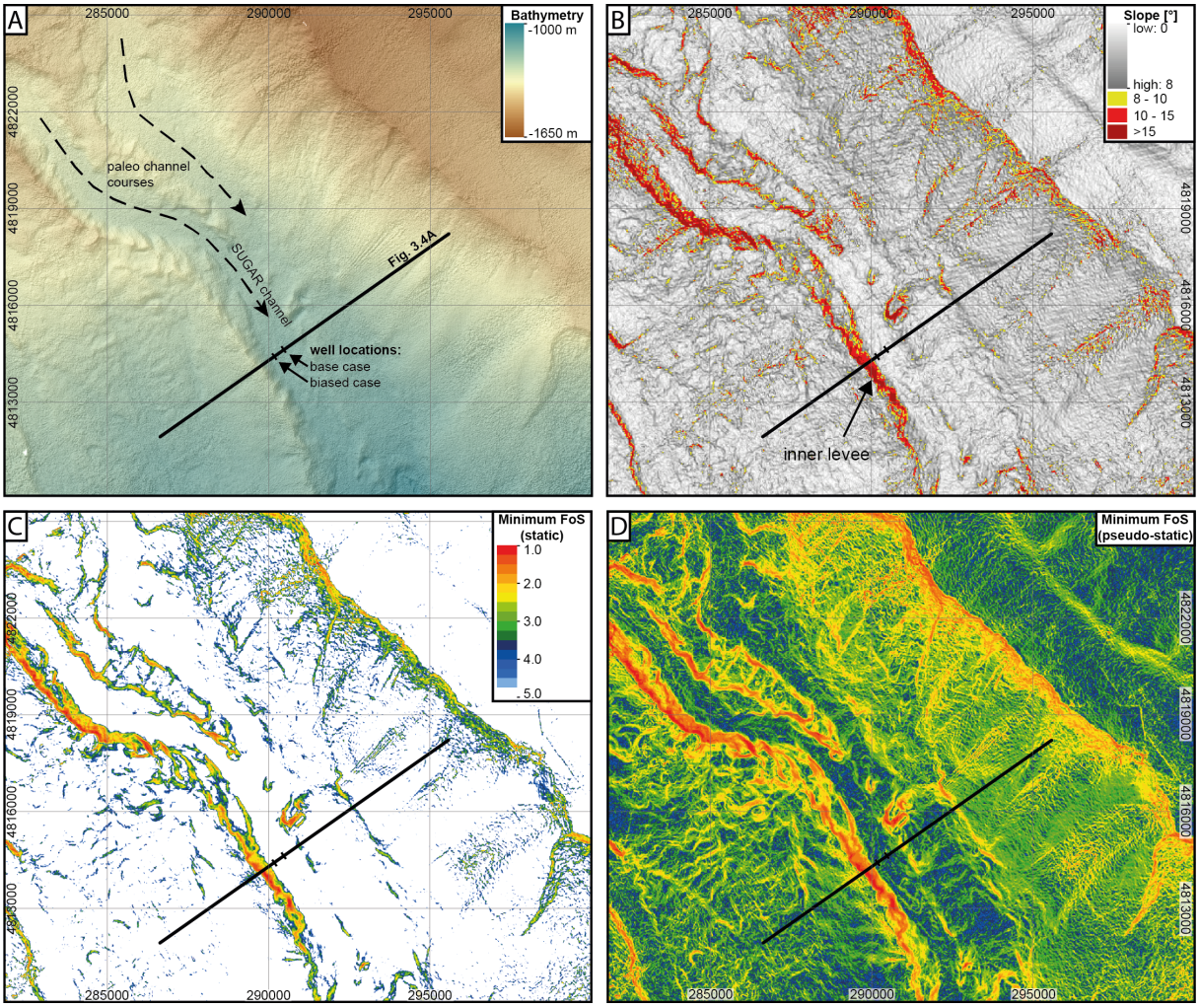

Fig. 3.3 A: Shaded relief bathymetry data from the study area. B: Slope angle calculated from the bathymetry data. C: Minimum Factor of Safety (FoS) under static conditions in the top 30 m of soil. D: Minimum FoS under pseudo-static conditions in the top 30 m of soil. The color scale is the same as in C. Coordinates are given in UTM zone 36N, the location is shown in Fig. 3.2.

Fig. 3.3B and Fig. 3.3C show the slope attribute and the deterministic minimum FoS under static condition, respectively. This is based on the 10 m x 10 m bathymetry dataset (Fig. 3.3A) and the parameters in Tables 3.1 and 3.3. In the study area, any area with slope inclinations exceeding 9° has the potential for slope failure as the associated deterministic FoS falls below 1.5. Most steep natural slopes are located along the paleo-channels at the inner levee walls, especially on the western levees (Fig. 3.3B). Under static conditions, some segments along the levee flanks appear critical with FoS lower than 1.5 (Fig. 3.3C). Because of the low FoS in the static case, we ran an additional pseudo-static slope stability analysis in which an inertial horizontal force was added to represent the effect of earthquake shaking. Earthquakes that triggered tsunamis happened in this area, such as the 1901 Black Sea earthquake with estimated magnitude of 7.2 (Matova, 2000). The simulation showed that for the

pseudo-static screening, the critical areas around the levee walls are larger compared to the static case (Fig. 3.3D).

3.5.2 2D geomechanical analysis

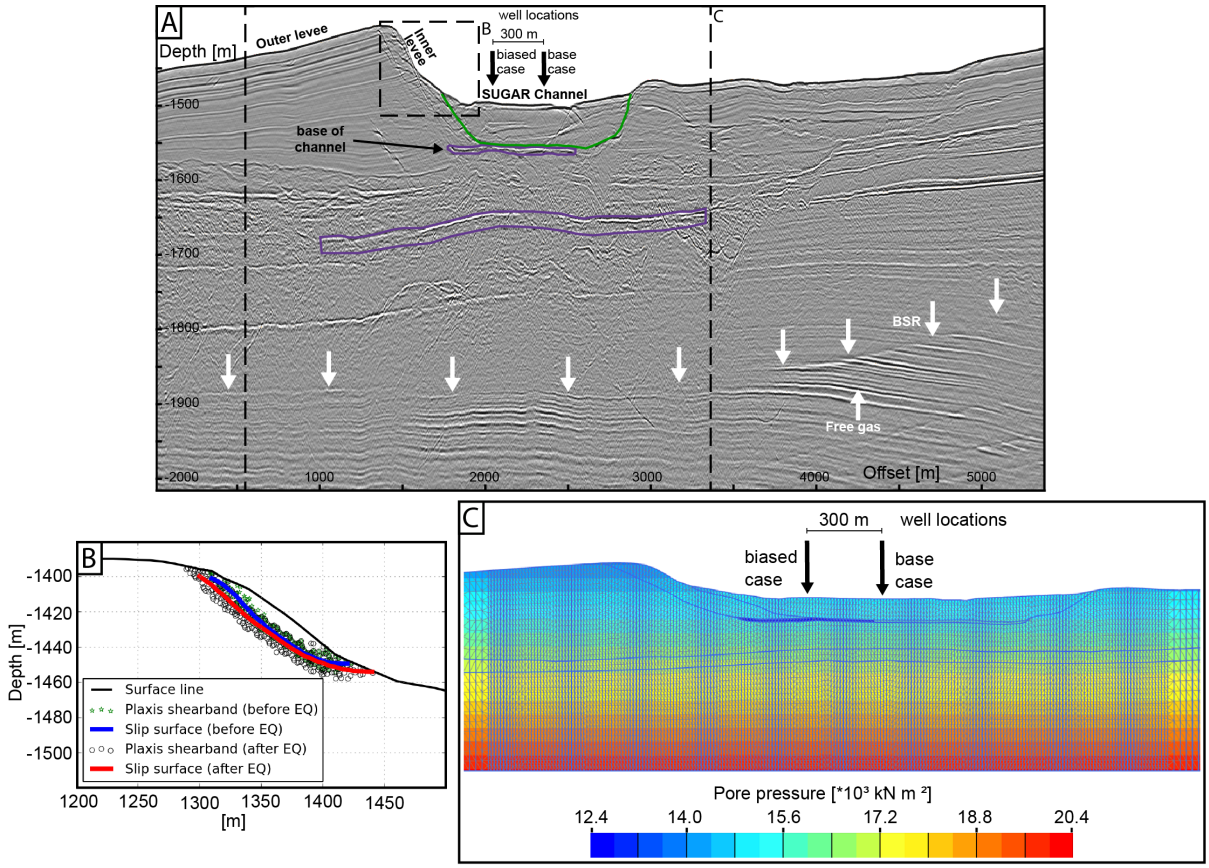

Fig. 3.4 A: 2D line 1107 across the SUGAR channel-levee system, which is located well above the base of the gas hydrate stability zone indicated by the BSR (white arrows) in about 380 m depth below the seafloor. The two hypothetical gas hydrate reservoirs (purple polygon) are located in about 60 m depth at the base of the most recent active channel (shallow reservoir), and in a depth of about 140 m (deeper reservoir). Green = outline of the SUGAR channel. The location of the profile is shown in Fig. 3.3. B: Comparison of the best-fit slip planes obtained from the shear bands under static and pseudo-static conditions. C: Total pore pressure distribution in the finite-element model based on the profile in A, with potential positions of the wells considered in this study.

Based on the screening results, we identified the western levee of the SUGAR channel as the most critical area in terms of slope stability (Fig. 3.3B). We therefore selected the seismic profile 1107, which crosses perpendicular to the levee slope and coincides with the area where most of the geophysical data were collected (Fig. 3.3). The geometry for the 2D geomechanical model was constrained from seismic interpretation and picking of prominent seismic horizons. In the seismic data, the channel facies of the most recent active channel system is clearly visible (Fig. 3.4A). At a depth of about 60 m below the channel seabed, a high amplitude reflection marks the base of the SUGAR channel. The levee at the western channel margin is characterized by well stratified seismic reflections. We interpret this seismic facies as overbank deposits that typically consist of fine-grained mud, clay

and silt (Damuth, 2002). In contrast, the base of a channel-levee system typically consists of coarse-grained sand and gravel (Damuth, 2002), which would provide ideal conditions for the exploitation of gas hydrates out of the pore space by using the depressurization method (e.g. Boswell, 2009).

Gas hydrates cannot be directly identified in reflection seismic data. However, seismic studies (Dannowski et al. 2016) and CSEM studies (Schwalenberg et al. 2016) conducted in the study area found indications for gas hydrates as shallow as 50 m below the seafloor with gas hydrate saturation up to 40 %. The thickness and spatial extent of this potential gas hydrate reservoir is still under debate and will require confirmation through drilling in the future. For this study and based on the observations and results mentioned above, we assumed a thin gas hydrate reservoir along the high-amplitude reflector at the base of the SUGAR channel. This shallow reservoir has an average thickness of about 6 m. In addition, we defined a second hypothetical gas hydrate reservoir following a distinct reflector at a depth of about 140 m below the seafloor and with a thickness of 30 m (Fig. 3.4A). This second reservoir served to assess the effect of reservoir depth on subsidence due to hydrate production. The base of the hydrate stability zone is about 380 m below the seafloor at this location (Figs. 3.1 and 3.4A).

The finite element model built in PLAXIS 2D was composed of 19,352 10-noded triangular elements. To minimize discretization effects and to capture the failure mechanism, the element size was gradually refined close to the reservoir (Fig. 3.4C). The soil parameters described in section 3.4.3 were applied to the overburden soils. To assess the present-day stability of the area, we initially calculated the slip zone with the least FoS under static conditions. The calculated slip plane is located at the steepest part of the levee, and has a horizontal length of about 120 m and a maximum thickness of 15 m, with a FoS of 1.27 (Fig. 3.4B). In the pseudo-static slope stability analysis, the slip plane is located slightly deeper at about 17 m and has a larger extent of about 140 m. The FoS is lower at about 1.01.

3.5.3 Effect of hydrate production on slope stability

In order to simulate gas production out of the hypothetical reservoirs, we investigate various production scenarios as a parametric study. This study focuses on the shallow hydrate reservoir, as there is more evidence for the presence of hydrate in this reservoir compared to the deeper target and because any effects on seafloor stability are expected to be stronger for the shallower reservoir. First, a well location was defined. The pore pressure at the well was then depleted along the entire vertical thickness of the reservoir. Within the depleted zone, the pressure was kept constantly low and the dissociation front spread out gradually into the reservoir over time. The pressure reduction was considered as 8 to 10 MPa based on the field scale production test in the Nankai Trough (Konno et al., 2017), which is sufficiently high for hydrates to dissociate under the pressure and temperature conditions in the study area (Fig. 3.1).

We tested the following scenarios:

- Depletion pressures of 8 MPa and 10 MPa
- 10 m to 150 m radius around the borehole for the area affected by hydrate dissociation indicative for the production time
- Well location at the center of the SUGAR channel (base case) and closer to the levee (biased case)
- production out of the shallow reservoir and production from the deeper reservoir.

Depletion pressure increase

Fig. 3.5 shows the effect of different depletion pressures on reservoir compaction and subsidence. For this parameter test, we assumed that constant pore pressure reduction affects the reservoir within 150 m around the well. The maximum depletion pressure (10 MPa in the entire dissociation zone) is representative for a target of 12 MPa depletion at the well. A simulation carried out in the Ulleung Basin of the Korean East Sea showed that the pressure target will only be achieved in a very narrow zone close to the well and decreases rapidly towards the margin of the reservoir (Kim et al., 2014), and similar results were shown for the production site in the Nankai Trough (Konno et al., 2017). The geomechanical simulation showed that higher depletion pressure increases the mean compaction rate of the reservoir, with a maximum compaction of 0.69 m for a 10 MPa depletion.

The subsidence at the seafloor is about 30 % smaller compared to the reservoir compaction, with a maximum subsidence of 0.41 m for the 10 MPa depletion case. The lateral extent of the deformation at the seabed is limited to the vicinity of the compacted reservoir and does not spread out to the failure surface at the levee margin. The FoS of the slip surface remains unaffected.

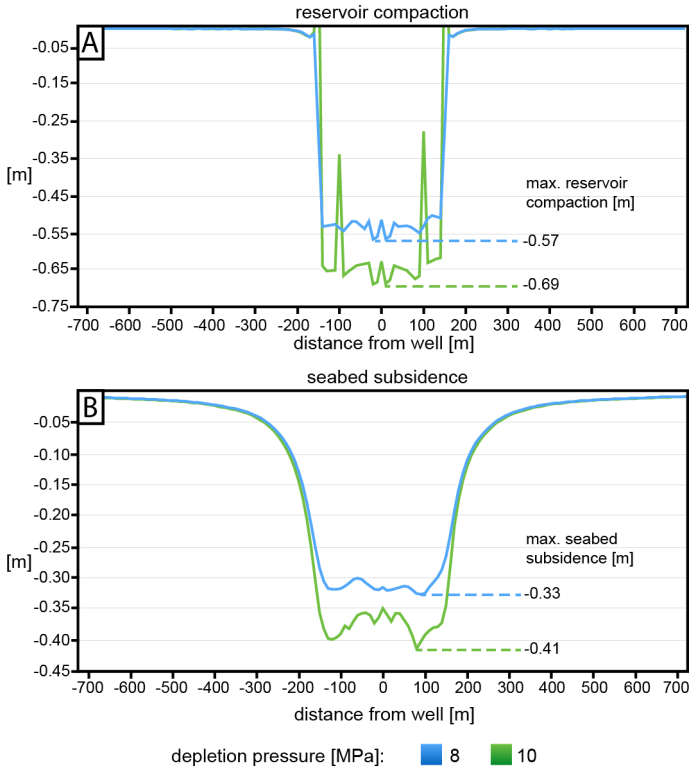

Fig. 3.5: Results from the parametric study for the shallow hydrate reservoir, showing reservoir compaction (A) and seabed subsidence (B) for depletion pressures of 8 and 10 MPa, assuming a maximum dissociation radius of 150 m around the borehole.

Production time

We simulated the production time by varying the size of the area affected by hydrate dissociation. Small radii of about several tens of meters around the well will be reached after a small production time of a few days (e.g. Kim et al., 2014, Konno et al., 2017), while the maximum case of a 150-m radius represents a longer production time of up to a few years. The dissociation area radii tested in this study varied between 10 m and 150 m. Fig. 3.6 shows the simulations for a maximum depletion pressure of 10 MPa. With increasing dissociation radius, the seabed subsidence increases both vertically and laterally. The lateral extent of the deformation remains in the vicinity of the compacted reservoir, but the vertical displacement at the seabed increases with the laterally spreading dissociation front in the reservoir (Fig. 3.6A). The FoS of the slip surface remains unaffected for the tested dissociation radii.

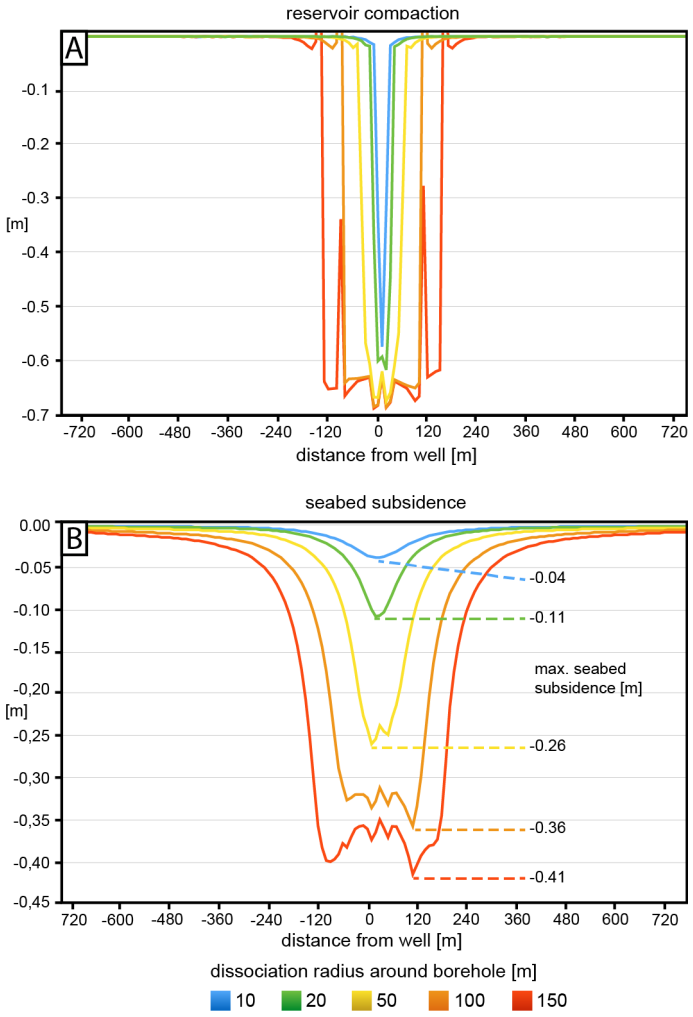

Fig. 3.6: Results from the parametric study for the shallow hydrate reservoir, showing reservoir compaction (A) and seabed subsidence (B) for a depletion pressure of 10 MPa for different hydrate dissociation radii around the borehole. The simulations indicate that the lateral extent of the subsided seafloor is directly coupled to the compacted reservoir.

Change of well location

Moving the well location from the center of the channel (base case) 300 m closer to the levee wall (biased case) results in a shift of maximum displacements of the reservoir compaction and seabed subsidence. Fig. 3.7 shows the simulations for a 150 m dissociation front around the well and a depletion pressure of 8 MPa. Although closer to the levee and its failure surface, the deformation at the seabed does not spread out towards the slip surface and the FoS remains unaffected for the biased well location.

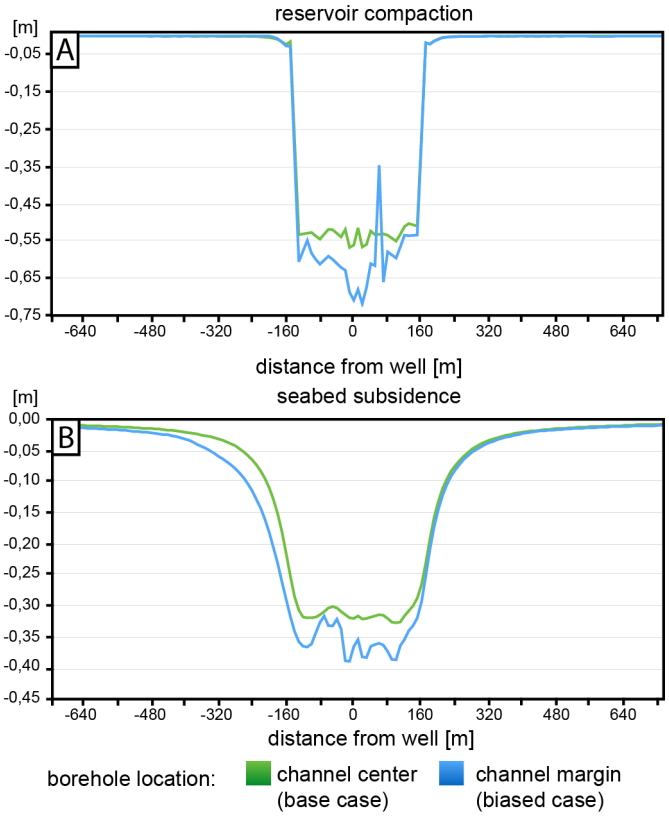

Fig. 3.7: Results from the parametric study, showing a comparison of reservoir compaction (A) and seabed subsidence (B) between two well locations in the channel center (base case) and the channel margin (biased case). The well locations are shown in Fig. 3.4C.

Reservoir depth

In order to compare production of a shallow reservoir in about 60 m depth with a deeper reservoir in about 140 m depth, we plotted the ratio of dissociation radius (representing production time) to depth of the reservoir against the ratio of maximum subsidence to maximum reservoir compaction (Fig. 3.8). Note that the simulation for the deep reservoir was only tested for the maximum depletion pressure of 10 MPa. The results indicate that for the deeper reservoir the subsidence is larger in relation to the compaction of the reservoir over time. However, the FoS of the slip surface remains unaffected at 1.27.

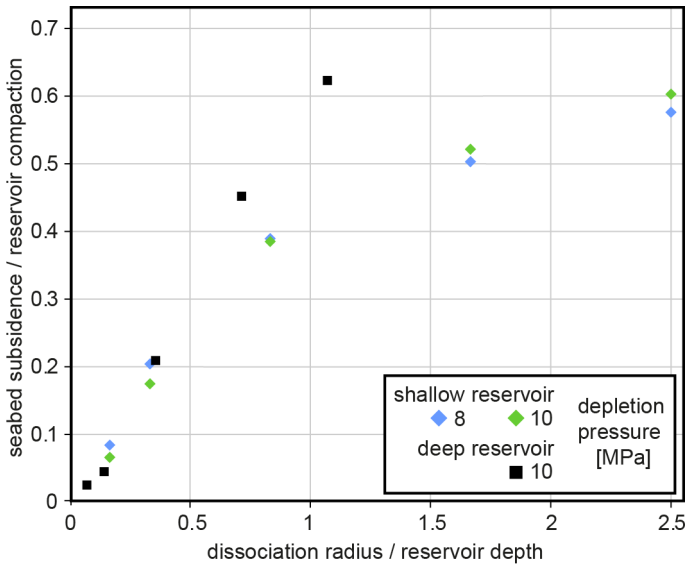

Fig. 3.8: Results from the parametric study, showing a comparison of the two hypothetical reservoirs, with the shallow reservoir located at about 60 m depth and the deeper reservoir at about 140 m depth below the seafloor (Fig. 3.4A).

3.5.4 Landslide dynamics (quasi-2D)

The results of the landslide dynamic simulations using the 2D slope stability output showed that the run-out reaches approximately 500 – 900 m for the static case and 600 m – 1000 m in the pseudo-static case (Fig. 3.9). The final deposit reaches a thickness of approximately 5 m in the static case (Fig. 3.9C) and 6 m in the pseudo-static case (Fig. 3.9D). The flow velocity at the toe peaks at 9 m s^{-1} and 14 m s^{-1} with marginally higher velocities for the pseudo-static case compared to the static case (Fig. 3.9E, F). During the remobilization, the maximum thickness of the flow is in the order of 8 - 20 m for the static case and about 250 m away from the landslide toe at failure (Fig. 3.9G) with maximum flow velocities around 9 to 15 m s^{-1} (Fig. 3.9I). For the pseudo-static case, the maximum flow thickness is on average 3 m thicker due to the larger volume which is mobilized (Fig. 3.9H) with maximum flow velocities around 10 m s^{-1} to 16 m s^{-1} (Fig. 3.9J).

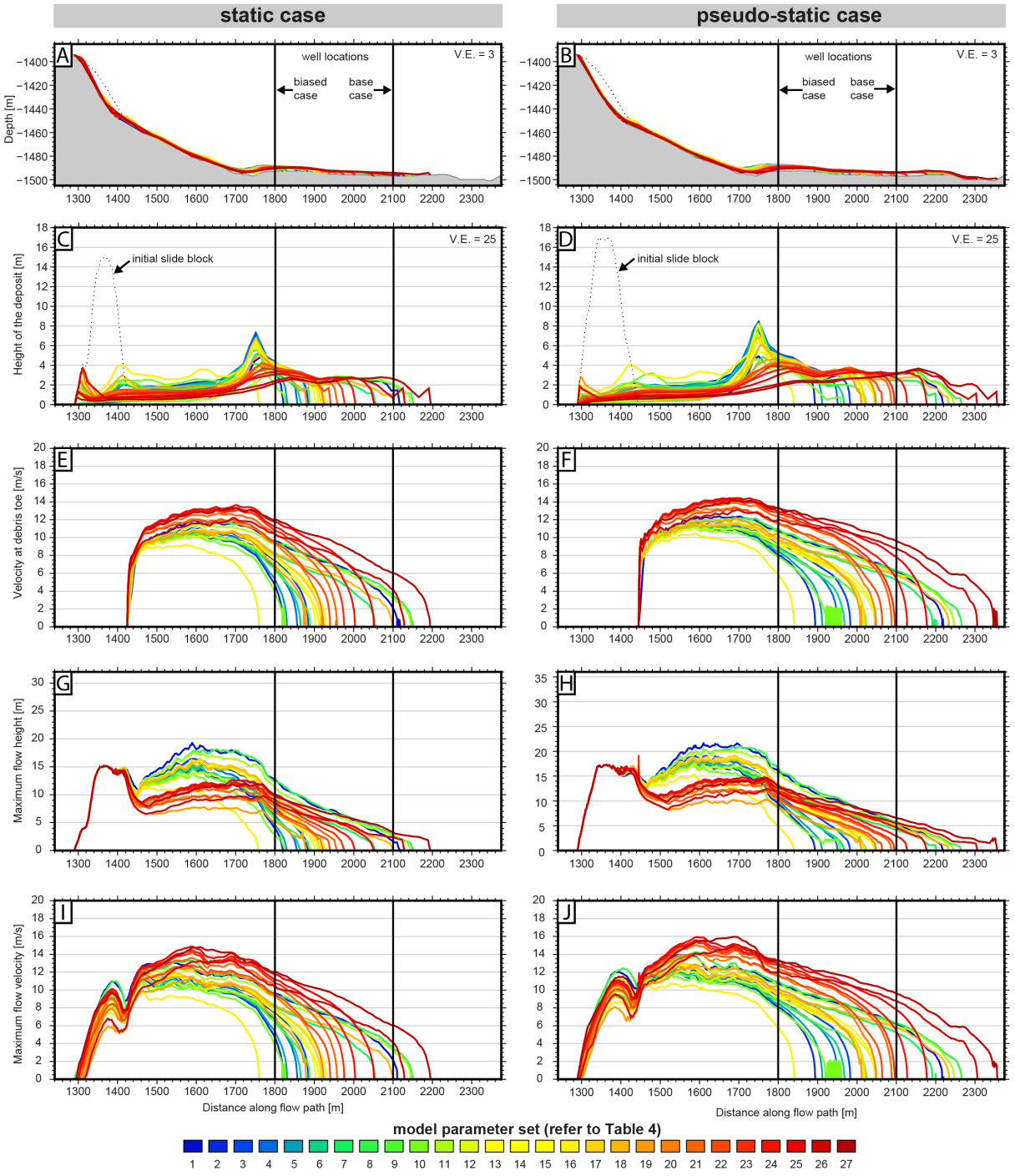

Fig. 3.9: Results from the quasi-2D landslide dynamics simulation for the static (left) and pseudo-static (right) cases. The model parameters for the 27 different runs (color coded) are presented in table 4. A, B: Final deposit of the mass projected on the topography (grey). The initial slide block is shown as a dotted line. C, D: Final deposit (thickness of the mass along the flow path. E, F: toe velocities during the flow. G, H: peak height at each point along the flow path. I, J: peak velocity at each point along the flow path.

3.6 Discussion

3.6.1 Slope stability before, during, and after production

The parameters used for the screening and geomechanical analysis of the area are conservative (i.e. gearing the model towards less stable slopes), but in the absence of specific knowledge of the subsurface conditions, they provide effective screening criteria. The screening of the study area revealed that the entire area is essentially stable, with only some segments along the inner levee flanks of the paleo channels that appear critical. Here, slope angles exceed 9°, which results in a FoS of <1.5 against slope failure. For engineering works to be conducted, the FoS value is typically required to be above 1.5 in the static case and 1.1-1.2 in the pseudo-static case (e.g. Eurocode 8 (CEN, 2004), depending on the type of facility). In our study, the 2D slope stability analysis for the western levee of the SUGAR channel revealed a FoS of 1.27 in the static case, which is typically not sufficiently high. In the pseudo-static analysis, the FoS is 1.01, which is considered critical. In case of an earthquake, a landslide would likely occur. Compared to the static case, a larger volume of soil may be mobilized as the slip plane is located deeper and more wide-spread.

The preconditioning factors of slope instability considered in this study are the change in geometry due to seabed subsidence, and shear strength reduction due to the removal of solid hydrate from the hypothetic reservoir during production. However, the post-production landslide stability model, which takes these effects into account, shows that the deterministic FoS remains unchanged at 1.27. The production of gas out of the hypothetical methane hydrate reservoir therefore has no effect on slope stability. The main reason why the strength reduction does not affect the initial FoS is that the relatively shallow depth of the hydrate reservoir (60 m) is still deeper than the calculated line of failure. Seafloor subsidence, although amounting to 0.4 m, remains confined to the immediate vicinity above the production sites, which are located in relatively flat terrain several hundreds of meters away from the steep levee flanks. Because of the extent of the hydrate reservoir, there is no point in moving the well location closer to the levee flank. The small differences in model results for the two well locations are due to the differences in geometry and slightly inhomogeneous thickness of the reservoir at both locations.

3.6.2 Potential hazards related to slope instabilities in the target area

One of the major hazards in the study area is the triggering of a landslide (i.e. by an earthquake). The analysis of landslide dynamics carried out in this study showed that a hypothetical slide may impact potential seafloor installations in both the base and the biased scenarios. The final slide deposit extends to the center of the channel with a depositional height of up to 5-6 m. In the base case the deposit may therefore reach the well (static case), and extend even beyond the well in the pseudo-static simulation. In the biased case, in which the well is located closer to the levee flank, the debris flow would reach the well site at a velocity of 4-12 m s^{-1}. Thus, a production platform would have to be strong enough to withstand such an impact or drilling has to be conducted at sufficiently great distance to the levee flank. Because the entire inner levee flank in this area dips at rather uniform steep angles, this recommendation does not only apply to the location of the 2D slope stability model, but also in upward or downward direction along the channel. In shallower water, the levee slopes generally become steeper which negatively affects the FoS. Further, many landslides in river deltas have a multiphase and

retrogressive development (Kvalstad et al., 2005, Kvalstad, 2007). After failure, the new slope may also be unstable and fail progressively in a back-stepping process over a relatively short period.

3.6.3 Limitations

In the absence of in situ geotechnical properties, several approximations and simplifications had to be made in order to create a geomechanical model for the study area. The largest uncertainty stems from the actual distribution of the gas hydrates as well as the in situ hydrate saturation. Changes of these parameters will have an impact on the modeling results and the assessment of geohazards. It is therefore necessary to obtain more accurate estimates of hydrate saturation through geophysical inversion of the existing data and future well logs to better constrain the amount and distribution of gas hydrates in the Danube deep-sea fan. Furthermore, the actual pore pressure distribution in the sediments is unknown and was therefore not considered in this study. Zones of overpressure may change the seafloor stability significantly since the effective stress (and therefore the shear strength) decreases with increasing pore pressure (e.g. Riboulot et al., 2016).

The model presented in this study consists of an isolated reservoir with constant pressure within the dissociation radius around the borehole. However, simulations showed that the target depletion pressure is only reached in a very narrow area around the well and decreases with further distance from the well (Kim et al., 2014, Konno et al., 2017). In this sense, the results presented in this study provide conservative estimates of slope stability changes. The applied mean depletion pressure of e.g. 10 MPa for the entire reservoir is considered representative for a higher depletion pressure target at the borehole (e.g. 12 MPa). A production simulation carried out for the Nankai hydrate production site found that a stepwise production method with waiting times in the order of ten days between two pressure reductions helps to reduce ground settlements (Zhou et al., 2014). Such a delayed depressurization process reduces gas production in the short term, but in the long-term, the total amount of produced gas will be similar to scenarios where the pressure target is achieved immediately.

Another limiting factor is that the FoS can be rather sensitive to small differences in slope geometry. Therefore, the potential for shallow seated small failures may be neglected due to the 10-m grid size of the bathymetric data. We also neglected the effect of the sloping seabed in the direction of the channel. Only a more sophisticated approach based on a 3D geometry model would give certainty as to the predicted failure loads in this complex bathymetric setting. A comparison between a 2D and a 3D approach for a different study area is e.g. presented in Sultan et al. (2011).

Finally, our modelling did not take into account fluid coupling of chemical disequilibrium. However, considering the uncertainties mentioned above, such in-depth modelling is currently not feasible but should be considered in a future model when more data becomes available.

3.7 Conclusions

The combined geomechanical analyses carried out in this study include slope stability investigations, analysis of landslide dynamics, and consequences of gas hydrate production on reservoir compaction and seabed subsidence, which may lead to secondary failures along the slope. The models were constrained from geophysical data combined with sparse geotechnical data. Screening indicated that the area may be considered stable in general, with critical slopes encountered at the inner levee flanks which are present along numerous paleo channel courses throughout the Danube deep-sea fan. The 2D slope stability modeling in the vicinity of a hypothetical gas hydrate reservoir in about 60 m below the seafloor suggests that the area is relatively safe against slope failure under static conditions (FoS around 1.27), but probably not sufficiently safe to allow developments of infrastructure at the seabed without taking specific mitigation measures into account. The simulation of hydrate production showed that the FoS is not significantly affected by the production process, as reservoir compaction and seabed subsidence remain confined to the immediate vicinity of the well sites, which lie in a sufficient distance from the main critical instability zone at the levee flank. The landslide dynamic simulation showed that if slope failure were to happen, the mobilized mass could impact at the production sites. It is more likely that seafloor facilities are damaged by a landslide triggered by an earthquake during drilling than by a landslide triggered by production itself. In general, it may be sufficient to keep a large enough distance away from the steep levee flanks to avoid any hydrate production-related slope failures.

3.8 Acknowledgements

The research leading to these results has received funding from the European Union Seventh Framework Programme (FP7/2007-2013) under the MIDAS project, grant agreement no. 603418, from the German Ministry of Education and Research (BMBF) and from the Federal Ministry of Economy and Energy (BMWi) through the SUGAR project (grant nos. 03G0819A, 03SX320A, 03G0856A). We would like to thank the captains and crews of RV MARIA S. MERIAN and RV Pourquoi Pas? cruises MSM34 and GHASS as well as the lab technicians for their excellent support. We further acknowledge Sebastien Garziglia for the analysis on the overburden soil parameters and Dieter Issler and Noel Boylan for developing the landslide dynamics code partly supported by NGI's internal R&D funding.

3.9 References

Bialas, J., Klaucke, I., and Haeckel, M. (Eds.), 2014. FS MARIA S. MERIAN Fahrtbericht / Cruise Report MSM-34/1 & 2 - SUGAR Site, 06.12.13-16.01.14, Varna – Varna. GEOMAR Report, N. Ser. 015. GEOMAR Helmholtz-Zentrum für Ozeanforschung Kiel, Germany, 111 pp., doi:10.3289/GEOMAR_REP_ NS_15_2014.

Boswell, R., 2009. Is gas hydrate energy within reach? Science 325, pp. 957-958, doi:10.1126/science.1175074.

Brinkgreve, R.B.J., Broere, W., and Waterman, D., 2007. PLAXIS 2D Manual. Delft University of Technology, Delft.

Carlton, B.D., Price, K., Vanneste, M., and Forsberg, C.F., 2017. Development and application of a regional slope stability assessment screening tool. 2nd International Workshop on Landslides in Sensitive Clays, Trondheim, Norway, 10 pp.

CEN, 2004. EN-1998-1: Eurocode 8: Design of Structures for Earthquake Resistance. European Committee for Standardization, Brussels, 229 pp.

Crutchley, G.J., Mountjoy, J.J., Pecher, I.A., Gorman, A.R., and Henrys, S.A., 2016. Submarine slope instabilities coincident with shallow gas hydrate systems: Insights from New Zealand examples. In: Lamarche, G., Mountjoy, J., Bull, S., Hubble, T., Krastel, S., Lane, E., Micallef, A., Moscardelli, L., Mueller, C., Pecher, I., and Woelz, S. (Eds.), Submarine Mass Movements and their Consequences. Advances in Natural and Technological Hazards Research 41, Springer, pp. 401-409.

Damuth, J.E., 2002. The Amazon-HARP Fan model: Facies distributions in mud-rich deep-sea fans based on systematic coring of architectural elements of Amazon Fan. CIESM Workshop 17, pp 19-22.

Dannowski, A., Bialas, J., Zander, T., and Klaeschen, D., 2016. Shear wave modelling of high-resolution OBS data in a gas hydrate environment in the Danube deep-sea fan, Black Sea. AGU Fall Meeting 2016, San Francisco, USA, 12-16 December 2016.

De Blasio, F.V., Engvik, L., Harbitz, C., and Elverhøi, A., 2004. Hydroplaning and submarine debris flows. Journal of Geophysical Research: Oceans 109, C01002, doi:10.1029/2002JC001714.

Degens, E.T., and Ross, D.A., 1974. The Black Sea – Geology, Chemistry, and Biology. The American Association of Petroleum Geologists, Tulsa, USA.

Fjaer, E., Holt, R.M., Horsrud, P., Raaen, A.M., and Risnes, R., 2008. Petroleum Related Rock Mechanics (Second Edition). Developments in Petroleum Science 53, Elsevier.

Garziglia, S., 2016. MIDAS. Complete geo-mechanical properties of gas hydrate bearing sediments from in situ geotechnical measurements. Scientific report, Ifremer, France, 22 pp.

Giardini, D., 1999. The global seismic hazard assessment program (GSHAP) – 1992/1999. Annali di Geofisica 42, pp. 957-974.

Griffiths, D.V., and Lane, P.A., 1999. Slope stability analysis by finite elements. Geotechnique 49, pp. 387-403.

Hansen, L.A.S., Callow, R.H.T., Kane, I.A., Gamberi, F., Rovere, M., Cronin, B.T., and Kneller, B.C., 2015. Genesis and character of thin-bedded turbidites associated with submarine channels. Marine and Petroleum Geology 67, pp. 852-879, doi:10.1016/j.marpetgeo.2015.06.007.

Imram, J., Harff, P., and Parker, G., 2001. A numerical model of submarine debris flow with graphical user interface. Computers & Geosciences 27, pp. 717-729, doi:10.1016/S0098-3004(00)00124-2.

Ker, S., and Riboulot, V., 2015. GHASS cruise report. Ifremer, France, 53 pp.

Kim, A.R., Cho, G.C., Song, K.I., and Kim, S.J., 2014. Settlement prediction in the Ulleung Basin due to gas hydrate production. Offshore Technology Conference, OTC25308-MS, Houston, Texas, USA, 5-8 May 2014, 10 pp.

Konno, Y., Fujii, T., Sato, A., Akamine, K., Naiki, M., Masuda, Y., Yamamoto, K., and Nagao, J., 2017. Key findings of the world's first offshore methane hydrate production test off the coast of Japan: Toward future commercial production. Energy & Fuels 31, pp. 2607-2616, doi:10.1021/acs.energyfuels.6b03143.

Kvalstad, T.J., Andresen, L., Forsberg, C.F., Berg, K., Bryn, P., and Wangen, M., 2005. The Storegga slide: evaluation of triggering sources and slide mechanics. Marine and Petroleum Geology 22, pp. 245-256, doi:10.1016/j.marpetgeo.2004.10.019.

Kvalstad, T.J., 2007. What is the current "best practice" in offshore geohazard investigations? A state-of-the-art review. Offshore Technology Conference, OTC18545, Houston, Texas, USA, 30 April - 3 May 2007, 14 pp.

Kvalstad, T.J., Yamamoto, K., Noguchi, S., Uchida, S., and Soda, K., 2011. Effect of gas hydrate production on seabed stability in the eastern Nankai Trough area. Proceedings of the 7th International Conference on Gas Hydrates (ICGH), Edinburgh, Scotland, 17-21 July 2011, 10 pp.

Matova, M., 2000. Recent geological activity along the northeastern Bulgarian Black Sea coast. Geological Quaterly 44, pp. 355-362.

Merey, S., and Sinayuc, C., 2016a. Experimental set-up design for gas production from the Black Sea gas hydrate reservoirs. Journal of Natural Gas Science and Engineering 33, pp. 162-185, doi:10.1016/ j.jngse.2016.04.030.

Merey, S., and Sinayuc, C., 2016b. Investigation of gas hydrate potential of the Black Sea and modelling of gas production from a hypothetical Class 1 methane hydrate reservoir in the Black Sea conditions. Journal of Natural Gas Science and Engineering 29, pp. 66-79, doi: 10.1016/j.jngse.2015.12.048.

Micallef, A., Masson, D.G., Berndt, C., and Stow, D.A.V., 2009. Development and mass movement processes of the north-eastern Storegga Slide. Quaternary Science Reviews 28, pp. 433-448, doi:10.1016/ j.quascirev.2008.09.026.

Morgenstern, N.R., 1967. Submarine slumping and the initiation of turbidity currents. In: Richards, A.F. (Ed.), Marine Geotechnique. University of Illinois Press, Urbana, Illinois, pp. 189-210.

Myshakin, E.M., Gaddipati, M., Rose, K., and Anderson, B.J., 2012. Numerical simulations of depressurization-induced gas production from gas hydrate reservoirs at the Walker Ridge 313 site, northern Gulf of Mexico. Marine and Petroleum Geology 34, pp. 169-185, doi:10.1016/j.marpetgeo.2011.09.001.

Özsoy, E., and Ünlüata, Ü., 1997. Oceanography of the Black Sea: a review of some recent results. Earth-Science Reviews 42, pp. 231-272, doi:10.1016/S0012-8252(97)81859-4.

Popescu, I., Lericolais, G., Panin, N., Wong, H.K., and Droz, L., 2001. Late Quaternary channel avulsions on the Danube deep-sea fan, Black Sea. Marine Geology 179, pp. 25-37, doi:10.1016/S0025-3227(01)00197-9.

Popescu, I., De Batist, M., Lericolais, G., Nouzé, H., Poort, J., Panin, N., Versteeg, W., and Gillet, H., 2006. Multiple bottom-simulating reflections in the Black Sea: Potential proxies of past climate conditions. Marine Geology 227, pp. 163-176, doi:10.1016/j.margeo.2005.12.006.

Riboulot, V., Cattaneo, A., Sultan, N., Garziglia, S., Ker, S., Imbert, P., and Voisset, M., 2013. Sea-level change and free gas occurrence influencing a submarine landslide and pockmark formation and distribution in deepwater Nigeria. Earth and Planetary Science Letters 375, pp. 78-91, doi:10.1016/j.epsl.2013.05.013.

Ross, D.A., and Degens, E.T., 1974. Recent sediments of Black Sea. In: Degens, E.T., Ross, D.A. (eds.), The Black Sea – Geology, Chemistry, and Biology. American Association of Petroleum Geologists, pp. 183-199.

Saeki, T., Fujii, T., Inamori, T., Kobayashi, T., Hayashi, Nagakubo, S., and Takano, O., 2008. Extraction of methane hydrate concentrated zone for resource assessment in the Eastern Nankai Trough, Japan. Offshore Technology Conference, OTC19311, Houston, Texas, USA, 5-9 May 2008, 8 pp.

Santamarina, J.C., Dai, S., Terzariol, M., Jang, J., Waite, W.F., Winters, W.J., Nagao, J., Yoneda, J., Konno, Y., Fujii, T., and Suzuki, K., 2015. Hydro-bio-geomechanical properties of hydrate-bearing sediments from Nankai Trough. Marine and Petroleum Geology 66, pp. 434-450, doi:10.1016/j.marpetgeo.2015.02.033.

Schwalenberg, K., Gehrmann, R., Rippel, D., Hölz, S., and Zander, T., 2016. Gas hydrate saturation estimates from the Danube Delta offshore Romania using marine controlled source electromagnetics. GIMS13 Gas in Marine Sediments, Tromsø, Norway, 19-22 September 2016.

Shipley, T. H., Houston, M. H., and Buffler, R. T., 1979. Seismic evidence for widespread occurrence of possible gas-hydrate horizons on continental slopes and rises. AAPG Bulletin 63, pp. 2204-2213.

Sloan, E.D., 1998. Clathrate Hydrates of Natural Gases. Marcel Dekker, New York.

Soulet, G., Delaygue, G., and Vallet-Coulomb, C., 2010. Glacial hydrologic conditions in the Black Sea reconstructed using geochemical pore water profiles. Earth and Planetary Science Letters 296, pp. 57-66, doi:10.1016/j.epsl.2010.04.045.

Sultan, N., Garziglia, S., and Colliat, J.L., 2011. Gas hydrate occurrences and seafloor deformation: Investigation of strain-softening of gas-hydrate bearing sediments and its consequence in terms of submarine slope instabilities. Offshore Technology Conference, OTC21294, Houston, Texas, USA, 2-5 May 2011, 18 pp.

Urlaub, M., Talling, P.J., and Masson, D.G., 2013. Timing and frequency of large submarine landslides: implications for understanding triggers and future geohazard. Quaternary Science Reviews 72, pp. 63-82, doi:10.1016/j.quascirev.2013.04.020.

Vanneste, M., Harbitz, C.B., De Blasio, F.V., Glimsdal, S., Mienert, J., and Elverhøi, A, 2011. Hinlopen-Yermak Landslide, Arctic Ocean – Geomorphology, Landslide Dynamics, and Tsunami Simulations. In: Shipp, R.C., Weimer, P., and Posamentier, H. (Eds.), Mass-Transport Deposits in Deepwater Settings. Society for Sedimentary Geology, Tulsa, Oklahoma, USA, pp. 509-527.

Vanneste, M., Sultan, N., Garziglia, S., Forsberg, C.F., and L'Heureux, J.S., 2014. Seafloor instabilities and sediment deformation processes: The need for integrated, multi-disciplinary investigations. Marine Geology 352, pp. 183-214, doi:10.1016/j.margeo.2014.01.005.

Waite, W.F., Santamarina, J.C., Cortes, D.D., Dugan, B., Espinoza, D.N., Germaine, J., Jang, J., Jung, J.W., Kneafsey, T.J., Shin, H., Soga, K., Winters, W.J., and Yun, T.S., 2009. Physical properties of hydrate-bearing sediments. Reviews of Geophysics 47, RG4003, doi:10.1029/2008RG000279.

Wong, H.K., Winguth, C., Panin, N., Dinu, C., Wollschläger, M., Georgescu, P., Ungereanu, G., Krugliakov, V.V., and Podshuveit, V., 1997. The Danube and Dniepr fans, morphostructure and evolution. GeoEcoMarina 2, pp. 77-102.

Yamamoto, K., Terao, Y., Fujii, T., Ikawa, T., Seki, M., Matsuzawa, M., and Kanno, T., 2014. Operational overview of the first offshore production test of methane hydrates in the Eastern Nankai Trough. Offshore Technology Conferency, OTC25243-MS, Houston, Texas, USA, 5-8 May 2014, 11 pp.

Yoneda, J., Masui, A., Konno, Y., Jin, Y., Egawa, K., Kida, M., Ito, T., Nagao, J., and Tenma, N., 2015. Mechanical properties of hydrate-bearing turbidite reservoir in the first gas production test site of the Eastern Nankai Trough. Marine and Petroleum Geology 66, pp. 471-486, doi:10.1016/j.marpetgeo.2015.02.029.

Zander, T., Haeckel, M., Berndt, C., Chi, W.C., Klaucke, I., Bialas, J., Klaeschen, D., Koch, S., and Atgın, O., 2017. On the origin of multiple BSRs in the Danube deep-sea fan, Black Sea. Earth and Planetary Science Letters 462, pp. 15-25, doi:10.1016/j.epsl.2017.01.006.

Zhou, M., Soga, K., Xu, E., Uchida, S., and Yamamoto, K., 2014. Numerical study on Eastern Nankai Trough gas hydrate production test. Offshore Technology Conference, OTC25169, Houston, Texas, USA, 5-8 May 2014, 19 pp.

4. New insights into the Kerch seep plumbing system in the Black Sea

Timo Zander[a], Matthias Haeckel[a], Ingo Klaucke[a], Christian Berndt[a], Joerg Bialas[a], Dirk Klaeschen[a], Cord Papenberg[a]

[a]*GEOMAR Helmholtz Centre for Ocean Research Kiel, Germany*

To be submitted to Marine Geology

4.1 Abstract

High-resolution 3D seismic data in combination with sidescan sonar data and pore water geochemical analysis give insights into the surface distribution and plumbing system of the Kerch seep site in the northwestern Black Sea. The study area is located in around 900 m water depth well within the gas hydrate stability zone (GHSZ) and comprises three individual seeps which are closely spaced in a paleo channel-levee system of the Don Kuban deep-sea fan. We show that the seep mounds are caused by sediment updoming due to gas overpressure. Each of the seeps hosts its own gas pocket underneath the domes, which is supplied with biogenic methane along narrow pipes through the GHSZ. Methane transport predominantly occurs in the form of gas bubbles. Our analysis suggests that the Kerch seep site is a relatively young and active seep system that lacks extensive carbonate crusts compared to the well-studied seep sites in the eastern Black Sea.

4.2 Introduction

Cold seeps are seafloor sites where fluids such as hydrocarbon gases, oil, or gas-rich pore waters rise from deeper strata to the shallow subsurface and eventually escape into the water column. Cold seeps consist of four main structural elements: fluid source, upward migration pathways, plumbing system and near-seafloor venting structures (Klaucke et al., 2006; Talukder, 2012; Koch et al., 2015; Luo et al., 2016). Most cold seep sites are dominated by methane (Judd, 2003; Bohrmann and Torres, 2006). Seeps are often indicators for active, deep petroleum systems, but the relationship between seafloor seepage and deep reservoirs, and in particular the migration of free gas through the gas hydrate stability zone (GHSZ) can be complex (Talukder, 2012). Multiple studies described cold seeps in many different geological settings at active (e.g. Stakes et al., 1999; Klaucke et al., 2008; Greinert et al., 2010) and passive continental margins (e.g. Sahling et al., 2008) around the world. At many of these seep sites, gas escape into the water column has been observed, also in areas within the GHSZ (Suess et al, 1999).

Microbial anaerobic oxidation of methane (AOM) and the coupled sulfate depletion in the sulfate-methane transition zone (SMTZ) is observed at all cold seep sites (Boetius et al., 2000). The analysis of these pore water profiles at active seep sites and comparison with background profiles provides insight into the processes involved at local seep sites, such as origin, quantification, and transport mechanisms of methane (e.g. Haeckel et al., 2004, 2007; Bhatnagar et al., 2008; Reigner et al., 2011; Koch et al., 2016).

Gas accumulations underneath the seafloor can be mapped using various geophysical equipment such as sediment echosounders or high-resolution reflection seismic experiments, because gas bubbles cause scattering and absorption of acoustic energy, which results in acoustic turbidity or blanking in sediment echosounder data (Judd and Hovland, 1992). Due to the strong impedance contrast, a gas-bearing zone underlying a gas-free zone in the sedimentary column also causes high-amplitude reflections or so-called bright spots with reversed amplitudes (Løseth et al., 2009), which are often observed directly underneath seep sites (e.g. Evans et al., 2007; Smith et al., 2014).

The surface expression of seeps is typically associated with a rough topography due to the buildup of carbonate crusts, mounds or domes. These structures can reach dimensions of up to several 100 m in diameter and heights of several tens of meters (Hovland and Judd, 1988). Dumke et al. (2014) compared surface expressions of 25 seep sites offshore New Zealand and defined four distinct types that reflect successive stages of seep development. Their observations were based on sidescan sonar images, which revealed different carbonate morphologies, ranging from extensive build-ups (type 1) to carbonate-free sites (type 4). The mechanisms leading to a bathymetric elevation are either uplift of sediments (e.g. due to formation of gas hydrate or gas overpressure) or accumulation of new material (e.g. mud release) on the seafloor (Serié et al., 2012; Koch et al., 2015).

As methane seepage plays an important role for benthic ecosystems, slope stability and as a window to underlying hydrocarbon systems it is important to better understand the functioning of these systems (Berndt, 2005). In this study we focus on the Kerch seep site in the Black Sea offshore Crimea Peninsula. The seeps at this site are located in 890–940 m water depth, i.e. within the GHSZ. They are described as seabed domes characterized by active gas escape (Römer et al., 2012). We use newly obtained high-resolution surface and subsurface data from the Kerch seep site to gain new insights into the plumbing system of these seeps. The objective is to provide further temporal and structural constraints on the way how free gas can migrate through the gas hydrate stability zone and how the seafloor domes form that were reported by Römer et al. (2012).

4.3 Geological Setting

The Don-Kuban paleo deep-sea fan is located in the northwestern Black Sea at the shelf break south of the Kerch Strait, which connects the Black Sea with the Sea of Azov (Fig. 4.1). It is the result of sediment discharge of the rivers Don and Kuban during sea level lowstands in glacial periods (Barg, 2007). The area hosts numerous active seep sites characterized by release of biogenic methane (Starostenko et al., 2010; Römer et al., 2012). These emission sites extend down to about 720 m water depth, which marks the upper limit of the GHSZ in the Black Sea for bottom water temperatures of 9°C (Sloan, 1998).

The Black Sea is characterized by an oxic surface layer extending down to about 150 m water depth and a gradual change towards anoxic conditions below this depth (Özsoy and Ünlüata, 1997). The anoxic conditions lead to burial of large amounts of organic matter in the Black Sea, providing ideal conditions for gas production in the sediments. Additionally, the anoxic water column facilitates the interpretation of water column imaging data, e.g. in terms of gas flares, as backscattering caused by fish can be excluded (Greinert et al., 2006).

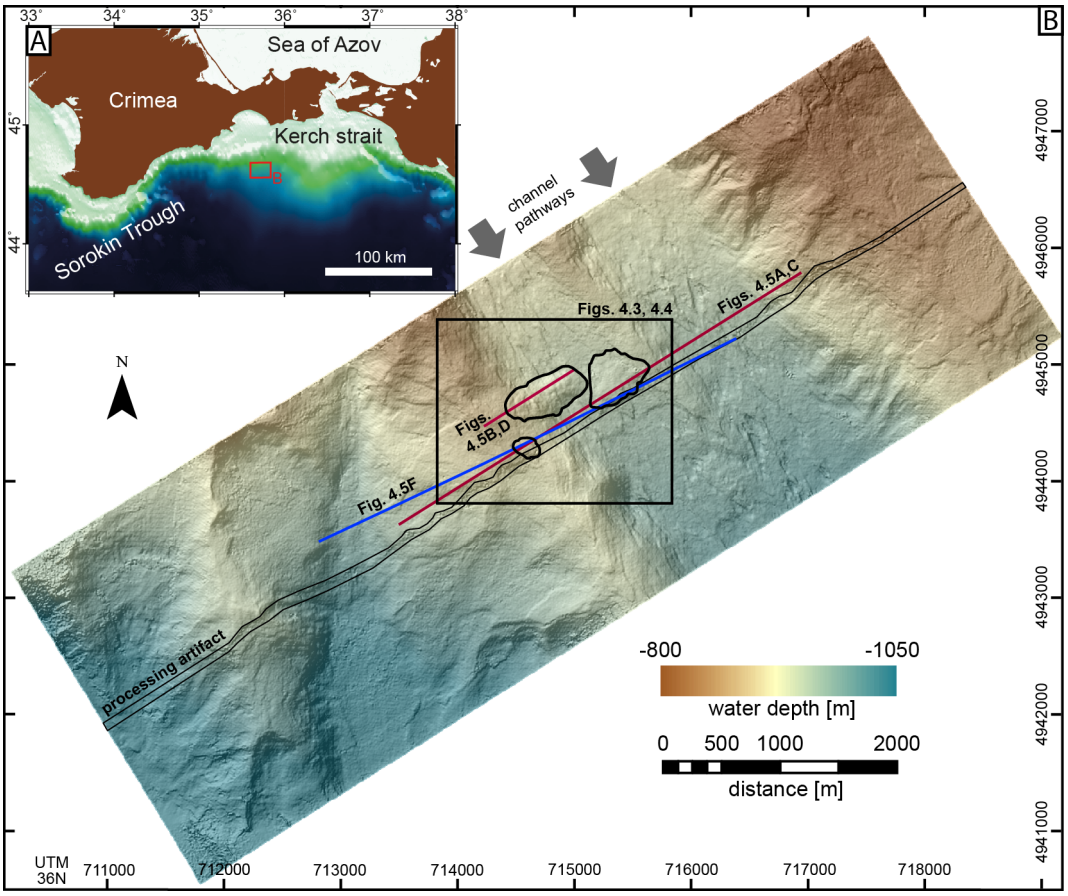

Fig. 4.1 A: Bathymetric map (GEBCO; http://www.gebco.net) showing the location of the study area in the northern Black Sea off the coast of Crimea (red rectangle). B: Seafloor pick of the 3D seismic survey. The three seeps in the channel-levee system of the Don-Kuban paleo deep-sea fan are marked by black polygons.

The Kerch seep area is located in a water depth of 890-940 m at a paleo channel-levee system of the Don Kuban deep-sea fan (Fig. 4.1). Although the Kerch seep area lies within the GHSZ, anomalous gas emissions into the water column have been observed, as evidenced by hydroacoustic flares that remained relatively constant throughout four years of monitoring (Römer et al., 2012). The seep site consists of cold seep mounds with an elevation of up to 10 m above the surrounding seafloor. Previous studies confirmed the presence of gas hydrate based on hydrate samples found in gravity cores from the mounds. In addition, elevated sediment temperature gradients were recorded at sites of fluid escape (around 60 °C/km compared to background values of 23 °C/km). According to Römer et al. (2012), the increased sediment temperatures are caused by upward flow of warm fluids from greater sediment depths. The temperature rise may also cause a shoaling of the base of the gas hydrate stability zone (BGHSZ).

Gas emissions at the seep mounds were observed mainly at the margins of the mounds, indicating that sediments are pushed up by free gas accumulations beneath shallow layers of gas hydrates. Gas migrates laterally towards the flank of the structures and then escapes into the water column, leading to an expansion of the seafloor formation (Römer et al., 2012).

4.4 Materials and Methods

This study is based on 3D high-resolution seismic reflection data, high-resolution sidescan sonar data and subbottom profiler data obtained during RV Poseidon cruise P427 in February/March 2012 (Bialas, 2012). The geophysical data are complemented by pore water geochemistry data derived from gravity cores and multiple cores collected during RV Meteor cruise M84/2 (Bohrmann et al., 2011).

4.4.1 3D seismic data

The 3D seismic data were collected using the P-Cable system (Planke et al., 2009) with 14 parallel streamers of 12.5 m length and 1.5625 m group interval. A 210 cubic inch GI gun was used as a seismic source with a shot interval of 7 s. The 3D seismic dataset covers an area of approximately 3 x 9 km² oriented perpendicular to the channel (Fig. 4.1). Seismic processing involved geometry correction, trace cleaning, band-pass filtering, normal-moveout correction, and post-stack time migration. In order to interpolate several small gaps in the cube area that could not be filled satisfactorily during acquisition, the cube was cut into time slices that were interpolated using the *surface* algorithm of the Generic Mapping Tool (GMT) software (Wessel and Smith, 1998). Due to a larger datagap in the center of the 3D cube, the interpolation method caused an elongated artifact (Fig. 4.1). The time slices were then stacked, resulting in a final bin size of 3.25 x 3.25 m^2. Due to the short length of the streamers, subsurface velocity information was not available and therefore a constant velocity of 1500 m s^{-1} was used for the time migration. Subsurface penetration of the seismic data is in the order of 800-1000 ms two-way traveltime (TWT) beneath the seafloor. Vertical resolution depends on the dominant frequency of the seismic wavelet and thus decreases with depth. A dominant frequency of 100 Hz for the upper 200 m of sediments in our data consequently results in a vertical resolution of approximately 4 m. Data analysis involved calculation of similarity attributes for time-gates ranging between 5 ms and 28 ms, which results in good imaging of faults, fractures, and other structural features in high resolution 3D seismic data.

4.4.2 Sidescan data

Sidescan sonar data were collected using GEOMAR's deep-towed DTS-1 system consisting of a modified EdgeTech dual-frequency sidescan sonar with an integrated sub-bottom profiler. The sidescan sonar's 75 kHz center frequency provided a 1.5 km wide swath and resulted in an across-track resolution of 5.6 cm. Survey speeds were 2.5-3 knots, allowing processing of the data to 1 m pixel size. Concurrently obtained sediment echosounder data have a frequency content of 2-8 kHz and a vertical resolution of a few decimeters for up to 40 m subsurface penetration in the Kerch area. Obtaining towfish position was difficult because USBL navigation was not available and the alternative layback method was complicated by the cable length counter not working properly. However, comparison of seafloor features imaged both in the sidescan sonar data and other datasets such as 3D-seismic data for which the absolute location is known with 1-2 m accuracy and micro-bathymetry of Römer et al. (2012) allowed us to constrain the likely cable length and resulted in satisfactory layback navigation of considerably less than 100 m in most part of the study area.

4.4.3 Hydrate stability modeling

In order to estimate the theoretical BGHSZ, we calculated the methane hydrate phase boundary using the SUGAR Toolbox (Kossel et al., 2013). Using the seafloor horizon picked in the 3D seismic data, we applied a regional thermal gradient of 23 °C/km and a bottom water temperature of 8.9 °C (Römer et al., 2012). The resulting horizon was shifted from the depth domain into the time domain to allow a comparison with the 3D seismic data. Due to the lack of seismic velocity data from the Don-Kuban deep-sea fan, we applied a seismic velocity profile from the Danube deep-sea fan in the western Black Sea, as both areas are characterized by similar depositional settings (Zander et al., 2017).

4.4.4 Gas column height

The gas column height required for creating a circular dome at the seafloor is calculated based on a thin-plate mechanical model which takes into account gravitational forces (Barry et al., 2012; Koch et al., 2015). In this model, rising gas pushes a thin layer of sediments upward before being breached. This results in gentle doming of the seafloor (Fig. 4.2A).

We calculated the required gas column heights as follows:

$$h_g = \frac{(P_{def}+P_{lit})}{g(\rho_w-\rho_{CH4})} \qquad \text{Eq. 4.1}$$

where h_g is the gas column height, P_{def} is the pressure accounting for sediment plate deformation, P_{lit} is the lithostatic pressure of the sediment plate, with $P_{lit} = \rho_s g h$ (ρ_s is the sediment bulk density, h is the plate thickness), g is the gravitational acceleration, ρ_w is the density of water and ρ_{CH4} is the density of methane.

According to Barry et al. (2012), P_{def} is calculated through

$$P_{def} = \frac{8}{3}\frac{E}{1-\nu}\frac{hw_{max}}{a^4}\left(\frac{2h^2}{1+\nu}+w_{max}^2\right) \qquad \text{Eq. 4.2}$$

where E is Young's modulus, ν is Poisson's ratio, a is the plate radius, and w_{max} is the maximum vertical displacement.

Two different dome geometries were tested to calculate the pressures required for the dome structures and the height of the gas column underneath. These geometries were circular shaped and closely match seeps B and C and the smaller sized seep A (Fig. 4.2B). For the plate thickness, we assumed a maximum of 10 m according to the observed blanking in the subbottom profile at this depth (Fig. 4.5F), but we also tested smaller plate thicknesses of 1-10 m. According to Römer et al. (2012), the smaller-sized seep A is elevated by "a few meters" above the surrounding seafloor, and we consequently used an estimated elevation w_{max} of 5 m. For the larger seep, Römer et al. (2012) noted an elevation w_{max} of 10 m. The Young's Modulus E was estimated to range between 140 kPa and 3000 kPa for fine-grained, shallow marine sediments (Barry et al., 2012). Furthermore, after Hamilton et al. (1971), E can be approximated with 350 MPa for silty clays in ~1 km water depth. We therefore included this value as an upper limit. All parameters are given in Table 4.1.

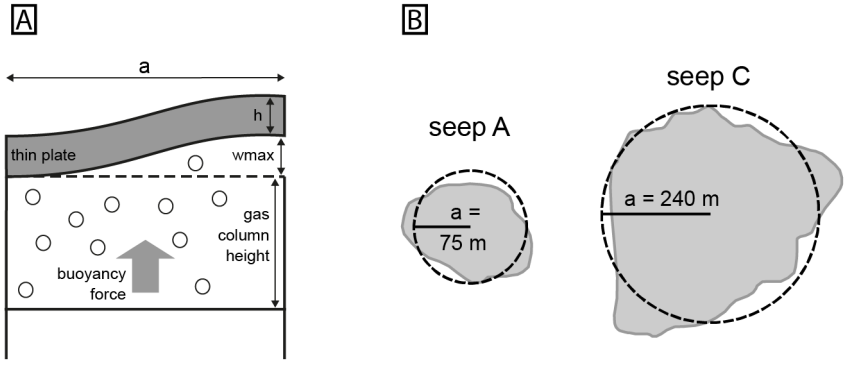

Fig. 4.2 A: Geometry of the plate bending after Barry et al. (2012) for a circular structure with radius a, plate thickness h, and a maximum vertical displacement w_{max}. The doming is forced through buoyancy of a rising gas column from underneath. B: For the calculation of the doming, we used circles with radius a as a representation of the surface extents of seeps A and C.

Table 4.1: Parameters for the calculation of the height of the gas column required to cause updoming of the sediments.

Parameter	**Notation**	**Value/range**	**Reference**
Poisson's ratio	ν	0.49	-
Sediment bulk density	ρ_s	2500 kg/m^3	clayey sediments
Pore water density	ρ_w	1030 kg/m^3	-
Density of methane	ρ_{CH4}	75.93 kg/m^3	Calculated for a water depth of 900 m and a temperature of 9 °C (Kossel et al., 2013)
Plate thickness	h	1-10 m	Gas accumulations as shallow as 10 m below seafloor indicated by subbottom profile
Radius	a	75 m (representative for seep A); 240 m (representative for seep C)	-
Maximum elevation	w_{max}	5 m (seep A), 10 m (seeps B & C)	Römer et al. (2012)
Young's Modulus	E	140 kPa – 350 MPa	Koch et al., 2015, Barry et al. (2012), Hamilton et al. (1971)

4.4.5 Pore water analysis

Pore water was extracted onboard the research vessel in the cold room (4 °C) using a low-pressure squeezer (argon gas at 3-7 bar). The pore water was filtered through 0.2 µm cellulose acetate Whatman filters and collected in recipient vials. Dissolved Cl and SO_4 were analyzed by ion chromatography, dissolved hydrogen sulfide by spectrophotometry, dissolved methane by gas chromatography, dissolved calcium by atomic emission, and dissolved total alkalinity by HCl tritration (see Haffert et al. (2013) for analytical details and errors). Core locations for pore water extraction are shown in Fig. 4.3A and Table 4.2.

Table 4.2: Sampling locations at the Kerch seep site. GC = Gravity Corer, MIC = Mini Corer

Core	Latitude (N)	Longitude (E)	Water depth [m]	Core length (m)	Remarks
GeoB 15519-1 (GC)	44°37.171'	35°41.763'	896	5.74	Background
GeoB 15519-2 (MIC)	44°37.105'	35°41.759'	896	0.45	Background
GeoB 15513-1 (GC)	44°37.386'	35°42.164'	878	5.58	T-logger
GeoB 15513-3 (MIC)	44°37.386'	35°42.164'	878	0.45	
GeoB 15516-1 (GC)	44°37.230'	35°42.282'	889	5.04	T-logger
GeoB 15516-3 (MIC)	44°37.243	35°42.286	888	0.42	
GeoB 15518-1 (GC)	44°37.182’	35°42.279	887	3.57	

In order to determine local rates of AOM and upward methane migration at the seep sites, we developed a numerical transport-reaction model according to Haeckel et al. (2007, 2008) using the parameters and boundary conditions presented in Table 4.3. The model considers concentrations of the pore water consituents chloride, methane, sulfate, hydrogen sulfide, calcium, and total alkalinity (simplified as the sum of HCO_3^- and HS^-). We therefore applied the partial differential equations governing early diagenetic processes after Berner (1980):

$$\frac{\partial \Phi C}{\partial t} = \frac{\partial}{\partial x}\left(\Phi D_s \frac{\partial C}{\partial x} - u\Phi C\right) + \Phi \sum_j R_j \qquad \text{Eq. 4.3}$$

where Φ is the porosity, C is the concentration of a solute, t is time, x is sediment depth, D_s is the effective diffusion coefficient (i.e., the molecular diffusion coefficient corrected by the sediment tortuosity), u is the vertical advection velocity of the pore water, and $\sum R_j$ represents the biogeochemical reactions the solutes are involved in. Steady state compaction is assumed by prescribing an exponential porosity depth profile, which was constrained by non-linear least-squares fitting to the porosity data:

$$\Phi(\mathrm{x}) = \Phi_\infty + (\Phi_\infty - \Phi_0)e^{-\beta x} \qquad \text{Eq. 4.4}$$

where β is the attenuation coefficient for the exponential decrease of porosity with depth. Sediment burial can be neglected at cold seep sites (Haeckel et al., 2008), and thus the pore water advection velocity is

$$u(x,t) = \frac{\Phi_0}{\Phi(x,t)} u_0 \qquad \text{Eq. 4.5}$$

Table 4.3: Parameters and boundary conditions used in this study

Parameter	Notation	Value/range	Reference
Maximum depth of calculation		10 m	-
Bottom water temperature		8.95 °C	-
Pressure		8.85 MPa	-
Pore water density	ρ_w	1025 kg m^{-3}	-
Sediment burial velocity at infinite depth	w_∞	0.02 cm a^{-1}	Jørgensen et al. (2004)
Porosity at sediment surface	Φ_0	0.94	-
Porosity at infinite depth	Φ_∞	0.62	-
Attenuation coefficient for the exponential decrease of porosity with depth	β	0.008	-
Chloride	Cl^-	360 mM (x=0, t) 210 mM (x=10 m, t)	-
Methane	CH_4	0.011 mM (x=0, t) L_{MB} (x=10 m, t)	-
Sulfate	SO_4^{2-}	18 mM (x=0, t) 0 mM (x=10 m, t)	-
Hydrogen sulfide	HS^-	0.3 mM (x=0, t) 7 mM (x=10 m, t)	-
Hydrogencarbonate	HCO_3^-	4 mM (x=0, t) 18 mM (x=10 m, t)	-
Calcium	Ca^{2+}	7 mM (x=0, t) 23 mM (x=10 m, t)	-
Methane concentration in equilibrium with the gas hydrate phase	L_{GH}	93.11 mM	Tishchenko et al. (2005)
Advection velocity at the sediment surface	u_0	0.2 – 5 cm a^{-1} (adjusted)	-
Rate constant of anaerobic concentration of methane oxidation	k_{AOM}	200 dm^3 $mmol^{-1}$ a^{-1} (adjusted)	-

4.5 Results

4.5.1 Seafloor morphology and acoustic characteristics

The Kerch seep site consists of three positive bathymetric features located in 890 – 940 m water depth. These seep mounds have an extent of 150-700 m and an elevation of up to 10 m above the surrounding seafloor (Fig. 4.3A). They are located in a NW-SE trending channel-levee system of the Don-Kuban deep-sea fan, which has a slope gradient of about 1.5-2° (Fig. 4.3B). Seep A developed on the crest of the western levee, seep B developed on the flank of the eastern levee, and seep C is located in the channel bed towards the eastern margin of the channel (Fig. 4.3).

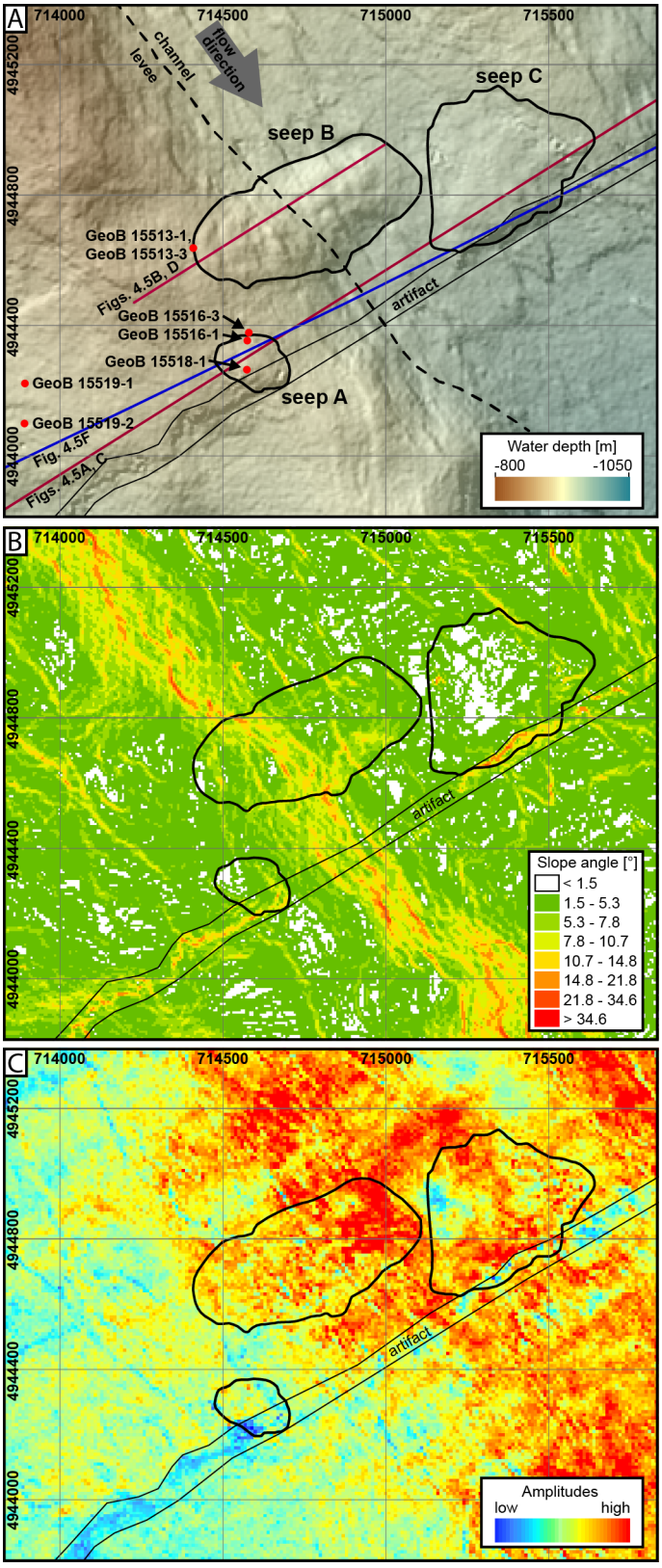

Fig. 4.3A: Shaded relief map based on bathymetry data from the seafloor horizon of the 3D seismic data. B: Slope angle calculated from the seafloor horizon. C: Seismic amplitudes derived from the seafloor horizon. Location is shown in Fig. 4.1, coordinate system is UTM 36N.

The amplitudes of the seafloor reflection in the seismic data are considerably higher for the channel bed than for the adjacent levee sediments (Fig. 4.3C). Similarly, the levees produce a homogeneous low backscatter return in the sidescan sonar images (Fig. 4.4A). Closer to the channel bed, the seafloor backscatter increases and shows an inhomogeneous distribution combined with patches of very high backscatter.

The sidescan sonar data suggest that seep B features the strongest relief of the three seeps, as indicated by shadows and increased backscatter intensity of the surface slopes facing towards the sidescan towfish (Fig. 4.4A). The central, elevated area of seep B is of low backscatter, similar to the backscatter signal of the surrounding levee. The western margin of seep B shows some patches of homogenous medium backscatter.

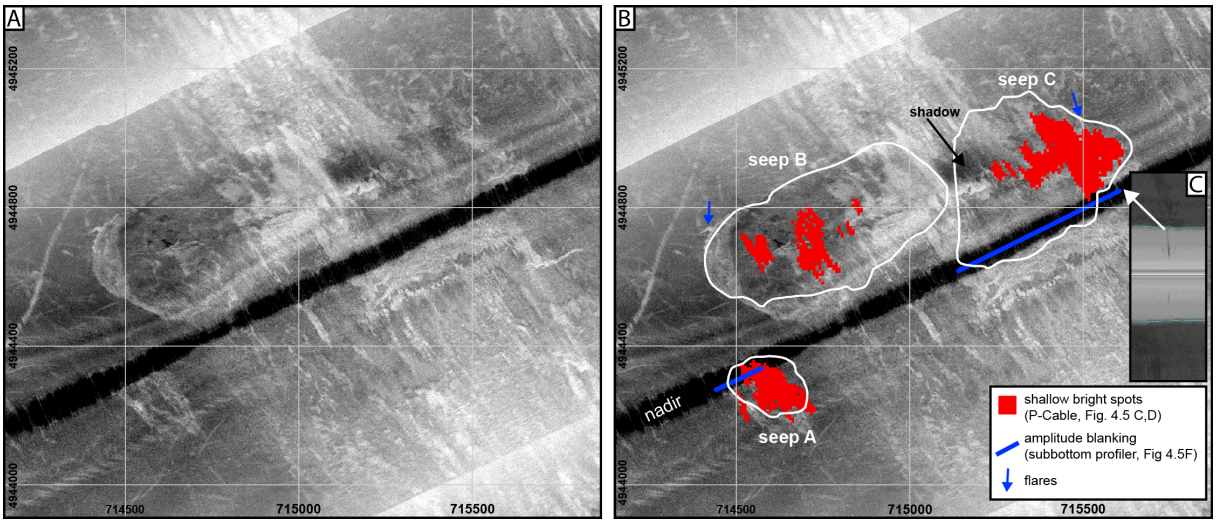

Fig. 4.4A: Processed sidescan sonar mosaic of the study area. The location of this image is shown in Fig. 4.1. High backscatter intensity is white. B: The same sidescan sonar image overlain with the seep outlines shown in Fig. 4.3. Locations of the near-surface bright spots interpreted in the 3D seismic dataset (Fig. 4.5C, D) are shown in red, the extent of the zones of acoustic blanking in the subbottom profiler (Fig. 4.5F) is shown by blue lines, and the locations of observed gas flares are marked by blue arrows. C: water column anomaly in raw sidescan data. Coordinate system is UTM 36N.

Seep C does not produce a clear image in the sidescan sonar data, especially at its western margin at the center of the channel (Fig. 4.4). The seep is characterized by a sharp medium to low backscatter contrast of the eastern and southern margins towards the surrounding sediments. In general, seep C shows less indications for topographic relief compared to seep B, and less elevation above the surrounding seafloor. The surface inclination of seep C is relatively uniform with inclination angles of less than 1.5 ° (Fig. 4.3B). The smallest seep of the study area, seep A on the crest of the levee, is characterized by four northwest to southeast trending linear patches of high backscatter intensity with patches of low backscatter in between.

In addition, two minor elevated backscatter features were observed in the sidescan mosaics (blue arrows in Fig. 4.4B): one on the western margin at seep B, and one on the northeastern margin at seep C. Seep C was also crossed directly by the sidescan towfish track, and a minor acoustic anomaly in the water column exists at this crossing (Fig. 4.4C).

4.5.2 Subsurface

We distinguish four facies units in the seismic data. Seismic unit 1 is situated in the bathymetric depression bound by seismic unit 2 and comprises the channel deposits of the channel-levee system (Fig. 4.5C, D). The unit extends for about 1500 m in SW to NE direction, with thicknesses ranging between 50 ms TWT towards the margins and 120 ms TWT at the center. The seafloor amplitudes at the top of unit 1 are the highest observed in our data (Fig. 4.3C). The reflectors are discontinuous and often chaotic. Their amplitudes are variable, and several scattered reflections are of very high amplitude and some of these have reversed polarity compared to the seafloor.

Seismic unit 2 comprising the levee sediments is found on either side of the channel (Fig. 4.5C, D). It consists of numerous, well-stratified continuous reflections that dip towards the central axis of the ridge-like structures. On the western side of the channel, unit 2 is about 150 ms TWT thick. Unit 2 features numerous near-vertical displacements of reflectors with offsets of up to 10 ms. Some of these discontinuities, which we interpret as faults, extend up to 500 m laterally (Fig. 4.5E), and their general orientation follows the strike direction of the levees (NW to SE). The shallow subbottom profile crossing this area shows that the faults reach up to 2-5 m beneath the seafloor (Fig. 4.5F).

Seismic unit 3 is situated below units 1 and 2. This unit varies in thickness between 10 ms TWT at the intersection point between units 1 and 2, and about 40 ms TWT below unit 2. The seismic amplitudes are generally high and the polarity of the major reflections in unit 3 is reversed compared to the seafloor reflection.

Seismic unit 4 comprises the sediments underneath unit 3. Unit 4 is generally seismically transparent, but several isolated and elongated reflectors can be identified. These reflectors are mostly parallel to the reflectors in unit 3 and the seafloor, and some are characterized by elevated amplitudes and a reversed polarity compared to the seafloor reflection (Fig. 4.5A-D).

4.5.3 Seep domes

The seafloor domes are underlain by shallow high amplitude patches with reversed polarity (Fig. 4.5C, D). The lateral extent of these patches is limited to the seafloor domes (Fig. 4.4B) except at seep A, where the outer margins are difficult to map due to the smaller bathymetric elevation compared to seeps B and C. The thickness of the high amplitude patches is in the range of 20-30 ms TWT (Fig. 4.5C, D). The subbottom profile shows blanking of the acoustic signal in 10 m depth below the seep sites (Fig. 4.5F). Below seep A two NW to SE trending linear features of about 100-150 m length are observed (Fig. 4.5E). These narrow anomalies are of about 200 m length and extend vertically through unit 3. In the similarity time slices, these two anomalies differ from typical narrow fault signatures as they both consist of two parallel lines of low similarity and a line of high similarity in between. This effect is caused by an upward bending of the well-stratified reflectors, which is most likely a velocity effect (pull-up) and does not reflect the stratigraphy.

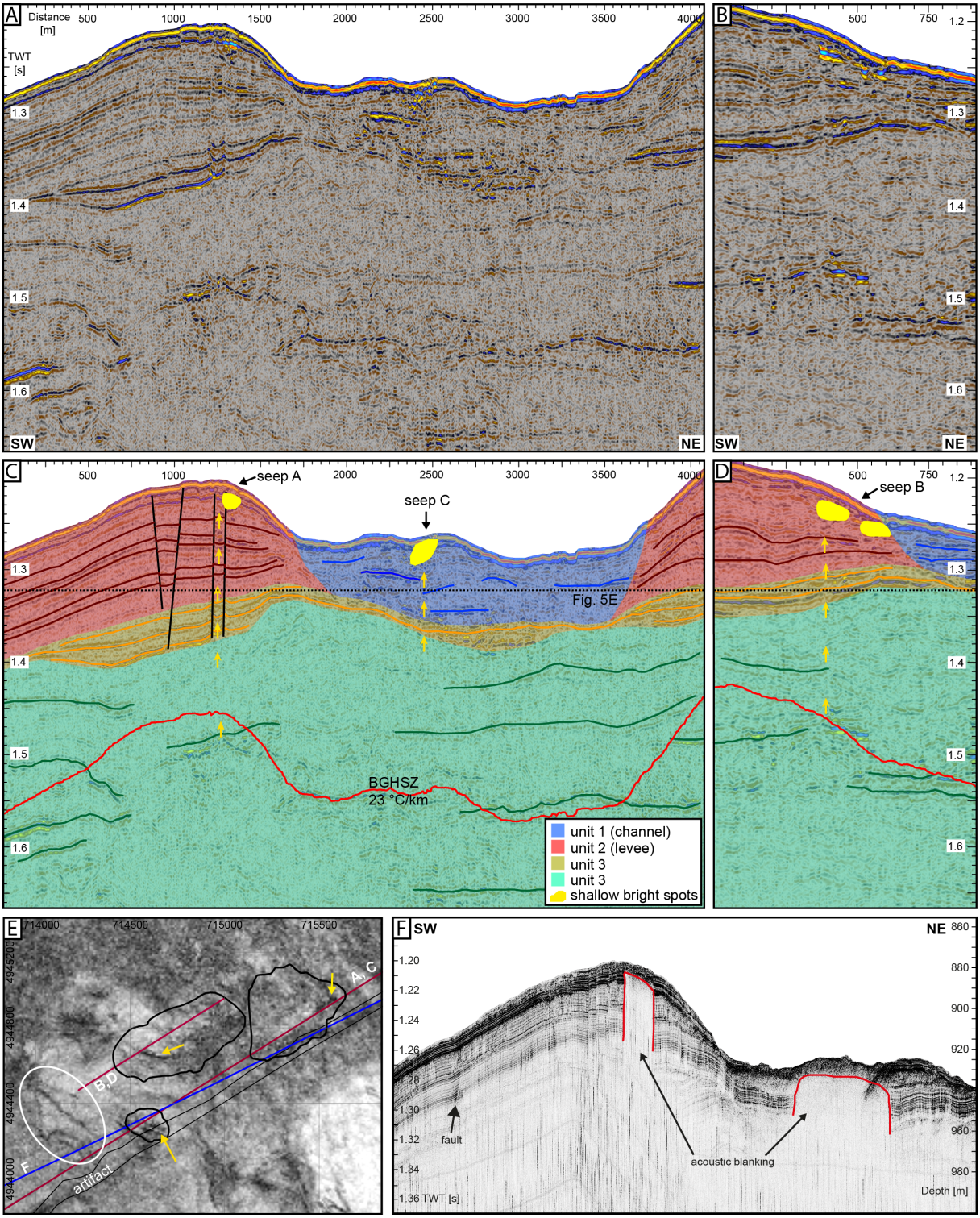

Fig. 4.5 A: 3D inline across the channel-levee system and seeps A and C. B: 3D inline across seep B. Locations of A and B are shown in Fig. 4.1. C: Interpreted section of A highlighting four main seismic units: Channel facies (unit 1, blue), levee facies (unit 2, red), unit 3 underlying the channel-levee system (orange), and unit 4 (green). Bright spot areas underneath seeps A and C are highlighted in yellow (lateral extent shown in Fig. 4.4B) and the most likely migration pathways for free gas are marked by yellow arrows. Several faults were identified in the levees (black lines). In the absence of a bottom simulating reflection (BSR), the theoretical depth of the BGHSZ was calculated for the regional geothermal gradient (red line). D: Interpreted section of B in the same style as in C. E: Similarity time slice of the area. Narrow elongated anomalies of low similarity are present within all of the seeps (yellow arrows). The faults in the levee facies are apparent as sharp

elongated zones of low similarity (white ellipse). The location of the time slice is shown in C and D. High similarity appears white. Coordinate system is UTM 36N. F: Subbottom profile across the seeps A and C. A prominent fault was identified within the top 20 m of the levee deposits. The area underneath the seeps is characterized by acoustic blanking beginning at around 10 m below the seafloor (red). Lateral extent of the blanking is shown in Fig. 4.4B.

Seep B on the levee flank is also situated above well-stratified levee sediments (Fig. 4.5B, D). A narrow low-amplitude anomaly of about 150 m length in NW to SE direction extends vertically into unit 3. Between seep C and unit 3, the chaotic reflectors of the channel bed show several patches of high amplitudes and inversed polarity (Fig. 4.5A, C). Towards the eastern margin of seep C, the similarity slices reveal a vertical narrow low-amplitude anomaly of about 100 m length, which connects the shallow bright spot with unit 3 (Fig. 4.5C, E). The identification of the lower termination of these vertical anomalies is difficult with the available seismic data.

A bottom-simulating reflection (BSR) typically indicating the interface between gas-hydrate-bearing sediments above and gas-bearing sediments below (Hyndman and Davis, 1992) could not be identified in the seismic dataset. However, at least at seep A, the vertical anomaly associated with the seep site appears to extend into the free gas zone beneath the modelled BGHSZ (Fig. 4.5C).

4.5.4 Pore water geochemistry

Background situation

Two cores taken from a reference site (GeoB 15519-1, 15519-2, Fig. 4.3A) are not influenced by methane gas seepage or fluid flow. The data show a decrease in Cl^- concentration from ~350 mM at the sediment/water interface to ~225 mM in 600 cm depth. This is a common observation in the Black Sea as it reflects the diffusion of the marine bottom water chloride into the limnic sediments (Manheim and Chan, 1974; Reitz et al., 2011). Sulfate depletes linearly from ~18 mM at the surface and is completely consumed in about 250-350 cm depth. Similarly, total alkalinity and sulfide show a maximum at the depth of sulfate penetration (sulfide: ~2 mM, TA: ~14 meq/l), and concentrations of methane are increasing from 5-7 mM to 8 mM below this depth (Fig. 4.6). A background temperature gradient of 23 °C/km has been measured with thermomisters attached to the gravity corer from reference station GeoB 15519-1.

Seep situation

The cores taken at the seep locations (GeoB 15513-1, 15513-2, 15516-1, 15516-3, 15518-1, Fig. 4.3A) show a sulfate penetration depth as shallow as 0 – 10 cm (Fig. 4.6). TA and HS^- peak around the same depth (TA: up to ~27 mM, HS^-: up to ~12 mM), and the methane concentrations increase as well (>20 mM at 10 cm depth). Gas hydrates were present in the form of platy chips in core 15513-1 (Römer et al., 2012). A temperature gradient of 60 °C/km has been calculated from station GeoB 15516-1, which was collected at the margin of seep A (Fig. 4.6). We modelled gas transport through fluid flow for different advection velocities between 0.2 cm a^{-1} and 5 cm a^{-1} in order to determine whether water flow is the dominant transport process. We fitted the resulting curves manually to the shallow methane increase, sulfate penetration, and temperature gradients.

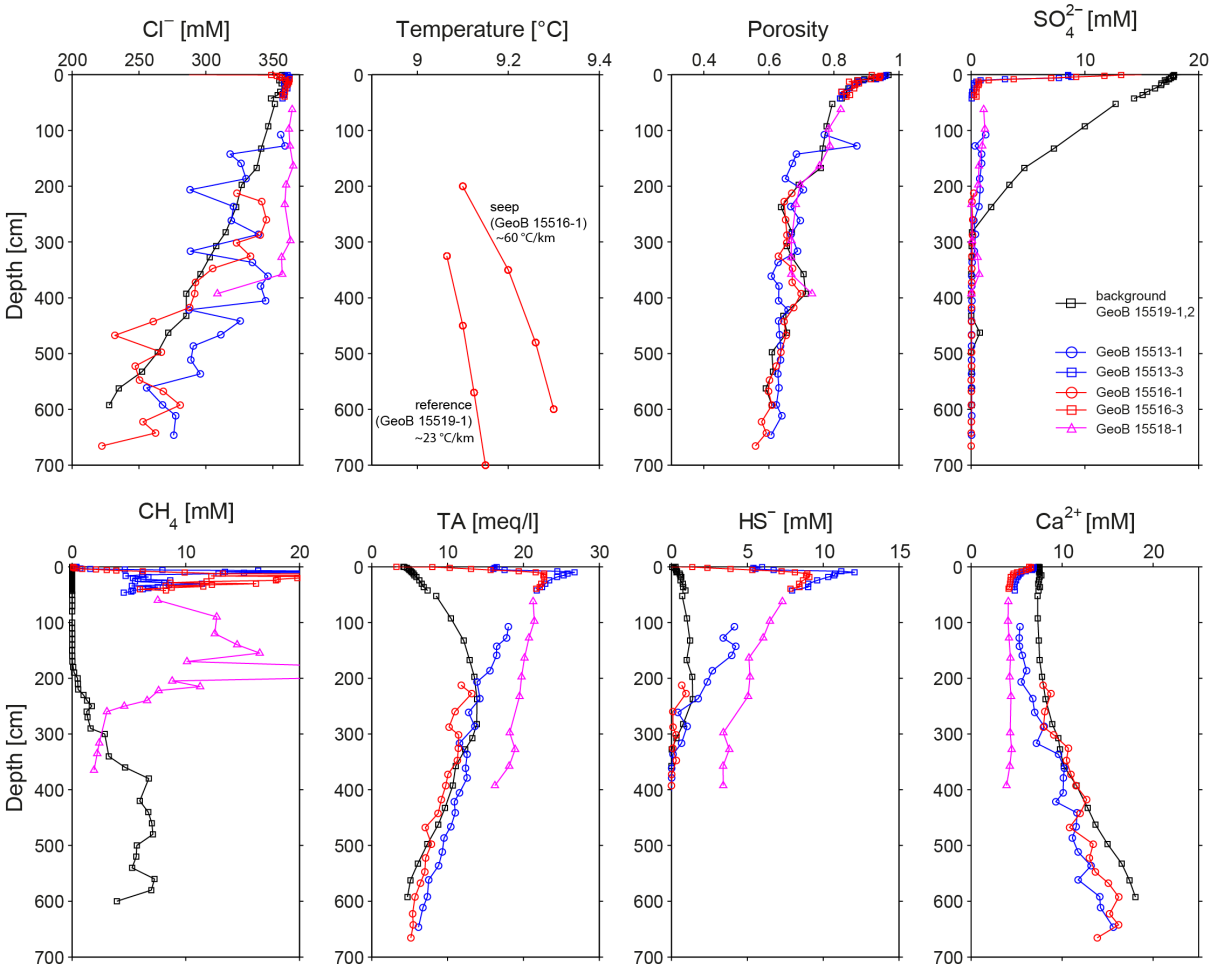

Fig. 4.6: Depth profiles of temperature and porosity and concentration depth profiles of Cl^-, SO_4^{2-}, CH_4, total alkalinity (TA), HS^- and Ca^{2+} from the gravity cores taken at a reference station and the seep sites. Core locations are shown in Fig. 4.3A.

4.5.5 Gas column heights

The results for the calculated gas column heights required for the updoming of the sediments are in the order of 3 – 27 m for both seep geometries, assuming a Young's Modulus E of 140 kPa (Fig. 4.7). The use of a larger value for E (350 MPa) requires larger gas column heights of 4 - 86 m for the seep A geometry (Fig. 4.7), and 3-28 m for the seep C geometry. For seep C, the gas column height increases only slightly compared to models in which a lower Young's Modulus E of 140 kPa is used.

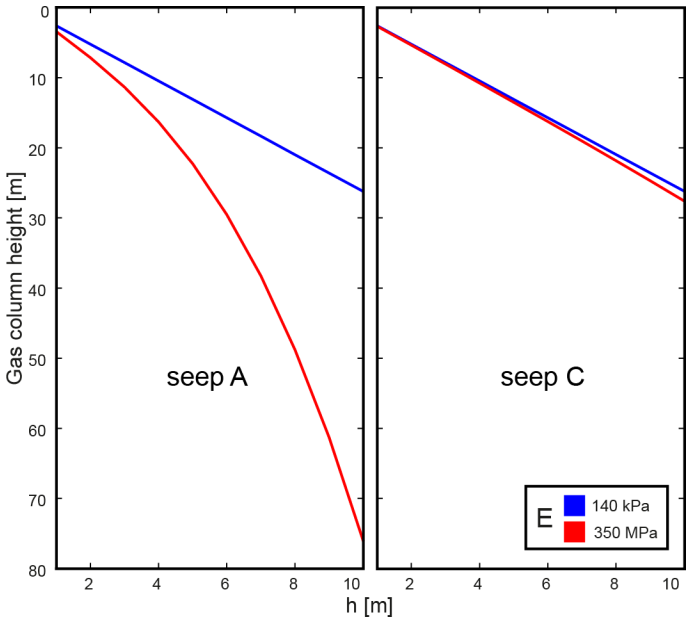

Fig. 4.7: Diagram of gas column height versus plate thickness for seeps A and C, shown for two different Young's Moduli E.

4.6 Discussion

4.6.1 Free gas distribution in the shallow subsurface

Combined with the flare mapping carried out by Römer et al. (2012), our diverse dataset allows detailed screening for gas signatures of the shallow subsurface of the Kerch seep site, providing a more complete picture of the actual subsurface gas distribution and plumbing system. Anomalies indicating the presence of free gas are present in all acoustic datasets and allow a detailed study of the advantages of the different methods in terms of resolution, depth penetration, and surface backscatter.

Gas escape into the water column was detected in the raw sidescan sonar data where the nadir of the towfish crossed the eastern margin of seep C (Fig. 4.4C). Furthermore, we interpret several high backscatter anomalies in the sidescan mosaic at the margins of the seeps as flares (Fig. 4.4B), which confirms the observations by Römer et al. (2012) that gas escape into the water column occurs mainly at the rims of the seep instead of the center.

Bright spots with reversed polarity are present at shallow sediment depths for each seafloor mound, indicating the presence of free gas underneath the seafloor mounds (Fig. 4.4B, Fig. 4.5C, D). Such anomalies are often observed in the shallow subsurface at vent sites (e.g. Evans et al. 2007, Wenau et al., 2014). These shallow gas pockets are most likely the source of the gas escaping into the water column. Acoustic blanking in the subbottom profile (Fig. 4.5F) indicates that gas is trapped as shallow as 10 m below the seafloor at seep A. The seismic datasets also show that the lateral extension of the gas pockets in the shallow subsurface is generally limited to the surface expression of the seeps and does not appear outside the seep area (Fig. 4.4B).

Although we do not observe a BSR in the seismic data, the presence of gas hydrates in the GHSZ is predicted as there is a sustained supply of methane from microbial generation within and underneath the BGHSZ. The calculated BGHSZ based on the background geothermal gradient (23 °C km^{-1}) may be shifted upwards due to elevated temperatures. The seismic data suggests that the three seeps are vertically connected to the free gas zone underneath the BGHSZ. Gas migration through the GHSZ occurs in the form of focused flow rather than diffusive flow. The elongated anomalies observed in the seismic data below each of the bright spots are interpreted as the vertical migration pathways for the free gas through the GHSZ. It is possible that small offset faults, which are apparent especially in the levees favor the gas migration through the GHSZ.

4.6.2 Gas transport mechanism

The undisturbed background sediment cores show an increase in TA and sulfide in about 250-350 cm depth, which is caused by the anaerobic oxidation of methane (AOM). At the seeps, the AOM front has moved upward to a depth of 0-10 cm due to the high methane flux from depth, which is indicated by the shallow sulfate penetration depth. In our model, we tested whether methane is transported by fluid flow (as suggested by Römer et al. (2012) in order to explain increased temperatures at the seep sites) or by gas bubbles. We therefore fitted the model results for both mechanisms to match the shallow AOM and the elevated geothermal gradient at the seep site.

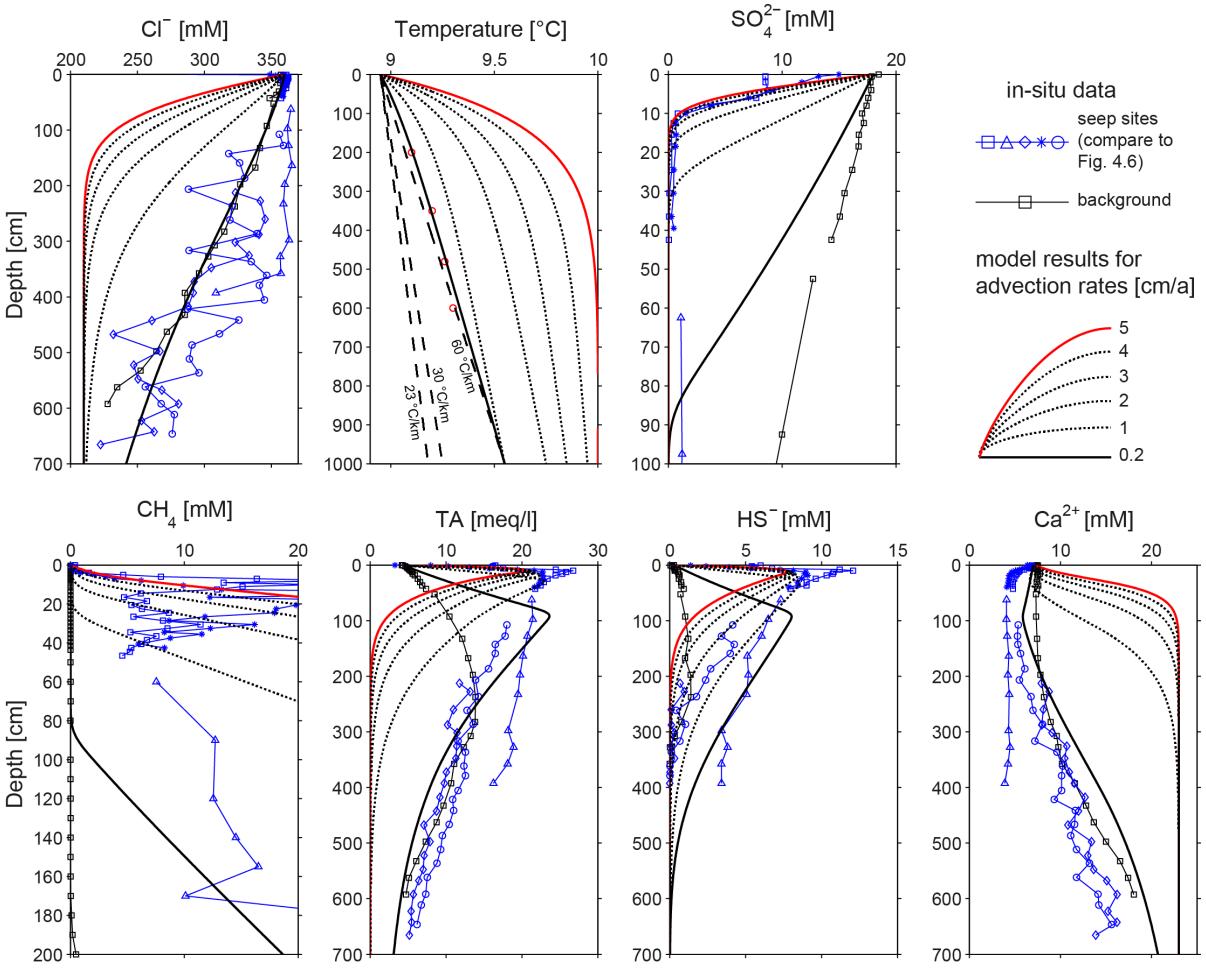

Fig. 4.8: Model results for upward fluid advection velocities of 0.2 – 5 cm a^{-1} in comparison to the observed pore water and temperature data shown in Fig. 4.6.

Fitting the model to the shallow methane increase and sulfate reduction through fluid flow requires an advection velocity of at least 5 cm a^{-1} to deliver sufficient methane (*Fig. 4.8*). The resulting Cl^- model curve, however, indicates a more rapid Cl^- decline compared to the observed data from the gravity cores at the seep site. Similarly, the temperature gradient would be significantly higher compared to the in situ temperature logs from the seep site. These results strongly suggest that methane is not transported by water flow at the seep site. Moreover, matching the model to the in situ temperature data at the seep site limits the fluid advection rate to <0.2 cm a^{-1}, which does not transport sufficient methane towards the shallow sediment column and disagrees with the shallow sulfate reduction front. These results strongly indicate that the system is dominated by methane transport through gas bubbles decoupled from upward fluid advection that may eventually be driven by non-steady state compaction.

The slightly elevated and scattered chloride data from the seep pore water data are likely the result of methane gas rising through the shallow sediments. The gas bubbles irrigate the pore water and enhance solute exchange with the bottom water. This process was discussed in detail for seep sites in the Sea of Okhotsk (Haeckel et al., 2007) and has also been suggested for seeps at the Hikurangi Margin off New Zealand (Schwalenberg et al., 2010; Luo et al., 2016), and offshore Taiwan (Chuang et al., 2013). The surface expression of irrigation tubes can be clearly identified in seafloor photographs from the Kerch seep sites with active bubble emission (Römer et al., 2012; their Figs. 7 and 8).

Active exothermic gas hydrate formation could explain the elevated temperature data at seep A, which were beyond the 60 °C/km gradient from core GeoB 15516-1 (Römer et al., 2012). Active gas hydrate dissociation and formation was suggested at the Dvurechenskii mud volcano in the Sorokin Trough (NW Black Sea) to act as a thermostat, thereby changing the heat flow in the shallow sediment (Feseker et al., 2009). Active gas hydrate formation also occurs at the seep sites in the eastern Black Sea (Heeschen et al., 2011).

4.6.3 Gas doming

If methane is transported via bubbles, updoming of the sediments at the three individual seeps is likely caused by gas overpressure. Carbonate build-ups as the cause of the dome structures can be excluded based on the sidescan sonar images, sediment echosounder data, and seafloor photographs of Römer et al. (2012). Furthermore, gas hydrate formation as the cause for the updoming can be ruled out since there is no evidence for high gas hydrate saturation or massive thick gas hydrate accumulations in the available data. The required gas column heights for the seep domes are in the order of 3-27 m for both of the tested geometries. Although the gas column heights for E of 350 MPa are up to three times higher for the seep A geometry compared to the gas column heights for E of 140 kPa (Fig. 4.7), we think that E is located more at the low end within 140 kPa to 3000 kPa as discussed by Barry et al. (2012). A variation of E within this range changes the resulting gas column heights only by a few centimeters. Compared to the thickness of the gas signatures identified in the seismic data (20-30 ms TWT, which corresponds to a thickness of 15-22.5 m for a seismic velocity of 1500 m s^{-1}), these calculated gas column heights (3-27 m assuming E of 140-3000 kPa) are consistent and plausible. These results strongly suggest that gas flux driven by buoyancy is causing the sediment updoming at the seep sites. Gas hydrate layers, although only small amounts have been recovered, likely support the permeability barrier and sealing at the center of the seeps, forcing the free gas to divert towards the margins of the domes as suggested by Römer et al. (2012).

4.6.4 Age of the seeps

The different mound morphologies and shallow distribution of the free gas underneath the domes may indicate that the three seeps reflect different development stages and did not necessarily develop at the same time. This is supported by the observation that each seep is associated with its own isolated gas pocket, which is fed individually from beneath the GHSZ (Fig. 4.4B). Seep B is most likely the most ancient one of the three seeps. It has a more complex morphology compared to the other two seeps, while at the same time the subsurface gas signature is smaller and more scattered. This might indicate that most of the gas, which led to the doming of the sediments, has already escaped into the water column or formed gas hydrates in the shallow subsurface. Seep A, on the other hand, is probably the youngest seep in this system. Due to its development on the crest of the levee, the gas had to have migrate through a thicker column of fine-grained, less permeable sediments compared to the other seeps. Seep A is also the most active seep of the three, as indicated by the larger number of flares (Römer et al., 2012) and by the distribution of the bright spots, which coincide with the surface expression of the seep. These observations indicate that the development of seep A is ongoing and it may grow laterally to an extent similar to the other two seeps.

These observations may further indicate that the migration pathways below seep B (and probably seep C as well) have been sealed over time, e.g. by the formation of gas hydrates in the lower part of the GHSZ. Consequently, more gas is transported towards the seabed before the pathways become sealed by hydrate formation. The complexity of gas bubble transport through a hydrate plug was demonstrated by Austvik et al. (2000), who showed that hydrate plugs remain porous and the bubbling gas forms small-scale channel pathways, which then get sealed over time by additional hydrate formation.

Unlike other seeps in the Black Sea, such as the Batumi seep site offshore Georgia (Klaucke et al., 2006), the Kerch seep site lacks extensive carbonate crusts at the surface, which is indicated by the low backscatter in the sidescan sonar data especially at seep B (Fig. 4.4) and the absence of high-amplitude normal-polarity reflectors in the pipe structures observed in the 3D seismic data. Some patches of elevated backscatter at the margin of seep B may have been caused by an increased volume roughness in the shallow subsurface (<10 cm depth) due to the presence of shallow carbonates, gas hydrates or free gas (Blondel and Murton, 1997). This observation indicates that the Kerch seep system is likely younger than e.g. the seep sites in the eastern Black Sea, which feature extensive carbonate buildups (Klaucke et al., 2006). Gulin et al. (2003) suggested that carbonate structures growing at methane seeps in the Black Sea originate from 5300-2900 years before present, which corresponds to the time of stabilization of the upper boundary of the anoxic zone in the water column after sea level rise since the last glacial maximum. As the Kerch seep site presently lacks such carbonate buildups, we propose that all three seeps correspond to seep type 4 (carbonate-free sites) after Dumke et al. (2014). We therefore suggest that the Kerch seep site is younger than 2900 years based on the estimations of Gulin et al. (2003).

4.7 Conclusions

The combined analysis of the Kerch seep site carried out in this study was based on high-resolution 3D seismic data, deep-towed sidescan sonar data, subbottom profiler data, and pore water analysis. The seep site is located in around 900 m water depth well within the GHSZ and comprises three seafloor domes. Each seep is underlain by isolated gas pockets, which are fed with methane gas migrating along individual narrow pathways through the GHSZ. Our calculations show that gas overpressure is likely the driver for the updoming of the sediments, and the required gas column heights are in the order of 3-27 m, which fits well to the observed gas signatures in the seismic data. Methane is transported through the sediment column towards the seep surface as free gas. Based on seismic expressions and surface backscatter of the seeps, we suggest that the Kerch seep site is a rather young seep system that lacks extensive carbonate crusts observed at other seep sites in the Black Sea.

4.8 Acknowledgements

The research leading to these results has received funding from the DFG project DOKUGAS (grant No. KL1846/3-1). We would like to thank the captains and crews of RV Poseidon cruise P427 and RV Meteor cruise M84/2 as well as the lab technicians at GEOMAR for their excellent support.

4.9 References

Austvik, T., Li, X., and Gjertsen, L.H., 2000. Hydrate plug properties: Formation and removal of plugs. In: Gas hydrates: challenges for the future. Annals of the New York Academy of Sciences 912, pp. 294-303, doi:10.1111/j.1749-6632.2000.tb06783.x.

Barg, I., 2007. Age and origin of the Kerch Strait and the Sea of Azov. Doklady Earth Sciences 412, pp. 17-18, doi:10.1134/S1028334X07010047.

Barry, M.A., Boudreau, B.P., and Johnson, B.D., 2012. Gas domes in soft cohesive sediments. Geology 40, pp. 379-382, doi:10.1130/G32686.1.

Berndt, C., 2005. Focused fluid flow in passive continental margins. Philosophical Transactions of the Royal Society A 363, pp. 2855-2871, doi:10.1098/rsta.2005.1666.

Berner, R.A., 1980. Early Diagenesis: A Theoretical Approach. Princeton University Press, Princeton, New Jersey.

Bhatnagar, G., Chapman, W.G., Dickens, G.R., Dugan, B., and Hirasaki, G.J., 2008. Sulfate-methane transition as a proxy for average methane hydrate saturation in marine sediments. Geophysical Research Letters 35, L03611, doi:10.1029/2007GL032500.

Bialas, J. (Ed.), 2012. FS POSEIDON Fahrtbericht / Cruise Report POS427 – Fluid emissions from mud volcanoes, cold seeps and fluid circulation at the Don-Kuban deep-sea fan (Kerch peninsula, Crimea, Black Sea), 23.02.-19.03.2012, Burgas, Bulagria – Heraklion, Greece. GEOMAR Report, N. Ser. 003. GEOMAR Helmholtz-Zentrum für Ozeanforschung Kiel, Germany, 28 pp, doi:10.3289/GEOMAR_ REP_NS_3_2012.

Blondel, P., and Murton, B.J., 1997. Handbook of seafloor sonar imagery. Wiley, Chichester.

Boetius, A., Ravenschlag, K., Schubert, C.J., Rickert, D., Widdel, F., Gieseke, A., Amann, R., Jørgensen, B.B., Witte, U., and Pfannkuche, O., 2000. A marine microbial consortium apparently mediating anaerobic oxidation of methane. Nature 407, pp. 623-626, doi:10.1038/35036572.

Bohrmann, G., and Torres, M., 2006. Gas hydrates in marine sediments. In: Schulz, H.D., and Zabel, M. (Eds.), Marine Geochemistry. Springer, Berlin, pp. 481-512.

Bohrmann, G., Akasu, E., Bahr, A., Bergenthal, M., Dehning, K., Diekamp, V., Domeyer, B., dos Santos Ferreira, C., Düßmann, R., Freudenthal, T., Haeckel, M., Hatsukano, K., Herschelmann, O., Hohnberg, H.J., Hüttich, D., Kaszemeik, K., Klein, T., Komakhidze, G., Kopiske, E., Körber, J.H., Lomnitz, U., Malakhova, T., Meinecke, G., Meyerdierks, D., Nadezhkin, D., Oelfke, S., Özmara, A., Pape, T., Piñero, E., Radulescu, V., Raeke, A., Reitz, A., Renken, J., Reuter, M., Römer, M., Rosiak, U., Sahling, H., Schmager, M., Stachowski, A., Tomczyk, M., Wangner, D., Wei, J., Wintersteller, P., and Wu, T., 2011. Report and preliminary results of RV Meteor cruise 84/2, Istanbul – Istanbul, 26 February – 02 April 2011. Origin and distribution of methane and methane hydrates in the Black Sea. Berichte aus dem Fachbereich Geowissenschaften der Universität Bremen 281, Bremen, Germany, 164 pp.

Chuang, P.C., Dale, A., Wallmann, K., Haeckel, M., Yang, T.F., Chen, N.C., Chen, H.C., Chen, H.W., Lin, S., Sun, C.H., You, C.F., Wang, Y., and Chung, S.H., 2013. Relating sulfate and methane dynamics to geology: Accretionary prism offshore SW Taiwan. Geochemistry, Geophysics, Geosystems 14, pp. 2523-2545, doi:10.1002/ggge.20168.

Dumke, I., Klaucke, I., Berndt, C., and Bialas, J., 2014. Sidescan backscatter variations of cold seeps on the Hikurangi Margin (New Zealand): indications for different stages in seep development. Geo-Marine Letters 34, pp. 169-184, doi:10.1007/s00367-014-0361-7.

Evans, R.J., Stewart, S.A., and Davies, R.J., 2007. Phase-reversed seabed reflections in seismic data: examples related to mud volcanoes from the South Caspian Sea. Geo-Marine Letters 27, pp. 203-212, doi:10.1007/s00367-007-0073-3.

Feseker, T., Pape, T., Wallmann, K., Klapp, S.A., Schmidt-Schierhorn, F., and Bohrmann, G., 2009. The thermal structure of the Dvurechenskii mud volcano and its implications for gas hydrate stability and eruption dynamics. Marine and Petroleum Geology 26, pp. 1812-1823, doi:10.1016/j.marpetgeo.2009.01.021.

Greinert, J., Artemov, Y., Egorov, V., De Batist, M., and McGinnis, D., 2006. 1300-m-high rising bubbles from mud volcanoes at 2080 m in the Black Sea: Hydroacoustic characteristics and temporal variability. Earth and Planetary Science Letters 244, pp. 1-15, doi: 10.1016/j.epsl.2006.02.011.

Greinert, J., Lewis, K.B., Bialas, J., Pecher, I.A., Rowden, A., Bowden, D.A., De Batist, M., and Linke, P., 2010. Methane seepage along the Hikurangi Margin, New Zealand: Overview of studies in 2006 and 2007 and new evidence from visual, bathymetric and hydroacoustic investigations. Marine Geology 272, pp. 6-25, doi:10.1016/j.margeo.2010.01.017.

Gulin, S.B., Polikarpov, G.G., and Egorov, V.N., 2003. The age of microbial carbonate structures grown at methane seeps in the Black Sea with an implication of dating of the seeping methane. Marine Chemistry 84, pp. 67-72, doi:10.1016/S0304-4203(03)00103-08.

Haeckel, M., Suess, E., Wallmann, K., and Rickert, D., 2004. Rising methane gas bubbles form massive hydrate layers at the seafloor. Geochimica et Cosmochimica Acta 68, pp. 4335-4345, doi:10.1016/ j.gca.2004.01.018.

Haeckel, M., Boudreau, B.P., and Wallmann, K., 2007. Bubble-induced porewater mixing: A 3-D model for deep porewater irrigation. Geochimica et Cosmochimica Acta 71, pp. 5135-5154, doi:10.1016/ j.gca.2007.08.011

Haeckel, M., Reitz, A., and Klaucke, I., 2008. Methane budget of a large gas hydrate province offshore Georgia, Black Sea. Proceedings of the 6th International Conference on Gas Hydrates (ICGH 2008), Vancouver, Canada, 6-10 July 2008, 10 pp.

Haffert, L., Haeckel, M., Liebetrau, V., Berndt, C., Hensen, C., Nuzzo, M., Reitz, A., Scholz, F., Schönfeld, J., and Weise, S.M., 2013. Fluid evolution and authigenic mineral paragenesis related to salt diapirism – the Mercator mud volcano in the Gulf of Cadiz. Geochimica et Cosmochimica Acta 106, pp. 261-285, doi:10.1016/j.gca.2012.12.016.

Hamilton, E.L., 1971. Elastic properties of marine sediments. Journal of Geophysical Research 76, pp. 579-604, doi: 10.1029/JB076i002p00579.

Heeschen, K.U., Haeckel, M., Klaucke, I., Ivanov, M.K., and Bohrmann, G., 2011. Quantifying in-situ gas hydrates at active seep sites in the eastern Black Sea using pressure coring technique. Biogeosciences 8, pp. 3555-3565, doi:10.5194/bg-8-3555-2011.

Hovland, M., and Judd, A.G., 1988. Seabed Pockmarks and Seepages: Impact on Geology, Biology and the Marine Environment. Graham and Trotman Ltd., Boston.

Hyndman, R.D., and Davis, E.E., 1992. A mechanism for the formation of methane hydrate and seafloor bottom-simulating reflectors by vertical fluid expulsion. Journal of Geophysical Research: Solid Earth 97, pp. 7025-7041, doi:10.1029/91JB03061.

Jørgensen, B.B., Böttcher, M.E., Lüschen, H., Neretin, L.N., and Volkov, I.I., 2004. Anaerobic methane oxidation and a deep H_2S sink generate isotopically heavy sulfides in Black Sea sediments. Geochimica et Cosmochimica Acta 68, pp. 2095-2118, doi:10.1016/j.gca.2003.07.017.

Judd, A.G., and Hovland, M., 1992. The evidence of shallow gas in marine sediments. Continental Shelf Research 12, pp. 1081-1095, doi:10.1016/0278-4343(92)90070-Z.

Judd, A.G., 2003. The global importance and context of methane escape from the seabed. Geomarine Letters 23, pp. 147-154, doi:10.1007/s00367-003-0136-z.

Klaucke, I., I., Sahling, H., Weinrebe, W., Blinova, V., Bürk, D., Lursmanashvili, N., Bohrmann, G., 2006. Acoustic investigation of cold seeps offshore Georgia, eastern Black Sea. Marine Geology 231, pp. 51-67, doi:10.1016/j.margeo.2006.05.011.

Klaucke, I., Masson, D.G., Petersen, C.J., Weinrebe, W., and Ranero, C.R., 2008. Multifrequency geoacoustic imaging of fluid escape structures offshore Costa Rica: Implications for the quantification of seep processes. Geochemistry, Geophysics, Geosystems 9, Q04010, doi:10.1029/2007GC001708.

Koch, S., Berndt, C., Bialas, J., Haeckel, M., Crutchley, G. J., and Papenberg, C., 2015. Gas-controlled seafloor doming. Geology 43, 571-57, doi:10.1130/G36596.1.

Koch, S., Schroeder, H., Haeckel, M., Berndt, C., Bialas, J., Papenberg, C., Klaeschen, D., and Plaza-Faverola, A., 2016. Gas migration through Opouawe Bank at the Hikurangi margin offshore New Zealand. Geo-Marine Letters 36, pp. 187-196, doi:10.1007/s00367-016-0441-y.

Kossel, E., Bigalke, N., Piñero, E., and Haeckel, M., 2013. The SUGAR Toolbox – A library of numerical algorithms and data for modelling of gas hydrate systems and marine environments. GEOMAR Report No. 8, 160 pp, doi:10.3289/geomar_rep_ns_8_2013.

Løseth, H., Gading, M., and Wensaas, L., 2009. Hydrocarbon leakage interpreted on seismic data. Marine and Petroleum Geology 26, pp. 1304-1319, doi:10.1016/j.marpetgeo.2008.09.008.

Luo, M., Dale, A.W., Haffert, L., Haeckel, M., Koch, S., Crutchley, G., De Stigter, H., Chen, D., and Greinert, J., 2016. A quantitative assessment of methane cycling in Hikurangi Margin sediment (New Zealand) using geophysical imaging and biogeochemical modeling. Geochemistry, Geophysics, Geosystems 17, 4817-4835, doi:10.1002/2016GC006643.

Manheim, F.T., and Chan, K.M., 1974. Interstitial waters of Black Sea sediments: new data and review. In: Degens, E.T., and Ross, D.A. (Eds.), The Black Sea – Geology, Chemistry and Biology. The American Association of Petroleum Geologists, Tulsa, USA.

Özsoy, E., and Ünlüata, Ü., 1997. Oceanography of the Black Sea: a review of some recent results. Earth-Science Reviews 42, pp. 231-272, doi:10.1016/S0012-8252(97)81859-4.

Planke, S., Erikson, F.N., Berndt, C., Mienert, J., and Masson, D., 2009. P-Cable high-resolution seismic. Oceanography 22, p. 85, doi:10.5670/oceanog.2009.09.

Regnier, P., Dale, A.W., Arndt, S., LaRowe, D.E., Mogollon, J., and Van Capellen, P., 2011. Quantitative analysis of anaerobic oxidation of methane (AOM) in marine sediments: A modeling perspective. Earth-Science Reviews 106, pp. 105-130, doi:10.1016/j.earscirev.2011.01.002.

Reitz, A., Pape, T., Haeckel, M., Schmidt, M., Berner, U., Scholz, F., Liebetrau, V., Aloisi, G., Weise, S.M., and Wallmann, K., 2011. Sources of fluids and gases expelled at cold seeps offshore Georgia, eastern Black Sea. Geochimica et Cosmochimica Acta 75, pp. 3250-3268, doi:10.1016/j.gca.2011.03.018.

Römer, M., Sahling, H., Pape, T., Bahr, A., Feseker, T., Wintersteller, P., and Bohrmann, G., 2012. Geological control and magnitude of methane ebullition from a high-flux seep area in the Black Sea – The Kerch seep area. Marine Geology 319-322, pp. 57-74, doi:10.1016/j.margeo.2012.07.005.

Sahling, H., Bohrmann, G., Spiess, V., Bialas, J., Breitzke, M., Ivanov, M., Kasten, S., Krastel, S., and Schneider, R., 2008. Pockmarks in the Northern Congo Fan area, SW Africa: Complex seafloor features shaped by fluid flow. Marine Geology 249, pp. 206-225, doi:10.1016/j.margeo.2007.11.010.

Schwalenberg, K., Haeckel, M., Poort, J., and Jegen, M., 2010. Evaluation of gas hydrate deposits in an active seep area using marine controlled source electromagnetics: Results from Opouawe Bank, Hikurangi Margin, New Zealand. Marine Geology 272, pp. 79-88, doi:10.1016/j.margeo.2009.07.006.

Serié, C., Huuse, M., and Schodt, N.H., 2012. Gas hydrate pingoes: Deep seafloor evidence of focused fluid flow on continental margins. Geology 40, pp. 207-210, doi:10.1130/G32690.1.

Sloan, E.D., 1998. Clathrate hydrates of natural gases. Marcel Dekker, New York.

Smith, A.J., Flemings, P.B., and Fulton, P.M., 2014. Hydrocarbon flux from natural deepwater Gulf of Mexico vents. Earth and Planetary Science Letters 395, pp. 241-253, doi:10.1016/j.epsl.2014.03.055.

Stakes, D.S., Orange, D., Paduan, J.B., Salamy, K.A., and Maher, N, 1999. Cold-seeps and authigenic carbonate formation in Monterey Bay, California. Marine Geology 159, pp. 93-109, doi:10.1016/S0025-3227(98)00200-X.

Starostenko, V.I., Rusakov, O.M., Shnyukov, E.F., Kobolev, V.P., and Kutas, R.I., 2010. Methane in the northern Black Sea: characterization of its geomorphological and geological environments. Geological Society, London, Special Publications 340, 57-75, doi:10.1144/SP340.5.

Suess, E., Torres, M.E., Bohrmann, G., Collier, R.W., Greinert, J., Linke, P., Rehder, G., Trehu, A., Wallmann, K., Winckler, G., and Zuleger, E., 1999. Gas hydrate destabilization: enhanced dewatering, benthic material turnover and large methane plumes at the Cascadia convergent margin. Earth and Planetary Science Letters 170, pp. 1-15, doi:10.1016/S0012-821X(99)00092-8.

Talukder, A.R., 2012. Review of submarine cold seep plumbing systems: leakage to seepage and venting. Terra Nova 24, pp. 255-272, doi:10.1111/j.1365-3121.2012.01066x.

Tishchenko, P., Hensen, C., Wallmann, K., and Wong, C.S., 2005. Calculation of the stability and solubility of methane hydrate in seawater. Chemical Geology 219, pp. 37-52, doi:10.1016/j.chemgeo.2005.02.008.

Wenau, S., Spiess, V., Pape, T., and Fekete, N., 2015. Cold seeps at the salt front in the Lower Congo Basin I: Current methane accumulation and active seepage. Marine and Petroleum Geology 67, pp. 894-908, doi:10.1016/j.marpetgeo.2014.07.032.

Wessel, P., and Smith, W.H.F., 1998. New, improved version of the generic mapping tools released. Eos Transactions 79, p. 579, doi:10.1029/98EO00426.

Zander, T., Haeckel, M., Berndt, C., Chi, W.C., Klaucke, I., Bialas, J., Klaeschen, D., Koch, S., and Atgın, O., 2017. On the origin of multiple BSRs in the Danube deep-sea fan, Black Sea. Earth and Planetary Science Letters 462, pp. 15-25, doi:10.1016/j.epsl.2017.01.006.

5. Conclusions and outlook

5.1 Summary of the key results

The work presented in this thesis has provided new insights into the complex gas and gas hydrate system of the Black Sea. The research objectives posed in the motivation of this thesis could be answered throughout the three individual case studies, which results are presented in the following. Additionally, further implications from these studies are given and an outlook for future studies is presented.

5.1.1 Multiple BSRs in the Danube deep-sea fan

The analysis of new high-resolution 2D seismic data reveals that the distribution of anomalous multiple BSRs is limited to the levees of a buried channel-levee system of the Danube deep-sea fan. Up to four BSRs overlying each other are observed. The shallowest BSR thereby mimics the theoretical base of the GHSZ calculated from regional geothermal gradients and salinity data.

Overpressured gas compartments can be excluded as the cause for the formation of the deeper BSRs, because the height of the necessary gas column would significantly exceed the vertical distance between two overlying BSRs. Instead, the results indicate that the deeper BSRs are paleo-BSRs, which could be related to paleo seafloor horizons located between the buried channel-levee system and the levee deposits of the Danube channel.

The BSR formation was favored by temperature and pressure conditions that were controlled by rapid sediment deposition rather than bottom-water temperature changes or sealevel variations. These changes are more distinctive in the Black Sea, and especially in the Danube area, because of the isolation of the Black Sea from the Mediterranean during sealevel lowstands. The BSRs are therefore interpreted to reflect stages of stable sealevel lowstands during glacial times. Their observation in seismic data indicates that small amounts of free gas are still present beneath each of the paleo-BSRs, and that buoyancy-driven upward gas migration is inhibited by the low gas concentrations. In addition, the paleo-BSRs may reflect the real geotherm (around 35 °C km^{-1}). These results suggest that the Danube area is not in a thermally steady state and is therefore still adapting to increasing bottom-water temperatures since the last glacial maximum.

5.1.2 Potential impacts of gas hydrate exploitation on slope stability

Hazards associated with gas hydrate production-induced slope failures in the Danube deep-sea fan were investigated based on a combination of multibeam echosounder data, 2D multichannel seismic data, and geotechnical samples. A three-step analysis was carried out, including (1) a preliminary area screening for critical slopes, (2) a 2D slope stability analysis, and (3) a run-out analysis for a hypothetical landslide. The analysis was based on a hypothetical gas hydrate reservoir located 60 m below the seafloor in water depths of about 1500 m.

Screening of the area based on multibeam bathymetry data shows that the area is generally stable, with some critical slopes at the inner levees of the paleo channels. The 2D slope stability model

reveals that the FoS against slope failure is around 1.27, with a calculated slip plane at the steepest part of the levee wall. The slip plane has a maximum thickness of 15-17 m and a horizontal length of about 120-140 m. Hydrate production with the depressurization method would increase the effective stress in the reservoir, resulting in reservoir compaction and seafloor subsidence in the order of 0.4 m. However, the simulation shows that the subsidence does not affect the FoS, and it is therefore unlikely that the production process would trigger a landslide. Should a landslide originate from the calculated failure plane, the mobilized mass would impact the production site with velocities of up to 10 m s^{-1}.

5.1.3 The Kerch seep site in the Don Kuban deep-sea fan

The Kerch seep site was investigated based on 3D seismic data, sidescan sonar data, and pore water data. The results show that each of the three seeps that constitute the Kerch seep site hosts its own gas pocket, which is supplied with biogenic methane via narrow pipes extending from the free-gas zone through the GHSZ. Methane is transported predominantly in the form of gas bubbles. The distinct seep mounds are caused by sediment updoming due to gas overpressure. Unlike other seep sites in the Black Sea, the Kerch seep sites represents a relatively young and active seep system that lacks extensive carbonate crusts at the seafloor.

5.2 Implications

BSRs in seismic data are, in general, well understood. In the hydrocarbon industry, the BSR is generally accepted as an indicator for the presence of gas hydrates and, more importantly, for the presence of free gas underneath. Knowledge of the BSR distribution is also useful in other aspects, e.g. to estimate the energy resource potential of an area by, e.g., the identification of positive high-amplitude reflections within turbidity zones. In addition, gas blow-out hazards can be mitigated by not drilling in areas where a BSR is observed.

In contrast, double or multiple BSRs are still not well understood. Our study of the multiple BSRs in the Danube deep-sea fan and a comparison with other examples of double BSRs from around the world (chapter 1.4.4) confirms that multiple BSRs are local features that can have a multitude of origins. Consequently, each of these sites have to be studied individually in order to understand the causes and implications of these anomalous BSRs.

The analysis of the multiple BSRs in the Danube deep-sea fan has provided new insights into the origin of these BSRs. Overpressured gas compartments can be excluded as the cause for multiple BSRs – not only in the Black Sea, but also in other areas, especially in cases where the BSRs clearly crosscut strata. The required pressures are too high and would rapidly exceed the lithostatic pressure, even when two overlying BSRs are only a few tens of meters apart. The absence of overpressured gas compartments in the Danube deep-sea fan implies that the multiple BSRs likely do not represent a potential hazard for drilling operations in the overlying hydrate bearing zone. Although free gas is present beneath the BSRs, it is of low concentrations. An important result is that in areas with multiple BSRs, low concentrations of free gas can remain in the sediment strata for several tens of thousands of years without starting to migrate towards shallower depths. These small gas accumulations therefore seem to be unaffected by recurring phases of sea level lowstands associated with changes in hydrostatic pressure in the order of 1-1.5 MPa.

The slope stability analysis in terms of potential exploitation of gas hydrates in the Danube deep-sea fan shows that the hazard of slope failure due to production is minor. The three-step approach to determine the hazard of triggering a landslide through hydrate production is very straightforward and consisted of a preliminary area screening for critical slopes, a 2D slope stability analysis, and a run-out analysis for a hypothetical landslide. This approach can be recommended for application to other suitable gas hydrate reservoirs around the world, as many are located in similar settings. The only drawback of the model was the lack of geotechnical samples from the study area, which is a major issue in submarine landslide studies in general (e.g. Vanneste et al., 2014). However, if more in situ geotechnical data become available, these can easily be integrated into the model to improve the accuracy.

The combination of high-resolution 3D seismic data and sidescan sonar data for the investigation of seep sites had been suggested by Talukder (2012) to get a deeper understanding of the complex plumbing processes involved at seep sites around the world. By complementing this dataset with pore water data, it was possible to determine the mechanism that led to the observed sediment updoming at the seep site. Moreover, the Kerch seep study comprises an in-depth analysis of the gas migration pathways and gas transport processes involved at the seep site. This multi-disciplinary approach is therefore recommended to be applied to other seep sites from around the world. In order to better constrain the gas column heights calculated for the Kerch seep site, geotechnical samples and better estimations of the thickness of the updoming sediment plate should be collected.

5.3 Outlook and recommendations for future research

5.3.1 Recommendations for future studies on the multiple BSRs

To improve the correlation of the multiple BSRs in the Danube deep-sea fan with different limnic stages of the Black Sea, a more accurate dating of the overlying sediment sequences is required. The present interpretation of the age of the sediment deposits, and especially of the buried channel-levee system where the multiple BSRs are observed, is based largely on the study of Winguth et al. (2000). The authors dated the sediment units by counting seismic sequences, but recent geologic interpretations (unpublished industrial data) suggest that some sequences might have been missed.

Are more accurate sequence stratigraphy model of the Danube deep-sea fan based on 2D seismic profiles is currently done by Orhan Atgın as part of his PhD thesis at the Dokuz Eylül University in Turkey. However, in order to get more accurate age estimations for the sediment sequences, drilling through the deposits of the Danube levee into the underlying layer A (Fig. 2.3), and ideally into the levee deposits of the buried channel-levee system, is required. Based on the study presented in Chapter 2, drilling sites were proposed for an upcoming RV Meteor cruise in the Danube deep-sea fan, which is scheduled for November 2017. During this cruise, the MeBo drilling device will be operated in the study area. The MeBo has a maximum penetration depth of 200 m below the seafloor and is therefore in theory capable of reaching into the shallowest sediment column of the buried channel-levee system.

In order to investigate our hypothesis that small amounts of free gas are present beneath each of the multiple BSRs, multi-phase flow simulations are currently carried out at GEOMAR by Christian Deusner and Shuphangi Gupta. In addition, an acoustic inversion of the high-resolution reflection seismic profiles may provide more insight into the concentration of free gas that may be present

underneath the BSRs. This method was recently applied by Crutchley et al. (2017) to long-offset streamer data from New Zealand's Hikurangi Margin. If the same approach would be applied to the Danube deep-sea fan, an accurate background velocity model would be required, which could be provided by the data from the OBS deployments in the area.

5.3.2 Recommendations for future studies on the gas hydrate reservoir and slope stability in the Danube deep-sea fan

The main challenge of out slope stability analysis for gas hydrate production include the uncertainty of the dimensions of the gas hydrate reservoir, the lack of reliable estimates of in situ gas hydrate saturations, and the lack of in situ geotechnical samples. The first two challenges, i.e., the dimension and properties of the gas hydrate reservoir, will be addressed by the upcoming RV Meteor cruise on which the MeBo drilling device will be operated. After a suitable target for a test dill (and eventually one or more sites for a later production) has been selected, a more detailed geotechnical study can be carried out in the area. The focus of this geotechnical should be the collection of sediment cores in the vicinity of the selected test site, i.e., along the nearby levee slope and in the channel bed. The cores should ideally penetrate below the deposits of hemipelagic sediments, i.e., at least 10 m beneath the seabed. This would allow sampling of both levee and the channel sediments to obtain their physical properties, which could then be used to improve the model results.

The slope stability modeling could further be improved by extending it to a full 3D model based on the 3D seismic data that are already available from the study area. The advantages of the 3D approach are that the full geometry of the area is taken into account, including the slope angle in the course direction of the channel. Furthermore, weaker, steep areas along the heterogeneous levee slope could be detected, which could not be taken into account in the 2D slope stability model as they may be located slightly offset to the profile. The 3D method would also allow determining a realistic sediment volume that may slide into the channel in case slope failure occurs.

Additionally, small-scale slumps and slides, especially along the levee walls, should be studied in more detail as they indicate the presence of weak sediment layers and failure planes. Identifying such slides in the existing multibeam bathymetric data can be challenging due to the resolution of the echosounder data (10 x 10 m^2), which may be too low to image the seafloor area affected by these slides. It is therefore recommended to map the area with AUVs or deep-towed sidescan sonars to acquire higher-resolution bathymetry and backscatter data for an improved detection of small-scale features.

5.3.3 Recommendations for future research on the Kerch seep site

One of the most interesting observations in the seismic data from the Don-Kuban paleo deep-sea fan is the absence of a BSR. As the area is characterized by active methane seepage and the confirmed presence of gas hydrates (Römer et al., 2012), the absence of a BSR is unusual and should therefore be studied in more detail. I would therefore suggest mapping the Don-Kuban deep-sea fan using similar seismic tools as in the Danube deep-sea fan, i.e., a streamer of >1km in length. This method would allow studying the deeper structure and sequences of the sedimentary succession of the fan, and it would also help to find out whether a BSR is absent in the entire area. The use of a long-offset streamer would also allow to get accurate seismic velocities in the subsurface, which could be used to create depth-migrated profiles.

Another useful dataset from the Kerch seep site is the data from repeated water column imaging surveys, which were performed during four different cruises since 2007: RV Meteor cruises M72/3 (2007), M84/2 (2011), RV Maria S. Merian cruise MSM15/2 (2010), and RV Poseidon cruise P427 (2012). This database can be used to study the temporal changes of gas flares, thus giving insight into the seep activity over time. A comparison between the 2007-2011 cruises was already presented in the study of Römer et al. (2012), but the extensive water column data from the P247 cruise has not yet been examined, and extending this database would be desirable. Ideally, a future cruise could also acquire an additional P-Cable 3D seismic dataset to obtain a second 3D snapshot of the subsurface, which could be used to investigate potential temporal changes of the gas distribution underneath the seeps. Combining the two datasets into a 4D dataset would also give insights into any short-term changes of the vertical gas migration pathways, such as lateral growing, clogging, or formation of new pathways.

Furthermore, an advanced CSEM survey would help identifying layers and zones of higher resistivity than the surrounding sediments. The CSEM method could confirm the presence and distribution of gas and gas hydrates in the subsurface underneath the seeps, as shown by studies of Schwalenberg et al. (2010) and Rippe et al. (2014) from the Hikurangi Margin in New Zealand.

5.4 References

Crutchley, G., Klaeschen, D., Pecher, O., and Henrys, S., 2017. How the gas hydrate system gives insight into subduction wedge dewatering processes in a zone of highly-oblique convergence on the southern Hikurangi margin of New Zealand. EGU General Assembly 2017, Vienna, Austria, 23-28 April 2017.

Rippe, D., Engels, M., Schwalenberg, K., and Scholl, C., 2014. Constraints on gas hydrate distribution from marine CSEM on Opouawe Bank, Hikurangi Margin, New Zealand. 22nd EM Induction Workshop, Weimar, Germany, 24-30 August, 2014.

Römer, M., Sahling, H., Pape, T., Bahr, A., Feseker, T., Wintersteller, P., and Bohrmann, G., 2012. Geological control and magnitude of methane ebullition from a high-flux seep area in the Black Sea – the Kerch seep area. Marine Geology 319-322, pp. 57-74, doi: 10.1016/j.margeo.2012.07.005.

Schwalenberg, K., Haeckel, M., Poort, J., and Jegen, M., 2010. Evaluation of gas hydrate deposits in an active seep area using marine controlled source electromagnetics: Results from Opouawe Bank, Hikurangi Margin, New Zealand. Marine Geology 272, pp. 79-88, doi:10.1016/j.margeo.2009.07.006.

Talukder, A.R., 2012. Review of submarine cold seep plumbing systems: leakage to seepage and venting. Terra Nova 24, pp. 255-272, doi:10.1111/j.1365-3121.2012.01066x.

Vanneste, M., Sultan, N., Garziglia, S., Forsberg, C.F., and L'Heureux, J.S., 2014. Seafloor instabilities and sediment deformation processes: The need for integrated, multi-disciplinary investigations. Marine Geology 352, pp. 183-214, doi:10.1016/j.margeo.2014.01.005.

Winguth, C., Wong, H.K., Panin, N., Dinu, C., Georescu, P., Ungureanu, G., Krugliakov, V.V., and Podshuveit, V., 2000. Upper Quaternary water level history and sedimentation in the northwestern Black Sea. Marine Geology 167, pp. 127-146, doi:10.1016/S0025-3227(00)00024-4.

List of Figures

List of Tables

Appendix

A.1 Supporting information: Chapter 2 – Heat flow simulation

Model description

The heat flow in the sediment was simulated using the 1D non-steady state transport equation:

$$\frac{\partial T}{\partial t} = \frac{\partial}{\partial x}\left(\frac{\lambda}{c_P} \frac{\partial T}{\partial x} + uT \right) \qquad \text{Eq. A.1}$$

where t is time, x is the depth, T is the temperature, λ is the thermal conductivity of the sediment matrix, u is the advection velocity, and c_p is the thermal capacity of the sediment matrix. In Equation A.1, the first term on the right side is equivalent to Fourier's law of conductive heat transport and the second term represents the convective heat transport due to advection (i.e. burial of bulk sediment).

The thermal conductivity λ and the heat capacity c_p of the bulk sediment were calculated from the respective values for solid phase and pore water, weighted by the respective volume fractions in the sediment:

$$\lambda = \phi\lambda_f + (1-\phi)\lambda_s \qquad \text{Eq. A.2}$$

where λ_f is the thermal conductivity of seawater and λ_s is the thermal conductivity of the solid phase, and

$$c_p = \phi c_f + (1-\phi)c_s \qquad \text{Eq. A.3}$$

where c_f is the heat capacity of seawater and c_s is the heat capacity of the solid phase. Sediment porosity was calculated in the model using an empirical relationship (Boudreau, 1997):

$$\phi(z) = \phi_L + (\phi_0 - \phi_L)e^{-\beta z} \qquad \text{Eq. A.4}$$

where ϕ_0 is the porosity at the sediment surface (x=0), ϕ_L is the porosity at a sediment depth of x=L, and β is the porosity attenuation coefficient (see Table A 1 for the parameter values).

The partial differential equation was solved using the 'pdepe' function of Matlab®. A constant bottom water temperature (T_{BW}) was chosen as upper boundary condition and a constant conductive heat flow (F_L) at the lower boundary.

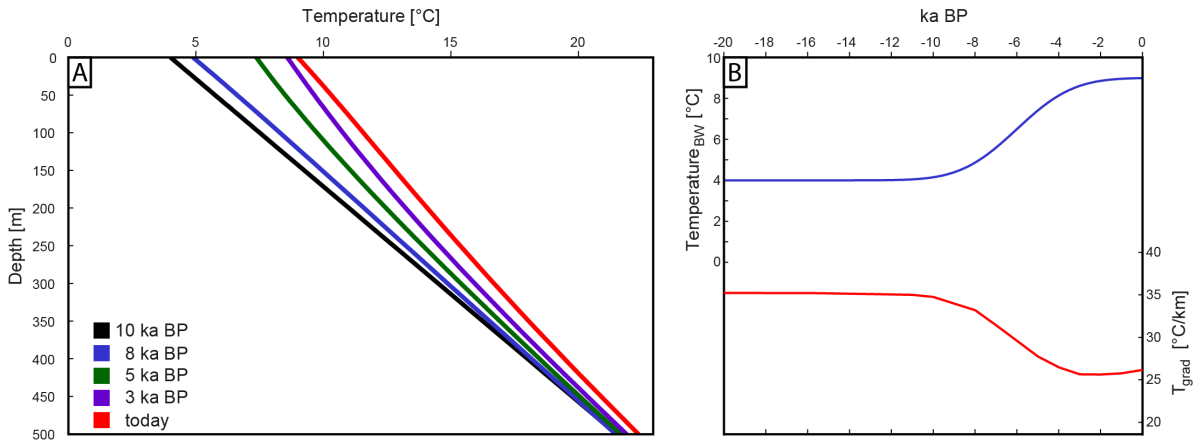

Fig. A 1: A: Bottom water warming from 4 °C to 9 °C and the change of the sediment temperature with depth since the last glacial maximum plotted for five timesteps. B: Bottom water warming (blue curve) and the temperature gradient of the top 400 m of sediments (red curve).

Table A 1: Summary of the parameter values used in the heat flow model

Parameter	**Symbol**	**Value [Unit]**	**Reference**
Length of the model column	L	15,000 [m]	-
Water depth	p	1500 [m]	This study
Salinity of bottom water	S_{BW}	22.3	Degens & Ross (1974)
Salinity in the GHSZ	S_{GHSZ}	3	[a]
Porosity at sediment surface (x=0)	Φ_0	0.7	based on DSDP42b Site379
Porosity at base of sediment (x=L)	Φ_L	0.38	based on DSDP42b Site379
Porosity attenuation coefficient	β	0.00008 [1/cm]	based on DSDP42b Site379
Heat capacity of seawater	c_f	$4.14 \cdot 10^6$ [J/(m^3 K)]	Kossel et al. (2013) [b]
Heat capacity of sediment	c_s	$2.15 \cdot 10^6$ [J/(m^3 K)]	Kossel et al. (2013)
Thermal conductivity of seawater	λ_f	0.63 [W/m/K]	Kossel et al. (2013) [b]
Thermal conductivity of sediment	λ_s	1.65 [W/m/K]	Kossel et al. (2013) [c]
Sedimentation rate	u	0.03 [cm/a]	Soulet et al. (2010) [d]
Temperature of bottom water (x=0)	T_{BW}	9 [°C]	Degens & Ross (1974)
Heat flow at base of sediment (x=L)	F_L	44 [mW/m^2]	Sclater et al. (1980)

[a] *Salinities of 2-5 are reported for the Danube area and DSDP42b Site 379. A value of 3 was used in the calculations. Variations between 2 and 5 do not alter the results significantly.*

[b] *Average value for p, T, S range in the GHSZ.*

[c] *1.3 W/m/K for Black Sea sediments with a porosity of 0.3.*

[d] *Average value for the past 10-15 ka.*

A.2 Supporting information: Chapter 2 – Time-sections and velocity profiles

The RMCS profiles were converted from time to depth using the velocity data from the semblance analysis. The velocity profile was smoothed and does not take into account possible local velocity anomalies, which are beyond the sensitivity of the seismic equipment due to the short offsets of 1050 m. We then defined a 3D velocity model for the HMCS survey by extrapolating seismic velocities derived from the RMCS profiles that cross the HMCS survey. The seismic sections presented in Fig. 2.2 (HMCS) and Fig. 2.3 (RMCS) are shown in TWT and include 1D velocity profiles for selected locations (Fig. A.2 and Fig. A.3).

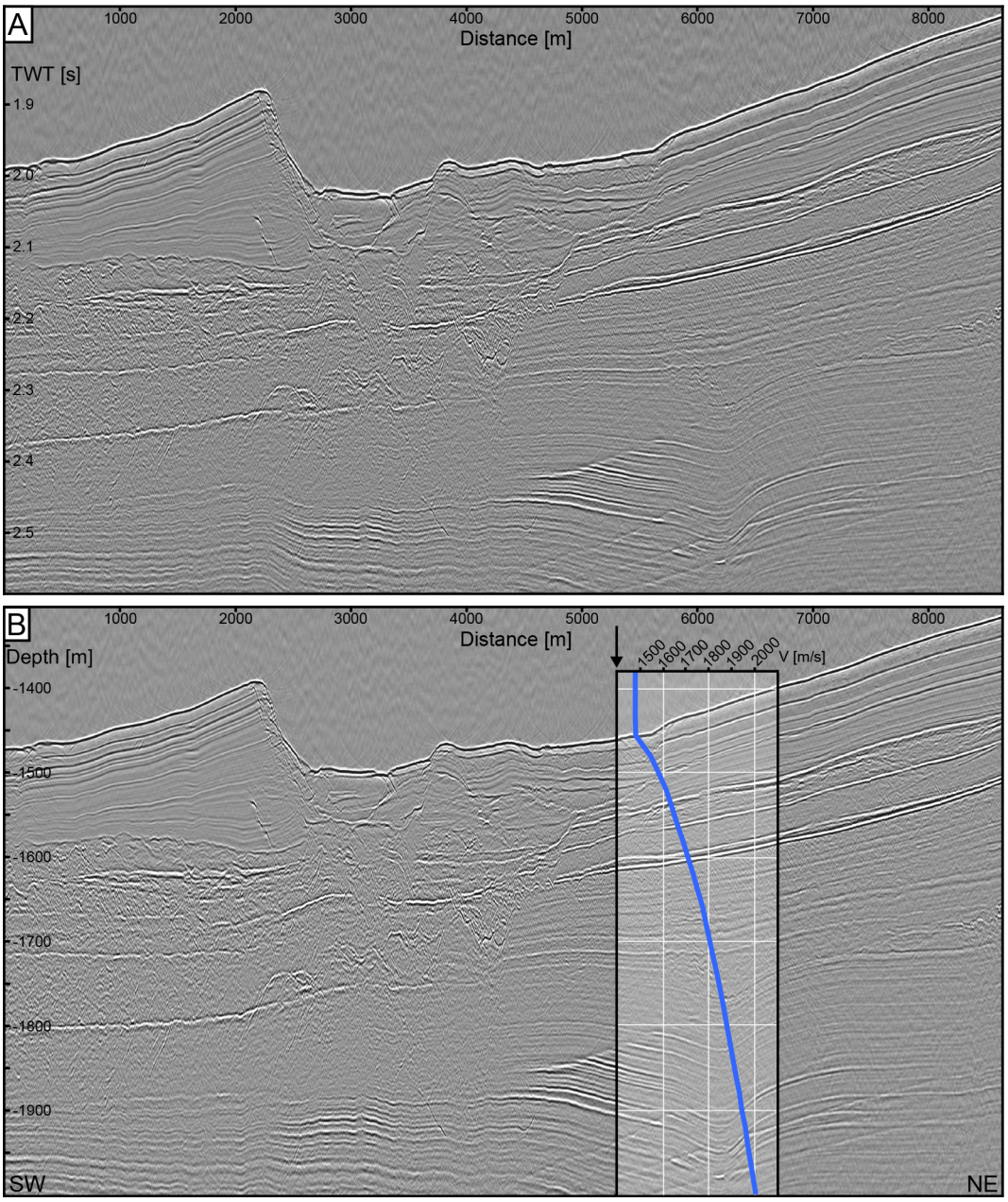

Fig. A.2 A: TWT-section of the HMCS profile presented in Fig. 2.2. B: Uninterpreted depth-section. Inset: 1D velocity profile. Location of the velocity profile is depicted by the black arrow.

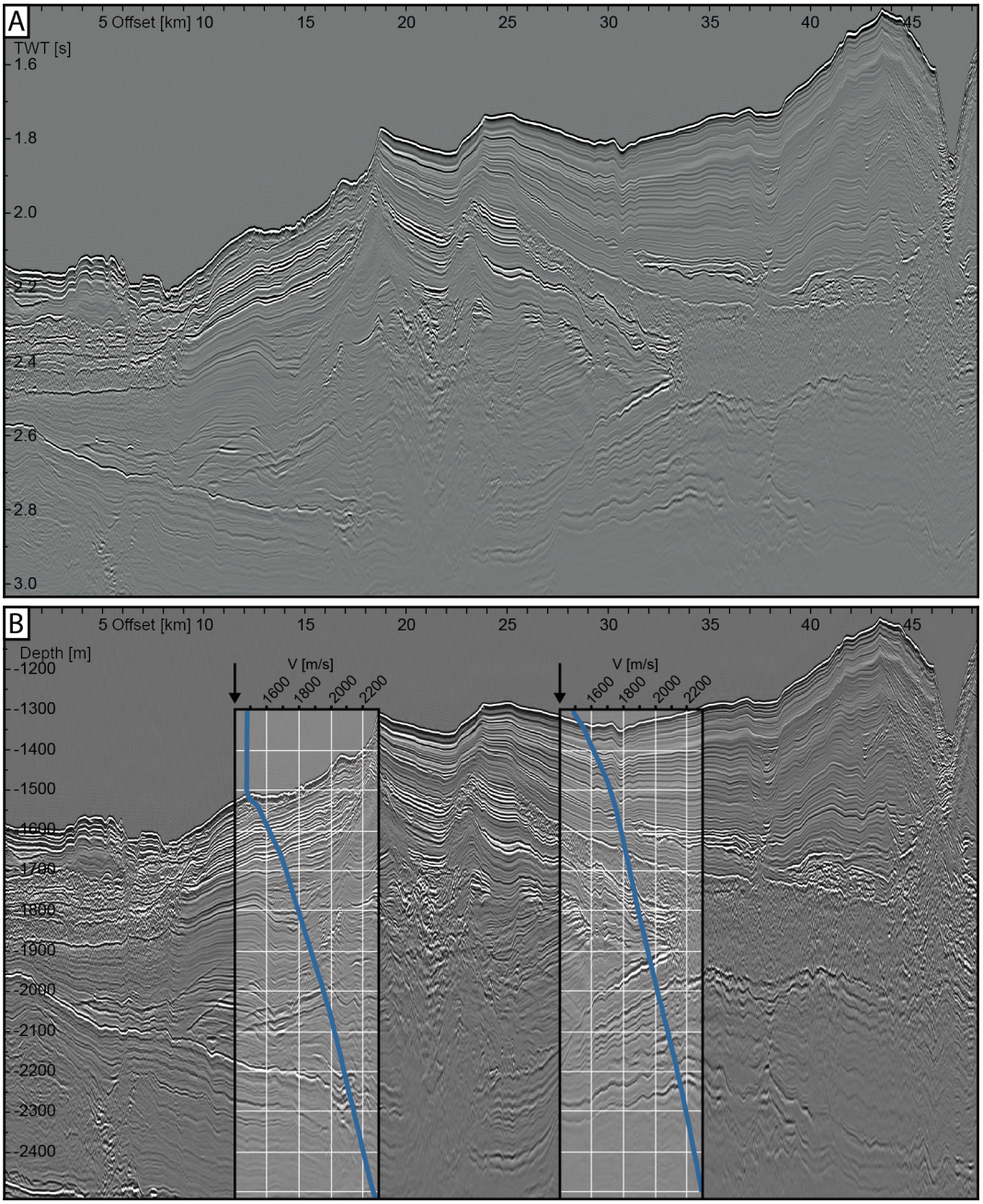

Fig. A.3 TWT-section of the RMCS profile presented in Fig. 2.3. B: Uninterpreted depth-section. Insets: 1D velocity profiles. Locations of the velocity profiles are depicted by black arrows.

A.3 Supporting information: Chapter 2 – Lithostatic pressure calculation

The lithostatic pressure depends on the density of the overburden (Ugwu, 2015) and is calculated by

$$P_L(z) = P_0 + g \int_0^z \rho(z) dz \qquad \text{Eq. A.5}$$

where P_L is the lithostatic pressure, z is the depth below the seabed, P_0 is the pressure at the seafloor, g is the gravitational acceleration, and ρ is the density.

The density was calculated from the P-wave velocity with the Gardner equation (Eq. A.6) (Gardner et al., 1974) which is valid for velocities between 1.5 < V_P < 6.1 km/s. Due to an increasing uncertainty for velocities of less than 2 km/s, we also calculated the density using the Nafe-Drake curve (Eq. A.7) as presented in Brocher (2005). This approach is valid for velocities between 1.5 < V_P < 8.5 km/s.

$$\rho = a{V_P}^b \qquad \text{Eq. A.6}$$

$$\rho = 1.6612V_P - 0.4721V_P^2 + 0.0671V_P^3 - 0.0043V_P^4 + 0.000106V_P^5 \qquad \text{Eq. A.7}$$

where ρ is the density, V_P is the P-wave velocity [m/s], a=0.31 and b=0.25.

We extracted a 1D velocity profile (Fig. A.2B) at the location of the model which is presented in Fig. 2.5. Compared to the lithostatic pressure gradient observed in the Gulf of Mexico (red dashed line in Fig. 2.5), the pressure values calculated with the Gardner equation are slightly higher (red line in Fig. 2.5), whereas the pressure values calculated with the Nafe-Drake curve are slightly lower (red dotted line in Fig. 2.5). Given that the velocity data had to be extrapolated and smoothed, the results of the two different approaches give a good estimation of the lithostatic pressure that might be encountered in this area.

References

Brocher, T., 2005. Empirical Relations between Elastic Wavespeeds and Density in the Earth's Crust. Bulletin of the Seismological Society of America, vol. 95, 6, 2081-2092. doi: 10.1785/0120050077

Gardner, G.H.F., Gardner, L.W., and Gregory, A.R., 1974. Formation Velocity and Density – The Diagnostic Basics for Stratigraphic Traps. Geophysics, Vol. 39, 6., 770-780.

Ugwu, G.Z., 2015. An Overview of pore pressure prediction using seismically-derived velocities. Journal of Geology and Mining Research, Vol. 7, 31-40.

B Extended Abstract: EAGE Near Surface Geosciences 2016

Potential Impacts of Gas Hydrate Exploitation of Slope Stability – A Study from the Danube Fan, Black Sea

Timo Zander[a], Jung Chan Choi[b], Maarten Vanneste[b], Christian Berndt[a]

[a]*GEOMAR Helmholtz Centre for Ocean Research Kiel, Germany*

[b]*Norwegian Geotechnical Institute, Oslo, Norway*

Presented at the Near Surface Geoscience 2016 – Second Applied Shallow Marine Geophysics Conference, 04.-08.09.2016, Barcelona, Spain

Abstract

We created a two-dimensional geomechanical model to analyse the hazard of hydrate production induced slope failures in a channel-levee system of the Danube paleo-fan in the Black Sea. Gas hydrates presumably have accumulated in coarse-grained sediments at the base of a paleo channel. The exploitation scenario is based on depressurization of the reservoir along a vertical drill hole. The model geometry is based on high resolution reflection seismic data. Initial results estimated the failure surface at the steepest part of the levee slope (>8° dip) with a Factor of Safety of 1.254, which is considered to be critically affected by seabed subsidence. Preliminary results show that the estimated subsidence at the seafloor after pore pressure depletion of the gas hydrate reservoir is only in the order of centimeters. The effect of production-induced subsidence on the stability of critical slopes will be minor. However, the inherent stability of the slope is still under marginal ranges, and the material properties and production scenario still have big uncertainties due to lack of information.

Introduction

Gas hydrates have been considered an energy resource for the past two decades as they store vast amounts of methane in the crystalline cage structures. Natural gas hydrates occur in continental margin sediments worldwide as well as permafrost areas and contain more energy than all other known fossil fuel sources combined (Trofimuk et al., 1981). The sandy sediments of the Danube deep-sea fan of the Black Sea have good reservoir conditions. 2D and 3D high-resolution reflection seismic datasets from a paleo channel-levee system in ~1500 m water depth of the Danube Fan (Bialas et al., 2014) reveal abundant evidence of gas hydrates and free gas, by the presence of a distinct bottom simulating reflection (BSR). The BSR originates from the impedance contrast between sediments containing gas hydrates above the base of the gas hydrate stability zone (BGHSZ), and sediments below containing free gas. In the study area, the gas hydrate stability zone (GHSZ) is about 350 m thick. High-amplitude reflections in the channel sediments above and also preliminary result from controlled source

electromagnetic (CSEM) profiles (Schwalenberg et al., 2015) point towards coarse-grained (sandy, gravelly) layers with high gas hydrate saturation.

For engineering and exploitation activities along a sloping seabed, the seafloor stability should be addressed (Kvalstad et al., 2011). In the study area, the bathymetric and seismic data reveal evidence for paleo-failures along the steep levee slopes, suggesting that the area may be prone to sediment failure. Furthermore, reducing the in situ pore pressure in the hydrate reservoirs to allow dissociation and exploitation, invokes an increase in effective stress and therefore a change in the geomechanical conditions within the overburden. As a result, gas production from shallow hydrate reservoirs may cause subsidence at the seafloor (Fjaer et al., 2008).

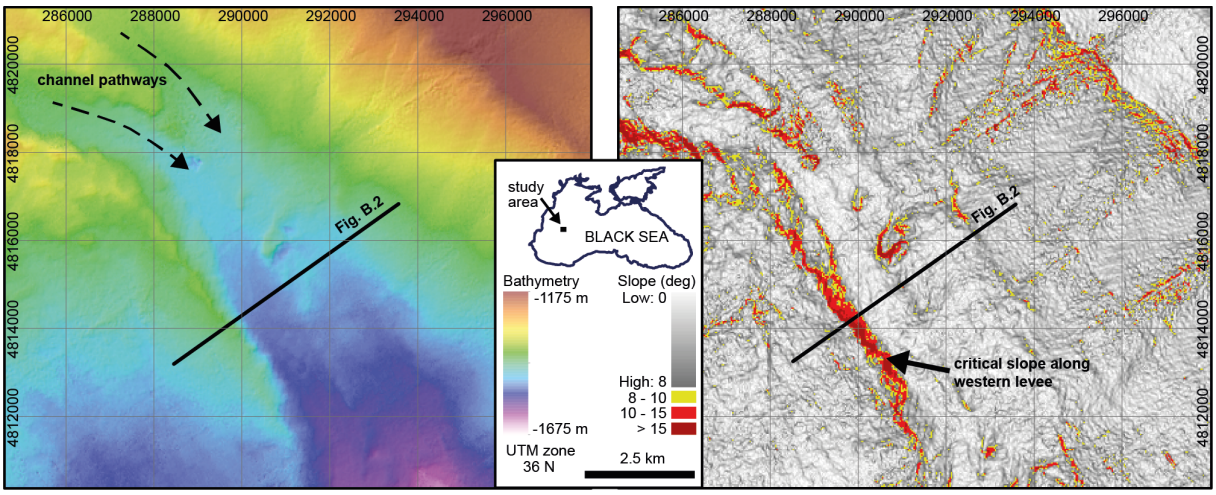

Fig. B.1 *left: multibeam bathymetry of the area. The study area is located in the paleo Danube deep-sea fan. The study area is located in an ancient channel-levee system in a water depth of about 1500 m. Right: The slope map highlights the steep slope angles (>8°) along the western levee of the paleo channel. To study the hazard of potential slope failures due to gas hydrate exploitation from a reservoir below the channel bed, a seismic cross section is selected for the finite element model (black line).*

Objectives

The main objectives of this study are:

1. How much compaction will be caused by gas production from an assumed gas hydrate reservoir in the study area?
2. Does the production-induced compaction affect seafloor subsidence, and if so, can it trigger seabed failures?
3. What will be the optimal strategy to avoid a production-related geohazard?

We note that there is a lack on in situ data from the study area, and therefore, part of the work is based on a parametric study or in-house knowledge and databases.

Slope stability assessment

This study focusses on analysing the hazard of slopes that may become unstable prior, during or after the production of gas hydrates and the induced seabed subsidence due to reservoir compaction. The steepest slope segments (> 8°) occur along the western levee of the SUGAR channel (Fig. B.1), and

this is the most critical zone. The channel-base is identified in the seismic data as layers of high amplitudes in about 60 m below sea floor (mbsf) (Fig. B.2) and preliminary analysis of a CSEM profile implies a 6 m thick zone of increased gas hydrate saturation in this zone (Schwalenberg et al., 2015). For our model, we postulate a second zone of gas hydrate-hosting sediments beneath a strong reflector in about 140 mbsf (Fig. B.2).

The parametric study runs along seismic line 1107 cutting through the channel and levee structure (Fig. B.2) where both CSEM and ocean bottom bottom seismometer data exist (Bialas et al., 2014). The geometry of the model – such as the channel pathway, channel base and outline of the reservoir – was derived from the interpreted key horizons in the depth-converted seismic data (Fig. B.2).

As direct borehole measurements from the study area are not available, we had to select a suitable range for the various geomechanical properties for the overburden and the reservoir from other studies, public domain data and in-house knowledge. The best sources from the Danube Fan are recently collected piezocone and pore pressure data from the Romanian area of the Danube Fan (Ker and Riboulot, 2015). The geotechnical properties for the gas hydrate bearing sands in the reservoir were parameterized in analogy to hydrate-bearing sediments of the Nankai Trough (Santamarina et al., 2015).

The production scenario adopts depressurization of the gas hydrate reservoir. To this end, a borehole is drilled vertically into the reservoir, and the pressure reduction is initialized along the entire reservoir thickness. Following pressure reduction, hydrate will start dissociating and the dissociation front will spread gradually from the well into the reservoir sediments. Simulations from Nankai show that the hydrate dissociation does not exceed much more than 100 m which is taken into account in our model, in addition to the consideration of spacing multiple boreholes.

Model approach and preliminary results

We carried out a 2D numerical modelling of the gas hydrate site using the commercial finite element software PLAXIS 2D (Brinkgreve et al., 2007). We defined a geometry for the finite-element model based on the geological interpretation of the seismic line. The sandy channel facies forms one layer, overlying the shallow gas hydrate reservoir as the second layer at a subsurface depth of about 60 m and an average thickness of 6 m. The neighbouring layer represents the levees at either sides of the channel. It consists of fine-grained overspill deposits. The deeper reservoir in about 140 m depth has an average thickness of about 30 m. It extends laterally to the edges of the model, considering that the seismic reflection data show sub-parallel continuous stratification in that depth interval.

The finite element modelling process is divided into two steps. First, the slip zone with the least factor of safety (FoS) is calculated under static conditions, as an assessment of the present-day stability of the area. This considers the resisting movement forces controlled mainly by shear strength against the driving forces, i.e. shear stress. The result for line 1107 is shown in figure 2, highlighting the shear strain increments along the calculated failure surface at the steepest part of the slope (8° dip). The slip zone has a length of about 120 m, and the FoS for the initial phase is 1.254, while a FoS below 1 means failure.

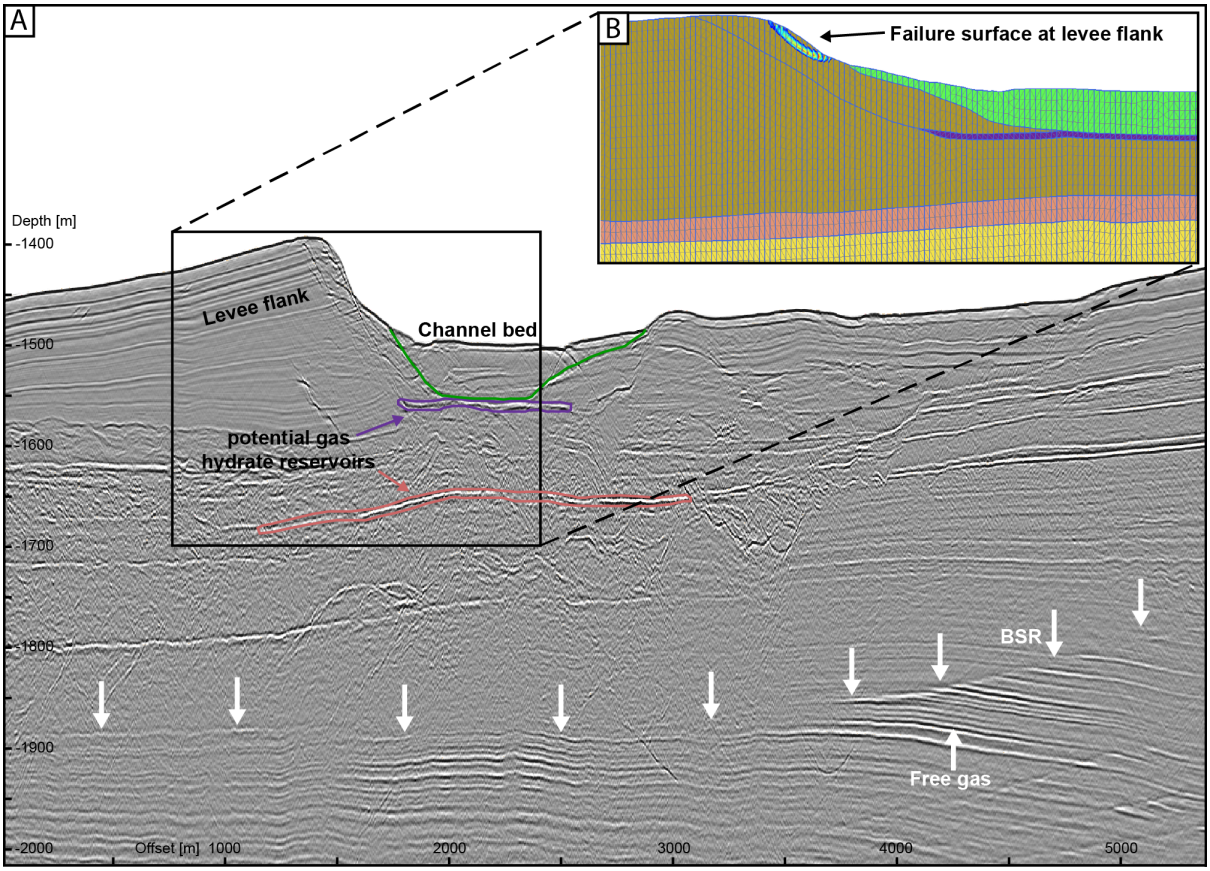

Fig. B.2 *A: seismic section showing the channel levee system in the study area. The entire channel-levee system is situated well above the base of gas hydrate stability zone, which is indicated by the BSR in about 350 m bsf (white arrows). Two potential gas hydrate reservoirs in coarse-grained sediments are highlighted (purple, light red). A simplified geometry was derived for the geomechanical model (B), taking into account the channel, levee and two potential reservoirs following high amplitude reflections identified in the seismic data (purple, light red). Note the different vertical exaggerations of the seismic plot and the geomechanical model.*

In the second step, we implement the depressurization of the reservoir. The pore pressure reduction leads to an increase in effective stress of the reservoir sands and thus the reservoir becomes compacted. Reducing the gas hydrate saturation further leads to a reduction in stiffness and shear strength. By varying different parameters such as borehole location, different radii for the hydrate dissociation front, ranges for the pressure reduction, and applying these studies to both shallow and deep reservoirs, a range of different scenarios and time scales is analysed. The impact of the reservoir compaction to the seabed can lead to a change of loading conditions and thus would reduce the initial FoS.

In a depletion scenario of the shallow gas hydrate reservoir with a production well at the centre of the channel bed, pore pressure reduction in the reservoir of 12 MPa, and a depletion radius around the borehole of 250 m shows the following results. The compaction of the shallow reservoir does not lead to a large subsidence at the seafloor. The maximum vertical displacement is in the order of 12 – 15 cm. The FoS remains stable since the change of slope inclination is negligibly small after the pore pressure depletion. However, locating the borehole closer towards the levee slope may have a different impact on the load conditions.

Conclusions

Based on geophysical data from the Danube deep-sea fan, we created a two-dimensional geomechanical model to analyse the hazard of hydrate-production-induced slope failures in a channel-levee system. Initial results estimated the failure surface at the levee slope that has a low Factor of Safety of about 1.25, which is considered to be critically affected by seabed subsidence. The estimated subsidence at the seafloor after pore pressure depletion of the reservoir is only in the order of centimetres. The preliminary estimation concludes that the effect of production-induced subsidence on the stability of critical slopes will be minor. However, the inherent stability of the slope is still under marginal ranges (less than 1.5); and the material properties and production scenario still have big uncertainties due to lack of information.

Acknowledgements

This project has received funding from the European Union's Seventh Programme for research, technological development and demonstration under Grant Agreement No. 603418. For more information, please visit the project website at eu-midas.net. Cruise MSM34 was supported by the Bundesministerium für Wirtschaft und Technologie (BMWi) and the Bundesministerium für Wirtschaft und Forschung (BMBF) as part of the SUGAR-project (SUbmarine GAs hydrate Resources), Grant No. 03G0819A.

References

Bialas, J., Klaucke, I., and Haeckel, M. (eds.), 2014. FS MARIA S. MERIAN Fahrtbericht / Cruise Report MSM-34 // 1 & 2 SUGAR Site. Berichte aus dem GEOMAR Helmholtz-Zentrum für Ozeanforschung Kiel, 15.

Brinkgreve, R.B.J., Broere, W. and Waterman, D., 2007. Plaxis 2D Manual. Delft University of Technology, Delft.

Fjaer, E., Holt, R.M., Horsrud, P., Raaen, A.M., and Risnes, R., 2008. Petroleum related rock mechanics 2nd edition. In: Developments in petroleum science 53. Elsevier.

Ker, S. and Riboulot, V., 2015. GHASS CRUISE REPORT. Ifremer, France.

Kvalstad, T.J., Yamamoto, K., Noguchi, S., Uchida, S., and Soda, K., 2011. Effect of gas hydrate production on seabed stability in the eastern Nankai trough area. Proceedings of the 7th International Conference on Gas Hydrates (ICGH), Edinburgh, Scotland.

Lu, H., Kawasaki, T., Ukita, T., Moudrrakovski, I., Fujii, T., Noguchi, S., Shimada, T., Nakamizu, M., Ripmeester, J., Ratcliffe, C. [2011] Particle size effect on the saturation of methane hydrate in sediments – Constrained from experimental results. Marine and Petroleum Geology 28, 1801 – 1805.

Santamarina, J.C., Dai., S., Terzariol, M., Jang, J., Waite, W.F., Winters, W.J., Nagao, J., Yoneda, J., Konno, Y., Fujii, T. and Suzuki, K., 2015. Hydro-bio-geomechanical properties of hydrate-bearing sediments from Nankai Trough. Marine and Petroleum Geology 66, 434 – 450.

Schwalenberg, K., Rippe, D. and Hölz, S., 2015. FS Maria S. MERIAN Ausfahrt MSM 35: Marine elektromagnetische Untersuchungen zur Exploration von submarinen Gashydratvorkommen im Donau-Delta, westliches Schwarzes Meer. 75. Jahrestagung der Deutschen Geophysikalischen Gesellschaft, Hannover, MG-P1.03.

Trofimuk, A.A., Makogon, Y.F. and Tolkachef, M.V., 1981. Gas hydrate accumulations – new reserve of energy sources. Geologiya Nefti I Gaza 10, 15 – 22 (in Russian).

C List of publications and presentations in the period of my PhD

Articles – peer-reviewed

On the origin of multiple BSRs in the Danube deep-sea fan, Black Sea

Zander, T., Haeckel, M., Berndt, C., Chi, W.C., Klaucke, I., Bialas, J., Klaeschen, D., Koch, S., and Atgın, O., 2017. Earth and Planetary Science Letter, 462, pp. 15-25. Doi: 10.1016/j.epsl.2017.01.006

High-resolution 2D seismic data reveal the character and distribution of up to four stacked bottom simulating reflectors (BSR) within the channel-levee systems of the Danube deep-sea fan. The theoretical base of the gas hydrate stability zone (GHSZ) calculated from regional geothermal gradients and salinity data is in agreement with the shallowest BSR. For the deeper BSRs, BSR formation due to overpressure compartments can be excluded because the necessary gas column would exceed the vertical distance between two overlying BSRs. We show instead that the deeper BSRs are likely paleo-BSRs caused by a change in pressure and temperature conditions during different limnic phases of the Black Sea. This is supported by the observation that the BSRs correspond to paleo seafloor horizons located in a layer between a buried channel-levee system and the levee deposits of the Danube channel. The good match of the observed BSRs and the BSRs predicted from deposition of these sediment layers indicates that the multiple BSRs reflect stages of stable sealevel lowstands possibly during glacial times. The observation of sharp BSRs several 10,000 of years but possibly up to 300,000 years after they have left the GHSZ demonstrates that either hydrate dissociation does not take place within this time frame or that only small amounts of gas are released that can be transported by diffusion. The gas underneath the previous GHSZ does not start to migrate for several thousands of years.

Extended Abstracts

Potential Impacts of Gas Hydrate Exploitation on Slope Stability – A Study from the Danube Fan, Black Sea

Zander, T., Choi, J.C., Vanneste, M., and Berndt, C., 2016. Presented at: Near Surface Geoscience 2016 – Second Applied Shallow Marine Geophysics Conference, 04.-08.09.2016, Barcelona, Spain. Doi: 10.3997/2214-4609.201602158

We created a two-dimensional geomechanical model to analyse the hazard of hydrate production induced slope failures in a channel-levee system of the Danube paleo-fan in the Black Sea. Gas hydrates presumably have accumulated in coarse-grained sediments at the base of a paleo channel. The exploitation scenario is based on depressurization of the reservoir along a vertical drill hole. The model geometry is based on high resolution reflection seismic data. Initial results estimated the failure surface at the steepest part of the levee slope (>8 ° dip) with a Factor of Safety of 1.254, which is considered to be critically affected by seabed subsidence. Preliminary results show that the estimated subsidence at the seafloor after pore pressure depletion of the gas hydrate reservoir is only in the order of centimeters. The effect of production-induced subsidence on the stability of critical slopes will be minor. However, the inherent stability of the slope is still under marginal ranges, and the material properties and production scenario still have big uncertainties due to lack of information.

Reports

Vanneste, M., Choi, J.C., Sauvin, G., Yang, S., Forsberg, C.F., Carlton, B., Kvalstad, T.J., Boylan, N., **Zander, T.**, Berndt, C., and Garziglia, S., 2016. Potential Impacts of Gas Hydrate Exploitation on Slope Stability and Sediment Deformation. MIDAS deliverable, D1.6, 50 pp.

Zander, T., Deusner, C., Garziglia, S., Kossel, E., Haeckel, M., Gupta, S., Berndt, C., Bialas, J., Badhani, S., and Vanneste, M., 2016. Seismic and geotechnical characterization of hydrated sediments in a sand-rich setting: field work and lab experiment results. MIDAS deliverable, D1.5, 51 pp.

Presentations

Haeckel, M., **Zander, T**., Burwicz, E., Bialas, J., Berndt, C., Dannowski, A., Hensen, C., Hölz, S., Jegen, M., Klaucke, I., Rottke, W., and Schwalenberg, K., 2017. The gas hydrate system of the Danube deep-sea fan in the Black Sea. 9th International Conference on Gas Hydrates, ICGH9, 25-30 June 2017, Denver, Colorado, USA.

Bialas, J., Dannowski, A., **Zander, T.**, Klaeschen, D., and Klaucke, I., 2017. Approaching hydrate and free gas distribution at the SUGAR-Site location in the Danube Delta. In: EGU General Assembly 2017, 23.-28.04.2017, Vienna, Austria.

Burwicz, E.B., **Zander T.**, Rottke, W., Bialas, J., Hensen, C., Atgın, O., and Haeckel, M., 2017. Estimating the gas hydrate recovery prospects in the western Black Sea basin based on the 3D multiphase flow of fluid and gas components within highly permeable paleo-channel-levee systems. In: EGU General Assembly 2017, 23.-28.04.2017, Vienna, Austria.

Choi, J.C., Vanneste, M., **Zander, T.**, Yang, S., Carlton, B., Forsberg, C.F., and Sauvin, G., 2016. Geomechanic assessment of hydrate-related geohazards: Case studies on Black Sea and western Svalbard continental margins. In: MIDAS Final Meeting 2016, 03.-07.10.2016, Ghent, Belgium.

Gehrmann, R., Schwalenberg, K., Hölz, S., **Zander, T**., Dettmer, J., and Bialas, J., 2016. Controlled source electromagnetic data analysis with seismic constraints and rigorous uncertainty estimation in the Black Sea. In: AGU Fall Meeting 2016, 12.-16.12.2016, San Francisco, USA.

Gehrmann, R., Schwalenberg, K., **Zander, T.**, and Dettmer, J., 2016. Analysis of controlled source electromagnetic data in the Black Sea: Regularized 2-D inversion with seismic constraints and trans-dimensional Bayesian inversion to estimate uncertainties. In: New Advances in Geophysics (NAG) Meeting 2016, Integrated Imaging of the Earth, 11.-12.02.2016, London, UK.

Schwalenberg, K., Gehrmann, R., Rippel, D., Hölz, S., and **Zander, T.**, 2016. Gas hydrate saturation estimates from the Danube Delta offshore Romania using marine controlled source electromagnetics. In: 13. Gas In Marine Sediments (GIMS13), 19-22.09.2016, Tromso, Norway.

Zander, T., 2016. Multiple BSRs in the Black Sea. In: TaiGer Meeting, 13.-15.04.2016, Kiel, Germany.

Zander, T., Choi, J.C., Vanneste, Garziglia, S., Deusner, C., and Berndt, C., 2016. Potential impacts of gas hydrate exploitation on slope stability in the Danube deep-sea fan, Black Sea. In: MIDAS Final Meeting 2016, 03.-07.10.2016, Ghent, Belgium.

Zander, T., Choi, J.C., Vanneste, M., Garziglia, S., Deusner, C., Berndt, C., and Haeckel, M., 2016. Geomechanische Studien zu Hang(in-)stabilitäten im Donaudelta. In: SUGAR Vollversammlung 2016, 25.-26.10.2016, Kiel, Germany.

Zander, T., Bialas, J., Berndt, C., Haeckel, M., Klaucke, I., Kunath, P., Klaeschen, D., Koch, S., and Papenberg, C., 2015. Gas hydrate accumulations and BSR anomalies in a channel-levee system of the Danube Deep-Sea Fan, Black Sea. In: MIDAS Annual Meeting 2015, 16.-20.11.2015, Sintra, Portugal.

Zander, T., Bialas, J., Berndt, C., Klaucke, I., Klaeschen, D., Koch, S., Papenberg, C., and MSM34 Scientific Parties, 2014. Gas Hydrate Distribution in Channel-Levee Systems of the Danube Deep-Sea Fan (Black Sea) revealed by new seismic data. In: MIDAS Annual Meeting 2014, 20.-24.10.2014, San Miguel, Azores, Portugal.

Zander, T., Bialas, J., Berndt, C., Klaucke, I., Klaeschen, D., Koch, S., Papenberg, C., and MSM34 Scientific Parties, 2014. Gas Hydrate Distribution in Channel-Levee Systems of the Danube Deep-Sea Fan (Black Sea) revealed by new seismic data. In: 12. Gas In Marine Sediments (GIMS12), 01.-06.09.2014, Taipei, Taiwan.

Zander, T., Klaucke, I., Bialas, J., Berndt, C., Klaeschen, D., and Papenberg, C., 2014. Are cold seep locations controlled by topographic or gas hydrate evolution? A view from the Kerch seep plumbing system in the Black Sea. In: 12. Gas In Marine Sediments (GIMS12), 01.-06.09.2014, Taipei, Taiwan.

Conference Posters

Dannowski, A., Bialas, J., Schwalenberg, K., Gehrmann, R., **Zander, T**., and Klaeschen, D., 2017. Shear wave modelling of high resolution OBS data with a comparison to CSEM data in a gas hydrate environment in the Danube deep-sea fan, Black Sea. 9th International Conference on Gas Hydrates, ICGH9, 25-30 June 2017, Denver, Colorado, USA.

Schwalenberg, K., Hölz, S., Gehrmann, R., Rippe, D., Dannowski, A., **Zander, T.**, Duan, S., Jegen, M., and Bialas, J., 2017. Gas hydrate occurrences in the Danube Delta, Western Black Sea: Results from 2D and 3D controlled source electromagnetics. In: EGU General Assembly 2017, 23.-28.04.2017, Vienna, Austria.

Dannowski, A., Bialas, J., **Zander, T.**, and Klaeschen, D., 2016. Shear wave modelling of high resolution OBS data in a gas hydrate environment on the Danube deep-sea fan, Black Sea. In: AGU Fall Meeting 2016, 12.-16.12.2016, San Francisco, USA.

Badhani, S., Bialas, J., Berndt, C., Klaucke, I., and **Zander, T.**, 2016. Possible evidence for a relationship between gas hydrate dissociation and submarine slope failure in the Danube deep-sea fan, Black Sea. In: 76. Jahrestagung der Deutschen Geophysikalischen Gesellschaft, 14.-17.03.2016, Münster, Germany.

Dannowski, A., Bialas, J., **Zander, T.**, and Klaeschen, D., 2016. High resolution shear wave modelling of OBS data in a gas hydrate environment in the Danube deep-sea fan, Black Sea. In: 13. Gas In Marine Sediments (GIMS13), 19.-22.09.2016, Tromso, Norway.

Dannowski, A., Bialas, J., **Zander, T.**, Klaeschen, D., and Koch, S., 2016. High resolution shear wave modelling of OBS data in a gas hydrate environment in the Danube deep-sea fan, Black Sea. In: 41. CIESM Congress 2016, 12.-16.09.2016, Kiel, Germany.

Schwalenberg, K., Rippe, D., Gehrmann, R., Hölz, S., and **Zander, T.**, 2016. Marine CSEM Investigation of submarine gas hydrate targets in the Danube Delta, western Black Sea. In: 23. Electromagnetic Induction Workshop (EMIW), 14.-20.08.2016, Chian Mai, Thailand.

Zander, T., Berndt, C., Haeckel, M., Klaucke, I., Bialas, J., and Klaeschen, D., 2015. Distribution and Origin of Multiple Bottom Simulating Reflectors in the Danube Deep-Sea Fan, Black Sea. In: AGU Fall Meeting 2015, 14.-18.12.2015, San Francisco, USA.

D List of Research Expeditions contributing to my PhD

23.02.2012 – 19.03.2012	Black Sea FS Poseidon Burgas (Bulgaria) – Heraklion (Greece) 3D seismic, OBS seismic, Deep-towed Sidescan, Subbottom profiler, Multibeam
09.12.2013 – 17.01.2014	Black Sea FS Maria S. Merian Varna (Bulgaria) – Varna (Bulgaria) 2D & 3D seismic, OBS seismic, Multibeam, Sediment Echosounder, Gravity Cores, Temperature lance
10.09.2014 – 05.10.2014	South China Sea Ocean Researcher V Kaohsiung (Taiwan) – Kaohsiung (Taiwan) 2D & 3D seismic, OBS seismic
01.09.2015 – 15.09.2015	Black Sea RV Pourquoi Pas? Constanta (Romania) – Constanta (Romania) 2D & 2D deep-towed seismic, sediment echosounder, Multibeam

E Acknowledgements

Many thanks to Christian Berndt, Jörg Bialas, and Ingo Klaucke, whose initiatives made this PhD thesis possible, and for the support, feedback, and ideas throughout the time. I am very thankful to Christian Berndt for the supervision and guidance, and for developing ideas on how we could put together exciting manuscripts from the conglomerate of data and interpretations.

I thank Wu-Cheng Chi for the supervision and guidance during my stay at the Academia Sinica in Taipei in early 2016. Although the time was rather short, I learned so much about heatflow modeling and connecting these models to real geophysical datasets. But I also got to know a lot about Taipei, and the field trip made this stay a truly unforgettable experience! Special thanks go to Pascal, Celine, Dai-Chieh, Kim, Wenzoe, and Yu-Sien for making the short time as comfortable as possible, for showing me around, and for the nice lunches around the campus.

I wish to thank Maarten Vanneste and Jung-Chan Choi for the guidance during my stay in the Offshore Geotechnics and Geohazards group at the Norwegian Geotechnical Institute in Oslo. Together, we managed to find a way to connect our geophysical data with geotechnical simulations and I really learned a lot about this complex field and about connecting the dots, even though some of the normally required data was not available. Thanks also to Bahman and Elin for the good company in the office, and also to Joonsang and Guillaume for the nice discussions during lunch.

Many thanks to different people that helped in the processing or interpretation steps. In particular, I would like to acknowledge: Dirk Kläschen for the introduction to and guidance through the seismic processing steps in Omega and the endless patience with all the tiny little hickups we ran into during that time; Stephanie Koch for the introduction to the onboard seismic acquisition processes that Sina and I oversaw during the fateful Taiwan cruise, and for the multiple discussions and coffees; Anke Dannowski for the multiple discussions and interpretation of the OBS data that greatly helped both of us in better understanding the complex seismic data of the Danube area; and Matthias Haeckel for his advice, introduction to the geochemical world, and patient guidance through the creation of the thermal and pore water models.

I would like to thank all members of the Geodynamics group at GEOMAR for the positive atmosphere during the past years. In particular, many thanks to my office mate Henning Schröder for the numerous discussions and laughs we had during that time. Many thanks also to Ines, Henning, Margit, Anke, Stephanie, Kuan-Ting, and Katrin for the company during lunches and breaks.

Further, I would like to thank the projects SUGAR, MIDAS, and STEMM-CCS for financing my PhD studies and for giving me the opportunity to attend various international project meetings and conferences where I presented my work. Many thanks also to the DAAD for financing my research stay in Taiwan.

Ines, thank you for all the time, support, advice, and encouragements you have given me, which was not easy with us living quite far apart during the past two years. Thank you for your suggestions and for proofreading the manuscripts and this thesis. Thanks also to my parents, family and friends for all your support.

This thesis was written using Microsoft Word (and yes, I possibly ran into every single bug this software has). I would also like to acknowledge GMT, Seismic Unix, Pecube, Plaxis 2D, ArcGIS, Kingdom Suite, Illustrator, and Matlab, which altogether consumed most of my time during the period of my PhD.

F Curriculum Vitae

Timo Zander

Date of birth	13 February 1986
Place of birth	Kiel
Citizenship	German
Adress	Sternstraße 10 24116 Kiel Germany

Education

Since 10/2013	Research associate at the Helmholtz Centre for Ocean Research Kiel, GEOMAR
08/2013	Diplom (equivalent MSc) in Geophysics
10/2006 – 08/2013	Studies in Geophysics at Christian-Albrechts-University of Kiel
05/2005	Abitur
08/1996 – 05/2005	Gymnasium Kronshagen